

2m14

NASA-CR-114671

STUDY OF 1980 COMET ENCKE-ASTEROID MISSIONS USING A SPIN-STABILIZED SPACECRAFT

Volume II TECHNICAL REPORT

October 1973

(NASA-CR-114671) STUDY OF 1980 COMET
ENCKE-ASTEROID MISSIONS USING A
SPIN-STABILIZED SPACECRAFT. VOLUME 2:
TECHNICAL REPORT (Martin Marietta Corp.)
373 p HC \$20.75
369
N74-12486
CSCI 22A G3/30 Unclass
23348

Prepared Under Contract No. NAS2-7564

by

MARTIN MARIETTA CORPORATION
Denver, Colorado 80201

for

AMES RESEARCH CENTER
NATIONAL AERONAUTICS AND SPACE ADMINISTRATION

STUDY OF 1980 COMET ENCKE-ASTEROID MISSIONS
USING A SPIN-STABILIZED SPACECRAFT

Volume II

TECHNICAL REPORT

by

W. J. Bursnall, E. G. Howard, W. R. McMinimy,
R. G. Shaffer, & J. M. Van Pelt

October 1973

Distribution of this report is provided in the interest of information exchange. Responsibility for the contents resides in the authors or organization that prepared it.

Prepared Under Contract No. NAS2-7564

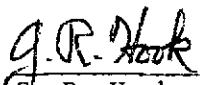
by

MARTIN MARIETTA CORPORATION
Denver, Colorado 80201

for

AMES RESEARCH CENTER
NATIONAL AERONAUTICS AND SPACE ADMINISTRATION

Approved:


G. R. Hook
Program Manager

ERRATA FOR NASA CR-114671

Page v

Change Appendix C to:

Probe Communications: Comet Gas Environment and
Electron Density Study

Page viii

Change Figure V-48 title to:

Comet Signal Strength vs Spacecraft-to-Encke Distance

Page II-26

In third sentence from bottom change:

"varies as R^{-2} " to "varies as R^2 "

Page III-10

In third paragraph change:

5.19×10^9 ft. to 5.19×10^9 ft./day

Page V-23

Change next to last complete sentence on page to:

The change in slope at 512 bps is caused by increasing
receiver loss at lowered data rates.

Page V-39

Change last bit rate from 256 to 512

Page V-123

Change $S = 29250 \text{ W/m}^2$ to $S = 5010 \text{ W/m}^2$

Page V-141

Second paragraph, second sentence change:

bround-based to ground-based

Page V-147

Add to last paragraph:

The first four figures -- V-39 through V-42 -- give: time to encounter, resolution, number of pixels subtended by coma and then by nucleus all as a function of spacecraft-to-Encke distance. The next five figures -- V-43 through V-47 -- contain: time to encounter, resolution, apparent visual magnitude, and number of pixels subtended all as a function of spacecraft-to-asteroid distance for both Toro and Geographos.

Page V-160

Add to bottom of page:

where N_c is the irradiance for a point source

Page V-161

Change second sentence to:

Figure V-48 shows the dependence of H on Δ , where both Δ and R are functions of time from encounter.

Add beside eq. (3):

valid when Δ is small enough such that B_c is constant across the FOV.

Page V-162

Change title to:

Comet Signal Strength vs Spacecraft-to-Encke Distance

Change legend similarly. Label abscissa " Δ ".

Page V-163

Replace first 2 lines with:

$$\pi r_c^2 \bar{B} = \int_0^{a_0} BdA = 2\pi \int_0^{r_c} Kdr$$

So $K = \frac{r_c \bar{B}}{2}$, \bar{B} = mean brightness, a_0 = comet cross-section area

Replace paragraph starting about center of page with:

In figure V-49, the brightness of the coma is plotted vs. distance from the center of the comet. The brightness is for the reference trajectory at about E-27 hours. At this time, Δ is about 1.8×10^6 km and the sun-Encke distance (R) is about 0.55 AU. Figure V-50 can be used to scale the brightness of figure V-49 to other times before encounter along the reference Encke trajectory. Using this scaled brightness, which accounts for the variation of both Δ and R with time from encounter, equation (3) can be used to find the illumination at the focal plane, E. The power per detector is then given by;

Page V-174

In title change 7.12 CM to 7.62 CM (3-inch)

Page R-2

Change Ref. II-11 to See Ref. V-2

Page R-7

Ref. V-2 should be TR 32-1590

Page B-9

Abscissa values at tick marks should be:

10^{-3} 10^{-2} 10^{-1} 10^0

FOREWORD

This report has been prepared in accordance with the requirements of Contract NAS2-7564 and under the direction of the NASA Contract Monitor, Edward L. Tindle. The data and conclusions presented are the result of a three-month technical effort conducted for the Ames Research Center by the Martin Marietta Corporation, Denver Division. The report is divided into the following volumes:

Volume I	Summary
Volume II	Technical Report

Volume I provides a concise overview of the study, and Volume II contains the detailed data and analyses which support the conclusions reached in the study. Volume II, in addition, provides a compilation of previous work accomplished under Martin Marietta sponsorship on several 1980 Encke mission modes which were not included in the study scope of the present contract.

ACKNOWLEDGEMENTS

The participation of the following individuals in this study is acknowledged. Their able efforts, though often limited in duration, contributed significantly to the study and are greatly appreciated.

Program Manager	G. R. Hook
Technical Director	W. J. Bursnall
Technical Team	
Science Analysis	Dr. E. G. Howard
Mission Analysis	J. M. Van Pelt
Spacecraft and Probe Design	R. G. Shaffer
Science and Subsystem Integration	W. R. McMinimy
Communications	J. D. Pettus
Attitude Control	J. W. McIntosh
	D. E. Maas
Propulsion	R. K. Kingery
Power	A. A. Sorenson
Thermal	M. T. Howerton
Mass Properties	W. D. Van Arnam
Navigation Analysis	J. W. Underwood
Gas Physics Analysis	C. T. Edquist
Particle Hazard Analysis	P. G. Kase
Imaging System Analysis	N. Ganiaris
Mass Spectrometer Analysis	J. O. Bunting

TABLE OF CONTENTS

	<u>PAGE</u>
FOREWORD	iii
ACKNOWLEDGEMENTS	iv
LIST OF FIGURES	vi
LIST OF TABLES	x
I. INTRODUCTION	I-1
II. ANALYSIS OF SCIENTIFIC REQUIREMENTS	II-1
A. Characteristics of Comet Encke	II-2
B. Comet Science Objectives	II-16
C. Instrument Payload Section	II-19
D. Coma Probe Utilization	II-26
E. Scientific Investigation of Asteroids Geographos and Toro	II-31
F. Summary of Expected Scientific Accomplishments	II-38
III. ANALYSIS OF MISSION OPPORTUNITIES	III-1
A. Encke-Dedicated Mission Characteristics	III-3
B. Encke/Asteroid Mission Characteristics	III-25
C. Navigation Feasibility	III-39
IV. SPACECRAFT SYSTEM DESIGN EVALUATION	IV-1
A. Description of Options Studied	IV-3
B. Probe Installation Concept	IV-10
C. Comparison of Spacecraft Concepts	IV-14
V. SUBSYSTEM DESIGN	V-1
A. Structures and Mechanisms	V-2
B. Communications	V-23
C. Probe Communications	V-42
D. Attitude Control	V-61
E. Propulsion	V-83
F. Electrical Power	V-112
G. Thermal Control	V-122
H. Data Handling	V-125
I. Science Instruments	V-129
J. Mass Properties	V-178
VI. CONCLUSIONS AND RECOMMENDATIONS	VI-1
REFERENCES	R-1
APPENDIX A - Prior Contractor Study Effort	A-1
APPENDIX B - Comet Particulate Model and Spacecraft Survivability	B-1
APPENDIX C - Comet Gas Environment and Electron Density Study	C-1

LIST OF FIGURES

<u>FIGURE NO.</u>		<u>Page</u>
II-1	Magnitude of Encke vs Distance (Time) to Encounter	II-6
II-2	Density of Water Products At 0.8 AU	II-8
II-3	Density of Several Species at 1.0 AU	II-12
II-4	Encke Major Features	II-13
III-1	Injected Weight Capability of Launch Vehicle	III-4
III-2	Region of Mission Interest	III-5
III-3	Spacecraft Approach Velocities at Encounter	III-6
III-4	Spacecraft Approach Angles at Encounter	III-7
III-5	Velocity Penalties for High Launch Declinations	III-8
III-6	Spacecraft Orbit Radius of Perihelion and Encke Intercept Radius	III-9
III-7	Comet Reference Mission Encounter Trajectory	III-11
III-8	Spacecraft/Comet Relative Motion Trajectory	III-12
III-9	Passage of Spacecraft Through Coma and Tail	III-13
III-10	Close Encounter Angular Motion	III-15
III-11	Probe Deployment Mode Comparison	III-17
III-12	Deployment Requirements - Bus Propulsion Mode	III-19
III-13	Geometry of Probe Entry	III-21
III-14	Bus to Probe Communication Parameter Variations	III-22
III-15	Summary of Asteroid Mission Options	III-26
III-16	Earth/Encke Leg Trajectory Variations	III-28
III-17	Encke/Geographos Missions	III-29
III-18	Encke/Toro Mission	III-30
III-19	Encke/Geographos/Toro Mission	III-31
III-20	Asteroid Lighting Conditions During Approach	III-34
III-21	Estimated Comet Ephemeris Accuracies with On-Board Sensor	III-49
IV-1	Spin Axis Points to Encke: Concept No. 1	IV-4
IV-2	Spin Axis Points to Earth: Concept No. 2	IV-5
IV-3	Spin Axis Perpendicular to Earth/Encke/Spacecraft Plane (Despun Platform): Concept No. 3	IV-6
IV-4	Spin Axis Perpendicular to Earth/Encke/Spacecraft Plane (Despun Mirror): Concept No. 4	IV-7

LIST OF FIGURES (CONTINUED)

<u>FIGURE NO.</u>		<u>Page</u>
IV-5	Spin Axis Perpendicular to Earth/Encke/Spacecraft Plan (Spin Scan Camera): Concept No. 5	IV-8
IV-6	Asteroid Maneuver Propulsion Installation	IV-11
IV-7	Probe Location Concepts	IV-13
IV-8	Estimated Time in Comet Tail for Spacecraft Weight Injected	IV-15
V-1	Spacecraft Primary Structure	V-3
V-2	• Encke Spacecraft - Boost Configuration	V-4
V-3	De-Spin Platform Concept for Concept No. 3	V-6
V-4	De-Spin Mirror Concept	V-7
V-5	Concept No. 1: Spin Axis Points to Encke	V-9
V-6	Concept No. 2: Spin Axis Points to Earth	V-11
V-7	Concept No. 3: Spin Axis Perpendicular to Spacecraft, Earth, Encke Plane, Utilizing De-Spun Platform	V-13
V-8	Concept No. 4: Spin Axis Perpendicular to Spacecraft, Earth, Encke Plane, Utilizing De-Spun Mirror	V-15
V-9	Concept No. 5: Spin Axis Perpendicular to Spacecraft, Earth, Encke Plane, Utilizing Spin-Scan Camera	V-17
V-10	Probe Equipment Arrangement Concept	V-19
V-11	Probe Structural Configuration Concept	V-21
V-12	Probe-To-Spacecraft Support and Separation Concept	V-22
V-13	Communications Block Diagram - Configuration 2	V-24
V-14	Communications Block Diagram - Configuration 1, 3, 4, and 5	V-25
V-15	Data Rate vs Range	V-31
V-16	380 MHz Viking '75 Orbiter Relay Antenna	V-48
V-17	Probe Flat Plate Antenna Outline Dimensions	V-49
V-18	Concept No. 2 Attitude Control System	V-64
V-19	Doppler Attitude Determination Accuracies	V-66
V-20	Despun Mirror Control System Block Diagram - Azimuth	V-72
V-21	Single Axis Gimbal Control System Block Diagram	V-73
V-22	Sun Aspect Angle and Sun Sensor Accuracy as a Function of Mission Time	V-76
V-23	Rate Stability Required vs Encke Encounter	V-79
V-24	Reaction Control System Schematic	V-86
V-25	Hydrazine Tank Blow Down	V-88
V-26	Typical N_2H_4 Engine Thrust Profiles	V-91

LIST OF FIGURES (CONTINUED)

<u>FIGURE NO.</u>		<u>Page</u>
V-27	Steady State Specific Impulse	V-92
V-28	Impulse Bit For Pioneer 10/11 1.2 LB _F Thruster (Duty Cycle: 0.125 Seconds ON/12.375 Seconds OFF)	V-93
V-29	Pulsing Specific Impulse for Pioneer 10/11 1.2 LB _F Thruster (Duty Cycle: 0.125 Seconds ON/12.375 Seconds OFF)	V-94
V-30	Bi-Propellant ΔV Maneuver System	V-97
V-31	GN ₂ RCS System	V-98
V-32	Solar Array Configuration	V-113
V-33	Power Subsystem Block Diagram	V-114
V-34	Probe Power Usage	V-117
V-35	Probe Power Subsystem	V-119
V-36	Thermal Control Concept	V-122
V-37	Thermal Analysis Diagram	V-123
V-38A	Non-Imaging Science and Spacecraft Engineering Data	V-126
V-38B	Imaging Science Data	V-126
V-39	Trajectory Distance <u>VS.</u> Time to Comet RCA	V-149
V-40	Resolution <u>VS.</u> (Time) Distance from Encke	V-150
V-41	Number of Pixels for Coma of Encke <u>VS.</u> Distance	V-151
V-42	Number of Pixels for Nucleus of Encke <u>VS.</u> Distance	V-152
V-43	Distance <u>VS.</u> Time to Encounter for Asteroids	V-153
V-44	Resolution <u>VS.</u> Distance for Geographos and Toro	V-154
V-45	Visual Magnitude <u>VS.</u> Time (Distance) of Geographos and Toro	V-155
V-46	Number of Pixels <u>VS.</u> Distance for Geographos	V-156
V-47	Number of Pixels <u>VS.</u> Distance for Toro	V-157
V-48	Comet Irradiance <u>VS.</u> Spacecraft-to-Encke-Distance	V-162
V-49	Brightness Distribution of Coma <u>VS.</u> Distance from the Nucleus	V-164
V-50	Brightness Ratio of Coma (For Various Spacecraft to Encke Distances, Δ)	V-165
V-51	Radius of Coma Imaging <u>VS.</u> Spacecraft Distance from Nucleus	V-168
A-1	1980 Comet Encke Mission Classes	A-4
A-2	Encke/80 Fast Flyby Characteristics	A-5
A-3	Encke/80 Flyby, Return to Earth Options	A-7
A-4	Typical Encounter Trajectories	A-9

LIST OF FIGURES (CONTINUED)

<u>FIGURE NO.</u>		<u>Page</u>
A-5	Relative Motion for Typical Encounters	A-10
A-6	Pre-Perihelion Encounter Flyby Geometry Options	A-11
A-7	Post-Perihelion Encounter Flyby Geometry	A-13
A-8	Asteroid Flyby Candidates	A-15
A-9	Combined Mission Characteristics	A-16
B-1	Encke Particle Flux vs Distance from Nucleus (Graph 1 of 2)	B-8
B-2	Encke Particle Flux vs Distance from Nucleus (Graph 2 of 2)	B-9
B-3	Spacecraft and Probe Survival for Encke Encounter	B-12
C-1	Number Density vs Distance from Nucleus	C-9
C-2	Flow Velocity vs Distance from Nucleus	C-10

LIST OF TABLES

<u>TABLE NO.</u>		<u>Page</u>
II-1	Comet Encke Physical Properties Summary	II-3
II-2	Observed Species for Encke	II-11
II-3	Major Comet Objectives for Investigation	II-17
II-4	Major Comet Science Objectives	II-18
II-5	Summary of Comet Observables for Measurement	II-20
II-6	Instrument Response for Comet Study	II-21
II-7	Coma Densities	II-27
II-8	Probe Science and Goals	II-30
II-9	Geographos Physical Properties Summary	II-33
II-10	Toro Physical Properties Summary	II-34
II-11	Major Asteroid Observables for Investigation	II-36
II-12	Major Asteroid Science Objectives	II-37
III-1	Comet Mission Parameter Variations During the Launch Period	III-16
III-2	Probe/Bus Relative Dispersions at Entry	III-24
III-3	Comparison of Asteroid Missions	III-35
III-4	Impact of Combining Asteroid Flybys Upon Basic Comet Mission	III-38
III-5	Effect of Ephemeris Uncertainties (Without On-Board Navigation)	III-41
III-6	Navigation Requirements for Reference Mission	III-44
III-7	Comparison of Retargeting Requirements Computed by Conic and Integrated Trajectory Programs (AIMS and MIT) (Encke/Geographos/Toro Mission)	III-44
III-8	Semi-Major Axes of Dispersion Ellipsoids at Target Encounter (Encke/Geographos/Toro Mission)	III-45
III-9	Statistical Parametric Values of the ΔV Budget for Individual and Total Trim Maneuvers (Encke/Geographos/Toro Mission)	III-46
III-10	Anticipated Dispersions in Target Approach Geometry	III-49
IV-1	Encke-Mission Science Instruments	IV-3
IV-2	Summary of Concept Characteristics	IV-12
IV-3	Spacecraft Mass Comparison	IV-16

LIST OF TABLES (CONTINUED)

<u>TABLE NO.</u>		<u>Page</u>
IV-4	Configuration Impact on Science	IV-18
V-1	Encke Encounter, 0.57 AU, S-Band Design Control Table	V-26
V-2	Encke Encounter, 0.57 AU, X-Band Design Control Table	V-27
V-3	Geographos, Toro Encounter - S-Band Design Control Table	V-28
V-4	Geographos, Toro Encounter - X-Band Design Control Table	V-29
V-5	Uplink Command Design Control Table, 64 Meter Net	V-30
V-6	Communications Features for an Earth Pointing Spacecraft	V-33
V-7	Communications Components, Weight and Power for an Earth Pointing Spacecraft	V-34
V-8	Major Communications Subsystems Characteristics for an Encke Pointing or an Encke, Toro, Geographos Spacecraft (Also Applies to Configurations 3, 4, & 5)	V-35
V-9	Communications Components, Weight and Power for an Encke Pointing Spacecraft or Encke, Toro, Geographos Pointing Spacecraft (Also Applies to Configurations 3, 4, & 5)	V-36
V-10	Telemetry Options for a S-Band Only Capability Considered For an Earth Pointing Spacecraft	V-37
V-11	Dual S-Band and X-Band Telemetry Options Considered for an Earth Pointing Spacecraft	V-38
V-12	Spacecraft Spin Axis Perpendicular to Earth Spacecraft Line (S-Band or X-Band)	V-39
V-13	Probe Communications Link Parameters	V-43
V-14	Relay Link Calculations, Wide Band FSK	V-44
V-15	Relay Link Calculations, Coherent PSK/PM 500 km Range, 1700 MHz, Uncoded	V-46
V-16	Ranges and Antenna Aspect Angles for Probe Relay and Probe Direct Links	V-47
V-17	380 MHz Wideband FSK Communications Equipment for Probe To Spacecraft Relay Link	V-51
V-18	1700 MHz Wide Band Communications Equipment for Probe to Spacecraft Relay Link	V-52
V-19	1700 MHz Coherent PSK/PM Communications Equipment For Probe To Spacecraft Relay Link - 128 bps	V-53
V-20	Probe Link Calculation - Direct To Earth	V-55
V-21	2300 MHZ Direct Probe to Earth Link Communications Equipment	V-57
V-22	Antenna Gain and Required Probe Transmitter RF Power for Various Spacecraft Attitudes, A 40° Probe Antenna Aspect Angle and 128 bps Data Rate	V-59

LIST OF TABLES (CONTINUED)

<u>TABLE NO.</u>		<u>Page</u>
V-23	Comparison of Weight and Power for Probe Relay With Earth Pointing Spacecraft and for Probe Direct to Earth Communications	V-60
V-24	Attitude Control System Components	V-63
V-25	Track Rate, Picture Rate for Close Encounter	V-70
V-26	Preliminary Experiment Pointing Error Analysis	V-78
V-27	Summary of Propulsion Requirements	V-84
V-28	Thruster Configuration Options	V-85
V-29	Typical Rocket Engine Assemblies	V-89
V-30	Approximate Burn Times Required for ΔV Maneuvers (2 Engines Firing)	V-89
V-31	Propulsion System Weight and Propellant Usage Summary	V-95
V-32	Propulsion System Requirements for the Earth-Encke-Geographos 1 Mission	V-99
V-33	Approximate Burn Time Required for ΔV Maneuvers with N_2H_4 System	V-100
V-34	Propulsion System Weight and Propellant Usage Summary - Encke-Geographos 1 Mission	V-101
V-35	Propellant System Requirements for the Earth-Encke-Geographos-Toro Mission	V-102
V-36	Approximate RCS Burn Times Required for ΔV Maneuvers (2 Engines Firing) with N_2H_4 RCS/SRM ΔV System Combination	V-103
V-37	Approximate RCS Burn Times Required for ΔV Maneuvers (2 Engines Firing) With N_2H_4 RCS/Bipropellant System Combination	V-105
V-38	RCS/Maneuver System Comparison	V- 109
V-39	RCS/Maneuver System Weight Comparison	V- 110
V-40	Power Profile Summary (Encke-Geographos-Toro Mission)	V- 115
V-41	Probe Sequence of Events	V- 120
V-42	Probe Equipment Power Requirements	V- 121
V-43	Surface Properties	V- 124
V-44	Data System Component Characteristics	V- 127
V-45	Minimum Imaging Timeline for Encke	V- 142
V-46	Minimum UV Timeline for Encke	V- 143
V-47	Minimum IR Timeline for Encke	V- 144

LIST OF TABLES (CONTINUED)

<u>TABLE NO.</u>		<u>Page</u>
V-48	Minimum Imaging Timeline for Asteroids	V-145
V-49	Minimum IR Timeline for Asteroids	V-148
V-50	Comet Threshold Position of Visibility from Imaging-Radiometry Study	V-159
V-51	Kinetic Energy of Species (ev)	V-172
V-52	Dissociation Energies and Ionization Potentials of Species	V-173
V-53	Magnetic Field Strength To Turn Species 90° Through a 3-inch Radius	V-174
V-54	Sensitivity of Mass Spectrometer	V-175
V-55	Baseline Detail Weight Statement Concept No. 2	V-179
V-56	Coma Probe Detail Mass Statement	V-181
V-57	Spacecraft Mass Data Comparison	V-182
A-1	Asteroid Flyby Characteristics	A-17
A-2	Mission Option Summary	A-19
B-1	Spacecraft and Probe Survivability (Particle Emission Rate - 60,000 g/sec; Particle Velocity 300 m/sec)	B-10
B-2	Spacecraft and Probe Survivability (Particle Emission Rate - 60,000 g/sec; Particle Velocity - 30 m/sec)	B-10
	Spacecraft and Probe Survivability (Particle Emission Rate - 6,000 g/sec; Particle Velocity - 300 m/sec)	B-11
B-4	Spacecraft and Probe Survivability (Particle Emission Rate - 6,000 g/sec; Particle Velocity - 30 m/sec)	B-11

I. INTRODUCTION

I. INTRODUCTION

A variety of ballistic fast-flyby mission options to the Comet Encke in 1980 were identified in corporate-sponsored studies by the Denver Division of Martin Marietta Corporation. The present study was undertaken to determine the feasibility and desirability of using low-cost, light-weight, spinning spacecraft for a selected group of these missions. The Atlas/Centaur/TE 364-4 was specified as the launch vehicle. Flight modes were limited to encounters at Encke prior to its perihelion passage. This allows a single spacecraft to pass through both the coma and tail, with the added potential of subsequent encounters of the asteroids Geographos and Toro. Post-Encke flybys of the asteroids Geographos or Toro, or both, were thus also assessed. Additionally, the utility of probes into Encke's coma was evaluated in terms of potential increase in scientific return and impact on spacecraft and mission characteristics.

The objective of this volume is to present the data and analyses that support the conclusions and recommendations resulting from the study. The scientific basis for the Encke missions is first discussed and includes a summary of the physical characteristics of Encke, a statement of scientific objectives and priorities, a definition of the spacecraft instrument payload, and a rationale for utilization and instrumentation of coma probes. Similarly, instrument payload modifications for asteroid encounter are arrived at by review and analysis of objectives and observables.

The discussion of mission opportunities begins with a review of Encke-dedicated parametric mission characteristics. Detailed data are presented for the reference mission selected as the baseline for science analyses and design studies. The coma-probe analysis is then described, including a comparison of several probe deployment techniques and associated propulsion requirements. Parametric bus/probe relative-geometry data are presented and form the basis for later communication link analyses. Probe dispersions due to deployment error sources and magnitudes are identified. Maneuver requirements and mission characteristics are compared for four post-Encke asteroid flyby cases (Geographos near perihelion, Geographos near 1 AU, Toro, and Geographos near perihelion plus Toro), and the impact of the asteroid(s) flyby on comet encounter is then analyzed. Five alternate spacecraft configurations

are compared in terms of their capability in meeting the science and mission requirements. Spacecraft-subsystem and probe-design features are then described. Finally, conclusions of the study are summarized, and recommendations are given for further activity.

THIS PAGE BLANK

II. ANALYSIS OF SCIENTIFIC REQUIREMENTS

II. ANALYSIS OF SCIENTIFIC REQUIREMENTS

In this section, physical models of Comet Encke and of asteroids Geographos and Toro are examined. While much remains to be learned, enough is known to identify the major areas of scientific investigation. These science goals then establish the instrumentation required. With the possible exception of a comet particulate-matter-composition detector, it will be shown that instruments are either available or could be modified for these missions. Included, also, is the study of a coma probe to more fully satisfy scientific objectives.

A. CHARACTERISTICS OF COMET ENCKE

In the following discussion, the available pertinent physical parameters of Comet Encke are presented. The description is not exhaustive, and some of our knowledge will be seen to be incomplete. It does, however, serve as a base from which to identify comet observables and science objectives. Those sections on dimensions, photometric, particulate, and gas-density models will be used the most in mission study. Table II-1 presents a summary of these values.

1. Description of Comet Model

There are three basic structural parts of a comet: nucleus, coma and tail. The comet model is discussed under these three headings.

a. The Nucleus - The nucleus has not been seen for Encke in the best Earth-based photography; however, it is inferred on theoretical bases by the need for a source of large amounts of gas and dust and on observational bases by brightness isophots and by the motion of fine structure and material in the ionized tail.

Size - Roemer (ref. II-1) has found that the measured brightness of the Encke nucleus (as distinguished from the larger coma) varies as the inverse square of the solar distance. This can be interpreted in terms of reflection from a small body of constant radius. With an albedo of 0.1 (the Moon) and a Lambert phase function, a nucleus radius of 1.6 km would correspond to a measured $AR_N = 0.24$, where R_N is the radius of the nucleus and A is the albedo. If the albedo varies from 0.02 (carbonaceous chondrites) to 0.7 (H_2O solids), the nuclear radius could be between 0.6 and 3.5 km.

TABLE II-1 COMET ENCKE PHYSICAL PROPERTIES SUMMARY

	<u>COMET FEATURE</u>	<u>RANGE OF VALUES</u>	<u>NOMINAL VALUE USED</u>
I.	NUCLEUS	STARLIKE TO DIFFUSE	STARLIKE
	DIMENSIONS (radius)	0.5 - 3.6 km	1.6 km
	MASS	$10^{14} - 5 \times 10^{17}$ g	2×10^{16} g
	ALBEDO	0.02 - 0.7	0.1
	PHASE CURVE	LAMBERT & MODIFICATIONS	LAMBERT
	MAGNITUDE	$H_N = 16.0 + 5 \log \Delta + 5 \log r$ + 0.3 (Phase Angle($^\circ$))	$\Delta =$ S/C-ENCKE DISTANCE IN AU $r =$ HELIOCENTRIC DIST. IN AU
II.	COMA	NEBULOUS AND DIFFUSE	NEBULOUS
	DIMENSIONS (radius)	10^4 - 10^6 km	2×10^4 km
	MAX GAS DENSITY (H_2O PRODUCTS)		
	NEAR NUCLEUS	10^{14} - 10^{12} molecules/cm ³	10^{13} molecules/cm ³
	NEAR 5000 KM	10^5 - 10^3 molecules/cm ³	10^5 molecules/cm ³
	MAGNITUDE	$H = 10.93 + 5 \log \Delta + 3.55(r^{1.8}-1)$	Same
	MAX. VEL. OF PARTICULATE MATTER	30-300 m/sec	300 m/sec
	PARTICULATE EMISSION RATE	6×10^4 to 6×10^3 g/sec	6×10^4 g/sec (per active 100 days)
III.	TAIL		
	LENGTH	10^5 - 10^7 km	10^6 km, ION TAIL ONLY
	WIDTH	10^4 - 10^6 km	4×10^4 km

Mass - After a refinement of the phase function, Marsden (ref. II-2) found a radius of 1.8 km for Encke's nucleus, (albedo = 0.1). For a density of 1.0 gm/cm^3 , this is a mass of $2 \times 10^{16} \text{ gm}$. With reasonable variations in assumed density and albedo, the mass could range from 10^{14} gm to $5 \times 10^{17} \text{ gm}$.

Rotation and Axis Alignment - Marsden (ref. II-2) has pointed out that the 0.04-deg/revolution non-gravitational acceleration of Encke can be accounted for if the gas flow from the nucleus were to occur in a concentrated direction. Sekanina (ref. II-3) has determined that as much as 30% of mass emitted by Encke's nucleus may be emitted in a single direction. These two ideas would imply that Encke's nucleus would be rotating retrograde with axis of rotation normal to the orbital plane. However, these calculations are very uncertain, and, for this study, a spinning nucleus with radial emissions in all directions has been assumed.

Mass Loss - Sekanina (ref. II-4) has found that the relative mass loss, $\frac{\Delta m}{m}$, required to explain nongravitational forces for comets is 0.01-1 percent per revolution. For Encke, $\frac{\Delta m}{m}$ has decreased from 0.24% to 0.03% per revolution between 1800 and 1967. Encke currently appears to be stable at the lower rates. This 0.03-percent-per-perihelion-passage-mass-loss-rate will be used later in the calculations of gas and particulate-matter models.

Chemical Composition - On the basis of Earth-based observations, the composition of the nucleus must be inferred from emission spectra of the coma and tail. Lines of CN, C₂, and C₃ probably are dissociation products from molecules of H₂O, NH₃, CH₄, and CO₂. Thus, elements of carbon, nitrogen, and oxygen formed the nucleus by condensation and accretion processes. Hydrogen is necessary to form the above molecules and to explain the lyman-alpha emission seen from the OAO observations. Highly volatile compounds, such as CH₄, may be trapped as clathrates. Magnesium, Iron, Silicon, and Calcium are probably present in solar abundance values. In order to identify the undissociated compounds and additional radicals, both neutral and ion mass spectrometers for in situ measurements are needed. Also, by flying on to the Apollo asteroids, Geographos and Toro, and obtaining good surface imaging, it may be possible to test the "dead-comet-core" hypothesis.

Evolution Model (Volatiles and Non-Volatile Core) - According to Sekanina (ref. II-3), the nucleus has a "core-mantle" structure. In this model, the mantle, or ray envelope, which was once large, gradually sublimated after heating on repeated perihelion passages. After more time, the nonvolatile core was exposed to solar radiation. Then, molecular desorption from the unprotected core's surface would replace free sublimation in producing the comet's atmosphere. The transfer of volatiles from the core's interior to the surface is provided by activated diffusion. The nucleus's ability to regenerate new material at the surface is further weakened with time. Eventually, the reservoir of volatiles is exhausted, and the comet is a dead, nonvolatile core. By measurements of volatile and particulate material in the coma, it will be possible to test such an evolutionary model.

Magnitude and Decline - Encke was first observed in 1786. During the succeeding 40 apparitions, its brightness has declined in absolute magnitude from ~ 8 to 14. That decline, along with the apparent absence of a dust tail in recent apparitions and a decrease in $\frac{\Delta_m}{m}$, indicates that Encke is a dying comet. Sometime around the year 2000, its death may be the birth of an asteroid. Therefore, Encke is an exciting target. It is important to measure a comet that is still active enough to be interesting, yet emits less material for possible spacecraft hazard and, finally, may be in the process of becoming an asteroid.

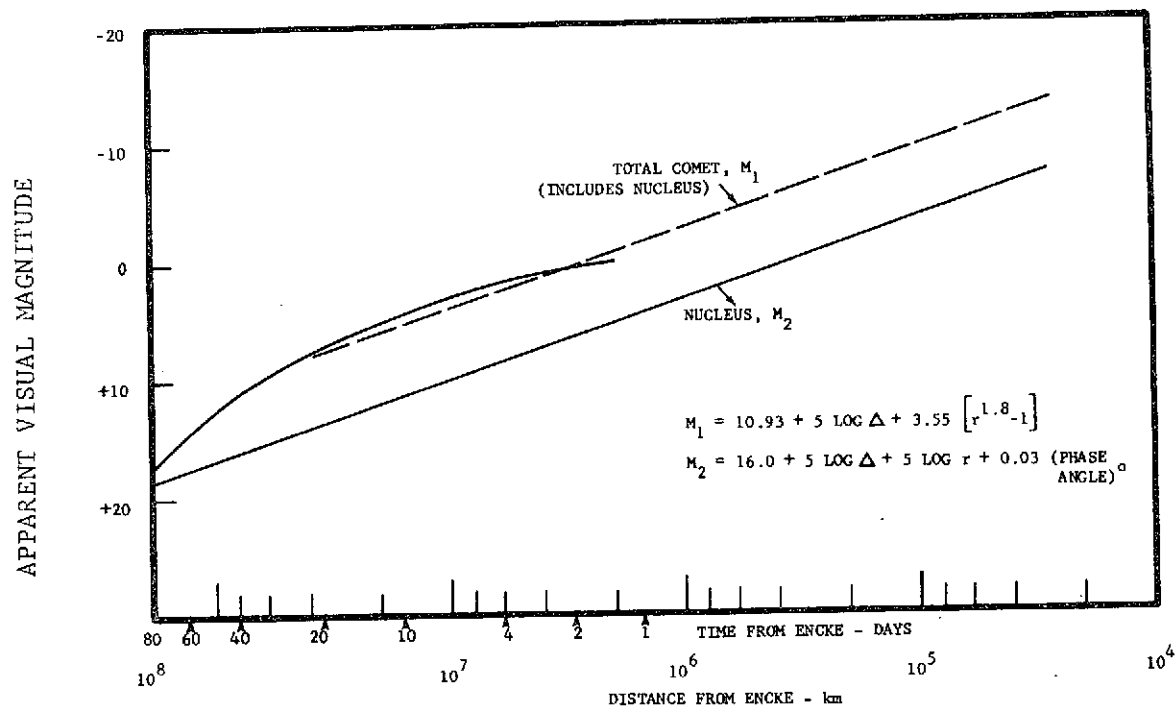
The magnitude of the nucleus can be stated as: (ref. II-5)

$$H_N = 16.0 + 5 \log \Delta + 5 \log r + 0.03 (\text{phase angle}^\circ)$$

where: r is heliocentric distance of comet in A.U.

Δ is Earth (or spacecraft) to comet distance in A.U.

The nucleus flux is $\sim 1\%$ of the comet total, or 5 to 6 magnitudes fainter than the integrated total comet. Figure II-1 plots this equation and the subsequent one for the total comet magnitude. These expressions constitute a photometric brightness model of the comet as a function of distance for the approach trajectory. This brightness will be used in later sections in comet-acquisition and imaging-systems radiometry studies (sec. V-I).

FIGURE II-1 VISUAL MAGNITUDE VS. DISTANCE TO ENCKE

b. The Coma - The coma is the atmosphere of the comet: a region in which ionization, photo-dissociation, and other processes occur for material from the nucleus.

Size - The coma diameter varies with the solar distance of the comet. At 1 AU, Encke's mean diameter is about 10^5 km. This diameter value decreases to about 40,000 km at 0.5 AU (ref. II-6), which is the value used in this study.

Gas Emission - In the simplest model of an expanding cometary coma (no icy-grain halo), the neutral gas, mainly H_2O products, leaves the nucleus at the speed of sound, or 300-700 m/sec at a surface temperature of 250-750°K. The flow speed stabilizes at ~ 1 km/sec. The number densities of H_2O and other molecules depends on the amounts in the nucleus but they decrease as the inverse square of the distance away from the nucleus to $\sim 10^4$ km, where photo-dissociation effects reduce the densities to near-zero values. Figure II-2 indicates one estimate of the number density of water products as a function of distance from the nucleus (ref. II-7).

The size of the region containing the parent molecules can be estimated from the photo-dissociation time, T , and the expansion speed of the undissociated gas, V . For $T = 0.25-2.5 \times 10^4$ sec at 0.5 A.U. and $V = 1.1$ km/sec, the radius is $VT = 0.25-2.5 \times 10^4$ km. It will be necessary to make in situ measurements by the mass spectrometers near the 5000 km region to have a high probability of parent molecule detection. A radius of closest approach value of 5000 km was selected in order to obtain meaningful mass-spectrometer measurements and still stay out of the particulate-matter hazards, as detailed in Appendix B.

The "daughter" products are eventually removed by photo-dissociation, photo-ionization, or collisions with solar wind particles. To conserve momentum, lighter products, like atomic hydrogen, would be heated by any excess energy above that required for dissociation. They should expand at higher speeds and reach greater distances (10^5 - 10^6 km from the nucleus) than other species. The distances and concentrations can be measured with an ultraviolet spectrometer. Halo's of hydrogen-Lyman alpha, atomic oxygen, and perhaps the hydroxyl radical will be sought, and they should be observable days before the coma entry or encounter.

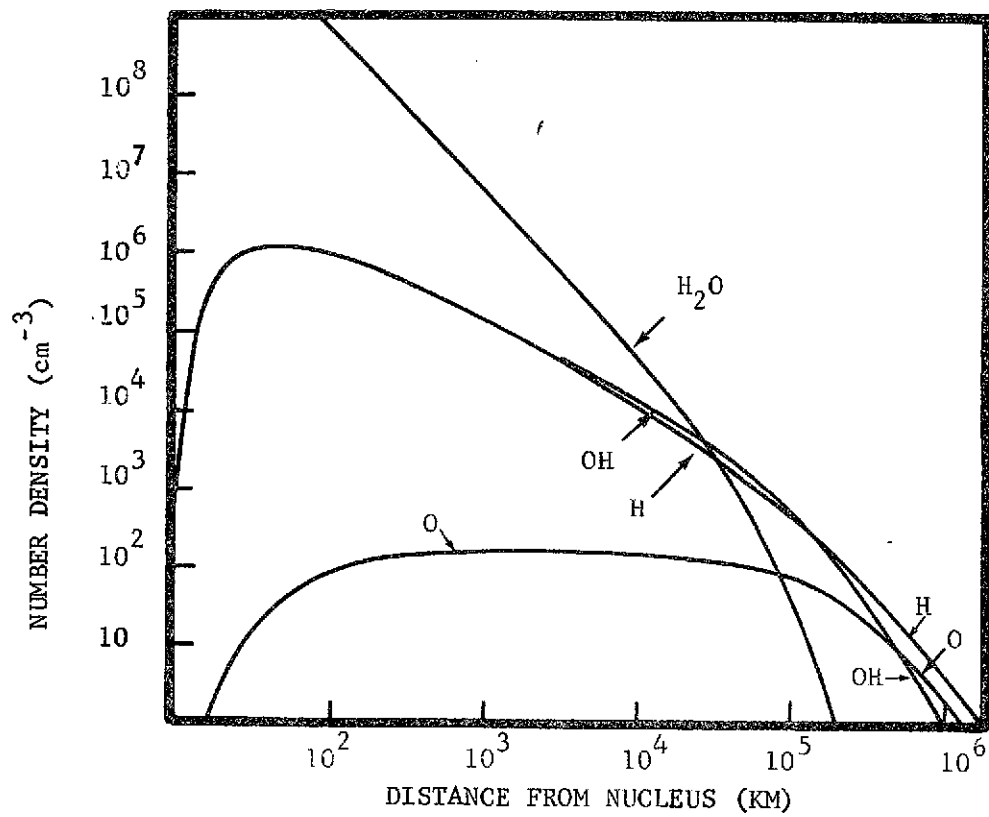


FIGURE II-2 DENSITY OF WATER PRODUCTS AT 0.8 AU
(ref. II-25)

Magnitude - The magnitude of the total comet is estimated (Sekanina, II-8) to be $N = 10.93 + 5 \log \Delta + 3.55 (r^{1.8} - 1)$. Where Δ is the distance from Earth (or spacecraft) to comet in AU, r is heliocentric distance to the comet in AU. The constant is 10.73 for the 1973/74 appearance. For 1980, the constant would be 10.93 if an average value of 0.1 is subtracted for each comet return as suggested by Sekanina (ref. II-8). This magnitude relation is plotted in Figure II-1 and is used in subsequent sections on comet acquisition and image-systems radiometry.

Icy Grain Halo Model - While not universally accepted, this model deserves mention for its mission effects. In order to explain the long life and the total amount of gas constituents in the coma, it is desirable to find a way to have gases emitted from the nucleus already in radical form. The solar flux is insufficient to account for the release of some of the excited material seen in the coma and tail.

One model (ref. II-9) has the nucleus surrounded by an icy halo. These icy particles are accelerated from the nucleus along with the neutral gas. If the icy particles were, in part, a clathrate (frozen radical gases), radicals would be able to reach a larger cometocentric distance.

If such an icy halo exists, its size depends on the size of the icy grains. For 0.3-mm grains, near Encke perihelion in 1980, the radius could be as large as 1000 km. A radius of 100 km is considered more likely (ref. II-6).

This icy halo could influence operation of the mass spectrometers on a coma probe. The halo might be bright enough, also, to effect the imaging system in its search for the nucleus. However, because of the halo's uncertainty as a model applied specifically to Encke, this study has not made special provisions for halo occurrence, with one exception. The radius of closest approach for the spacecraft, 5000 km, is outside of the region where particulate-matter damage would be expected if such an icy halo should exist.

Volatile Mass Emitted - A mass loss of 6×10^{12} g per perihelion passage has been estimated for Encke (ref. II-10). For a 100-day active period, this corresponds to $\sim 6 \times 10^5$ g/sec. This mass-loss is derived from the mass-loss mentioned in the earlier discussion of the nucleus. The mass-loss value is also the basis for particulate-matter loss in the next section.

An uncertainty of an order of magnitude has been applied to this emitted-mass number in models of the particulate-matter emission.

Nonvolatile Mass Loss - The absence of continuum radiation in the coma of Encke suggests either the coma wind is too weak to blow much material from the nucleus, or that all the small grains have been blown off. A value of 10% of the volatile mass loss or 6×10^4 g/sec of nonvolatile material (ref. II-6) is used in this study. An uncertainty of an order of magnitude for the mass-loss value will be considered in later applications.

Spectrum (Gas Constituents) - Table II-2 lists the gas species seen in Encke's spectra; CN, C₂, and C₃ are the strongest lines. These neutral molecules (dissociated products of more complex molecules) radiate in the visible through resonance fluorescence. Other species strongly expected are CO₂⁺, N₁, N₂⁺, CH⁺, Na, and OH⁺.

The "onion-skin" head of the coma is due to CN and CO⁺ emissions which overlap, and, to a lesser degree, due to scattering from dust particles. The number densities of water and water products has been stated (fig. II-2) in the discussion of coma gas emission. Unfortunately, number densities on species other than water are not well known; the available information is summarized in Figure II-3 (ref. II-11).

c. The Tail (Solar Wind Interaction Region) - The comet must interact with the solar wind, and several important processes are involved. The solar wind may contribute to dissociation and ionization of comet neutral parent molecules, the solar wind sweeps ionized constituents of the coma into the tail, and the solar wind must blow around the comet providing a possible shock, and contact discontinuity surface.

Bow Shock Model - The solar wind may produce a collisionless shock in the process of decelerating around the ionized coma. Biermann (ref. II-12) has located the shock at 10^6 to 10^7 km upstream, as shown in Figure II-4. The bulk flow would drop from 400 km/sec to 100 km/sec or less at the shock, it would then slow to a few km/sec, and it would finally slow to a near-zero velocity at a contact discontinuity located $\sim 5 \times 10^4$ km from the nucleus.

While the above model is analogous with Earth's magnetosphere, it is

TABLE II-2 OBSERVED SPECIES FOR ENCKE

SPECIES	WAVELENGTH (Å)
CN - - - - -	3880
	{ 4740
C ₂ - - - - -	{ 5160
	{ 5640
C ₃ - - - - -	4050
CH - - - - -	4280
NH - - - - -	3360
NH ₂ - - - - -	6300
OH - - - - -	3090
	{ 4000
CO ⁺ - - - - -	{ 4260
	{ 4550
N ₂ ⁺ - - - - -	3910

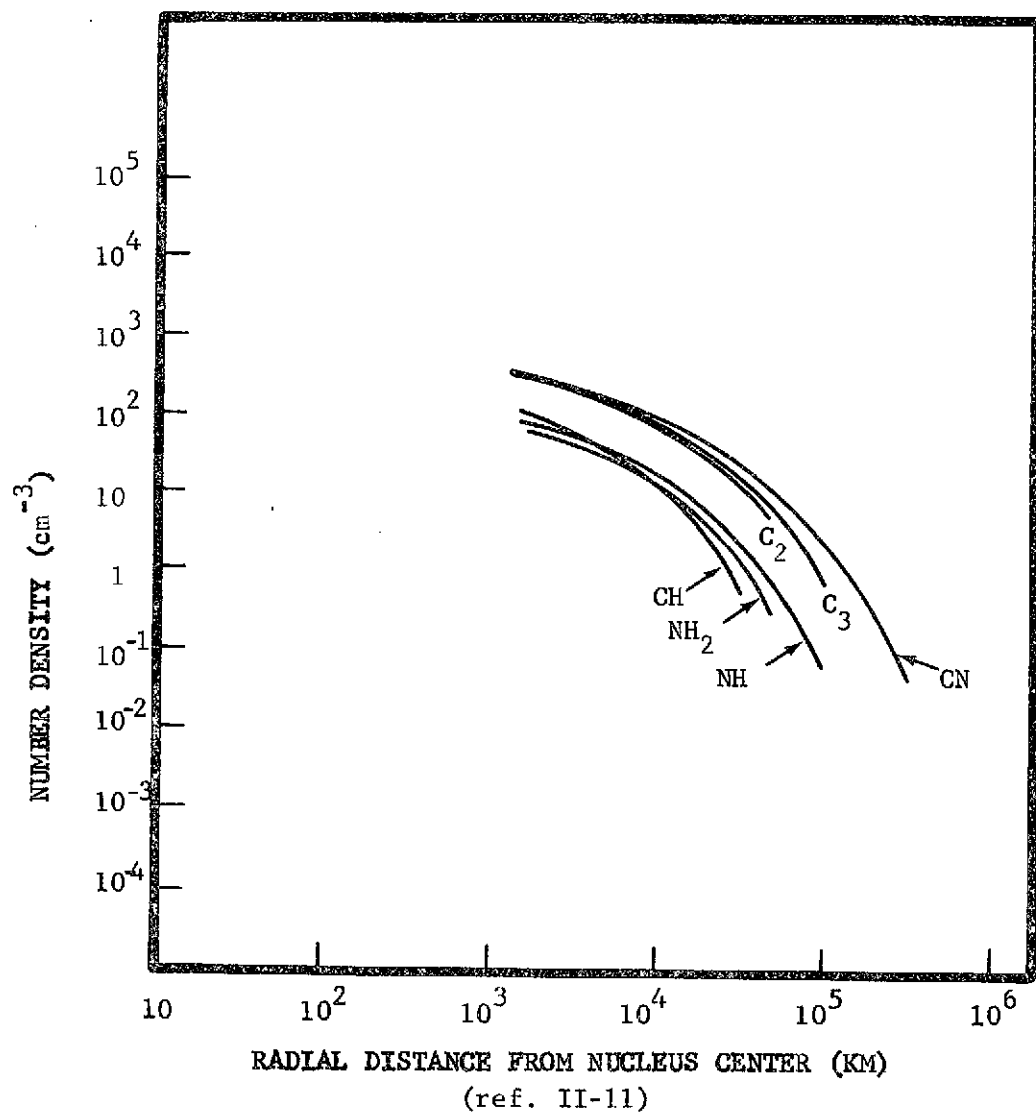


FIGURE II-3 DENSITY OF SEVERAL SPECIES AT 1 AU

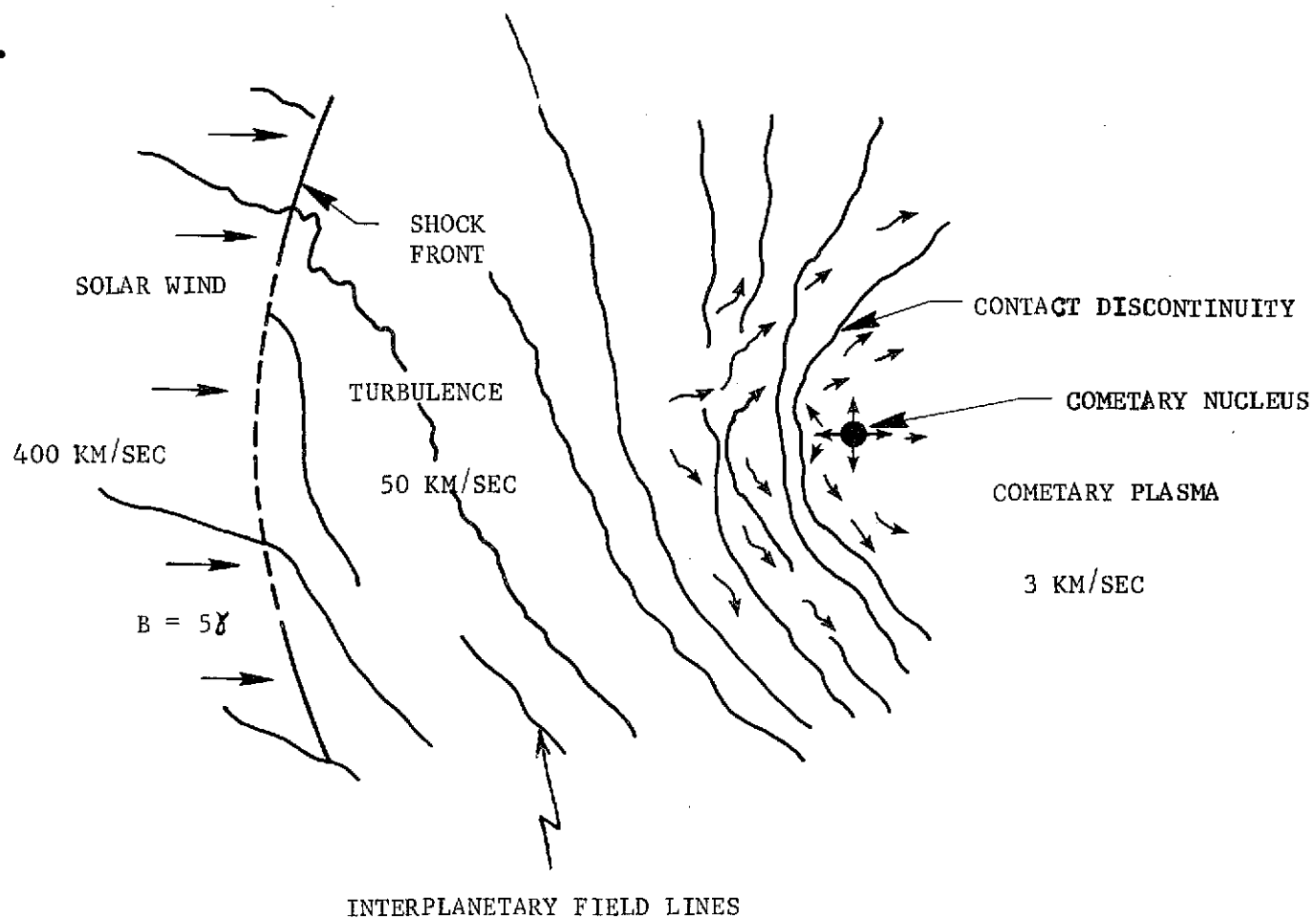


FIGURE II-4 ENCKE MAJOR FEATURES (ref. II-6)

not known if the cometary plasma exerts a pressure sufficient to balance the solar wind at the distance indicated. Location distances of the bow shock at contact discontinuity are poorly known. Yet, these distances are critical to correct comet models of solar wind interaction. The bow shock and contact surface discontinuity can be measured with particles-and-fields instruments, primarily a magnetometer, a plasma probe, a plasma wave detector, and a Langmuir probe.

No Bow Shock Model - Charge exchanges between solar wind and comet, and photoionization may occur in such a way that there is smooth deceleration (i.e., no shock). A contact surface would still exist, regardless of whether or not there is a shock. The particles-and-fields experiments mentioned above are needed to define the bow shock and to locate contact boundaries.

Principal Interaction Regions - Figure II-4 shows the solar wind flow around a comet in general terms for shock or no shock (ref. II-12). In condensed form, the process is this, a transition occurs in the fringe of the interaction region from supersonic to subsonic flow of the solar wind. In the subsonic region, the cometary and solar plasma mix and the magnetic field is compressed against the contact surface. Plasma within the contact surface is all cometary, produced by photoionization of neutral coma gas. Details of how this coma plasma produces a contact surface are not well known. The comet plasma could be lost by recombination near the contact surface, or by being blown into the wake of the comet ion tail.

Principal Motions and Magnetic Field in the Comet Tail - The maintenance of the tail and its observed fine structure may require electrodynamic processes not clearly understood. Magnetic fields in the tail appear to be evidenced by observed narrow (6000 km) plasma stream widths (ref. II-13). Using an expression for the Larmor radius, $r_L = V_{mc}/ZeH$, it would be possible to investigate plasma stream widths.

Spectrum - Lines of CO^+ , N_2^+ , CN_2^+ , CH^+ , and OH^+ have been seen in comet tails. The CO^+ and N_2^+ have lifetimes $\sim 10^6$ sec (ref. II-15). Molecular bands seen in the tail range from 3378 to 5048 Å. Encke does not show the continuum spectra typical of scattering on dust grains.

An ultraviolet and visual spectrometer would be able to investigate the above constituents in the tail. An infrared spectrometer would also be useful for observing some molecular-band transitions and for searching for the continuum due to dust grains.

Type-I and Type-II Tails - As stated earlier, the type-I tail is formed by ionized constituents swept from the coma. It is shorter than the type-II dust tail and is basically parallel (within $\sim 5^\circ$) to the comet/Sun vector. Dust tails of type-II are curved and are several times broader than the type-I widths. Sometimes observations show a type-III tail, which has even greater curvature, and which is thought to be due to smaller dust particles. Encke has been observed to have only a type-I tail. A length of 10^6 km is used for study purposes, but a smaller value would be well-explored since the reference trajectory traverses the comet from the head through the tail. A small type-II tail that is too faint to be seen from Earth may be found at Encke. The particulate-matter and IR instruments, in particular, should be able to detect a type-II tail, if present, in the flyby mode.

2. Major Areas of Uncertainty

The photometric equations and particulate-matter values (table II-1 and fig. II-1) are two areas which have a high impact on the spacecraft design. Fortunately, those areas have been modeled with some accuracy over a possible range of values. Uncertainties of the particulate-matter model are discussed in Appendix B. The decrease in total comet brightness by 0.1 magnitude per apparition has been factored into our photometric equation by the constant 10.93 in the previous section (table II-1). Other areas of model uncertainty (e.g., nucleus size, mass emission, ionized-tail length) have been called out in the preceeding section. Here, a brief summary of the several other assumptions or minimal model values needed for the comet mission is presented.

A single nucleus of at least 0.5-km radius is needed to orient cameras for closest approach. No special provisions have been made for large ice or clathrate halos extending to a 100-km radius around the nucleus. The degree of visibility of the nucleus due to dust and gas emissions is not known. However, the atmosphere must be reasonably transparent for the solar flux to

activate the nucleus thereby producing the whole range of comet activity. It is thought that the nucleus will be within a few hundred kilometers of the central condensation, or maximum brightness, of the coma; thus, no asymmetrical shapes or large displacements of the nucleus were modeled.

Because of encounter at 16 days before perihelion, we expect the radius of the coma to be at least 20,000 km, although it could be 50,000 km at that heliocentric distance. Coma activity is unpredictable, and, should the gases leave prior to encounter, some of the coma science could be compromised.

An ion tail is assumed for Encke, near encounter, but it is not always observed from Earth at each apparition. Regardless of the tail length, assuming only that it is there, useful measurements will be made with the reference mission. Even though no dust tail is assumed, its presence would be detected with the subsequent payload selected.

B. COMET SCIENCE OBJECTIVES

From the comet model discussed in Section A, a list of comet observables, along with the type of measurements anticipated, was developed and is shown in Table II-3. Table II-4 shows the major scientific questions or objectives related to more specific instrumentation. Table II-4 also gives more indication of the use of instruments and their allocation toward the solution of major science objectives.

1. Scientific Objectives

In accordance with the wide range of observables and energy processes possible at the comet, considerable breadth in science objectives is required. Since a first flyby (and flythrough) of a comet is in every sense an exploratory venture, there is no strong rationale for special emphasis given to any one scientific discipline. The philosophy, then, is to learn as much about the comet and asteroids in a fast flyby as is feasible with an economical, spinning spacecraft. This can be done best by carrying a range of instruments for as many disciplines as feasible.

Table II-4 (cited earlier) indicates some of the major unsolved questions concerning comets and shows the primary and secondary instruments that would provide scientific data to answer the questions. Imaging contributes to

TABLE II-3 MAJOR COMET OBSERVABLES FOR INVESTIGATION

	<u>COMET OBSERVABLES</u>									
	NUCLEUS IMAGING	COMA IMAGING	PARENT MOLECULES	PARTICULATE MATTER	CONTACT SURFACE	TRANSITION REGION	ION SPECIES	NEUTRAL MOLECULES	SHOCK DECELERATION	TAIL STRUCTURE
<u>INSTRUMENT DISCIPLINE</u>										
1. Imaging	●	●		○	○					●
2. Optical Spectroscopy		○		○	○		●	●	●	
3. Mass Spectroscopy			●		○		●	●	○	○
4. Dust Particles	○			●						○
5. Plasma & Fields					○	●			○	○

● Prime Investigations

○ Secondary Investigations

TABLE II- 4 MAJOR COMET SCIENCE OBJECTIVES

SCIENTIFIC INSTRUMENTS

LEGEND: • Prime Investigations
 o Secondary Investigations

QUESTIONS

	IMAGING	UV SPECTROMETER	VISUAL SPECTROMETER	ION MASS SPECTROMETER	NEUTRAL MASS SPECTROMETER	DUST ANALYZER	LANGMUIR PROBE	PLASMA WAVE	MAGNETOMETER	PLASMA PROBE	IR SPECTROMETER
1. Is there a "Rocky" nucleus?	•										o
2. How does gas flow from nucleus?	o	o		•	•						
3. How do particles flow from nucleus?	o					•					o
4. What are parent molecules?		o			•						o
5. What is gas molecule radial distribution?	o	•	o	•	o						
6. What is ionized gas distribution?	o		o	•							
7. How is contact surface maintained?	o			o			•	o	o	•	
8. What is extent/concentration of neutral species halos?	o	•									
9. Is there a deceleration shock?							o	•	•	o	
10. What is electron density of solar wind around comet?								•		o	
11. What are the magnetic field values?									•		
12. Does comet have energetic particle production mechanism?									o	o	
13. What is ion concentration in tail?				•			o		o		
14. What is dust concentration in tail?						•					o
15. Do pre-solar wind conditions influence comet ionization processes?								o	o	•	

answering questions concerning the coma. The UV spectrometer complements the coma imaging work. IR and visual spectrometers appear the least useful, but are still important. Ion and neutral mass spectrometers will permit in situ measurements of gas species, and they complement the remote UV investigations. The particulate (i.e., cosmic dust) detector has inherently limited use, but it is unique, in that direct composition of comet particles can be obtained in no other way. Finally, the whole range of questions concerning tail structure and particle and field phenomena need several instruments that complement each other in that area.

2. Comet Observables

Table II-3 summarized the instruments into five disciplines and showed the major observational features of the comet to which the disciplines apply.

To summarize, Table II-5 lists the major comet observables and the instruments to be used. Further instrument descriptions will be given in the next section. The impact of asteroid flyby on comet science is discussed in Chapter IV.

C. INSTRUMENT PAYLOAD SELECTION

In section II-B, a preliminary selection of science instruments was derived. In order to measure the wide range of comet observables and to provide data for the major scientific comet questions, a wide range of instruments was found necessary. A summary is given first of the rationale for science discipline, followed by the rationale for instrument selection. Table II-6 provides a summary of the science-instrument spectral and dynamic ranges for comet study. A detailed payload description will be given in section V-I. The effect of placing the instruments on the spinning spacecraft will be discussed in section IV-C.

1. Rationale by Science Disciplines

Imaging - A high priority is placed on locating and imaging the nucleus; hence, a narrow angle, high resolution camera is needed. A wide angle camera should be useful in comet acquisition using background stars and in the coma and close to the nucleus to provide wide angle reference for the narrow angle imaging.

TABLE II-5 SUMMARY OF COMET OBSERVABLES FOR MEASUREMENT

<u>INSTRUMENT CATEGORIES</u>	<u>COMET OBSERVABLES</u>
TELEVISION, WIDE AND NARROW ANGLE	<p> GROUND BASED COMPARISONS NUCLEUS IMAGING INNER COMA DETAILS TAIL FINE STRUCTURE </p>
SPECTROSCOPY ULTRAVIOLET AND VISUAL	<p> UV EMISSIONS IN COMA AND TAIL IDENTITY AND ABUNDANCE OF RADICALS HIGH SPATIAL RESOLUTION OF SPECTRA </p>
SOLID PARTICLES	<p> PARTICLE MATERIAL FROM NUCLEUS DUST IN TAIL </p>
PLASMA PROPERTIES	<p> SOLAR WIND MATERIAL UPSTREAM CONTACT SURFACE MAINTENANCE TAIL EXTRUSION AND DYNAMICS </p>
PARTICLES AND FIELDS	<p> MAGNETIC FIELDS IN TAIL ELECTROMAGNETIC WAVES IN TRANSITION REGION AND TAIL </p>
MASS SPECTROMETRY ION AND NEUTRALS	<p> IDENTITY AND ABUNDANCE OF CONSTITUENTS IN COMA AND TAIL </p>

TABLE II-6 INSTRUMENT RESPONSE FOR COMET STUDY

INSTRUMENT	SPECTRAL-DYNAMIC RANGE
TV IMAGING SYSTEM	
(a) WIDE ANGLE CAMERA	FOV: $11^{\circ} \times 14^{\circ}$, SHUTTER SPEED: 3ms - 6144ms SILICON TARGET: 3800 Å - 12,000 Å (1.2 m)
(b) NARROW ANGLE CAMERA	FOV: $1.1^{\circ} \times 1.4^{\circ}$, SHUTTER SPEED: 3ms - 6144ms SILICON INTENSIFIER TARGET (SIT): 3200 Å - 6200 Å
ULTRAVIOLET SPECTROMETER	CHANNEL 1 1100 Å to 1700 Å CHANNEL 2 1900 Å to 3400 Å
ION MASS SPECTROMETER (BENNETT RF TYPE)	MOLECULAR DENSITY 1.0 to $10^6/\text{cm}^3$ MASS RANGES: 1.0 to 6.0 AMU, 7.0 to 45 AMU
NEUTRAL MASS SPECTROMETER	MASS RANGE: 1.0 to 6.0 AMU, 7.0 to 45 AMU
PLASMA PROBE (ELECTROSTATIC ANALYZER)	ENERGY RANGE: 5.0 eV to 70.0 keV DYNAMIC RANGE: 3×10^5 COUNTS/SEC FOV: PERPENDICULAR AND PARALLEL TO ORBIT PLANE
COSMIC DUST ANALYZER (IMPACT IONIZATION)	PARTICLE DIAMETER: 100 mm to 1 mm
PLASMA WAVE DETECTOR	FREQ. RANGE 10 Hz to 2×10^5 Hz DELTA E: 1 V/m to 20 mV/m, DELTA B-1. MILLIGAMMA to 1 GAMMA
TRIAXIAL FLUXGATE MAGNETOMETER	LOW RANGE: ± 25 GAMMA HIGH RANGE: ± 100 GAMMA
LANGMUIR PROBE	N_e : $2 \times 10^5 \text{ cm}^3$, T_e : 1700°K
VISUAL SPECTROMETER	3800 Å to 7500 Å

Optical Spectroscopy - Many excited gases in the coma emit primarily in the UV only, and possibly in infrared wavelengths. Better spectra and spatial information is expected and new lines may be seen in the coma. Visual spectrometry would add spatial information and would identify lines not seen through Earth's atmosphere (e.g., atomic oxygen).

Mass Spectroscopy - In situ measurements of neutral molecules in the inner coma lead to identification of complex molecules in the nucleus. The distribution of radicals and ions in the coma and tail has direct bearing on energy processes.

Dust Particles - In situ measurements of flux, density, and composition will help to narrow the range of models of the origin of comets from among interstellar grains. Dust particle composition is a key to comet formation.

Plasma and Fields - Magnetohydrodynamic processes in the ion tail are important in themselves, in order to understand the solar wind and to extrapolate back to the contact surface region.

2. Rationale for Instrument Selection*

Television Imaging - One of the primary goals of an early comet mission is to image the comet's nucleus. The selection of the imaging instrument followed review and analysis of various camera systems presently in use or being developed for future space missions. The two classes of imaging experiments considered are:

- a) Vidicon Frame-Type Cameras
- b) Spin-Scan Cameras

The above systems were studied to assess their resolution and photometric capability to 1) resolve a 3.2-km diameter target, and 2) distinguish the small bright nucleus against a more diffuse, but relatively bright, coma background. Each of the camera systems offers certain advantages: The spin-scan camera offers reduced image smear and shorter exposure times. The vidicon system offers increased flexibility in the selection of a target (photocathode) with appropriate spectral response, sensitivity, and pixel spacing.

* See Section V-1 for a more detailed description of these instruments.

The spin-scan systems will be shown in chapter V-I to be less effective than vidicons for the radiometric detection of the comet and the comet nucleus and for their capability to image the faint coma edges important for coma fine-structure analysis.

A vidicon camera system has been chosen for this mission, specifically, the dual camera configuration presently used in the MM'71 spacecraft. A wide-angle and a narrow-angle camera are included in this system. A silicon intensifier target (SIT) is used in the narrow-angle camera.

This system offers an optimum combination of the size, weight, performance, and optical properties needed to obtain the required science return.

Cosmic Dust Analyzer - Measurement of the flux, mass, and elemental composition of comet dust will be performed using a combination instrument: an acoustic momentum sensor operating in conjunction with an impact ionization analyzer. A complete instrument of this type has not been previously flown. Otto Berg, at Goddard Spaceflight Center, has flown impact ionization detectors, but with some limitations on full analysis. Dr. S. Auer, at Max Planck Institute, proposed a combined time-of-flight and impact ionization instrument for the Grand Tour missions. At the present time, Dr. J. F. Friichtenicht (TRW Systems) is working on a laboratory model of an impact ionization analyzer. Data on the progress of his study were presented to the NASA Science Advisory Committee on Comets and Asteroids earlier this year.

In conclusion, it is proposed that a combined experiment, rather than individual instruments be flown to measure flux, mass, and composition.

Ultraviolet Spectrometer - In order to observe the UV emission and absorption lines that are expected to be seen near the coma and tail of the comet, a measurement range extending from 1100 Å to 3400 Å is required.

Several instruments covering the above spectral range were reviewed. As a result, the instrument proposed for the Mariner Venus Mercury 1973 mission was selected. The experiment is a miniaturized, single-channel version of the unit flown on Mariners 6 and 7. The instrument is an Ebert (grating) spectrometer using a photomultiplier tube as the detecting element. It offers low weight, relatively small size, and a low operating power level.

Langmuir Probe - Several types of instrumentation have been used on spacecraft to measure electron density. Typical instruments of this class are retarding potential analyzers (RPA), planar ion traps, and Langmuir probes.

A Langmuir probe has been selected for this mission primarily because of its simplicity and measurement range. The particular experiment has been flown on the OGO vehicles, and a modified version has been proposed for advanced Pioneer spacecraft. The Langmuir probe does not require the use of suppressor grids to minimize density errors resulting from photoelectrons generated within the instrument during exposure to solar UV radiation. Spacecraft-produced electric fields (RF) also have less effect on instrument performance in the case of the Langmuir probe than in the RPA.

Plasma Probe - The instrument selected to provide data regarding the ion and electron fluences covers a spectral range for electrons of 5 eV to 70 keV. The selected instrument is a modified version of the experiment used on the Pioneer 6 through 9 spacecrafts and the Pioneer 10/11 vehicles. The plasma probe experiment is a curved-plate electrostatic analyzer using channeltron multipliers as the detectors.

This type of instrument is considered a good choice since very high sensitivity is not required (ref. II-14).

Mass Spectrometers - In order to make simultaneous measurements regarding the fluences of both neutrals and ions in the vicinity of the coma and nucleus, two types of mass spectrometers have been chosen.

The neutrals will be measured using a quadrupole instrument, while the ions will be observed with a Bennett RF Mass Spectrometer.

It is recognized that both species could be observed with the quadrupole instrument. However, the optimum observation time occurs when the instrument's acceptance cones are parallel to the spacecraft's velocity vector (the ram direction). For a spin-scan mode, this is approximately 1/9 of the spacecraft rotational period for a $\pm 20^\circ$ instrument acceptance angle. This results in a collection efficiency of approximately 10% per revolution. A combined instrument would have to share ram direction time, and, hence would obtain fewer total scans. Because of the share requirement, if one instrument is used, and,

due to the relatively short observation time during transit of the coma, a maximum number of observations could be made using the proposed, two-instrument configuration.

Magnetic sector spectrometers are capable of making very accurate measurements; however, the magnet, ion pumps, and ion sources result in increased magnetic field levels in the vicinity of the instrument. In view of the fact that the spacecraft will also carry a sensitive magnetometer, any increase in spacecraft remanence would require more stringent magnetic cleanliness controls. For this reason, as well as their reduced mass and volume, the quadrupole and Bennet instruments are considered good choices for this mission.

Finally, the design of the entrance apertures and momentum (or velocity) filters will require special care due to the high spacecraft velocity during passage through the coma and tail. The spacecraft relative velocity is expected to be approximately 18 to 26 km/sec.

Plasma Wave Detector - The instrument selected for this mission was based on an experiment flown on OGO-E. Its purpose was to measure plasma phenomenon in the region of the Earth's geomagnetic shock front and transition regions. It is anticipated that the comet/solar wind interactions will be similar to those observed between the solar wind and the Earth's geomagnetic field. For this reason, a comparable instrument to that flown on OGO-E has been included in the spacecraft science payload. Hydromagnetic wave phenomenon and electric field oscillations will be measured in order to verify whether or not the comet/solar wind interactions are comparable to those observed during the mission of OGO-E.

The instrument fulfills the stated science objectives, with a minimum expenditure of power and with a low instrument weight.

Magnetometer - The instrument chosen for this measurement is a tri-axial fluxgate magnetometer. The fluxgate instrument was selected in place of the more sophisticated helium-vector-type unit. Although the fluxgate is less sensitive, its mass and power requirement is smaller. Extensive use has been made of this type of magnetometer. Sensitivities of the order of 0.1 gamma typical, and read out accuracies of ± 0.25 gamma are easily obtained. Estimates of field amplitudes in the solar plasma, bow shock region, tail, and internal

regions of the coma indicate that this type of instrument is capable of observing the orthogonal components of the ambient field accurately. It is proposed that the experiment be designed to have two range scales. The lower level range will be capable of measuring field levels of ± 25 gamma, while the high range will extend to ± 100 gamma.

D. COMA PROBE UTILIZATION

A coma probe is recommended to greatly increase the coma science investigation of Encke in the areas of complex molecule detection and particulate matter flux. A secondary benefit comes from spatial sampling provided by the existence of a probe. No strong science rationale was found for more than one probe.

1. Probe Objectives and Strategy

Rationale - The selection of the spacecraft radius-of-closest-approach to be 5,000 km was a careful trade between the desire for parent-molecule-detection maximization and possible particulate-damage minimization. By means of a single probe, it is possible to greatly maximize the molecule detection without jeopardizing the spacecraft.

The science rationale for a probe is direct and in two parts. A single, spin-oriented, medium-size probe was the result of study: 1) to extend scientific measurements to regions closer to the nucleus than could be accomplished by the parent spacecraft; and 2) to provide limited spatial correlations between measurements on the probe and spacecraft.

Gas Densities - The exact radial extent of the region containing the parent molecules around the nucleus is not well known, but it can be estimated rather easily from the lifetimes of molecules, if photodissociation is the prime energy source of molecule release. From observations (ref. II-15) the lifetime, T , of typical parent molecules is $\sim 10^4 - 10^5$ seconds at 1 AU and varies as R^{-2} for other heliocentric distances. The velocity of molecules emitted from the nucleus is ~ 1 km/sec and is not strongly distance dependent. A rough estimate then shows the expected effective radius of parent molecules to be $VT = 2.5 \times 10^3$ to 2.5×10^4 km near 0.5 AU.

A choice of 5000 km is near the low end of this expected range, and should therefore provide a reasonable chance of parent-molecule detection if our model of photodissociation mechanisms is correct.

For purposes of preliminary planning, Table II-7 shows the estimated average densities in Encke's coma, as taken from the Yerkes conference (ref. II-15).

TABLE II-7
COMA DENSITIES

	<u>COMA REGION, kms</u>	<u>DENSITY, molecules/sec.</u>
Inner	$< 5 \times 10^3$ km	5×10^6 cm ⁻³
Intermediate	$3 \times 10^3 - 3 \times 10^4$ km	5×10^4 cm ⁻³
Outer	$> 5 \times 10^4$ km	5×10^3 cm ⁻³

For the limited case of water and the water-dissociated products of O, OH, and H, some additional modeling has been done by Delsemme et al., (ref. II-9). Figure II-2 shows that the number of molecules varies inversely as distance to the nucleus.

Finally, the estimate of other species, such as C₂, NH, and CN are shown in Figure II-3, taken from Reference II-11. These estimates clearly show the ~3.5 orders of magnitude increase in number density between the approximate coma limits of 10⁵ km and 10³ km. The increase continues to smaller distances and is especially pertinent for the probe.

Particulate Matter - The probe is needed to measure the radial gradient in the particulate flux. The particulate-flux model developed in Appendix B shows an increase in number and flux density with distance from the nucleus for a wide range of particle masses.

Because the cross-sectional area of the probe is smaller than that of the spacecraft, it therefore has a higher probability of no penetrations than has the spacecraft at the same distance. Appendix B shows the probe penetration probability as a function of distance. Note that the probe should be able to reach the 500-km level or lower and still survive in the tail for several hours.

Spatial Sampling - The spatial and temporal correlations between spacecraft and probe are the second part of the probe rationale. With respect to the mass spectrometers, it is advised that duplicate instruments be flown on the spacecraft and probe even though it will be shown later that some configurations do not permit orientation of the mass spectrometers in the ram direction at all times. Since the detection and abundance measurements are a critical scientific objective, the use of separate ion and neutral mass spectrometers on both the spacecraft and the probe did not seem unreasonable for complete and maximum coverage in this scientific discipline.

The possibility of molecule detection by the probe may, indeed, be the only hope of detecting the very complex molecules CH_3 and NH_3 , which are keys to understanding gas molecules in the nucleus. If the same species can be seen by spacecraft and probe, it will be very important to theoreticians to correlate detection time and location.

Spatial correlations of particulate matter are also needed to determine asymmetrical flows and possible temporal concentrations during the encounter time. For both gas-molecule emission and particulate-matter flux, direction rates, and temporal variations are deemed valuable to a comet mission.

Tail Considerations - Finally, the coma probe will likely survive to enter the tail of the comet as shown in Appendix B. It is therefore important that there be instruments on the probe to measure electron density, and it would be strongly desirable to also measure magnetic fields. A magnetometer was not placed on the probe in this study, because the probe was considered for a coma mission only by the groundrules. The addition of a magnetometer would be given first priority if another instrument could be added. Even if the probe provides only a few minutes of tail particle-and-field data, the temporal and spatial rates of magnetic fields and electron density will prove valuable to understanding plasma physics processes.

Single Probe - A final word on probe strategy concerns the lack of recommendation for more than one probe on scientific grounds. Two reasons often advanced for multiple probes do not seem sufficient. These are 1) to insure at least one probe survival due to possible particle damage, and 2) to insure at least one probe gets close to the nucleus. Both reasons are slightly

negative, implying the "shotgun" approach and lack of knowledge in particulate matter and position accuracy.

Briefly, the analysis of the particulate-flux penetrations, (see Appendix B) even under conservative conditions, indicate that the probe will survive to reach the tail. With on-board approach navigation, a 2σ average uncertainty between spacecraft and nucleus is ~ 500 km. On top of this value is a smaller probe-release uncertainty of under 100 km at the 2σ level. Additional details are given in Section III-C. The point here is that the probe-release uncertainties are not so large as to justify multiple probes being scattered in order to get near a specified level.

Additional reasons for more than one probe might be related to the need for additional spatial measurements. The assymmetrical emission of material and the direction of Encke's pole, for example, are not known well enough to justify distributed samples or to find optimum intercorrelation lengths between spacecraft and probe. It does not seem possible to ask for several probes on spatial sampling arguments. In the tail, where the interaction of magnetic fields, plasma waves, and the electron density needs to be better understood, a multi-probe strategy appears more feasible. One probe satisfied the requirements for parent-molecule and particulate detection. The addition of more than one probe does not seem justifiable for increased science return.

2. Probe Instruments

The probe instruments selected are a result of the probe strategy of the previous section. The instruments are in three categories: mass spectroscopy, cosmic dust, and particles-and-fields measurements. Table II-8 lists the probe science goals and instrument selection.

Two mass spectrometers, neutral and ion, were selected to be identical to the spacecraft instruments. The correlative rational has been explored previously. The operation effectiveness of these instruments improves greatly with decreasing distance for the nucleus, as stated in Section V-I.

The probe cosmic-dust detectors are vital instruments for extending the number-density investigations coloser to the nucleus. The detectors are envisioned as simple plates of accoustical panels to be attached to the probe.

TABLE II- 8 PROBE SCIENCE AND GOALS

PAYLOAD	GOALS
COSMIC DUST	EXTEND MEASUREMENTS CLOSER TO NUCLEUS FIND SPATIAL ANISOTROPIES
ION MASS SPECTROMETER	DETECT IONS NEAR NUCLEUS LEARN OF ENERGY PROCESSES
NEUTRAL MASS SPECTROMETER	IDENTIFY COMPLEX MOLECULES DETERMINE RADIAL DISTRIBUTION
LANGMUIR PROBE	MEASURE ELECTRON DENSITY IN COMA MEASURE ELECTRON DENSITY IN TAIL
(MAGNETOMETER-RECOMMENDED)	MEASURE MAGNETIC FIELD IN COMA MEASURE MAGNETIC FIELD IN TAIL

The dust detectors on the probe do not measure composition as the spacecraft instrument does. The composition device might saturate at a lower level, and its inlet could require careful orientation. The accoustical panel will permit number-density and directional data to be obtained.

The particles-and-fields instruments consist of a Langmuir probe to measure possible electron densities in the coma and the tail (if the probe survives, which is expected). The addition of a magnetometer is recommended, especially when the probe is in the tail. In initial studies, the probe was designed for the coma only.

E. SCIENTIFIC INVESTIGATION OF ASTEROIDS GEOGRAPHOS AND TORO

In this section, the scientific goals for asteroid investigation are discussed. Then descriptions of the physical properties of Geographos and Toro are presented as models. Observables, instruments, and objectives are correlated by the same matrix approach used for the comet science. Finally, the addition of one instrument (an IR spectrometer) complements the comet payload for asteroid investigations. There are two principal reasons for asteroid study: implications concerning the origins and the evolution of the solar system.

Solar System Origin - Asteroids may be the Rosetta Stones of the early solar system. The small asteroids could be composed of rock and other material that has not been modified substantially since their formation. The ejecta blankets and regolith mixtures on asteroid surfaces should be visible to flyby imaging.

If meteorite studies can be tied to asteroid groups, then meteoritic results on condensation, cooling, etc. can be tied to specific parts of the solar system. In the early solar system, various temperatures, pressures, and cooling rates occurred in different places. The unscrambling of the dynamic evolution of asteroids can permit chronological and spatial reconstruction of solar system formation.

Solar System Evolving - There are still dynamical changes, accretion/fragmentation process, development of regoliths, and formation and decay of comets that asteroid study can clarify. Early in the history of the solar system, accretion seemed to be the prime process. Today, bodies seem to be losing more particles to space than they are gaining, i.e., a fractionation

process. Close-up studies of asteroids will help in the understanding of these processes.

Finally, but of great importance, is the question of whether some asteroids may be dead comets. Comparison of images of a comet nucleus with asteroid images, and comparison of comet particulate matter with asteroid regolith may answer this question.

1. Description of Asteroid Models

a. Geographos

Physical Properties - Geographos (1620) is probably a prolate spheroidal shape, $1.6 \text{ km} \pm 0.1 \text{ km}$ wide and $4.2 \text{ km} \pm 0.5 \text{ km}$ long. This is based on fitting laboratory models to the asteroid light curve (ref. II-16). For a conservative spherical shape, a value of 1.62 km minimum is used. Rotation is retrograde with a sidereal period of $5^{\text{h}} 13^{\text{m}} 23^{\text{s}}.91 \pm 0^{\text{s}}.03$. The direction of the axis of rotation is equivalent to an ecliptic longitude of $200^{\circ} \pm 8^{\circ}$ and ecliptic latitude of $60^{\circ} \pm 4^{\circ}$.

Photometric Values - The brightness of Geographos is $B = 16.08 + 5 \log \Delta + 5 \log r + 0.030$ (phase angle in degrees) mag/degree. The albedo is 0.16 (at 0.4μ), as determined recently by IR polarimetry (ref. II-58).

Additional Information - Geographos has the largest amplitude (2.03 magnitudes) in its light curve of any asteroid observed. If this effect were all due to shape, the length to width ratio would be as high as 6:1. However, one end of Geographos may be rougher or of a different shape than the other.

b. Toro

Physical Properties - Toro (1685) probably has an elongated, irregular shape. An effective circular radius of $2.2 \text{ km} \pm 0.4$ (p.e.) is used. Rotation is direct with a sidereal period of $10^{\text{h}} 11^{\text{m}} 44^{\text{s}} \pm 4^{\text{s}}$. The direction of the rotation axis is equivalent to an ecliptic longitude of $200^{\circ} \pm 20^{\circ}$ and ecliptic latitude of $55^{\circ} \pm 5^{\circ}$.

Photometric Values - The brightness of Toro is: $B = 14.90 + 5 \log \Delta + 5 \log r + 0.037$ (Δ, r) (phase angle) in degrees. The albedo is 0.14 (B filter) by Reference II-17.

TABLE II-9 GEOGRAPHOS PHYSICAL PROPERTIES SUMMARY

	<u>ASTEROID FEATURE</u>	<u>RANGE OF VALUES</u>	<u>NOMINAL VALUE USED</u>
I.	PHYSICAL PROPERTIES		
	Dimensions (Radius)	WIDTH 1.4 to 1.8 km LENGTH 3.7 to 4.7 km	1.62 km radius, circular
	Rotation Period	$5^{\text{h}} 13^{\text{m}} 23.91 \pm 0.03$	$5^{\text{h}} 14^{\text{m}}$, retrograde
	Axis of Rotation	$\lambda_{\text{o}} = 200^{\circ} \pm 20^{\circ}$ $B_{\text{o}} = 60^{\circ} \pm 5^{\circ}$	$\lambda_{\text{o}} = 200^{\circ}$ $B_{\text{o}} = 60^{\circ}$
II.	PHOTOMETRIC VALUES		
	Brightness	$B = 16.08 + 5 \log \Delta + 5 \log r$ $+0.030$ (phase angle) in deg.	Δ = S/C-Geographos Dist. in AU r = Heliocentric Dist. in AU
	Albedo (4π)	0.16	0.16
III.	ADDITIONAL DATA		
	Amplitude Range (magnitude)	2.03 magnitudes	2.03 magnitudes
	Light Curve Variation	Partially due to shape	Some variation in shape, albedo variation

TABLE II-10 TORO PHYSICAL PROPERTIES SUMMARY

<u>ASTEROID FEATURES</u>	<u>RANGE OF VALUES</u>	<u>NOMINAL VALUE USED</u>
I. PHYSICAL PROPERTIES		
Dimensions (radius)	1.8 to 2.6 km	2.2 km radius, circular
Rotation Period	$10^h 11^m 44 \pm 4^s$	$10^h 12^m$, Direct
Axis of Rotation	$\lambda_o = 200^\circ \pm 20^\circ$ $B_o = 55^\circ \pm 5$	$\lambda_o = 200^\circ$ $B_o = 55^\circ$
II. PHOTOMETRIC VALUE		
Brightness	$B = 14.90 + 5 \log \Delta + 5 \log r$ $+0.037$ (phase angle) in degrees	Δ = S/C-Toro Dist. in AU r = Heliocentric Dist. in AU
Albedo	0.14	0.14
III. ADDITIONAL DATA		
Amplitude Range (magnitude)	0.8	0.8
Light Curve Variation	Partially due to shape	Some reddening with phase Absorption band at 0.97 may be F_e^{+2}

Additional Information - Variations exhibited in the light curves are mostly due to shape, but some albedo variation over the surface has been detected. At optical wavelengths, the surface texture appears to be a dusty regolith, perhaps rougher than the moon. From UBV photometry, some reddening with increasing phase is detected also. A deep band near 0.97 microns has been detected and may be due to F_e^{+2} in octahedral coordination, perhaps in a pyroxens. Table II-10 summarizes the physical properties of Toro.

2. Asteroid Observables and Order of Importance

Tables II-11 and II-12 show the same matrix information for asteroids as was shown for comets. Here imaging and IR are clearly the predominate instruments. This is another way of stating that asteroid science is surface-morphology-oriented without emphasis on gaseous and particulate emissions as on a comet flyby mission.

Photometry and polarimetry could also add to asteroid science, as shown in Tables II-11 and II-12. Significant work has already been done in ground-based programs. For effective far-distance operation of the photometer/polarimeter on the spacecraft, considerable effort would need to be made in the development of telescope optics for the instrument. The merits of this have not been pursued.

The instruments shown on Table II-12 are inherited from the comet mission. Other instruments have been suggested, but it is believed that the major scientific questions listed can be answered with the baseline payload. Upon further study, or new rocket/ground-based data, scientists may decide to stress specific areas of the comet/asteroid unknowns. They may then choose to reduce the instrument payload, but it does not appear justifiable at this time.

3. Science Instrument Payload - Addition of an IR Spectrometer to the Basic Comet Payload

Only one change in the comet payload is highly recommended for asteroid investigations; that is, the addition of an IR spectrometer. The scientific rationale and timeline for the instrument are discussed in other sections. Briefly, the IR spectrometer will measure Bond albedos and temperature properties, will measure surface roughness, and will search for clues to

TABLE II-11 MAJOR ASTEROID OBSERVABLES FOR INVESTIGATION

SCIENTIFIC DISCIPLINES/INSTRUMENTS	ASTEROID INVESTIGATION AREAS									
	SIZE, SHAPE, ROTATION	SURFACE FEATURES	SURFACE COMPOSITION	ALBEDO STUDIES	PARTICULATE ENVIRON.	PLASMA ENVIRON.	FIELDS ENVIRON.	THERMAL MAPS	SURFACE ROUGHNESS	FAR DIST. PHOTOMETRY
IMAGING	●	●	○	○					●	○
IR RADIOMETRY	○		●	○	○			●	○	
POLARIMETRY	○		○	●				○	○	●
DUST ANALYZER					●					
OPTICAL SPECTROSCOPY										○
MASS SPECTROSCOPY						○				
PARTICLE AND FIELDS						●	●			

LEGEND: ● = Prime Investigation
○ = Secondary Investigation

TABLE II-12 MAJOR ASTEROID SCIENCE OBJECTIVES

LEGEND: ● = Prime Investigation
○ = Secondary Investigation

MAJOR SCIENTIFIC QUESTIONS FOR ASTEROIDS

	IMAGING	UV SPECTROMETER	VIS. SPECTROMETER	ION MASS SPECT.	NEUTRAL MASS SPECT.	DUST ANALYZER	LANGMUIR PROBE	PLASMA WAVE	MAGNETOMETER	PLASMA PROBE	IR RADIOMETER	POLARIMETER
1. Is the asteroid body a decayed comet nucleus?	●										○	
2. Are surface features of comet nucleus & asteroid similar?	●											○
3. Is particulate matter of comet similar to asteroid regolith surface?						●						
4. What is size, shape of asteroid?	●											○
5. What is polarization in light-curve of asteroid?	○										○	●
6. What is minearological composition (surface material) of asteroid?	○										●	○
7. Does asteroid have any residual heat?	○										●	
8. Does asteroid have any magnetic field?									●			
9. Does asteroid have accompanying space debris?	○					●						
10. How long has asteroid been in present orbit?	●					○					○	
11. What is density (mass) of asteroid?	●											○
12. Orientation of axis and rotation rate?	●											○
13. Surface reflectivity, albedo curves?	○										○	●
14. Surface roughness of asteroid?	○										●	○
15. Detailed crater counts.	●										○	○

chemical composition at far, close, and near-encounter distances.

If the IR instrument cannot be added to the comet payload, then it may be advisable to replace the visual spectrometer with the IR device. While a valuable comparison with Earth-based spectroscopy may be lost, the IR spectrometer can provide some compensating measurements at the comet. It would attempt to scan the nucleus, see complex molecular transitions in the coma, and look at particulate dust in the comet tail.

A photometer/polarimeter was considered briefly as a desirable candidate for the asteroid mission payload. However, the asteroid photometric model seemed to indicate that these instruments would need enlarged optics for operation at long distances from the asteroid. It did not appear feasible or possible to use the narrow angle television optics for a photometer/polarimeter detector. Thus, in keeping the add-on instruments to a bare minimum to enhance asteroid mission success, the photo-polarimeter was omitted from the baseline design.

Both the TV and IR instruments require a closer approach at the asteroid than at the comet. To do quality surface morphology, a maximum distance of 500 km is recommended. Distances greater than 1000 km would degrade the image resolution and the IR science objectives stated above.

F. SUMMARY OF EXPECTED SCIENTIFIC ACCOMPLISHMENTS

In Chapter II, comet and asteroid observables and major scientific questions were examined. The "representative payload" subsequently selected permits comprehensive exploration of the comet and provides exciting new imaging and infrared investigation of the asteroids.

Surprises may occur at the comet that make some measurements more difficult than expected. (Examples could be unusual dust, ice grains, or, multiple nucleus.) Such surprises, however, could also be fortuitous for other instruments. The comet and asteroid models are not so uncertain as to seriously detract from the earlier scientific goals.

The expected science returns are restated briefly according to the measurements to be made.

Imaging - The nucleus should be detected in a number of frames near encounter. It will be the first close-up look at a comet nucleus and should provide new information for theorists on formation and emission processes. Within the coma and tail, images from the wide and narrow-angle nested cameras would indicate spatial structure. Streamer widths and electromagnetic kinks may be seen in the tail. Farther from encounter, the imaging system will provide data on overall morphology of the comet and tail which will match and then improve upon spatial resolution from Earth-based photography.

UV Spectrometer - The UV spectrometer will permit images of the Lyman-alpha halo at far distances from the comet. Additional halos, such as atomic oxygen and OH, may be found in the UV wavelengths. Closer to the coma, the radial distribution of well known species, such as NO, CO_4^+ , N_2 , N_2^+ , CO, H_2 , atomic oxygen and molecular hydrogen, will be measured. This measurement will help to narrow possible comet models for energy processes and species lifetimes very near the nucleus, new constituents may be discovered.

Visual Spectrometer - These instruments will work similarly to the UV device, but in visual wavelengths. Lines well-studied and known from Earth-based spectroscopy will be explored at equal spectral resolution and much higher spatial resolutions. Again, the radial distributions will be a key to modeling the coma dynamics of the comet. Some new, weak lines and/or coma asymmetries may be discovered due to the higher sensitivity of the measurements.

Mass Spectrometer (Neutral and Ion) - The comet coma seen from Earth results from resonance fluorescence of ionized species. The parent molecules' identification and location are sought as a key to comet modeling. At various distances, depending upon which energy processes dominate, the more complex species are ionized and fractionated. Again, the in situ measurements as a function of position will sort out which energy processes are acting.

Dust Analyzer - The volatile species will be studied remotely by energy transitions, and directly by mass spectrometers. The non-volatile particulate matter will be seen by imaging if dense enough, but its composition is a key to nucleus history and temperature processes. The dust detector will operate most effectively near the nucleus and in the tail to identify particulate matter and to measure the velocity and direction of emission. The early history

of the nucleus and the dynamics of present-day nucleus will thereby be investigated.

Langmuir Probe - As the comet interacts with the solar wind, a deceleration region and contact surface will be generated. The Langmuir probe will make vital measurements of the temperature and number density of electrons and protons. Flow patterns, spatial location, and interaction zones will tell much about the comet macrostructure in the solar wind.

Plasma Wave Detector - When charged particles contained within the solar wind interact with themselves or with the comet boundaries, various modes of electromagnetic waves can be generated or excited. Measurement of shocks, wave transitions, and permitted oscillation modes in multi-frequency searches will further define comet boundaries. In the tail, magnetohydrodynamic phenomena will be identified with the plasma wave device.

Magnetometer - A residual magnetic field is not anticipated at the comet nucleus or asteroid, but changes in the solar magnetic field around the targets are expected. The magnetometer will help in setting limits on upstream comet boundaries, and in setting levels, temporal variations, and twisting of magnetic fields in the tail. The magnetic field strength and variations will be needed to understand tail hydromagnetic modes.

Plasma Probe - The solar wind composition, velocity, and orientation have been studied in interplanetary space and near Earth. Since the comet is immersed within, and its tail is shaped by, the solar wind, it will be important to know plasma conditions prior to comet entry. Once in the comet, solar wind values will be modified, but the boundary of the contact surface between comet and solar wind needs definition and should be observable. The tail length, orientation, and ionization will be correlated to the solar wind plasma measurements before, during, and after encounter.

IR Spectrometer - This instrument, while sized for the asteroids, can perform very meaningful investigations at the comet. These would include trying to scan the nucleus at closest range in order to obtain temperature, albedo, and possible surface composition data. Its use to search for complex molecule transitions within the coma would be of less time criticality, although some of these transitions are better observed in the IR than in the UV.

Finally, in the tail, the instrument would try to obtain the temperature and spectra of the particulate matter.

Asteroid Imaging - With a close approach distance, e.g., 500 km, the asteroid surface would be viewed at high resolution for the first time. Results of good high resolution images would permit crater counts, fault detection, and the identification of the regolith or rippled surfaces. The time that the asteroid has been in its present orbit could then be analyzed. A link between the comet's nucleus and particulate matter and the asteroid surface would also be investigated.

Asteroid IR - The IR spectrometer will measure the total Bond albedo and the asteroid temperature at far distances. At intermediate ranges, the surface roughness and structure will be measured from the spectra of scattered light. Finally, at the closest approach, selected absorption bands will be searched for information about mineral and surface composition. This composition data may be a greater clue to link asteroid and comet than will be the imaging data.

THIS PAGE BLANK

III. ANALYSIS OF MISSION OPPORTUNITIES

III. ANALYSIS OF MISSION OPPORTUNITIES

In 1972, Comet Encke/80 was selected as a desirable mission for study by Martin Marietta's Advanced Planetary Missions group. Complete launch energy contours were generated for fast flyby missions that encountered the comet from before to after perihelion. In addition to being desirable missions because of a strong scientific interest in Comet Encke, they are attractive as possible precursor missions to Comet Halley in 1986. A further discussion of the pre-contract study effort is given in Appendix A.

Because of increased interest in combining the Encke '80 mission with later asteroid encounters and also because of scientific interest in obtaining in situ measurements while the comet was still active, contract study effort was directed toward pre-perihelion encounters where these conditions exist.

Section A discusses the rationale which led to the selection of the comet flyby reference mission from the parametric data, and also discusses the characteristics of the selected mission, including launch energy requirements, heliocentric trajectory conditions, approach geometry, and expected variation during the launch period opportunity.

The last portion of this section concentrates on the coma probe mission analysis and compares three techniques for probe deployment. Velocity requirements are shown for a selected mode and relative bus/probe geometry, and dispersion data are also presented.

Section B presents the opportunities available for flying comet/asteroid missions singly or in combination with the Apollo asteroids, Geographos and Toro. The various missions are compared in terms of launch energy requirements, maneuver requirements, and asteroid approach conditions. Finally, the impact of asteroid retargeting upon the comet encounter conditions is discussed.

Section C considers the navigation feasibility of two selected mission modes, including the effects of Encke and asteroid ephemeris uncertainties and expected target dispersions. A targeting strategy is presented, including propulsive maneuver requirements. A comparison is also made of expected target dispersions with and without on-board optical navigation knowledge. The latter data concentrate on the basic flyby mission.

A. ENCKE-DEDICATED MISSION CHARACTERISTICS

1. Reference Mission Selection

The launch vehicle selected for injected-weight comparisons is the Atlas/Centaur/TE364-4. Data on overall spacecraft injected weight as a function of launch energy are presented in Figure III-1. The effects of velocity penalties for launch azimuths other than due East are also shown. These data are from Reference III-1. All of the injected weights presented in this and later sections are based upon this data.

The reference mission was chosen early in the study, and the rationale for selection was primarily scientific. By launching when the Earth is near the comet plane's ascending node (8-28-1980) and arriving at the comet on 11-20-1980 (16 days prior to its perihelion passage on 12-6-1980), the spacecraft has the unique opportunity to fly nearly directly down the comet's tail and thus obtains in-situ measurements for the longest period. The reference injected weight for this mission is 335 kg (739 lb) with a flyby velocity of 18.3 km/sec (60040 fps). Figure III-2 shows the basic C3 contours over the region of interest, with the reference mission centered on a 10-day launch period.

Figures III-3 through III-6 present the other basic parametric data superimposed upon the C3 contours. These data include the comet relative approach velocity, the approach angle (phase angle at encounter), the launch asymptote declinations required (and corresponding velocity penalties), and the spacecraft heliocentric radius at comet encounter and also at perihelion (for thermal design considerations).

Referring to the contour data, observe that later comet arrivals can reduce approach velocities to 12 km/sec (39400 fps), but with greatly reduced injected weight 250 kg (550 lb) and with high negative approach angles and low intercept radii. Moving toward the minimum-C₃ region increases approach velocity to 26-28 km/sec (85000-92000 fps), allowing substantial injected weight increases 560 kg (1235 lb), but with higher positive approach angles, and relaxed thermal loads.

Further discussion concerning the latter region will continue in Section B, where the results from the combined comet/asteroid missions are presented.

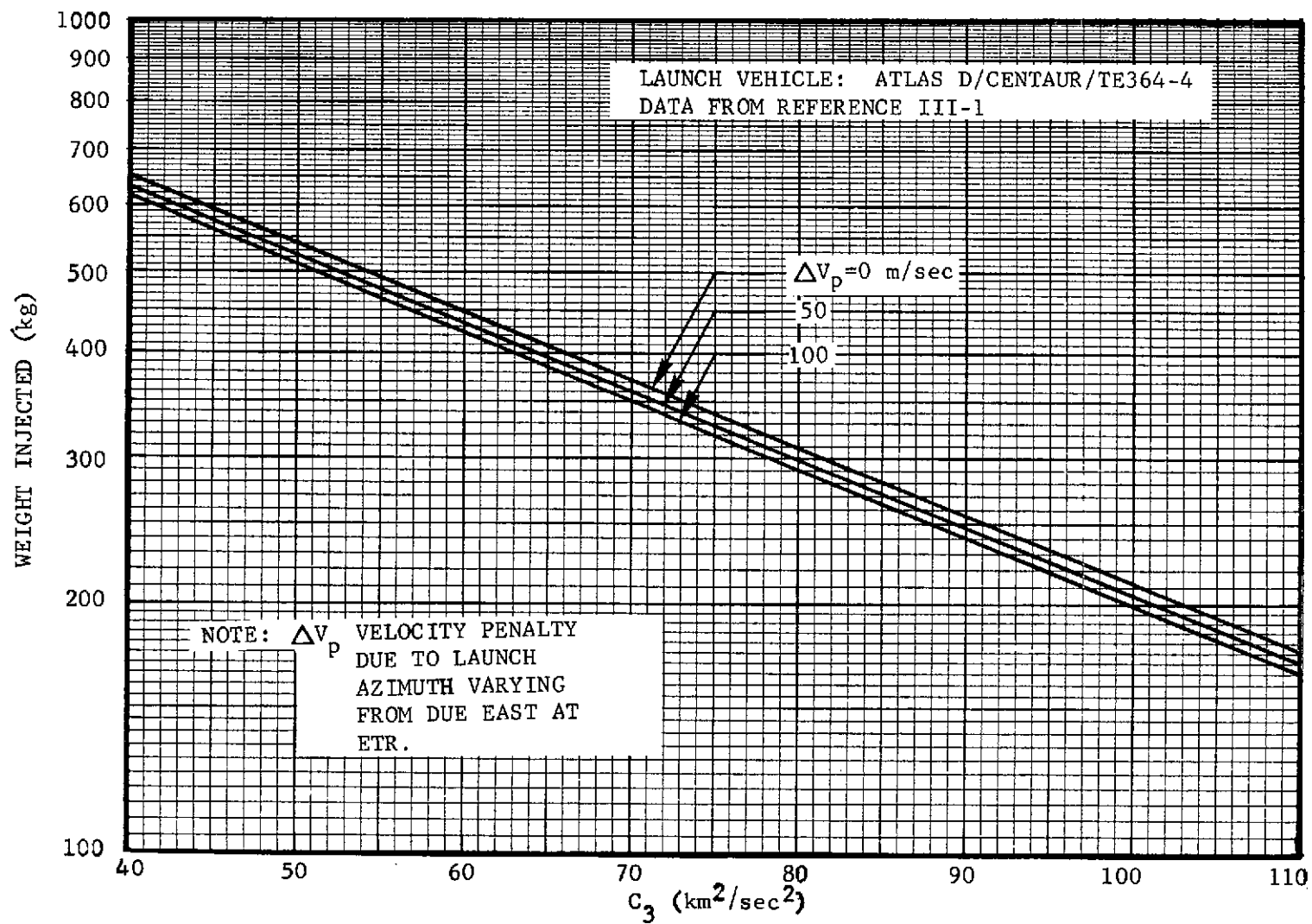


FIGURE III-1 INJECTED WEIGHT CAPABILITY OF LAUNCH VEHICLE

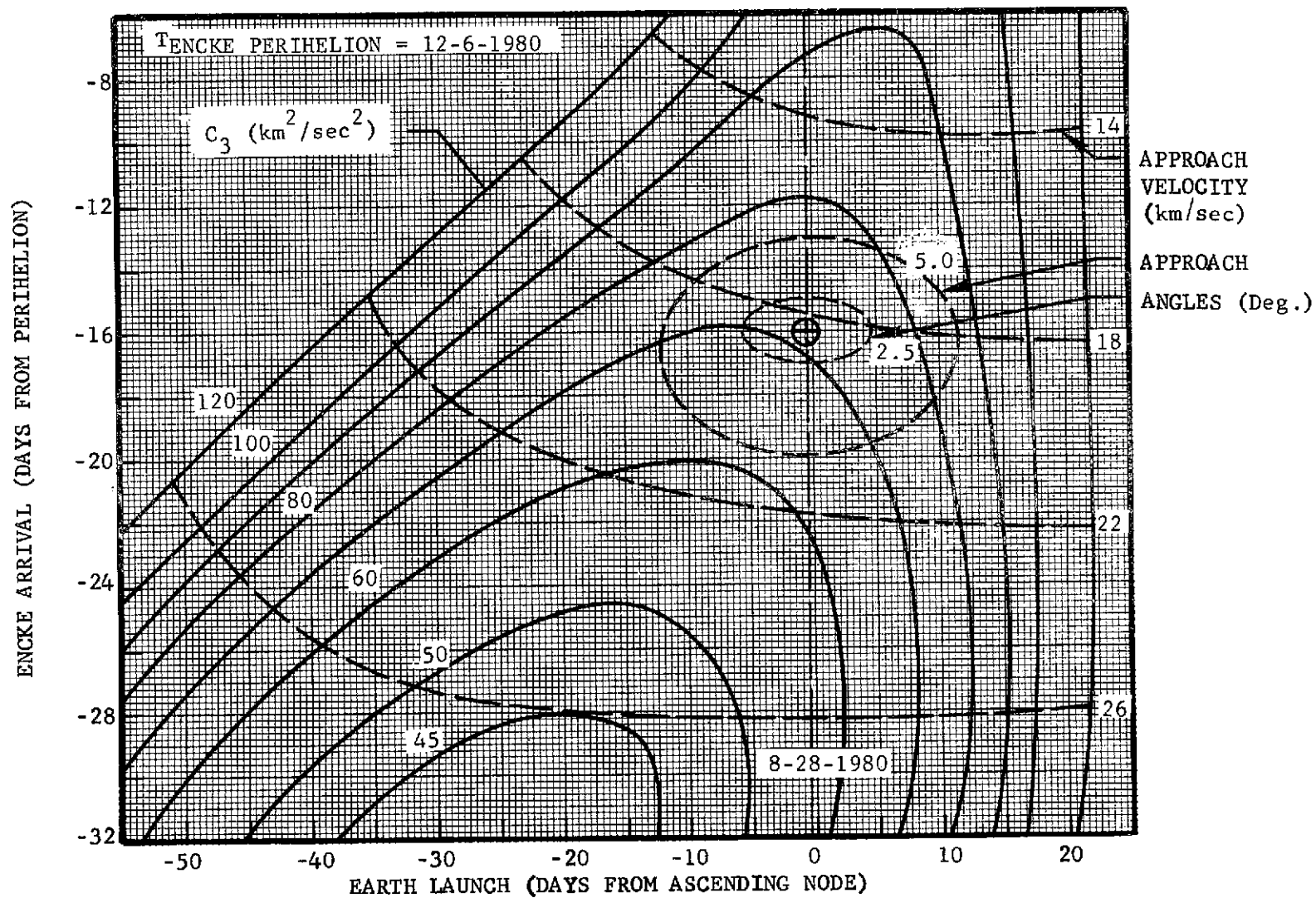


FIGURE III-2 REGION OF MISSION INTEREST

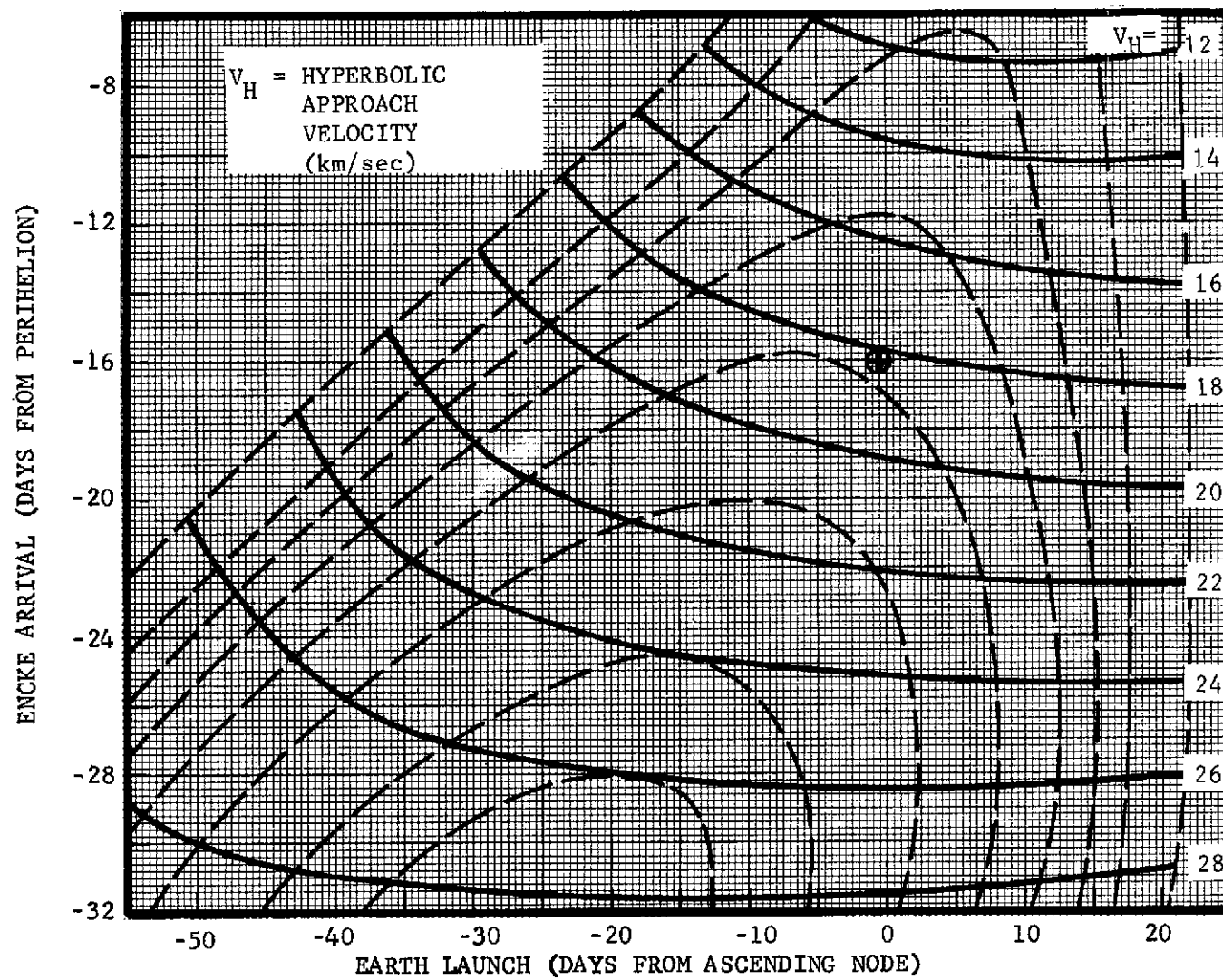


FIGURE III-3 SPACECRAFT APPROACH VELOCITIES AT ENCOUNTER

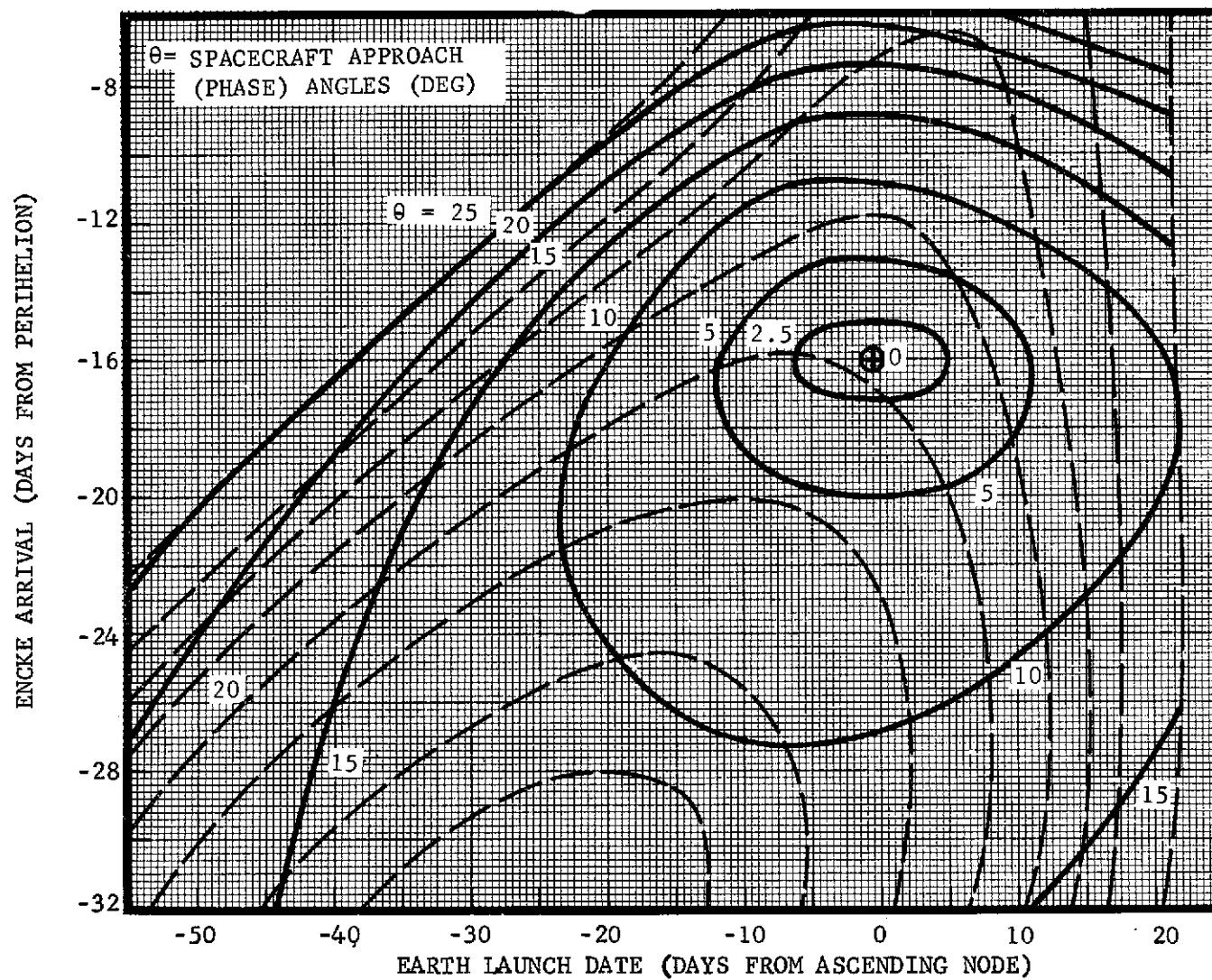


FIGURE III-4 SPACECRAFT APPROACH ANGLES AT ENCOUNTER

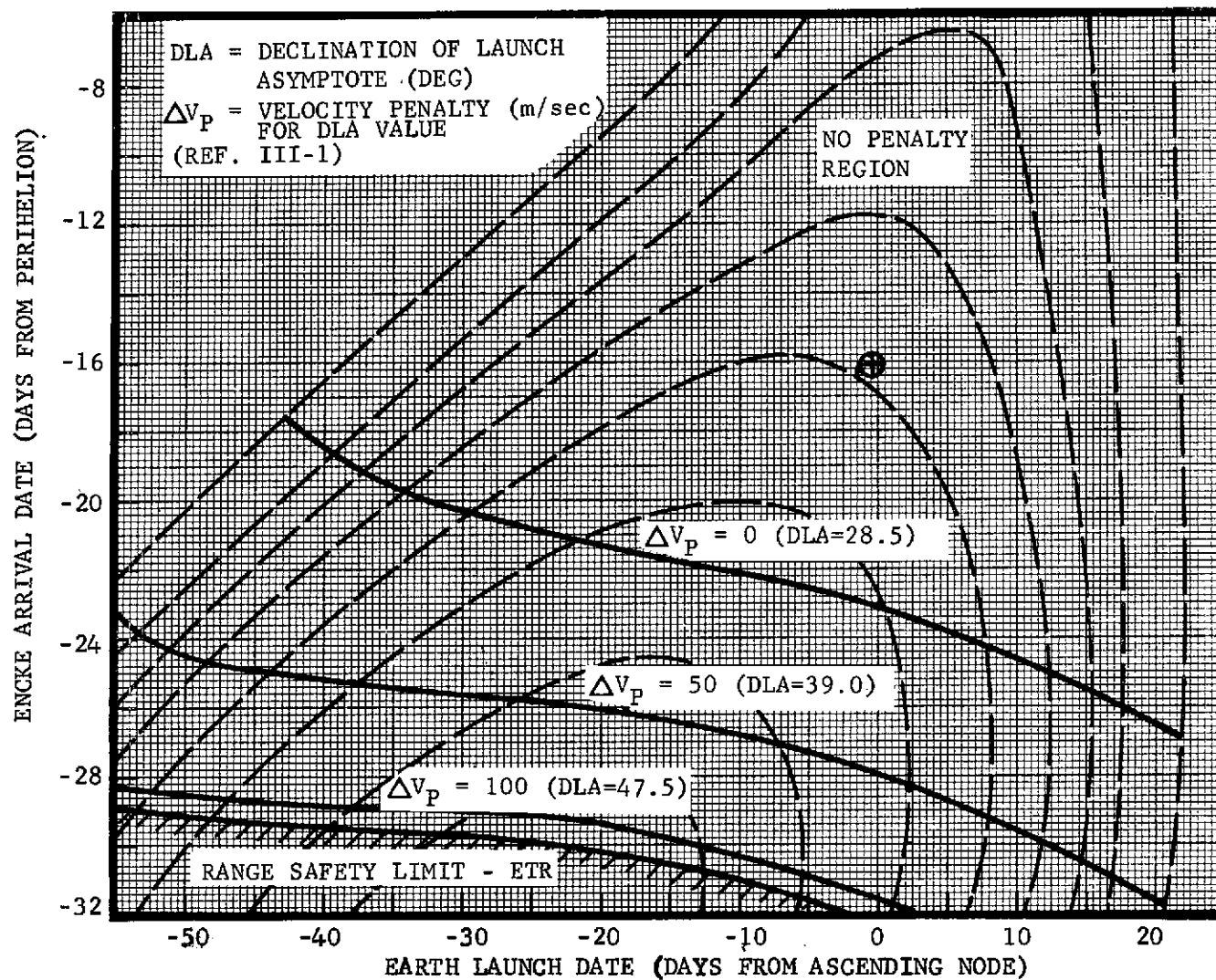


FIGURE III-5 VELOCITY PENALTIES FOR HIGH LAUNCH DECLINATIONS

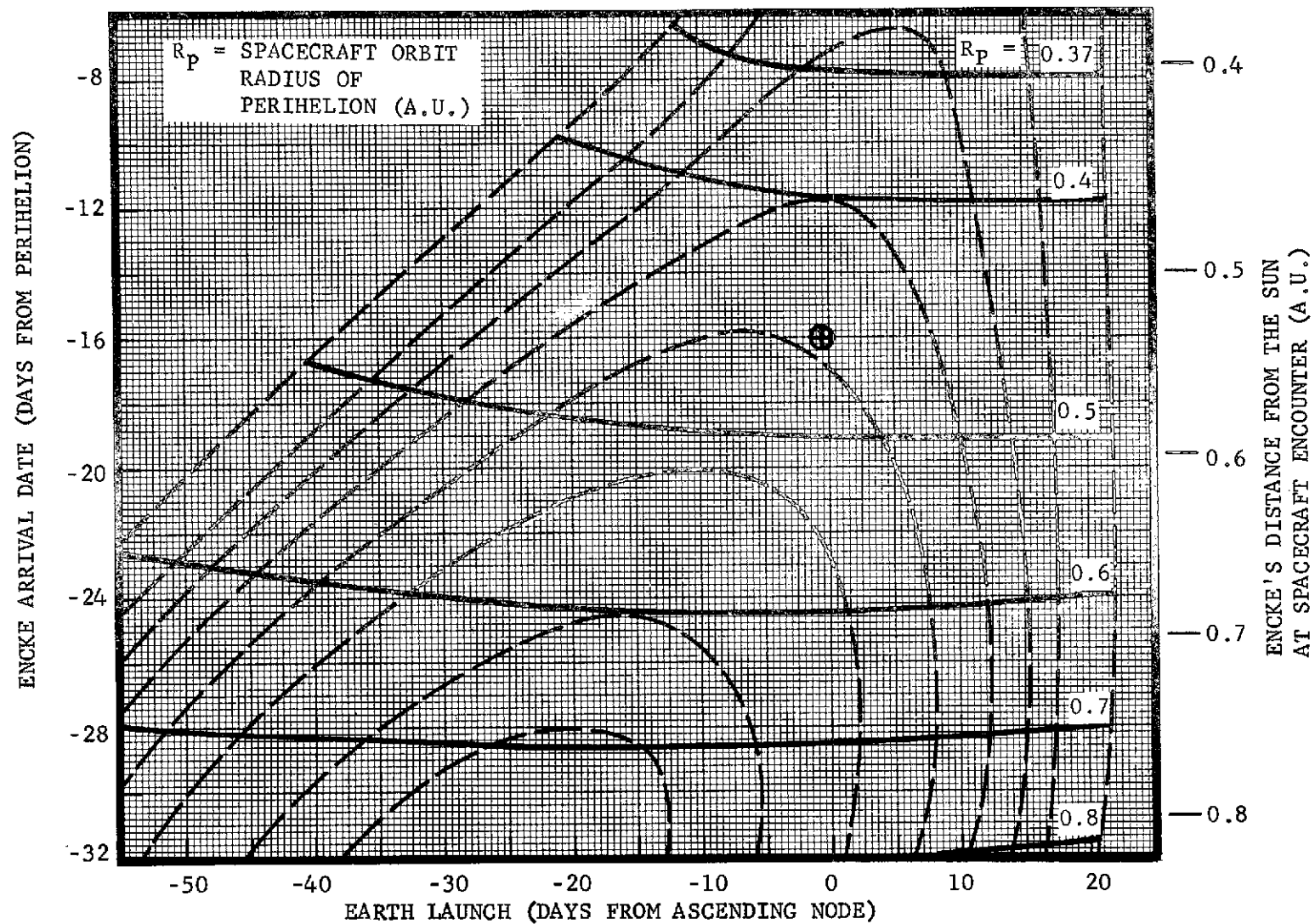


FIGURE III-6 SPACECRAFT ORBIT RADIUS OF PERIHELION AND ENCKE INTERCEPT RADIUS

2. Reference Mission Characteristics

The heliocentric spacecraft trajectory for the reference mission is presented in Figure III-7. Distance and angle relationships with the Sun, comet, and Earth are also depicted. Communication distances between the Earth and spacecraft gradually increases to 0.57 AU for the 85-day period from launch to Encke encounter, but rapidly increases to 0.91 AU during the 20 day period following, with spacecraft orbit perihelion of 0.45 AU reached at 18 days after encounter. Actual mission duration would be about 85 days plus several days for tail observation and data readout. Distance from the Sun at encounter is 0.53 AU.

Figure III-8 shows the spacecraft motion relative to the moving comet and tail during a period from 15 days before encounter to 15 days after encounter with intermediate time ticks given. All relative motion shown is in the plane of the paper, which is also the plane of the spacecraft orbit and comet. Relative motion of the spacecraft directly parallel to the comet tail from ahead of the comet to a tail exit is clearly shown. The spacecraft is actually being overtaken by the comet as shown in the previous figure.

The earliest interception of a possible bow shock would occur at about six days before encounter at a distance of 10^7 km (3.281×10^{10} ft) relative to the comet. Relative spacecraft velocity is 1.58×10^6 km per day (5.19×10^9 ft) with Sun-spacecraft-Earth angle remaining relatively constant. Lower and upper bounds on the approach angle are -30 deg. (corresponding to the late arrival data region on fig. III-2) and +15 deg. (corresponding to the low C_3 region) and are also shown.

Figure III-9 shows a close-up sketch of the spacecraft passage through the coma and tail of the comet. Tail passage time is nominally limited to about 13 1/2 hours in duration because of the relative velocities and curvature of the approach trajectory. As discussed in Section II, a flyby radius of 5000 km (16.4×10^6 ft) was selected. Also selected at this point was targeting for an in-plane (nucleus equator) passage to the left ($\theta_{AIM} = 180$ deg) to maximize tail passage time. For later comparisons, the following simplified model was assumed for the coma and tail:

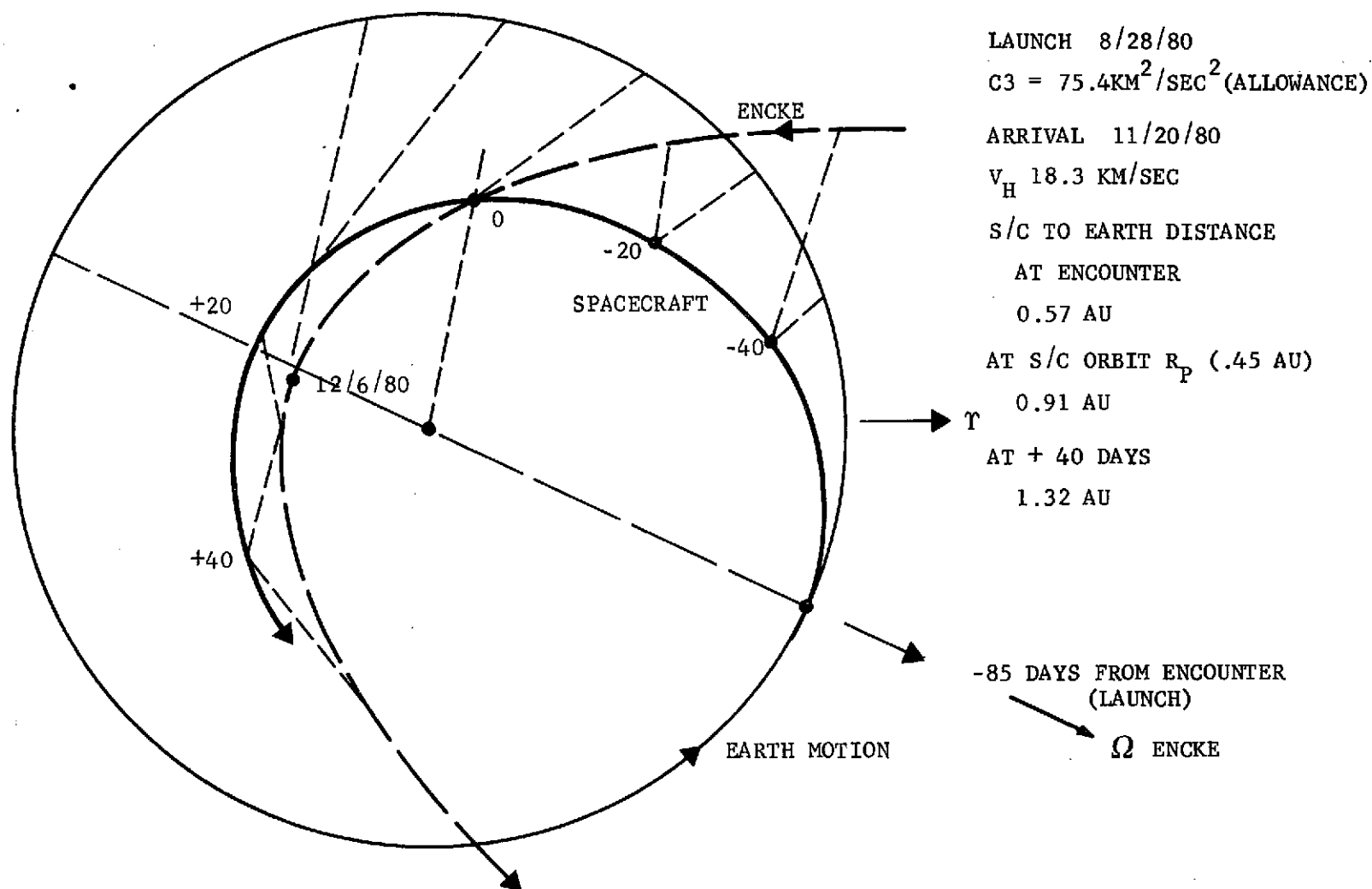


FIGURE III-7 COMET REFERENCE MISSION ENCOUNTER TRAJECTORY

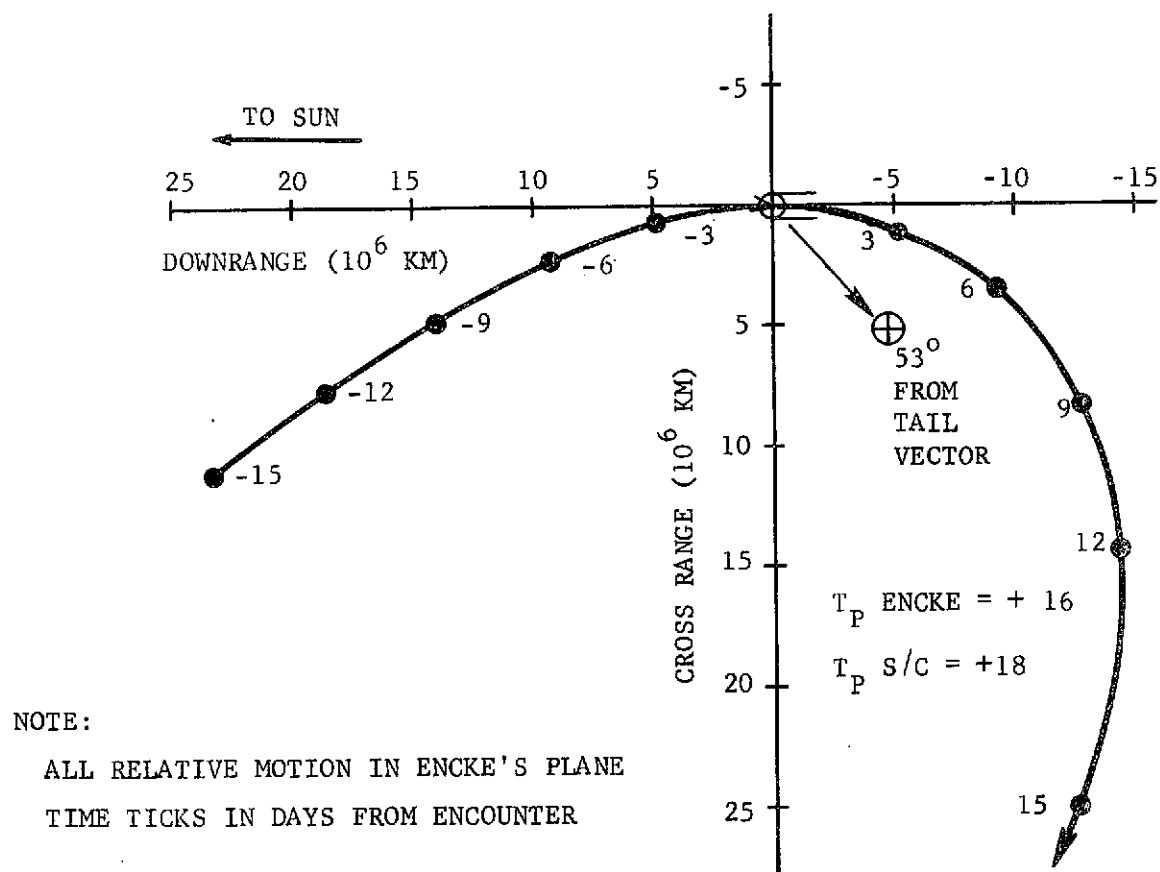


FIGURE III-8 SPACECRAFT/COMET RELATIVE MOTION TRAJECTORY

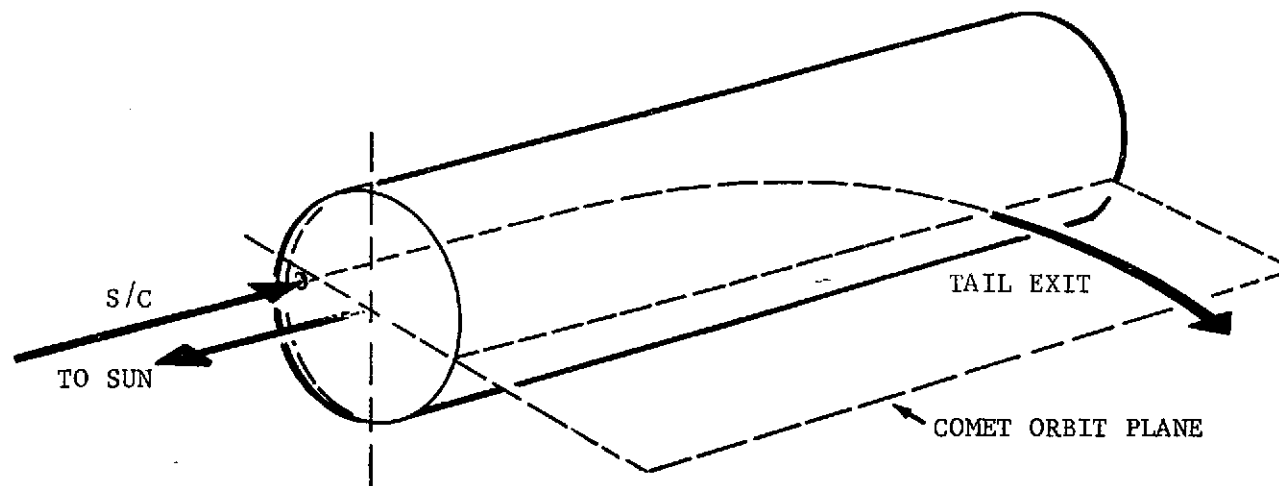


FIGURE III-9 PASSAGE OF SPACECRAFT THROUGH COMA AND TAIL

Spherical coma 40000 km diameter (131×10^6 ft)

Cylindrical tail 1×10^6 km length (656×10^7 ft)

Tail points directly away from the sun.

Another feature of the tail passage mode selected is the possibility of a solar transit of the nucleus. Under perfect targeting conditions, the transit would start at about 4 1/2 hours after encounter and last about 4 hours. Targeting dispersions could greatly reduce the duration or eliminate the occurrence of a transit.

The close-encounter angular motion of the spacecraft trajectory (relative to the nucleus) is shown in Figure III-10. Since the spacecraft motion is parallel to the comet tail during this period, the spacecraft lead angle and nucleus phase angles are equal and the relative motion is primarily in or near one plane (comet's plane). The phase angle is less than 10 degrees at 30 minutes before closest approach and rapidly goes through 160 deg. of travel in 1 hour. Passage time through the coma is 35 minutes. (The nucleus is in a near fully sunlit phase for several days prior to encounter).

Table III-1 shows the comet mission parameter variations for a 10-day launch period, with the reference mission centered in the period. The design C_3 of $75.4 \text{ km}^2/\text{sec}^2$ (hyperbolic excess velocity of 8.68 km/sec or 28490 ft/sec) is reached at the end of the period, corresponding to the reference injected weight of 335 kg (739 lb). Encke arrival time is fixed in all cases.

Only minor variations occur in the launch asymptote declination (DLA), approach velocity (V_{HP}), approach angle, comet intercept distance from the Sun, spacecraft orbit inclination and perihelion, and Sun/Encke/Earth angle at encounter.

The major influence of the time of launch is on the time spent in the comet's tail. For the planned equatorial passage to the left (maximizes tail passage time) the tail passage time can vary from about 9 hours to 13 1/2 hours.

3. Coma Probe Mission Analysis

a. Comparison of Deployment Techniques and Requirements - Figure III-11 shows a typical bus flyby and probe entry (30 deg. probe aspect angle) for the

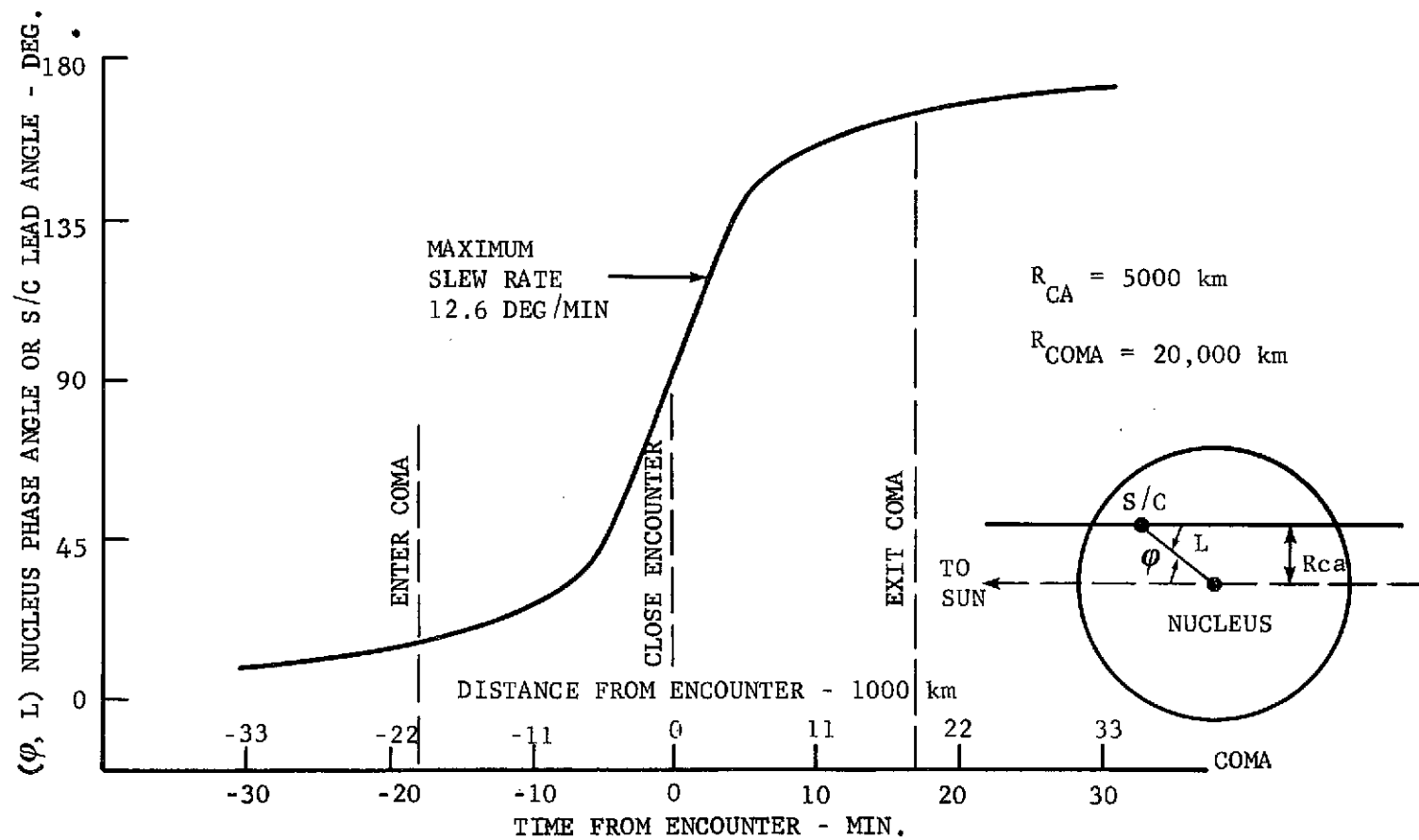


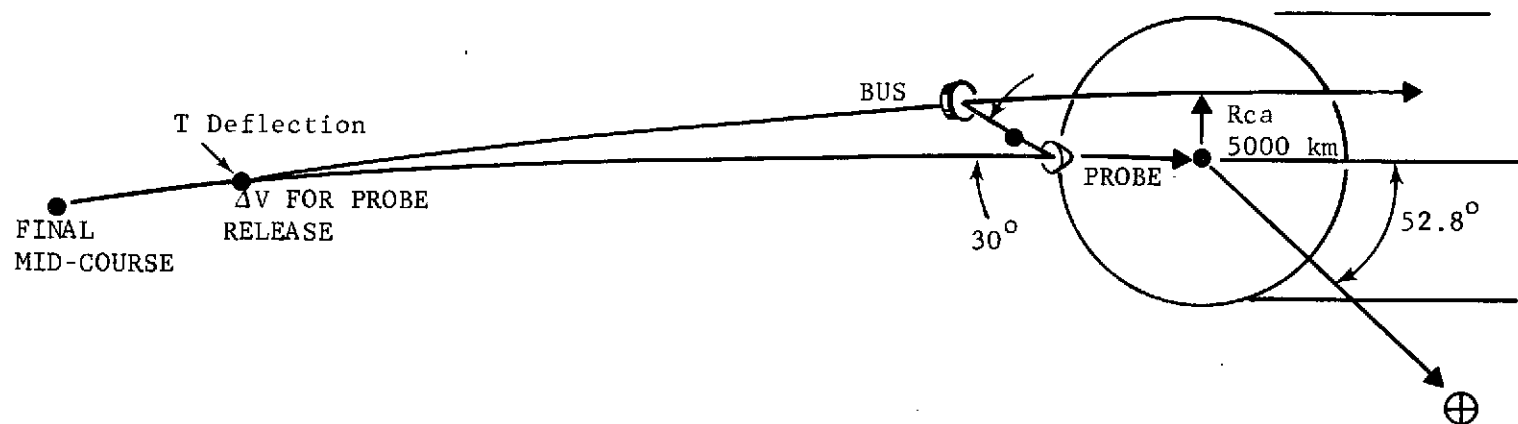
FIGURE III-10 CLOSE ENCOUNTER ANGULAR MOTION

TABLE III-1 COMET MISSION PARAMETER VARIATIONS DURING THE LAUNCH PERIOD

	EARTH LAUNCH (DAYS FROM REFERENCE)*		
	<u>-5</u>	<u>0</u>	<u>5</u>
C3 (km^2/sec^2)	69.8	71.2	75.4**
DLA (Deg.)	17.5	16.5	15.3
V_{HP}	18.6	18.3	18.1
APPROACH ANGLE (Deg)	-2.59	0	+2.51
R INTERCEPT (A.U.)	0.53	0.53	0.53
Δ INCLINATION (Deg)	-1.09	0	+1.03
SUN/ENCKE/EARTH ANGLE (Deg)	119	127	135
R_p OF S/C (A.U.)	0.456	0.453	0.451
TAIL PASSAGE TIME (Hrs.)	9	13 1/2	9
TRIP TIME (Days)	90	85	80

* REFERENCE: Earth Launch 8/28/80; Encke Arrival 11/20/80 (Fixed)

** Design C3 Value (335 kg Injected Wt.)



BUS PROPULSION

$$\Delta V_B = 29 \text{ m/s}$$

E - 4 Days

No Probe Propulsion

No Probe Att. Control

Uses Existing Bus R.C.S.

PROBE PROPULSION

$$\Delta V_P = 29 \text{ m/s}$$

E - 4 Days

Probe Propulsion

Probe Att. Control

FIGURE III-11 PROBE DEPLOYMENT MODE COMPARISON

three probe deployment modes which were investigated. The final mid-course maneuver is shown at 5 days before encounter with the deflection maneuver and probe release at E-4 days. The basic flyby trajectory was also used for the probe reference trajectory.

The bus propulsion mode suggests a minimum change from the basic flyby mission, except that the bus is targeted for the nucleus and deflected for the 5000 km flyby radius after the probe is spun up and released. The ΔV maneuver required for the bus is 29 m/sec or 95 ft/sec (ΔV up and back at 30 deg.).

For the probe propulsion mode, the ΔV requirement is identical but the bus is targeted for the flyby condition with the probe deflected down and forward at 30 deg. at E-4 days. This mode requires separate probe propulsion and attitude control.

In the last method, an increased spin rate on the bus (from 5 rpm to 60 rpm) is used to deploy off-center probe(s) without requiring chemical propulsive maneuvers on either the bus or the probe. The small ΔV which is developed with this method (~ 6 m/sec or 20 ft/sec) requires probe deployment at about 19 days before encounter, where large comet ephemeris knowledge errors may still exist.

The last method discussed does not appear feasible. The bus propulsion mode, however, represents a minimum change from the basic configuration and is therefore recommended.

Figure III-12 presents the deployment requirements for the bus propulsion mode and considers bus deflection times from 10 days before encounter until 2 days from encounter with probe aspect angles in the 20 to 40 deg. range.

It is desired that the final mid-course maneuver occur as late as possible (3-5 days from encounter) to take advantage of latest ground tracking comet ephemeris knowledge and also to minimize dispersions from the final mid-course maneuver.

If the final mid-course maneuver occurs during the period discussed

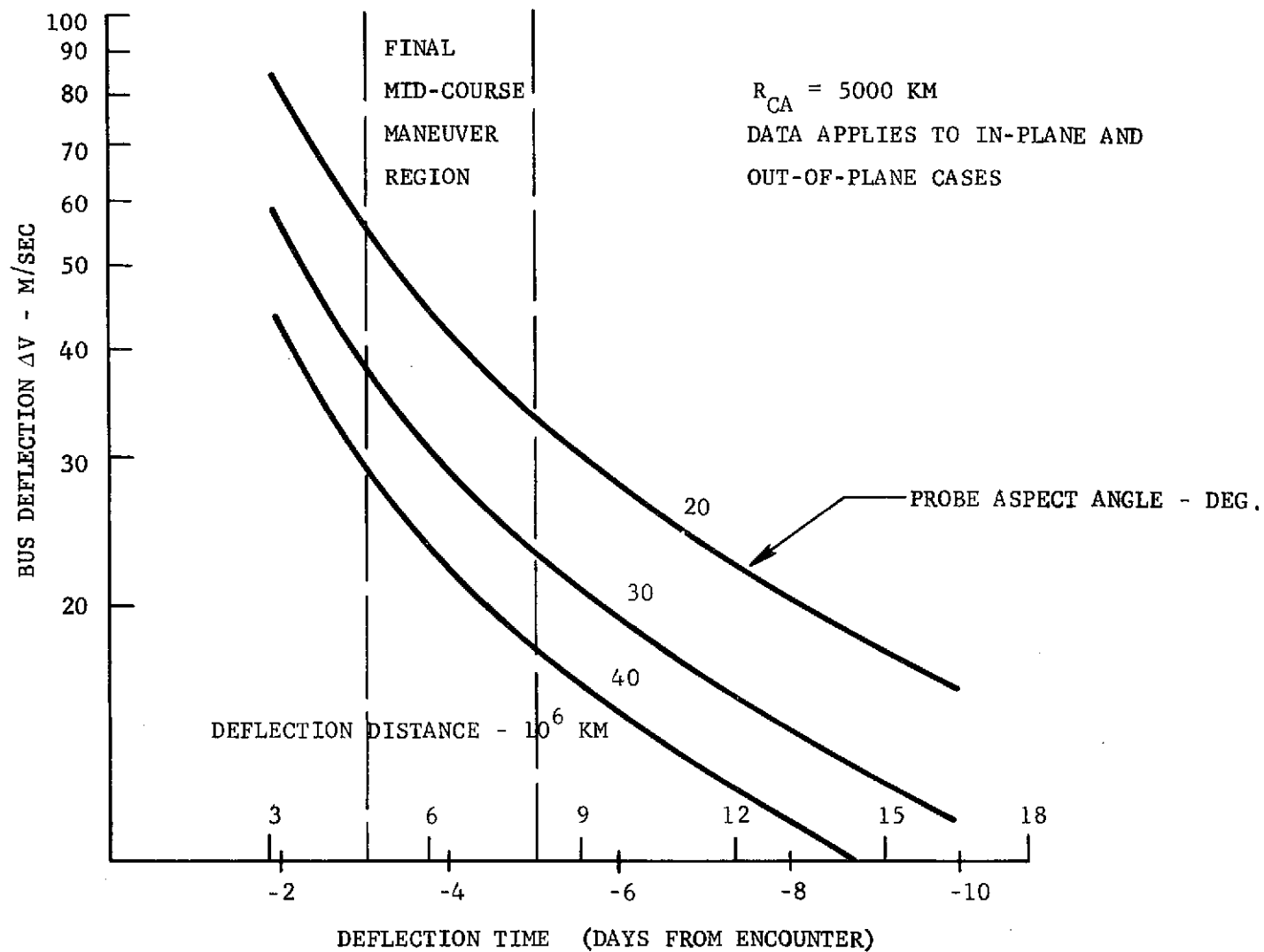


FIGURE III-12 DEPLOYMENT REQUIREMENTS - BUS PROPULSION MODE

and one day is allowed for attitude reorientation and stabilization, the bus deflection maneuver would occur between 2 and 4 days before encounter. The ΔV required for a 30 deg. probe aspect angle would then lie between 30 and 60 m/sec (100-200 ft/sec).

b. Relative Bus/Probe Geometry - Figure III-13 depicts the period from probe separation and the bus deflection maneuver until passage of the bus into the tail region. As previously mentioned, the deflection maneuver would probably occur between 4 days and 2 days before encounter. All motion shown is in or near the plane of Encke. The total angular direction to the Earth (Sun-spacecraft-Earth angle = 127 deg.) is indicated with the Earth-pointing vector shown actually directed about 21 deg. below the comet plane.

The angular relationship of the Earth relative to the motion of the bus or probe in comet-centered coordinates remains very nearly constant during the range of deflection times considered. This would be particularly useful for direct link probe communications with the Earth.

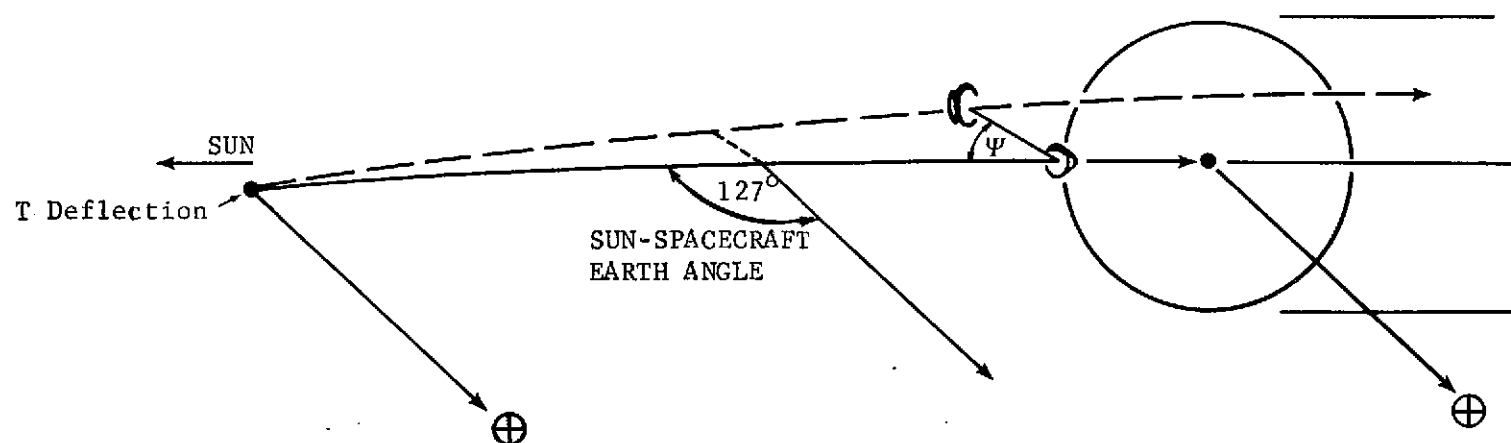
As shown in Figure III-14 and also indicated in Figure III-13, the probe aspect angle also remains fairly constant (varying less than 1 degree) from deflection through entry which would simplify probe to bus communication systems. Communication distance from the bus to probe varies nearly linearly with time from deflection (a maximum of 15000 km or 49.2×10^6 ft) reached for a phase aspect angle of 20 deg. Earth communication distance lies between 0.51 A.U. and 0.57 A.U. during the period of interest.

The invariance of the probe aspect angle and the linearity of the bus to probe communication distance from deflection time through entry is due mainly to the lack of a significant gravity field at the comet.

c. Probe Dispersion Analysis - As the study progressed, probe communication link studies indicated a preference for the 40 deg. probe aspect angle, with the preferred bus deflection maneuver time remaining in the 2 days to 4 days before encounter region. The probe dispersion analysis was therefore conducted for those conditions.

Again, due to the linearity of the problem, probe dispersions relative to the bus (actually caused by bus deflection maneuver dispersions) can easily

NOTE: ALL MOTION NEAR ENCKE PLANE (PLANE OF PAPER)



T Deflection = (E-4 to E-2 DAYS)

ψ = PROBE ASPECT ANGLE

FIGURE III-13 GEOMETRY OF PROBE ENTRY

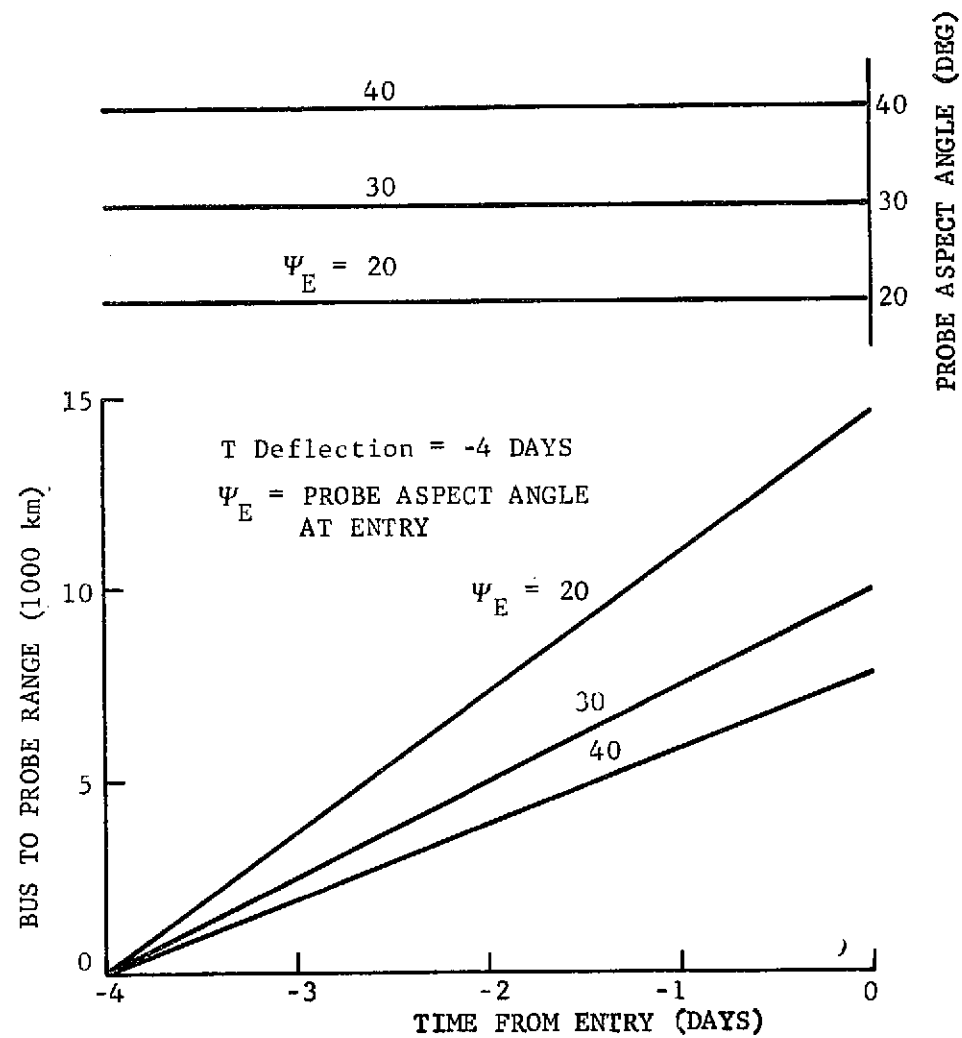


FIGURE III-14 BUS TO PROBE COMMUNICATION PARAMETER VARIATIONS

be estimated with the following relationships:

$$1) Y_E = \Delta V t_D \sin \psi_E$$

$$2) X_E = \Delta V t_D \cos \psi_E$$

$$3) Z_E = \Delta V t_D \sin \phi \text{ (nominally 0)}$$

where: ΔV = Magnitude of Bus Deflection Maneuver

t_D = Deflection Time

ψ_E = Probe Aspect Angle at Entry

Y_E = Cross Range Distance from Bus to Probe at Entry
(approximately equal to radius of closest approach)

X_E = Downrange Distance

Z_E = Out of Plane Distance from Bus to Probe At Entry

ϕ = Out of Plane Attitude Angle

By taking partial derivatives of the various parameters relative to downrange and crossrange distance for a nominal flyby radius of 5000 km (16.4×10^6 ft) and estimating 3σ dispersions in ΔV (due to thruster impulse uncertainty), deflection time initiation, and thrust vector pointing (approximately equals ψ_E), the following dispersions are observed as shown in Table III-2. Maximum dispersions of about 200 km (due primarily to the 1.5 deg. uncertainty in thrust vector pointing) are shown. These dispersions represent only the bus to probe knowledge uncertainties and are independent of the dispersions relative to the nucleus, which will be discussed under the navigation analysis.

TABLE III-2 PROBE/BUS RELATIVE DISPERSIONS AT ENTRY

Time of Deflection (days) (2 to 4)		
A. Cross Range Variation (km)		
1. Due to ΔV		5.0
2. Due to Attitude		157.7
3. Due to t_D		2.9
4. Total R_{SS} value		157.8
B. Down Range Variation (km)		
1. ΔV		6.0
2. Attitude		130.9
3. t_D		6.9
4. Total R_{SS} Value		131.2
C. Out of Plane Variation (km)		203.6
Assumed (3σ) Dispersions:		
Thrust Impulse	0.1%	
Thrust Attitude	1.5 deg.	
Deflection Time	0.03% (100 sec at 4 days)	
Nominal Condition:		
t_D	= 2 (days)	
ψ_E	= 40 (deg)	
ΔV	= 45 (m/sec)	
ϕ	= 0 (deg)	

B. ENCKE/ASTEROID MISSION CHARACTERISTICS

Preliminary investigations at Martin Marietta in 1972 and early 1973 indicated a potential for combining the Encke 80 mission with a flyby of the asteroids Geographos or Toro for under 500 m/sec (1640 ft/sec) ΔV maneuver penalty. A possible opportunity for combining both asteroids with the comet mission appeared feasible for less than 1 km/sec (3281 ft/sec) ΔV maneuver penalty. Further discussion of the pre-contract study effort in this area is contained in Appendix A.

1. Asteroid Encounter Options

The basic flyby mission requires less than 1/2 revolution of the spacecraft about the Sun with a duration of less than 1/3 year. Because of timing relationships between the comet and asteroids, the combined missions require more than one revolution about the Sun. (From 1 3/4 revolutions for Geographos 1 encounter to 2 1/4 revolutions for an encounter with Toro). These combined mission durations vary from about 1 1/3 to 1 2/3 years.

Figure III-15 pictorially summarizes all of the missions (including the reference mission) on the basic C_3 contour chart. These data summarize the results of the study as far as optimized ΔV maneuver requirements for retargeting to an asteroid (or asteroids). These data were generated on the basis of minimizing the ΔV required to achieve a 10-day launch period (within reasonable C_3 limits).

In general, an opportunity exists to maneuver in the first revolution about the Sun (shortly after encountering Encke) or in the second revolution. Usually, one opportunity is slightly displaced from the other on the contour chart, and may have a different ΔV requirement. The second revolution opportunity appears to be somewhat lower generally in ΔV required.

For comparison purposes, a contour has been shown for the reference mission. This contour corresponds to an approach angle of about 2.5 deg. at Encke, with the reference case centered on a 10-day launch period.

The four Encke/Asteroid(s) mission considered in this study are as follows:

- 1) Encke/Geographos 1 (Encounter with Geographos occurs near its

FIGURE III-15 SUMMARY OF ASTEROID MISSION OPTIONS

perihelion)

- 2) Encke/Geographos 2 (Encounter with Geographos occurs after the asteroid passes perihelion and is near 1 A.U. from the Sun)
- 3) Encke/Toro (Encounter with Toro occurs near its perihelion)
- 4) Encke/Geographos/Toro (similar to (1) and (3))

As seen in Figure III-15, velocity requirements vary from 130 m/s (427 FPS) to 670 m/s (2200 FPS) for the singly-combined missions and require 940 m/sec (3084 FPS) for the double combined mission.

Figure III-16 indicates how the Earth-Encke leg is affected by the various missions. Flight duration varies from 70 to 100 days for the combined missions, compared to the reference mission time of about 85 days. The main difference is in the radius of intercept at the comet. This varies from .53 A.U. (for the reference mission) to .76 A.U. for the missions involving Geographos 1. These effects are caused primarily by the greatly differing launch energies, as will be discussed.

2. Maneuver Requirements for Asteroid Flyby

Figures III-17 through III-19 present typical heliocentric trajectories for the four combined asteroid missions investigated. As previously indicated, optimization studies show that executing the ΔV maneuver on the second revolution about the sun achieves the same or lower velocity penalties compared to maneuvering on the first revolution (although this of course is an option if other requirements would dictate). The data in this section is therefore based upon maneuvering in or near the second revolution.

Because of the close proximity of the ascending nodes and inclinations of the orbits of Encke and Geographos, two opportunities exist for encountering the asteroid. Figure III-17 shows both of these missions (Geographos 1 and Geographos 2) pictorially on the same trajectory for simplicity of presentation.

For the Geographos 1 mission (intercept near perihelion on 12-21-81) launch typically occurs about three weeks before the reference mission and arrives about 12 days earlier. C_3 is reduced to about $47 \text{ km}^2/\text{sec}^2$ ($506 \times 10^6 \text{ ft}^2/\text{sec}^2$)

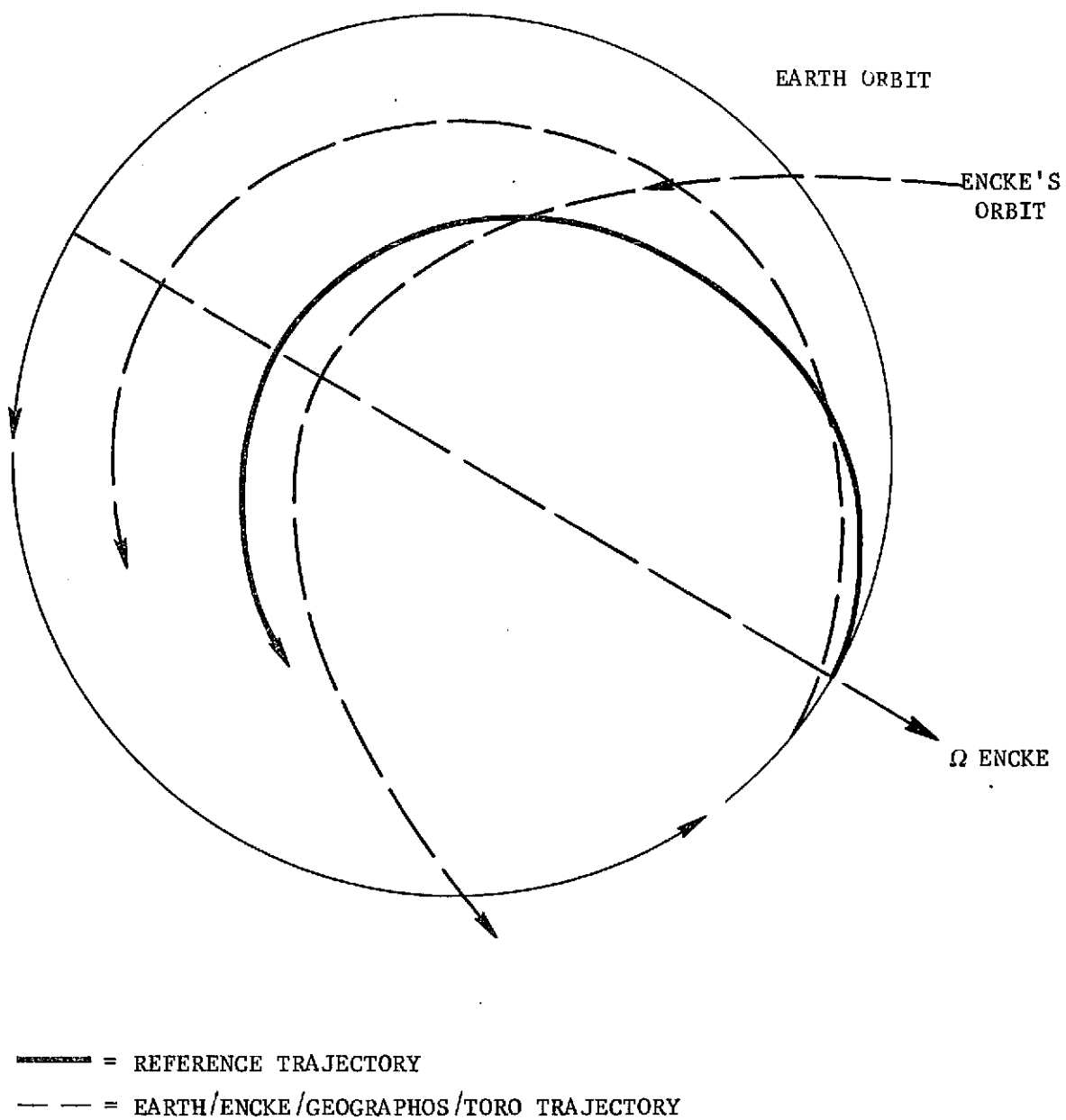


FIGURE III-16 EARTH/ENCKE LEG TRAJECTORY VARIATIONS

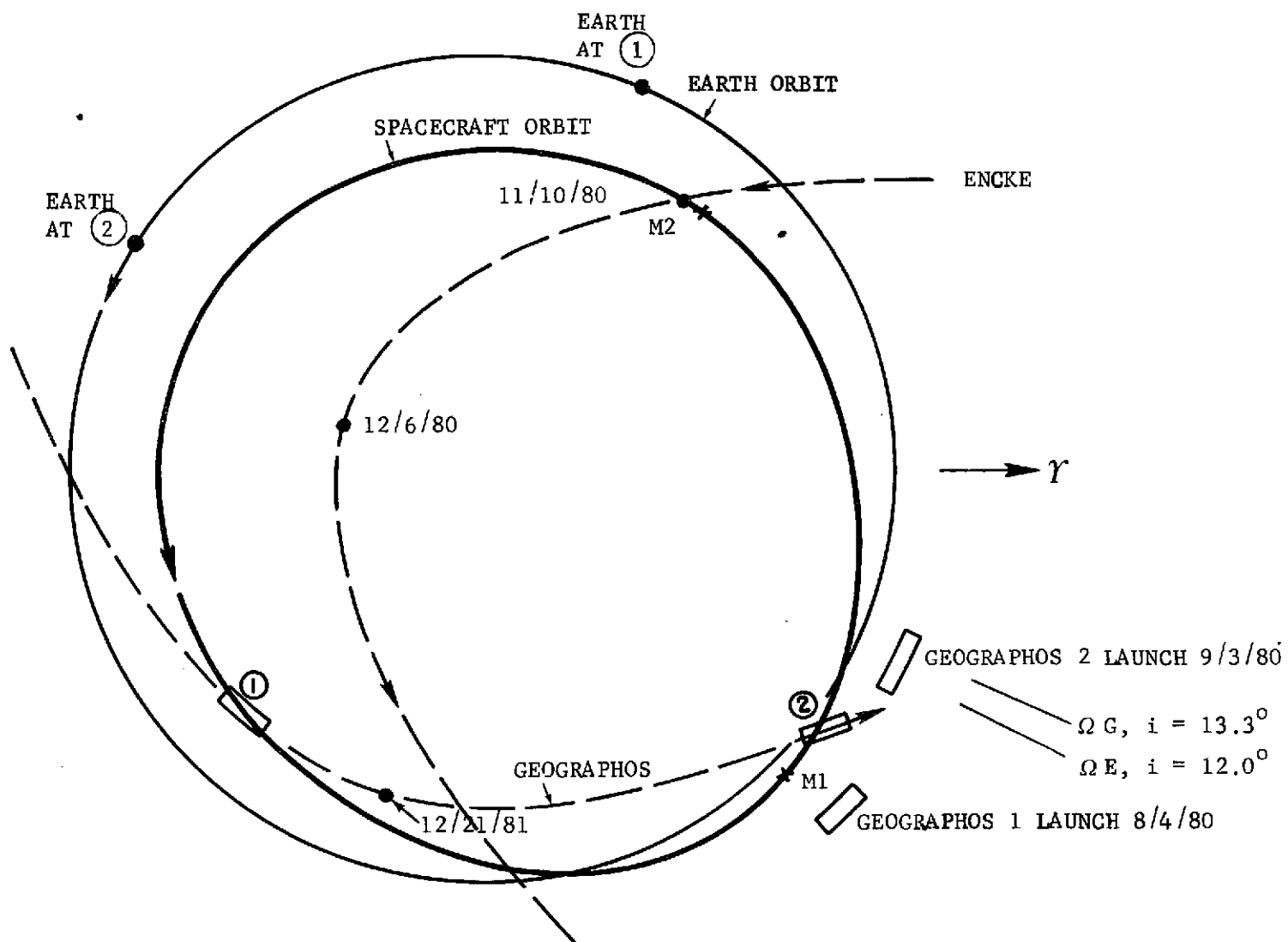


FIGURE III-17 ENCKE/GEOGRAPHOS MISSIONS

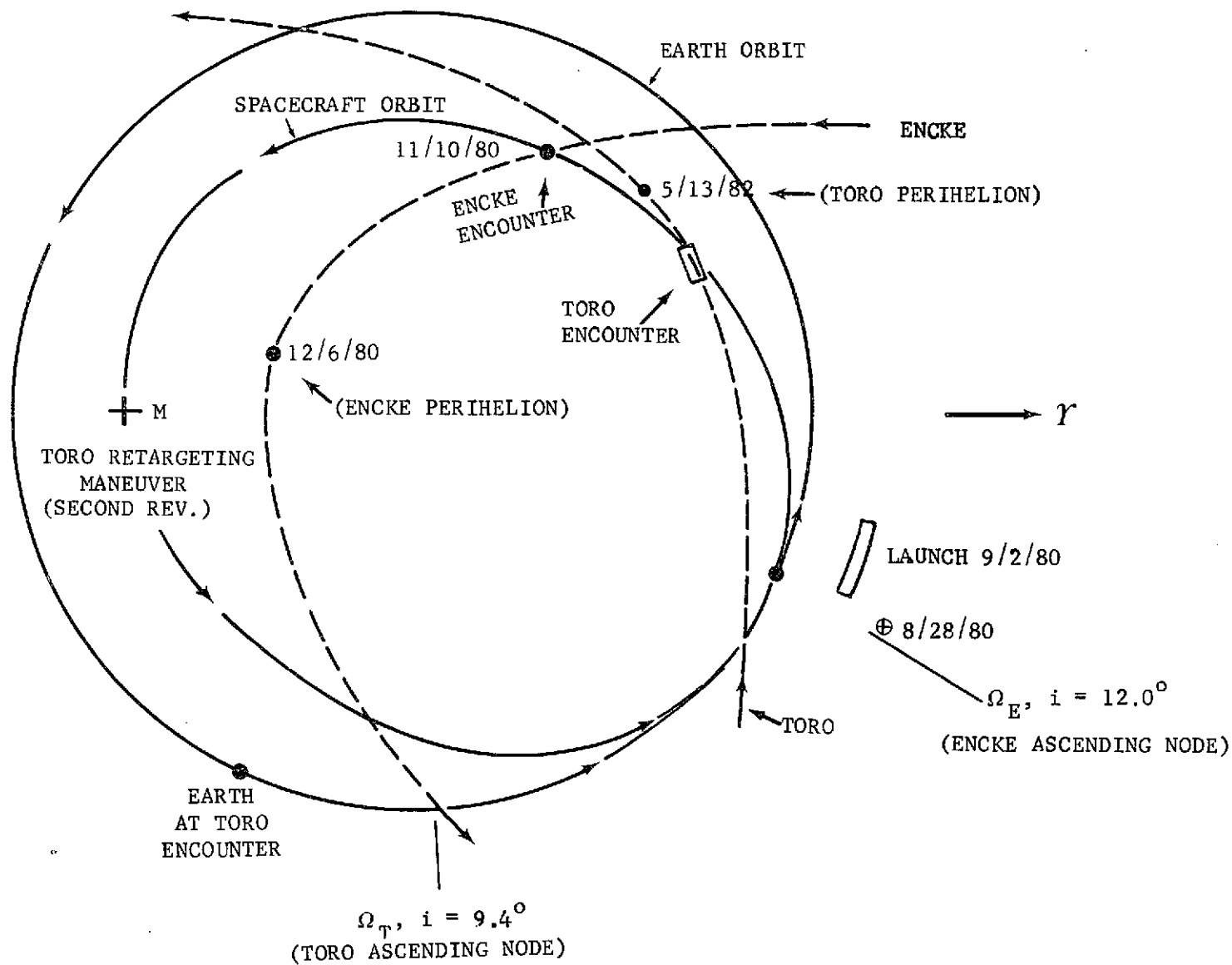


FIGURE III-18 ENCKE/TORO MISSION

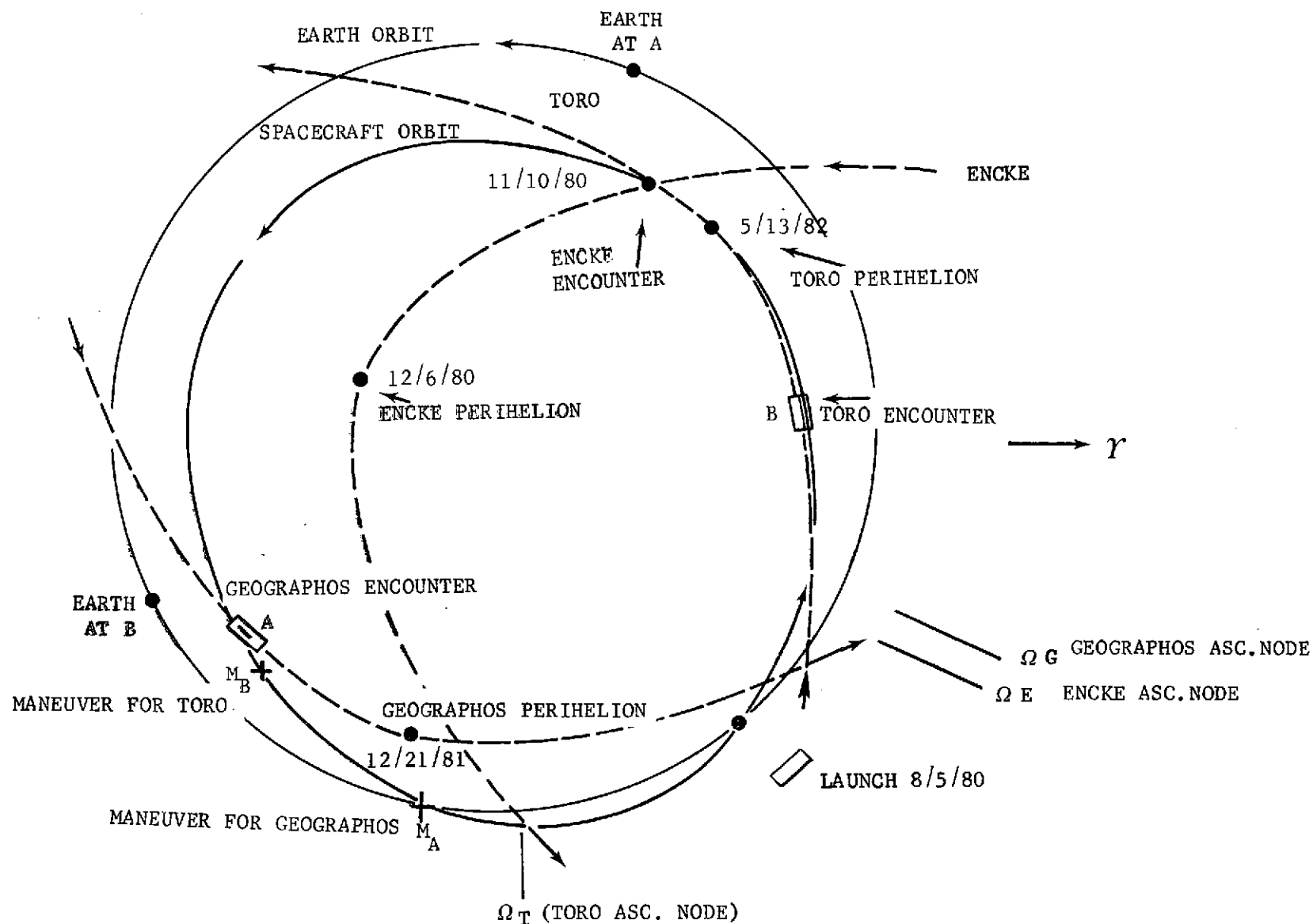


FIGURE III-19 ENCKE/GEOGRAPHOS/TORO MISSION

which allows an injected weight of 550 kg (1213 lb). The maneuver ΔV of 130 m/sec (427 ft/sec) is executed at M1 (as shown in Figure III-17) on about (5-28-1980) and intercept with Geographos occurs at Pt. 1 on (12-1-1981). The total mission time is 485 days and the spacecraft orbit perihelion is 0.69 AU.

For the Geographos 2 mission, the launch period overlaps that of the reference mission and arrives typically about seven days earlier at the comet. A launch energy of $70 \text{ km}^2/\text{sec}^2$ ($754 \times 10^6 \text{ ft}^2/\text{sec}^2$) is required for this mission, producing a spacecraft injected weight of 370 kg (816 lb). The maneuver ΔV required for a 10-day launch period is 670 m/sec (2200 ft/sec) and is executed at M2 (shown in Figure. III-17) on 7-28-1981. Intercept with Geographos occurs at Pt. 2 on 2-23-1982. The total mission time is 538 days and spacecraft orbit perihelion is 0.54 AU.

For the single mission to the asteroid Toro (intercept near its perihelion on 5-13-1982), launch typically occurs at the same time period as the reference mission, and arrives at Encke about 10 days earlier. A C_3 of $68 \text{ km}^2/\text{sec}^2$ ($732 \times 10^6 \text{ ft}^2/\text{sec}^2$) is required for this mission and the orbits of the asteroid and the comet are more displaced from each other than for Geographos (see Figure III-18). An injected weight of 380 kg. (838 lb) is delivered. The maneuver ΔV is 615 m/sec (2018 ft/sec) is executed at point M on 10-22-1981 and intercept with Toro is reached on 5-2-1982. The total mission time is 608 days and the spacecraft orbit perihelion is 0.64 AU.

For the double combined mission, intercept is required at Geographos 1 (as shown in Figure III-19) to produce the correct location and timing to encounter Toro within the next revolution. Launch occurs at essentially the same time as required for the single Geographos 1 mission (see overlapping contours in fig. III-15), and has similar launch/encounter conditions. Injected weight is 560 kg (1235 lb). The first maneuver ($\Delta V = 200 \text{ m/sec}$ or 656 ft/sec) occurs typically at M_A in Figure III-19 on 5-28-1981 and encounters Geographos on 12-1-1981. As near after encounter as practical (within one or two days) a second maneuver of 740 m/sec (2428 ft/sec) is required to intercept Toro on 4-17-1982. The total mission time is 622 days and spacecraft orbit perihelion is similar to the Geographos 1 mission (0.64 AU).

3. Comparison of Asteroid Mission Characteristics

Because of the importance of asteroid lighting conditions for imaging experiments (and optical navigation, if present), Figure III-20 is presented. Lighting phase angles are shown as a function of time from 80 days before encounter with the target asteroid until 10-20 days after encounter. In all cases the phase angle during the previous encounter with Encke is very near to a fully lit phase of the nucleus (0 to 12 deg).

Lighting conditions for the Geographos 1 encounter (on both the single and double missions) are very good throughout the 80 day pre-encounter period (13 to 34 deg) with a phase angle at final encounter of 29 deg. Approaching Toro during the double asteroid mission produces phase angles varying from a low of 20 deg. to an encounter phase angle of 78 deg.

For the single mission to Toro, phase angles are substantially higher (going from an initial angle of 40 deg. and intercepting Toro with a moderately dark-side encounter condition of 114 deg).

The most serious lighting situation occurs during the single mission to Geographos 2. A phase angle of 90 deg. occurs at 69 days from encounter and becomes progressively greater until encounter where a highly darkened condition (158 deg) is realized. If acquisition could be made and an accurate flyby insured, good lighting conditions would exist (approaching 22 deg.) within minutes after close approach.

A comparison of the primary asteroid mission characteristics are summarized and related to the reference comet flyby mission in Table III-3. As previously mentioned, the duration of the asteroid missions vary from 1 1/3 years to 1 2/3 years (from 1 3/4 to 2 1/4 revolutions about the sun), compared to 3 months for the reference mission.

In all cases (for a 10-day launch period) injected weights are increased over the reference mission, with the most significant improvements occurring in the two missions involving Geographos 1. Injected weight varies from a minimum of 335 kg (739 lb) for the reference mission to 550 to 560 kg (1213 to 1235 lb) for the Geographos 1 missions. All of the asteroid combined missions are

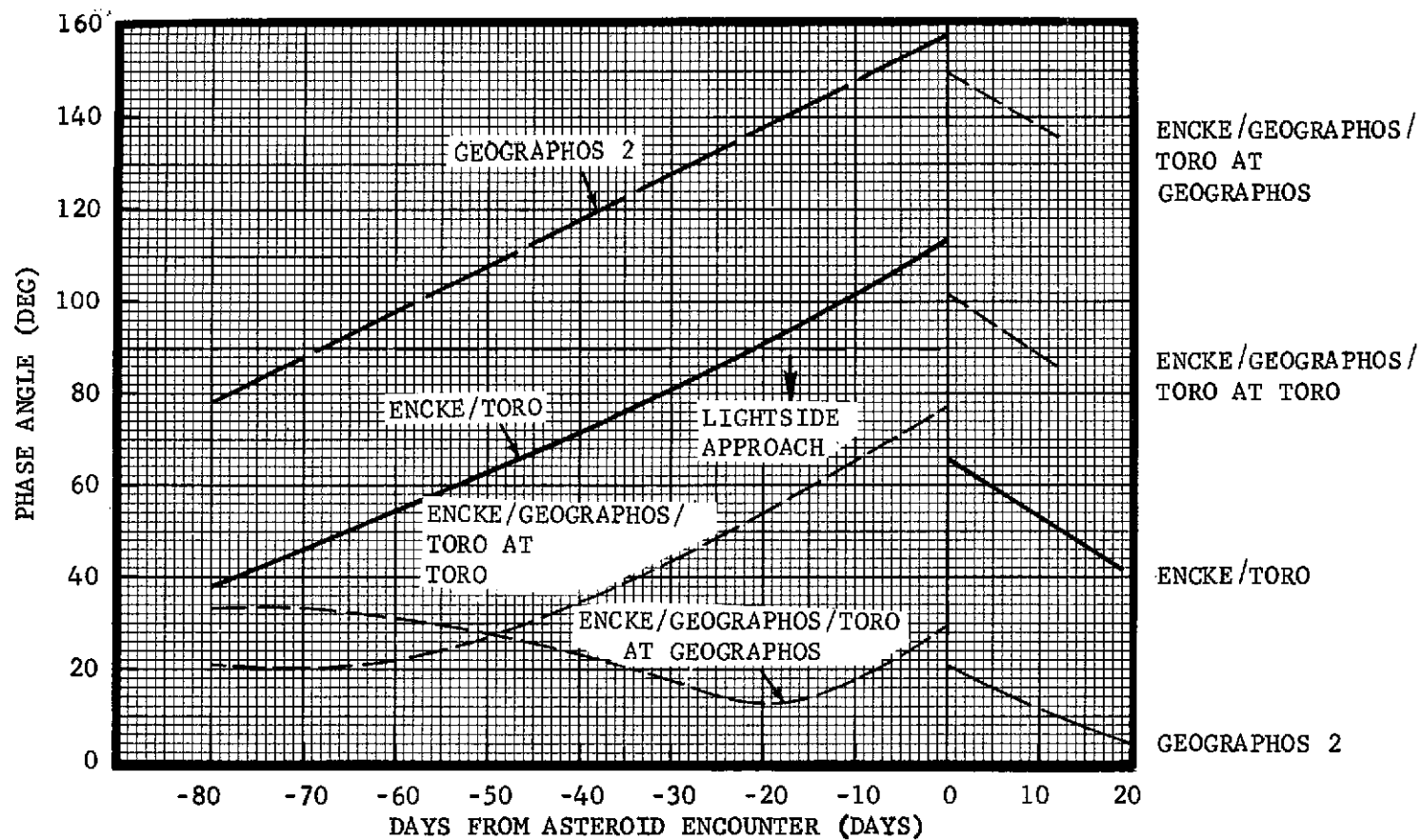


FIGURE III-20 ASTEROID LIGHTING CONDITIONS DURING APPROACH

TABLE III-3 COMPARISON OF ASTEROID MISSIONS

	REFERENCE FLYBY MISSION	GEOGRAPHOS 1 MISSION	GEOGRAPHOS 2 MISSION	TORO MISSION	GEOGRAPHOS/TORO MISSION
Required C_3 (km^2/sec^2)* ($\text{ft}^2/\text{sec}^2 \times 10^6$)	75.0 (807)	47.0 (506)	70.0 (754)	68.0 (732)	46.0 (495)
Injected Weight (kg) (lb)	335 (739)	550 (1213)	370 (816)	380 (838)	560 (1235)
ΔV Maneuver/s (m/sec) (ft/sec)	0 (0)	130 (427)	670 (2200)	615 (2018)	200/740 (656/2428)
V_{HP} at Encounters (km/sec) (ft/sec $\times 10^3$)	18 (59)	26/13 ** (85/43)	23/14 (75/46)	25/11 (82/36)	26/13/8 (85/43/26)
Mission Duration (days)	85+	485+	538+	608+	622+
Encounter Phase Angles (deg)	0	12/29	9/158	10/114	12/29/78
Sun/Body/Earth Angles (deg)	127	122/16	120/0	121/10	122/16/15
Tail Passage Time (hrs) ***	9-13½	1.2-1.3	1.8-2.3	1.5-1.7	1.1-1.2
Earth to S/C Distance at Encounter (AU).	0.57	0.35/1.78	0.44/2.04	0.38/1.77	0.35/1.78/1.78

*Corresponds to 10-day launch period in all cases.

** Indicates Encke/asteroid values (typical).

*** Assumes that tail passage time is maximized by varying targeting point (θ_{AIM}) for a constant flyby radius of 5000 km.

characterized by higher comet approach velocities (23-26 km/sec or 75000 to 85000 ft/sec) compared to the reference value of 18 km/sec (59000 ft/sec). Asteroid encounter velocities are significantly lower (8-14 km/sec or 26000-46000 ft/sec).

As mentioned previously, the spacecraft orbit perihelions are generally increased for the asteroid missions (relaxed thermal input) because of the lower launch energies. Those values vary from 0.54 A.U. to 0.69 A.U. (with corresponding increases in comet intercept radii, as shown in Figure III-16) compared to the reference mission value of 0.45 A.U.

Because of the multiple revolutions (about the Sun) for the asteroid missions, the communication distance at asteroid encounter(s) is substantially increased (from 1.7 A.U. to 2.0 A.U.) compared to the reference value of 0.57 A.U.

Comet encounter phase angles (approach angles) are increased (9-12 deg) compared to the reference value of 0. The main effect of this influence is to reduce tail passage time to 1 to 2 hours (compared to 9 to 13½ hours for the reference flyby case).

The Geographos 1 mission appears to be the most attractive single asteroid mission because of the low launch energy, low retargeting maneuver velocity of 130 m/sec (427 ft/sec), and low encounter phase angle (29 deg). Time in the comet tail exceeds one hour.

Both the single Geographos 2 and Toro missions do not offer large increases in injected weights (a maximum of 380 kg or 838 lb) over the reference mission value of 335 kg (739 lb). Both missions require over 600 m/sec (about 2000 ft/sec) retargeting maneuver velocity.

Since the communication angle with Earth (Sun Geographos-Earth angle) for Geographos 2 is near zero at encounter, the spacecraft probably cannot be tracked from the Earth or communicated with for several weeks before encounter. The Geographos approach also has a darkside encounter condition (158 deg phase angle). For these reasons, it is recommended that the Geographos 2 mission be dropped from further consideration.

For the case of Toro (single mission) the communication angle is low near encounter (10 deg), and tracking and communication look feasible.

A semi-darkside approach does exist (114 deg. phase angle), but is not as severe as for Geographos 2. Because of the previously mentioned low injected weight for the larger retargeting maneuver velocity, this should be considered a marginal mission.

The double combined mission has essentially the same attractive features for launch conditions and arrival conditions at Geographos (weight injected is 560 kg or 1235 lb). It does of course require the cost and complexity of a second maneuver (740 m/sec or 2428 ft/sec) but has the advantage of visiting the second asteroid with improved conditions (over the single Toro mission) in encounter phase angle (78 deg. compared to 114 deg.) and encounter velocity (8 km/sec or 26000 ft/sec compared to 11 km/sec or 36000 ft/sec). This mission also looks desirable.

4. Impact of Asteroid Flyby on Comet Encounter

From the preceding discussion, the following primary impacts of combining asteroid flyby missions with the basic comet mission can be summarized, (Table III-4).

TABLE III-4 IMPACT OF COMBINING ASTEROID FLYBYS UPON BASIC COMET MISSION

- o Requires additional propulsion system and propellant
retargeting ΔV from 130 m/sec (427 ft/sec) to 940 m/sec (3094 ft/sec)
- o Increases comet flyby velocity
from 18 km/sec (59K ft/sec) to 26 km/sec (85K ft/sec)
- o Increases total mission duration
from 3 months up to 1 year 8 months
- o Decreases tail passage time
from 13 1/2 hrs (maximum) to 1 hr. (minimum)
- o Increases injected weight available
from 335 kg (739 lb) up to 560 kg (1235 lb)

C. NAVIGATION FEASIBILITY

1. Introduction

The navigation analysis was limited to the investigation of two sample missions. These missions selected were the reference mission (simplest from a navigation standpoint) and the double combined mission to Geographos and Toro (most complex). The targeting strategy for these missions and propulsive maneuver requirements for a 99 percentile level are discussed.

In parallel with this work, has been a continuing effort to obtain information on comet and asteroid(s) ephemeris errors for the 1980 opportunity to evaluate target dispersions. Informal contacts have been made (refs. III-2 and III-3) with Dr. B. G. Marsden (Smithsonian Astrophysical Observatory) and Dr. Elizabeth Roemer (Lunar and Planetary Laboratory, Tucson, Arizona) in this area. Because of the magnitude of the expected one-sigma ephemeris errors (typically expected to exceed 1000 km without on-board navigation), it will be shown that the influence of targeting dispersions due to position knowledge and maneuver execution can be neglected. The effects of these ephemeris uncertainties on the science results are also presented.

A brief assessment of on-board optical navigation requirements and capabilities for the reference mission was conducted, and the possible application of this technique to the combined mission is discussed.

Finally, dispersions in the approach geometry for the various targets (with and without on-board navigation) are tabulated and discussed.

2. Targeting Strategy and Propulsion Requirements

a. Reference Mission - A navigation analysis has been performed for the reference mission and the results and assumptions are summarized in Table III-5. The strategy selected assumed that the first mid-course maneuver would be made at 5 days after launch and the final mid-course maneuver at 5 days before encounter. This strategy should provide adequate tracking prior to the first and final mid-course maneuvers. The final mid-course maneuver time is a trade between accuracy of comet ephemeris knowledge and mid-course propellant expenditure. This maneuver can be executed later if desired at a ΔV cost that will be approximately inversely proportional to time from encounter.

The post-launch trajectory dispersions are caused primarily by the TE364-4 stage injection errors (as noted) and required a first midcourse correction allowance (99 percentile value) of 101.2 m/sec (332 ft/sec). The second mid-course maneuver (99 percentile value) would require 12.1 m/sec (40 ft/sec). The total ΔV allowance ($\Delta V_{.99}$) for the mid-course corrections on the reference mission is 106.6 m/sec (350 ft/sec).

The dispersions at Encke arrival (particularly in radius of close approach of the nucleus) are completely dominated by the ephemeris errors, so that the errors from tracking knowledge and execution at the final mid-course maneuver can be neglected. If updated ephemeris knowledge were transmitted to the spacecraft at the time of the final mid-course maneuver, the ΔV budget for the final maneuver (at E-5 days) would change by approximately 2.3 m/sec (7.6 ft/sec) per 1000 km (3.281×10^6 ft) change in targeting radius.

b. Encke/Geographos/Toro Mission - A typical Encke/Geographos/Toro trajectory within the 10-day launch period shown on Figure III-15 was analyzed (ref. III-5) as being representative of a complex comet/asteroid mission. The

TABLE III-5 NAVIGATION REQUIREMENTS FOR REFERENCE MISSION

INJECTION ERRORS - ATLAS D/CENTAUR/TE364-4 (ref. III-4)

Sigma Position	1.4 km Radially
Sigma Velocity	6.7 m/s Along V vector

MID-COURSE CORRECTIONS

1. Launch + 5 Days

Mean $\Delta V = 38.5$ m/s

Sigma $\Delta V = 21.0$ m/s

$\Delta V_{.99} = 101.21$ m/s (99 percentile)

2. Encounter - 5 Days

Mean $\Delta V = 4.7$ m/s

Sigma $\Delta V = 2.46$ m/s

$\Delta V_{.99} = 12.05$ m/s

3. Total $\Delta V_{.99}$ Required = 106.6 m/s

EPHEMERIS ERROR

1000 km (estimated one-sigma value)

launch date for this mission was 8-4-1980 and the Encke arrival date was 11-8-1980.

It should be noted that the magnitude of the retargeting maneuvers differ between the simple conic program (for calculating contours) and the integrated trajectory program (for the navigation analysis). The major difference in the two total velocities, however, was due to a decision to make the second maneuver 2 days after Geographos encounter (rather than immediately after encounter.) Table III-6 shows a comparison of these planned mid-course maneuver magnitudes. The larger value was actually used for the propulsion analysis (See Chapter V).

Six additional trim maneuvers were chosen as follows:

Launch + 5 Days (L+5)

Encke Encounter - 5 Days ($E_E - 5$)

First Maneuver + 10 Days (PMC1 + 10)(i.e., first planned midcourse maneuver.)

Geographos Encounter - 5 Days ($E_g - 5$)

Second Maneuver + 10 Days (PMC2 + 10)

Toro Encounter - 5 Days ($E_T - 5$)

The following tracking schedule was assumed for the analysis:

5 days of tracking after Earth orbit insertion

30 days before each pre-encounter maneuver

30 days bracketing PMC1 (PMC1-20 to PMC1+10)

30 days bracketing PMC2 (PMC2-20 to PMC2+10)

Further assumptions were made concerning dynamic noise, measurement noise, solar radiation pressure effects, and station location errors. Dynamic noise is assumed to perturb the flight with a spherical acceleration dispersion (radius = 3 mm/sec^2). The execution error model chosen for the analysis was as follows:

$$\begin{aligned}\sigma_{\text{Proportionality}} &= 3.33 \times 10^{-3} \\ \sigma_{\text{Resolution}} &= 3 \times 10^{-6} \text{ km/s} \\ \sigma_{\text{Pointing}} &= 1/3 \text{ deg}\end{aligned}$$

A measurement noise variance was assumed, equivalent to the JPL value of 1 mm/sec for a 60 sec count time. Uncertainty in the solar radiation pressure was modeled as an acceleration corresponding to a location midway between the orbits of Earth and Venus. The equivalent station location errors assumed are as follows, and completes the explicit set of assumptions used in the analysis.

$$\begin{aligned}\sigma_{RS} &= 4.05 \text{ meters (distance from Earth spin axis)} \\ \sigma_{\lambda} &= 3.70 \text{ meters (longitude)} \\ \sigma_Z &= 10 \text{ meters (Z-height)} \\ \sigma_{\lambda\lambda} &= 0.9 \text{ (longitude correlation between stations)}\end{aligned}$$

Table III-7 presents the dispersions produced by the assumed trim maneuver schedule. The trajectory control and knowledge are mapped forward to the target times (indicated in the last column) and result in ellipsoids whose semi major axes are listed in the first two columns. The final dispersions noted are 54 km (177×10^3 ft) at Encke, 184 km (603.7×10^3 ft) at Geographos, and 271 km (889×10^3 ft) at Toro. Note again that the dispersions at the target are dominated by the target ephemeris errors, as noted in Table III-5.

In Table III-8, the mean and sigma values for each trim maneuver are listed. The ΔV budget for each maneuver is shown for the 99 percentile level (as was selected for the reference mission). Also shown is the total $\Delta V_{.99}$ trim budget of 105.5 m/sec (346 ft/sec) which when combined with the 960 m/sec (3150 ft/sec) retargeting maneuver budget produces a total propulsion ΔV requirement of 1065.5 m/sec (3496 ft/sec).

It has also been observed for this mission, that velocities may be difficult to observe during the last four tracking arcs because the low inclinations to the plane of the sky during these periods. The geocentric declinations are also low during the tracking period for the first retargeting maneuver and also during the near-Toro tracking. Changing the retargeting maneuver positions suggests one possible improvement which could be made. Another good possibility would be to use more sophisticated tracking techniques (eg. QVLBI).

TABLE III-6 COMPARISON OF RETARGETING ΔV REQUIREMENTS COMPUTED BY
CONIC AND INTEGRATED TRAJECTORY PROGRAMS (AIMS AND MIT)
(ENCKE/GEOGRAPHOS/TORO MISSION)

MANEUVER	TIME	$\frac{\Delta V}{(m/sec)}$ (MIT)	$\frac{\Delta V}{(m/sec)}$ (AIMS)
* PMC 1	** E _g - 187	122.4	166.4
PMC 2	E _g + 2	<u>837.6</u>	<u>739.2</u>
	TOTAL	960.0	905.6

* PMC = Planned Mid-Course Maneuver for Retargeting

** E_g = Geographos Encounter

TABLE III-7 SEMI-MAJOR AXES OF DISPERSION ELLIPSOIDS AT TARGET
ENCOUNTER* (ENCKE/GEOGRAPHOS/TORO MISSION)

MANEUVER	TIME	SEMI-MAJOR AXIS (KM)		TARGET POINT
		BEFORE MANEUVER	AFTER MANEUVER	
MC1	L+5	522,257	1935	E _E
MC2	E _E -5	1938	54	E _E
MC3	PMC1 + 10	33841	1304	E _g
MC4	E _g -5	1331	184	E _g
MC5	PMC2+10	120896	1157	E _T
MC6	E _T -5	1159	271	E _T

* MC = Mid-Course

Subscripts: E = Encke; G = Geographos; T = Toro

TABLE III-8 STATISTICAL PARAMETRIC VALUES OF THE ΔV BUDGET FOR
INDIVIDUAL AND TOTAL TRIM MANEUVERS
(ENCKE/GEOGRAPHOS/TORO MISSION)

MANEUVER	TIME	MEAN ΔV m/s	SIGMA ΔV m/s	$\Delta V_{.99}$ m/s
MC1	L+5	32.9	18.1	86.8
MC2	E _E -5	4.72	2.46	11.92
MC3	PMC1+10	1.01	0.44	2.26
MC4	E _g -5	2.97	1.74	8.13
MC5	PMC2+10	6.83	3.12	15.78
MC6	E _T -5	2.43	1.54	6.98

Total Budget ($\Delta V_{.99}$ Total) 105.5 m/s

Equivalent f Sigma Level = 2.923 Sigma

3. Effect of Comet and Asteroid Ephemeris Errors

Because of the importance of imaging the nucleus of the comet (and sampling the coma and tail environment) and also imaging the asteroid at close distances, the subject of ephemeris errors is very important. Table III-9 shows the impact of assumed ephemeris knowledge uncertainties upon the feasibility of the various missions without on-board navigation. This certainly emphasizes the need for a concerted effort to improve the knowledge of ephemeris data on both the comet (1980 apparition) and the two asteroids of interest, irrespective of whether or not on board navigation is a consideration. The degree to which such an effort should be extended may be influenced by the presence of an on-board system as will later be discussed.

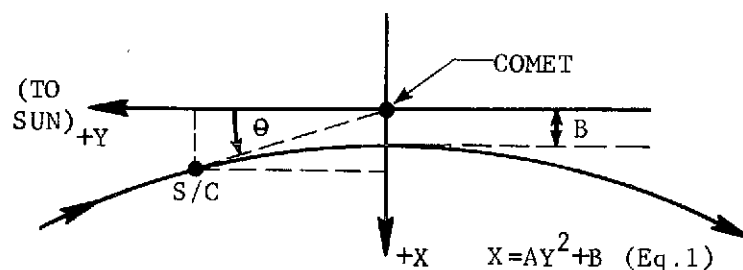
TABLE III-9 EFFECT OF EPHEMERIS UNCERTAINTIES
(WITHOUT ON-BOARD NAVIGATION)

Assumed (3-sigma) Position Error (km)	1500	3000	4500
1. Encke Flyby and Probe Missions (Flyby desired at 5000 km)			
Minimum Flyby Radius (Safety Zone)-km	3500	3500	3500
Nominal Flyby Radius (Targeted)-km	5000	6500	8000
Maximum Flyby Radius - km	6500	9500	12500
Quality of Flyby Science	Acceptable Imaging and Mass. Spec.	Acceptable Imaging Marginal Mass Spec.	Marginal Nucleus Imaging Poor Mass Spec.
Quality of Probe Science (2-sigma errors accepted)	Acceptable	Marginal	Poor
2. Missions Involving Geographos (500 km flyby desired)			
Quality of Imaging Science	Poor	Poor	Poor
3. Missions Involving Toro (500 km flyby desired)			
Quality of Imaging Science	Poor	Poor	Poor

4. Assessment of On-Board Navigation Requirements and Capabilities

A brief investigation was made to assess the potential of on-board navigation for the basic reference mission. Because of the uniqueness of the reference trajectory (in comet's plane and zero approach angle) it was possible to approximate the spacecraft/comet relative motion (as shown in Figure III-8) with a parabola at near encounter conditions.

This approximation then allowed a closed-form solution with the following simplifying assumptions.



- 1) B is nominally zero (A calculated to be $2.94 \times 10^{-8}/\text{KM}$).
- 2) B is taken to be the miss distance. The quantity B is estimated by observing Θ (angle between line of sight and Comet/Sun vector) during approach (starting at E-6 days).
- 3) Approach velocity (V_H) was assumed constant during the observation periods (E-6 to E-5 and E-6 to E-2 days).
- 4) Parameters A and B solved for separately.
- 5) Mariner-class optical system assumed (i.e., narrow F.O.V. camera selected for science package).

Errors due to noise only were analyzed assuming a weighted least squares filter with no weight given to the "a priori" estimate. Bias error was found to RSS in with the noise to produce an effectively noisier instrument, i.e.:

$$\sigma_B = \left[\sigma_N^2 + \sigma_{\text{Bias}}^2 \right]^{\frac{1}{2}} K$$

Where: σ_N = Data Noise
 $K = \left[\frac{1}{D} \right]^{\frac{1}{2}}$
 D = Data Rate

For: $\sigma_N = \sigma_{\text{Bias}} = 1 \text{ pixel}$

The resultant $\sigma_B = 52.5 \text{ km at E-5 days.}$

An estimate was also made for the out-of-plane error (σ_z) assuming it to be essentially uncoupled from the in-plane problem. For this out-of-plane case the spacecraft relative velocity was assumed equal to the range rate, which again permitted a closed form solution.

Figure III-21 summarizes the results of this investigation for the following conditions:

1) In-Plane Errors

- a) One day of tracking (E-6 to E-5) versus four days of tracking (E-6 to E-2)
- b) Noise only errors (1 pixel and 5 pixels)
- c) Noise plus bias (1 pixel and 5 pixels combinations)
- d) Data rates (TV pictures per day = 10, 5 and 2)

2) Out-Of-Plane Errors

Considers noise only errors (1 pixel and 5 pixels) and the maximum data rate (10 per day) for the two tracking arcs.

The results indicate that to obtain in-plane accuracies near the acceptable reference trajectory region of Table III-9 one day of tracking at a data rate of two TV pictures per day would provide satisfactory performance with the maximum values of 5 pixels of noise and 5 pixels of bias assumed. Similar results are indicated for the out-of-plane case.

By increasing the data rate to 5 pictures per day and a one day tracking arc, σ_B should be reduced to under 200 km (for the intermediate noise and bias error levels).

Further reductions (approaching 100 km error or less) would probably be realized by increasing the tracking arc to four days.

5. Expected Dispersions in Approach Geometry

Table III-10 presents a summary of anticipated dispersions in target approach geometry, based upon subjective evaluations of presently predicted ephemeris errors with and without on-board optical navigation. All errors

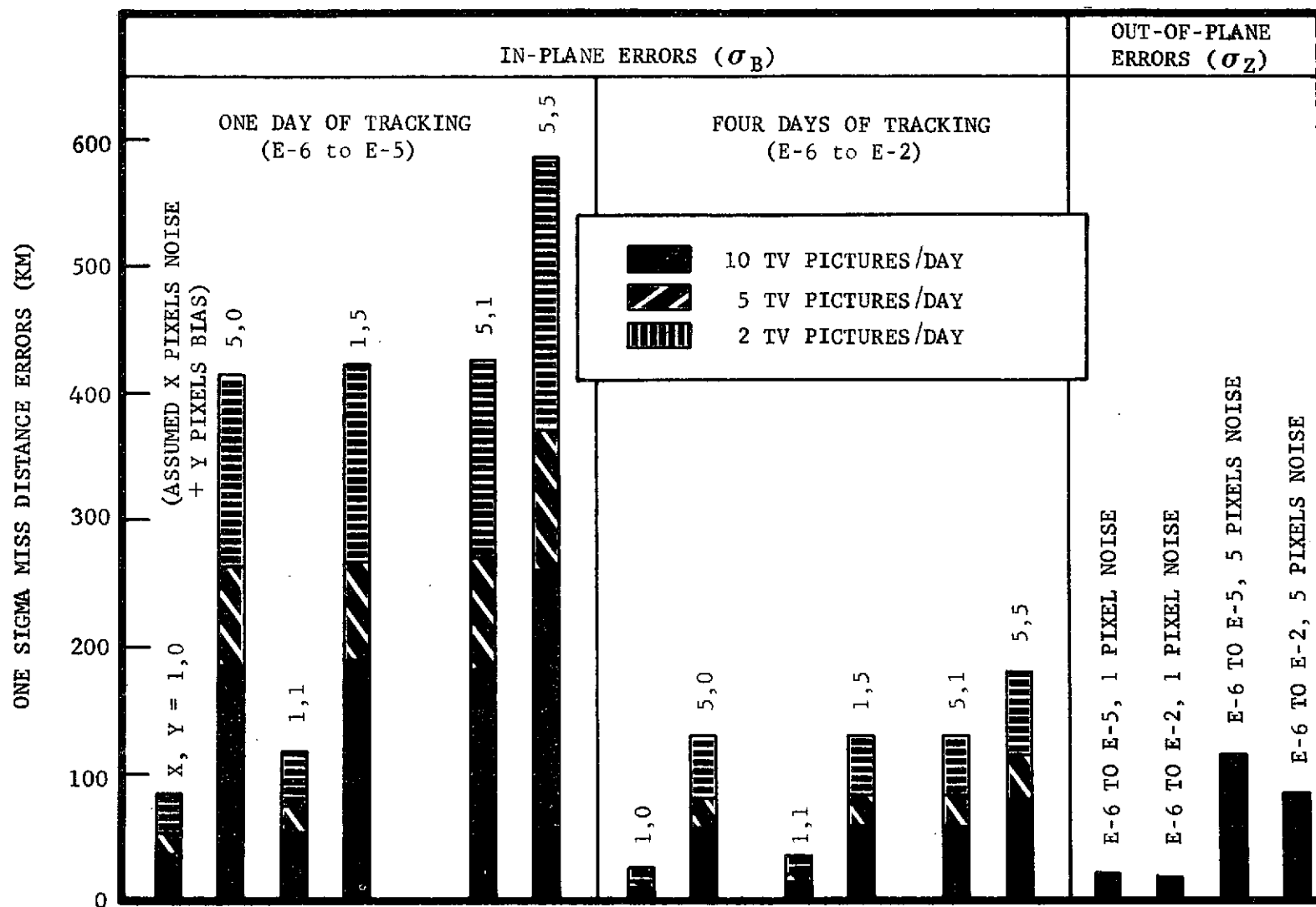


FIGURE III-21 ESTIMATED COMET EPHEMERIS ACCURACIES WITH AN ON-BOARD OPTICAL SENSOR

TABLE III-10 ANTICIPATED DISPERSIONS IN TARGET APPROACH GEOMETRY

	ENCKE MISSION (5000 km Flyby)	AT GEOGRAPHOS 1 (500 km Flyby)	AT TORO (500 km Flyby)
A. WITHOUT ON-BOARD NAVIGATION			
1. 3-Sigma Position Error Anticipated (km)	3000	4000-8000	8000-12000
2. Possible Effect Upon Mission	Acceptable Imaging Marginal Mass Spec. Marginal Probe Mission With 2-Sigma Errors	Unacceptable Asteroid Imaging	Unacceptable Asteroid Imaging
B. WITH ON-BOARD NAVIGATION*			
1. 3-Sigma Position Error Anticipated (km)	500-1000	Probably Exceeds 1000	Probably Exceeds 1000
2. Possible Effect Upon Mission	Acceptable In All Areas With And Without A Probe	Probably Acceptable -Investigate Further	Questionable Acceptability - Investigate Further

* Assumes intermediate noise and bias error levels (2-3 pixels); 2 pictures per day; 4 days of tracking.

are 3-sigma anticipated error values, except where noted.

The 3000 km (9.84×10^6 ft.) predicted position uncertainty for the Encke 1980 opportunity assumes that a significant effort will be mounted to dedicate several observatories to tracking the comet at forthcoming close approach opportunities so that better observational data is available for improving the model of non-gravitational forces. It also assumes that one or more observatories will operate in conjunction with other mission operational facilities to update ephemeris knowledge during the actual flight.

The degree to which the preceding effort would progress would probably depend upon the decision concerning optical sensors (as indicated in Reference III-7). If the decision were made early to include optical navigation on the spacecraft, it might not be necessary to have as intensive an effort to reduce ephemeris errors of the comet.

The ability to determine, from Earth, the angular position of Geographos and Toro relative to a star background would seem to be better than for Comet Encke (as suggested in Reference III-2). However, due to the large tracking distances (approaching 2 AU) before encounter, the anticipated ephemeris position errors are substantially higher. The anticipated errors are 4000-8000 km (13.1×10^6 - 26.2×10^6 ft.) for Geographos and 8000-12000 km (26.2 - 52.5×10^6 ft.) for Toro.

Since the desirable flyby radius is 500 km with the imaging system used, the anticipated miss uncertainties (without optical sensors) would be unacceptable. Position error uncertainties with on-board navigation probably would exceed 1000 km (3.28×10^6 ft.), although much analysis is needed in this area to put reasonable limits on these numbers.

The major conclusions that can be drawn from our current knowledge can be summarized as follows:

- 1) The basic flyby mission without probes can probably be performed without optical sensors, but a concerted effort is needed between now and 1980 (and during the mission) to improve Earth-based ephemeris knowledge of the comet.
- 2) The basic flyby mission with probe(s) is marginal for probe

science return without optical navigation.

- 3) As long as it is desirable to obtain knowledge on asteroid surface characteristics (and not just overall size or shape) it appears necessary to have on-board optical navigation.
- 4) Geographos 1 looks more attractive because of its low encounter phase angle (29 degrees) than Toro, as a candidate mission. Toro has a phase angle at encounter of ~ 78 degrees for the double-combined mission and ~ 114 degrees for the single mission, making acquisition more difficult.

IV. SPACECRAFT SYSTEM DESIGN EVALUATION

IV. SPACECRAFT SYSTEM DESIGN EVALUATION

The direction taken in the design phase of this study was based on several primary guidelines:

- Utilize light-weight, spinning spacecraft;
- Incorporate existing equipment to the maximum extent possible; and
- Base designs on the capability provided by the Atlas/Centaur/TE364-4 launch vehicle.

In the selection of subsystem components and spacecraft configuration details, extensive use was made of the results of studies performed for NASA/ARC by Martin Marietta Corporation and other contractors on advanced planetary missions.

The foregoing chapters have provided the science and mission background necessary for the establishment of general design requirements and constraints to be met by the spacecraft. The succeeding chapter on subsystem and science instrument designs includes individual summaries of pertinent requirements affecting the selection of preferred equipment. The purpose of this chapter is to assess the feasibility of spacecraft system design in terms of meeting the requirements imposed by science objectives and instruments, mission characteristics, and subsystem interfaces.

The science payload selected for the 1980 Encke mission opportunities is comprehensive in scope and demanding of spacecraft resources and capabilities. Visual imaging of small bodies (comet nucleus and asteroids) at high spacecraft/target relative velocities is in particular, a difficult task. The conflicting pointing requirements of the optical instruments and the "ram," or relative-velocity-oriented instruments (mass spectrometers and plasma probe), place additional constraints on system design. Accommodation of the science payload, along with the achievement of balanced subsystem performance, was approached in this study as follows. A basic spaceframe/solar array concept was selected and five variations of this basic concept were synthesized to evaluate several alternatives for meeting total system requirements imposed by the Encke reference mission and the selected instrument payload. Then, necessary modifications were made, first to accommodate probes, and then, to accomplish the combined comet-asteroid missions.

In the following sections, the five configurations will be described and then evaluated with respect to: 1) Performance in the various mission options; and 2) Ability to meet scientific objectives. Chapter V (Subsystem Design) contains detailed supporting material for the present chapter and will be referenced as appropriate.

A. DESCRIPTION OF OPTIONS STUDIED

The five spacecraft configuration concepts developed in the study are shown in Figures IV-1 through IV-5 and, for ease of reference, are identified by number. With the exception of Concept 5, each incorporates the payload shown in Table IV-1. In Concept 5, the two television cameras are replaced by a single spin-scan camera. All concepts incorporate a high-gain antenna

TABLE IV-1
ENCKE-MISSION SCIENCE INSTRUMENTS

Narrow Angle (NA) Television Camera
Wide Angle (WA) Television Camera
Ultraviolet Spectrometer
Visible Spectrum Radiometer
Ion Mass Spectrometer
Neutral Mass Spectrometer
Plasma Probe
Plasma Wave Detector
Langmuir Probe
Cosmic Dust Analyzer
Triaxial Fluxgate Magnetometer

for continuous Earth pointing. The achievable data rates, in conjunction with a data system tape recorder, are adequate for the science measurement sequences defined in Section V-I. The common solar array arrangement (section V-F) can provide the power required by the selected subsystems and payload. All configurations also have a common hydrazine monopropellant reaction control system (section V-E) which is used for midcourse navigation maneuvers as well

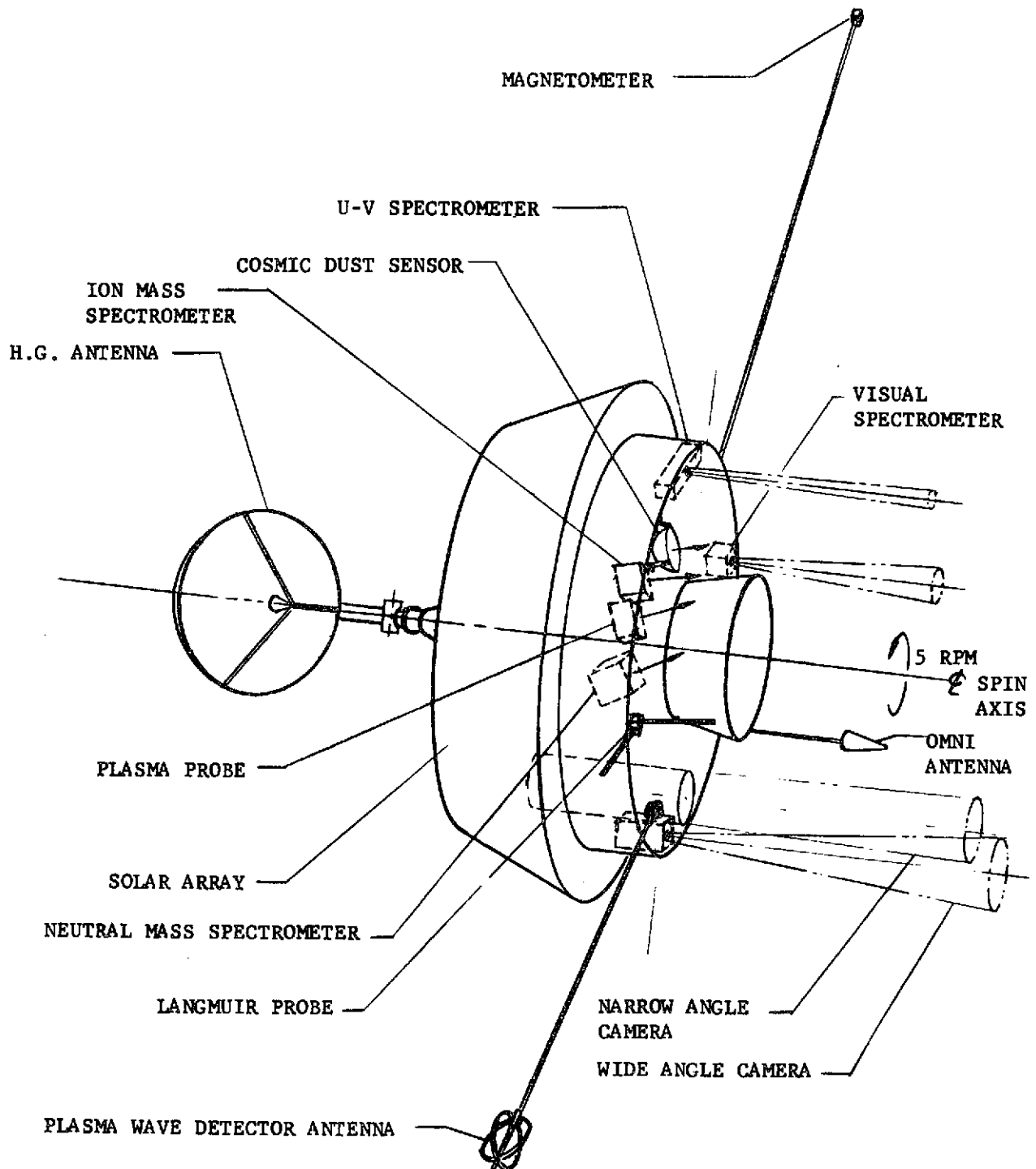


FIGURE IV-1 SPIN AXIS POINTS TO ENCKE - CONCEPT NO. 1

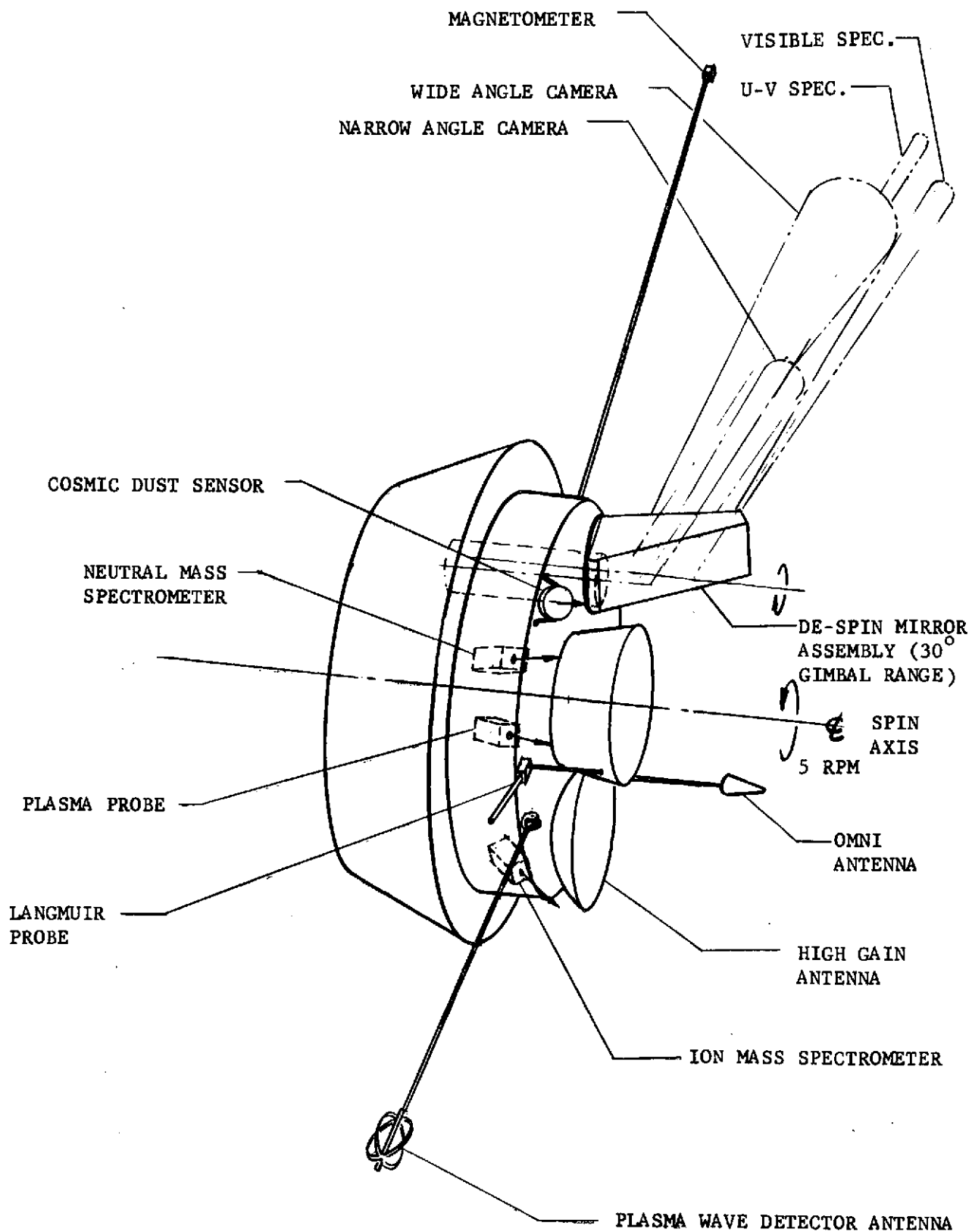


FIGURE IV-2 SPIN AXIS POINTS TO EARTH - CONCEPT NO. 2

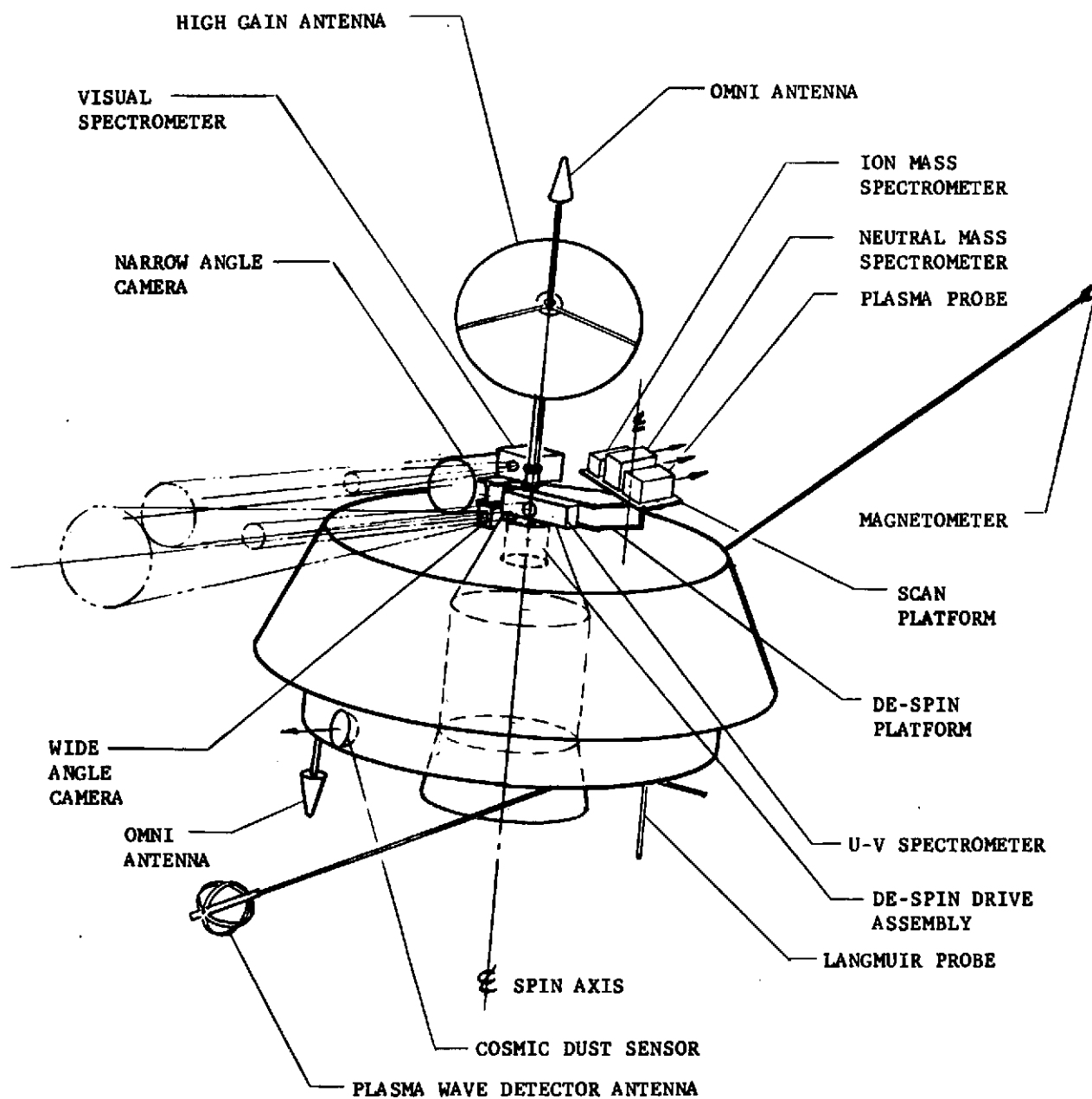


FIGURE IV-3 SPIN AXIS PERPENDICULAR TO EARTH/ENCKE/SPACECRAFT PLANE
(DE-SPUN PLATFORM) - CONCEPT NO. 3

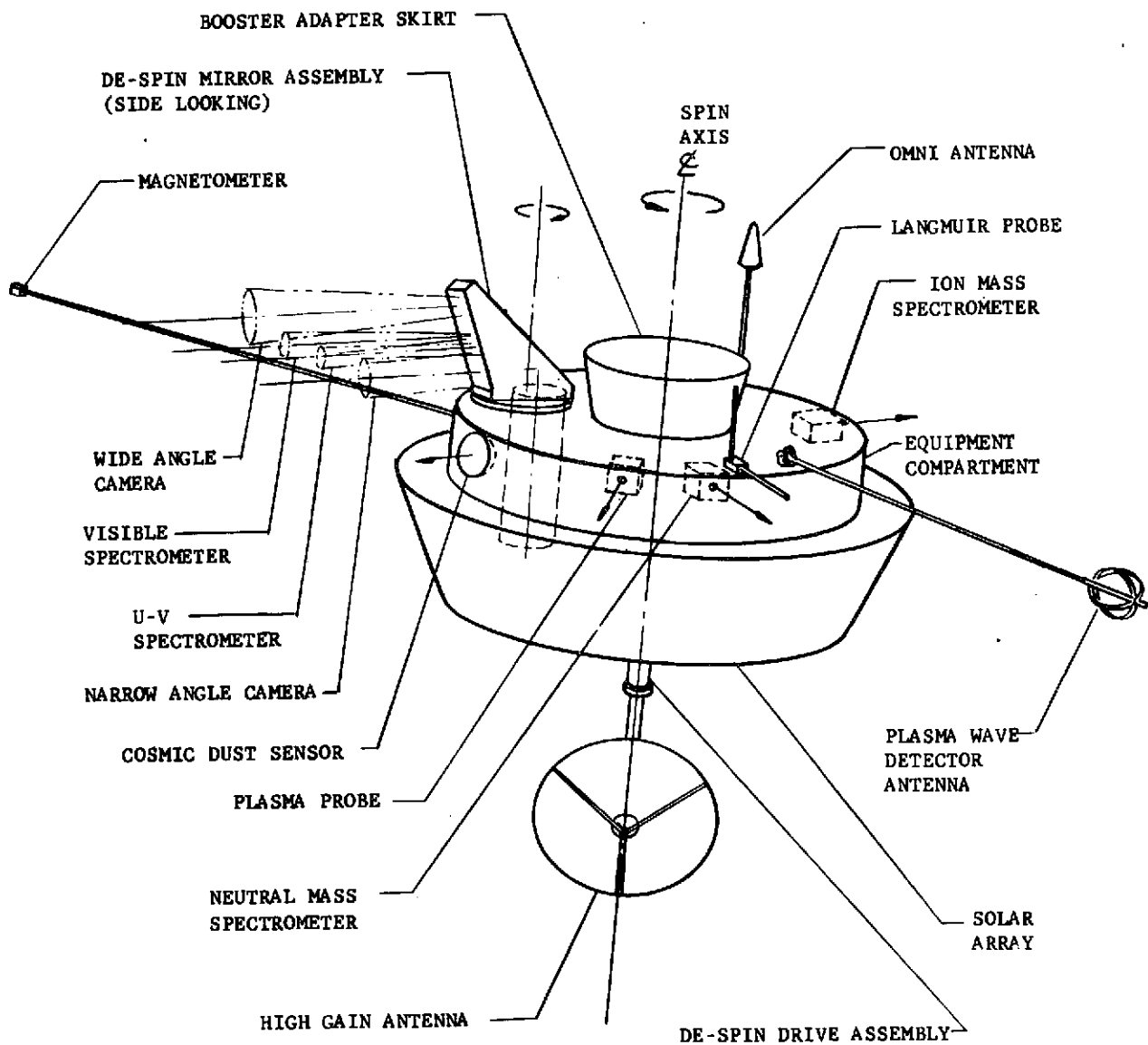


FIGURE IV-4 SPIN AXIS PERPENDICULAR TO EARTH/ENCKE/SPACECRAFT
PLANE (DE-SPUN MIRROR) - CONCEPT NO. 4

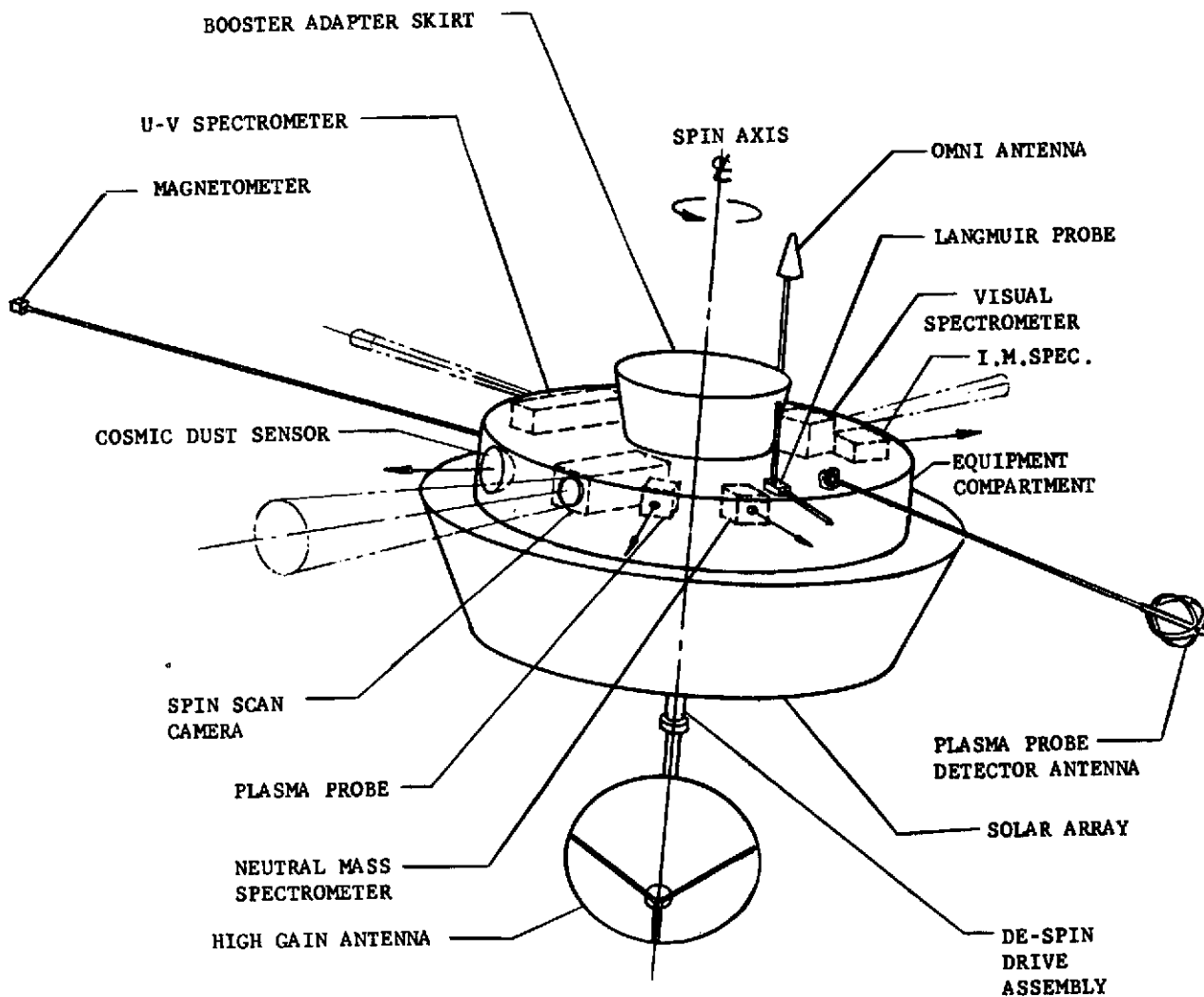


FIGURE IV-5 SPIN AXIS PERPENDICULAR TO EARTH/ENCKE/SPACECRAFT PLANE (SPIN SCAN CAMERA) - CONCEPT NO. 5

as attitude control. Variations in the attitude control systems, discussed in Section V-D, are related to the methods incorporated in each spacecraft concept for instrument pointing.

The five concepts evolved in an effort to maintain a high level of scientific accomplishment within reasonable limits of subsystem performance. A major consideration, in each case, was to minimize the effects of high target-approach velocity and spacecraft spin on the quality of imaging data. (The associated common problems of acquiring and tracking the target are discussed in section V-D and V-I.) In Concept 1, for example, the science instruments are rigidly installed on the equipment compartment with their lines of sight parallel to the spacecraft spin axis which is pointed toward the target body. Smear of the television image is thus limited to twist (due to spacecraft rotation). Spin axis precession is the method used to track the target. The ram instruments are also shown as rigidly installed, but canted at 20° to operate in a spin scan mode aligned with the relative velocity vector up till E-4 min during comet fly-through.

In Concept 2, the spin axis is pointed toward Earth, and communication is maintained with a fixed-dish antenna. The visual instruments are shown rigidly mounted and pointed along the spin axis. A despun, single-axis gimbaled mirror is used to track the target body. The ram instruments are shown rigidly mounted, but canted approximately 50 degrees from the spin axis. This provides proper orientation in a spin-scan mode. The notable feature of Concept 3 is the de-spun platform for both the visual and ram-directed instruments. In this configuration, the television system is subjected to the least smear. The ram instruments are mounted on an additional scan platform to maintain proper viewing. The high gain antenna is also on the despun platform and has its own scan motor, thus permitting continuous Earth pointing. An attitude with the spin axis perpendicular to the plane containing Earth, Encke, and the spacecraft is maintained in this concept to preclude gimbaling of the despun antenna. Since the Encke encounter occurs above the ecliptic plane, the spacecraft spin axis must be tilted to maintain pointing. An "antenna-down" orientation is therefore required to avoid sunlight on the thermal control louvers.

The orientation of Concept 4 is the same as for Concept number 3. However, the visual instruments are fixed to the spacecraft and view the target through a despun mirror assembly. The mirror, in this case, is fixed at 45 degrees and is much smaller 69 cm (27 in) by 43 cm (17 in) than the gimbaled-127 cm -(50 in) mirror of Concept 2.

Concept 5 was generated to incorporate spin-scan imaging. All instruments are fixed and, therefore, operate in a spinning mode. As shown, the spin-axis is oriented in the same manner as the two previous configurations.

Table IV-2 summarizes the significant differences in the five concepts investigated.

For the missions which include asteroid encounters, additional propulsion capability is required. The Encke-Geographos mission can be performed by merely increasing RCS tankage. For the other asteroid missions, however, it has been determined that a bipropellant main propulsion system must be added to all the spacecraft concepts as shown in Figure IV-6. Concept 2 (Earth-pointing) requires, in addition, that a second high-gain antenna be installed opposite to the one shown in Figure IV-2. Because of Earth-Sun geometry, the spacecraft must be "flipped" about 40 days after Encke encounter to maintain illumination of the solar panels.

B. PROBE INSTALLATION CONCEPT

The coma probe design developed in this study (Section V-A) is quite simple compared to probes designed to penetrate dense planetary atmospheres. The absence of a sensible "atmosphere" in the comet (Appendix C) removes the requirement for extensive aerodynamic and thermal control provisions. As a result, the Encke-mission probe is a simple cylinder.

It was concluded in Chapter II that a single probe was an appropriate complement for the Encke spacecraft. Figure IV-7 shows the location of the installed probe which would be separated from the spacecraft with explosive nuts and springs to impart the necessary separation velocity.

For spacecraft Concepts 1 and 3, the probe will be located in the aft end of the booster adapter cone. For the asteroid missions, this adapter

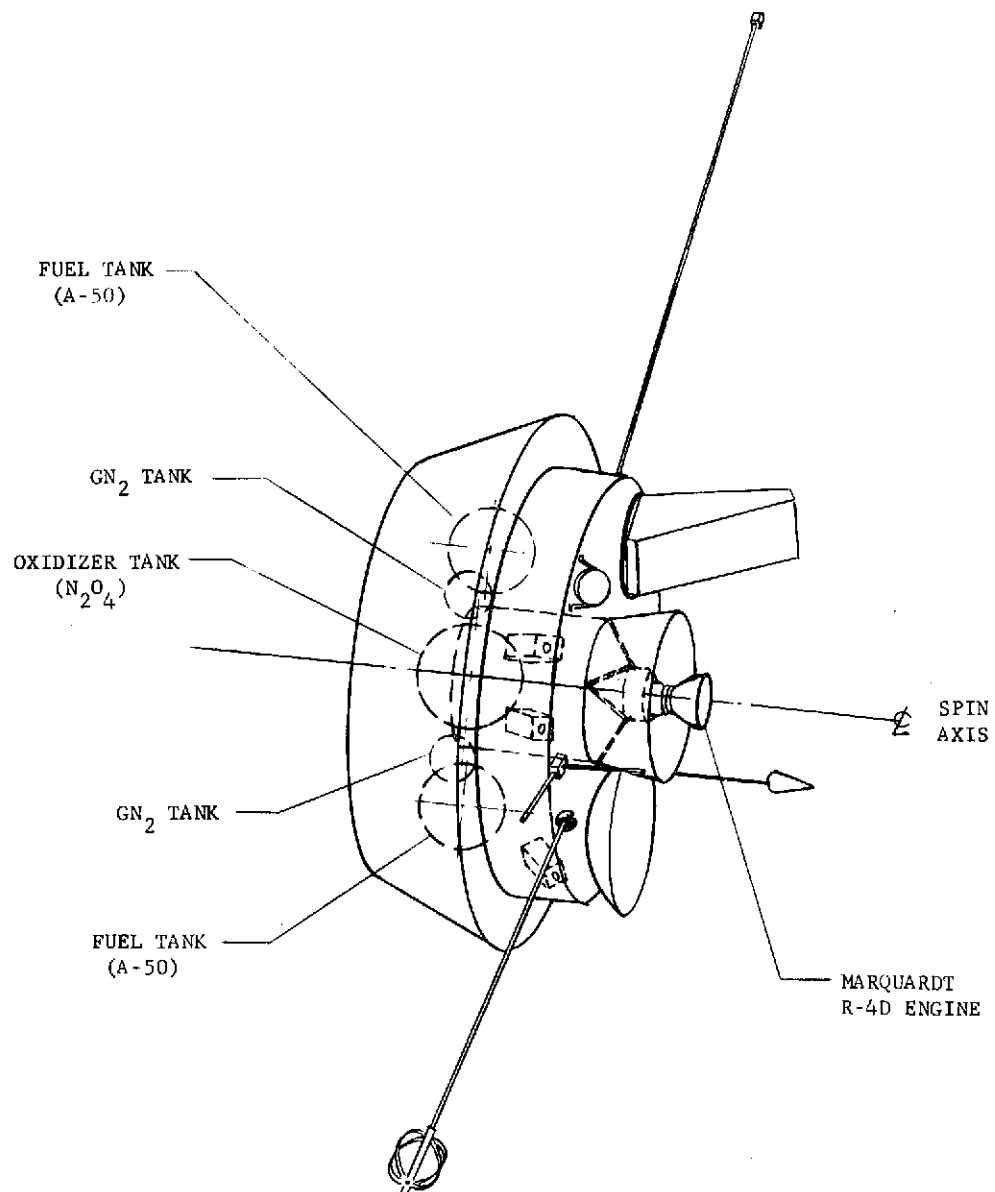
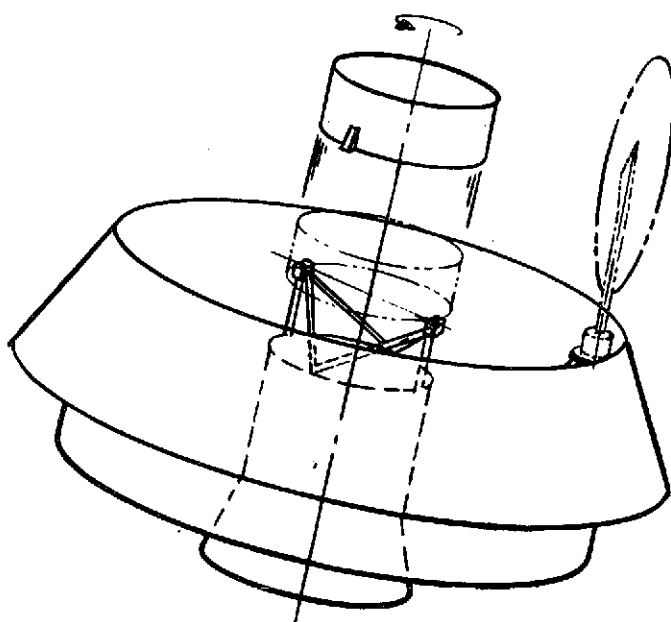


FIGURE IV-6 ASTEROID MANEUVER PROPULSION INSTALLATION

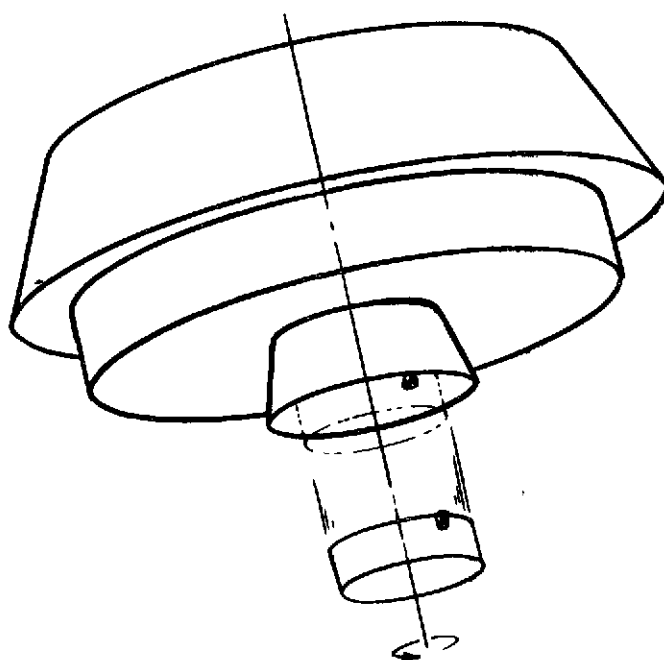
TABLE IV-2 SUMMARY OF CONCEPT CHARACTERISTICS

	<u>1</u>	<u>2</u>	<u>CONCEPT</u> <u>3</u>	<u>4</u>	<u>5</u>
<u>Characteristics</u>					
Spin-Axis Direction	to Target	To Earth	*	*	*
Antenna	Despun	Fixed	Despun	Despun	Despun
Optical Instruments	Fixed	Fixed	Despun	Fixed	Spin Scan
	Point S/C	Despun Mirror	Platform	Despun Mirror	
Ram Instrument	Fixed	Fixed/ Canted	Despun Platform	Fixed	Fixed

* Perpendicular to Earth-Spacecraft-Encke Plane



FORWARD PROBE CONCEPT



AFT PROBE CONCEPT

FIGURE IV-7 PROBE LOCATION CONCEPTS

location is occupied by a required additional propulsion system. The probe then will be installed on the aft end of the vehicle but offset from the center enough to clear the booster adapter structure. This location may require a balancing mass to be installed and jettisoned with the probe. For Concept 2, the probe could be installed above the central cylinder for all missions. The additional high gain antenna required on the forward end for the asteroid missions would be offset from the center and would rotate aside to provide enough clearance for probe separation. For Concepts 4 and 5, the probe is installed above the central cylinder for all missions. The despun high-gain antenna must be positioned off-center to provide clearance for probe separation.

C. COMPARISON OF SPACECRAFT CONCEPTS

In this section, the five spacecraft concepts will be compared with respect to mission performance compatibility, effects on science accomplishment, and technical requirements.

1. Mission Performance Compatibility

Table IV-3 is a summary of the mass of each spacecraft concept, with and without probes, on three of the five missions investigated. It was shown in Chapter III that the mission to Encke with a subsequent encounter of Geographos near one AU was not an acceptable mission. The Encke-Toro mission has also been deleted as an acceptable option because the low allowable spacecraft weight (375 kg) is not consistent with the required addition of a main propulsion system to provide a 615 m/sec velocity change. The three missions shown, therefore, represent the preferred options within mission and launch vehicle constraints.

The spacecraft masses shown for the Encke-only mission are, with the exception of Concept 3, within launch vehicle capability of the reference mission which maximizes the time spent in the comet environment. The higher mass of Concept 3 and of all the concepts in a probe mode can be launched to Encke by the Atlas/Centaur TE364-4 by varying encounter conditions at Encke with a resulting reduction in tail-passage time (fig. IV-8). It has been concluded that this results in a minimal effect on science

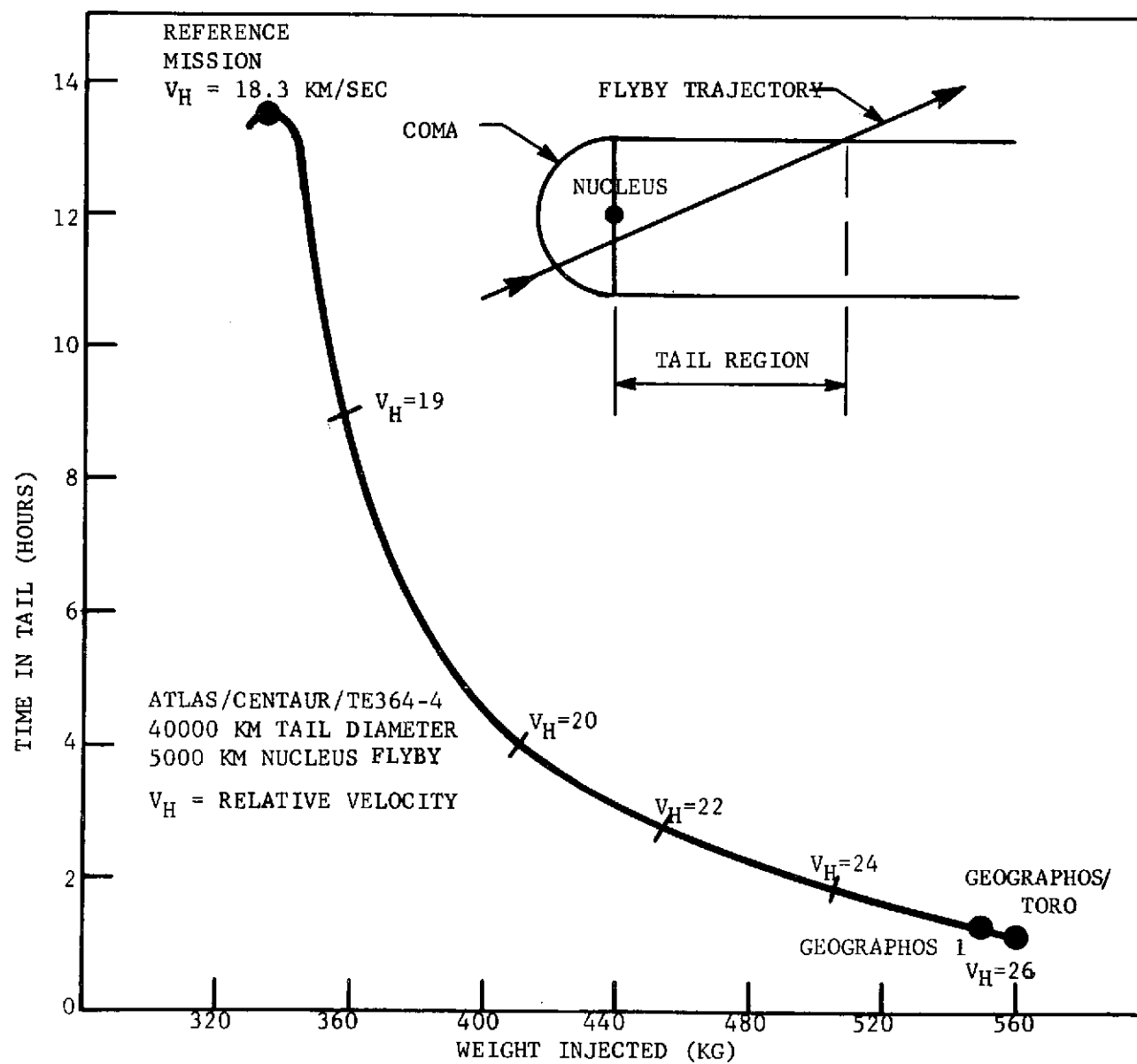


FIGURE IV-8 ESTIMATED TIME IN COMET TAIL FOR SPACECRAFT WEIGHT INJECTED

TABLE IV-3 SPACECRAFT MASS COMPARISON

CONCEPT	MISSION MODE				
	ENCKE-ONLY		ENCKE-GEOGRAPHOS		ENCKE-GEOGRAPHOS-TORO
	<u>NO PROBE</u>	<u>PROBE</u>	<u>NO PROBE</u>	<u>PROBE</u>	<u>NO PROBE</u>
1	332 kg	388 kg	370 kg	432 kg	569 kg
2	326	382	365	424	561
3	358	415	397	455	609
4	332	388	370	432	570
5	299	353	337	394	515
L/V Capability	Minimum = 335 (Ref. Mission)		550		560

NOTE: Spacecraft Mass Estimates Include 10% Design Margin

accomplishment. A considerable launch-performance margin is available in the Encke-Geographos mission, even with a probe installed on the spacecraft. The double-asteroid mission, however, presents a considerably different situation. When no probes are carried, Concepts 2 and 5 are compatible with the mission-imposed weight constraint on this mission. Concepts 1 and 4 are less than two percent above this constraint, and design refinements or science modifications could yield acceptable weights. For the configurations carrying probes, none of the resulting weights are within launch vehicle capacity when the nitrogen-tetroxide/Aerozine-50 propulsion system is used for the major course-change maneuvers. A brief analysis (Section V-E) showed that an advanced space-storable propulsion system would not provide sufficient performance to carry a probe on this mission option except for Concept 5.

2. Configuration Impact on Science Accomplishment

The five spacecraft configurations studied are all spinning spacecraft, but each differs in pointing or despun complexity. In this section, the impact on science for each of the configurations is assessed. The imaging and optical instruments (i.e., UV, Visual spectrometer, and IR) are covered first, followed by mass spectrometers, plasma probe, and cosmic dust detector. The remaining particle and field detectors prefer the spinning spacecraft mode and are not appreciably effected by the five spinning configurations. Table IV-4 lists the major discussion points.

Configuration 1 - (Encke Pointed) - Since the imaging and other optical instruments are target oriented, this configuration is attractive from the standpoint of instrument installation simplicity. A rotational smear is inherent in this pointing mode but is not a serious problem for short exposure times. However, attention must be given to camera alignment and spacecraft stability to maintain pointing for long exposure time (5-6 sec).

Some optical constraints occur near the nucleus or RCA in configuration number 1. At about E-6 minutes, the spacecraft axis precession become high enough to cause nutations which could interfere with the camera imaging. One way around this problem is to preposition the axis and allow a few minutes for nutation damping beginning before picture sequences near RCA. In the tail

TABLE IV-4 CONFIGURATION IMPACT ON SCIENCE

<u>SCIENCE CATEGORY</u>	<u>SPACECRAFT CONCEPT</u>				
	<u>No. 1</u> <u>(ENCKE POINT)</u>	<u>No. 2</u> <u>(EARTH POINT)*</u>	<u>No. 3</u> <u>(DESPUN)</u>	<u>No. 4</u> <u>(PERPENDICULAR)*</u>	<u>No. 5</u> <u>(SPIN-SCAN)</u>
Imaging/Optical	Good until near RCA	Good until RCA	No Restrictions	No Restrictions	Limited by camera technology
Mass Spectrometer	Full ram until near RCA, then restricted measurements	Partial ram in spin- scan throughout encounter	Full ram throughout encounter	Partial ram in spin- scan throughout encounter	Partial ram in spin- scan throughout encounter
Plasma Probe	Full ram until RCA, partial thereafter	OK (in spin- scan mode)	Full ram	OK (in spin- scan mode)	OK (in spin- scan mode)
Cosmic Dust	Full ram until RCA, partial thereafter	OK (in spin- scan mode)	OK (in spin- scan mode)	OK (in spin- scan mode)	OK (in spin- scan mode)

* Incorporates Despun Mirror

imaging sequences, a requirement for the spacecraft to maneuver, would be needed to look down the tail vector or at selected angles for photometric studies.

The mass spectrometer if boresighted down the relative velocity direction would operate well until about E-15 minutes of encounter. At that time, the spacecraft would have rotated to the extent that the ram velocity would be outside of the mass spectrometer acceptance angle. This is an important period during the mission. If the coma radius is only 20,000 km, at the mission rate of 18.3 km/sec, there are only 37 minutes of prime mass spectroscopy measurements in the coma.

The above loss of ram direction for the mass spectrometers could be eased by offsetting the mass spectrometer to the radius vector by 20° . This will add ~ 7 minutes of ram direction to the near encounter-spectrometer measurement time. Eventually, however, the "ram direction is lost at \sim E-6 min. A hinge mechanism (or one-axis platform) might be used then, but at an increase in complexity.

The plasma probe would not be Sun oriented but it would be Encke oriented in the present configuration without spacecraft maneuvering. The plasma probe would be well suited for comet/solar wind plasma in the early encounter. After RCA, reorientation of plasma probe for tail measurements seems advisable. Finally, the cosmic dust detector should operate well, as did the plasma probe, with Encke orientation. In lieu of better knowledge, particulate matter is assumed to come off of the nucleus in a uniform, radial direction. For tail measurements, the particulate detector should be reoriented for best operation.

Configuration 2 - (Earth Pointed) - This mode is preferred for communications with Earth. The optics instruments rely on a despun mirror that is gimballed to keep the target in constant view of the instruments. This, again, allows advantageous long viewing exposures for the optical instruments. The view is restricted to approximately 240° per revolution, because of spacecraft structure in the field of view, but this should be a minor inconvenience.

The limited size of the mirror can constrain viewing very near RCA. A condition occurs where the nucleus viewing is parallel to the spin axis and

the mirror is not long enough to permit this completely parallel viewing. The solution might be to swing the mirror out of the way at this point. Another solution is to target differently.

With equatorial passages by the nucleus, the mirror starts to look into the spacecraft at about E-5m. By targeting for a south pole passage at Encke, the nucleus viewing is extended to E=0. For IR measurements to E+15 m would be desirable. A mirror in the measurement train must be allowed for in instrument design. Light scattering and absorption should not prove to be a major problem in spectroscopic work of UV and IR instruments. The mirror may require protection against contamination or surface damage.

The mass spectrometers are ram directed only a portion of each spin in configuration 2. This is a limitation on the mass spectrometer's operation near the nucleus. A quick calculation has shown they operate 1) as a cosine function of acceptance angle and 2) as a percentage loss due to spinning. Multiplying the percentages above (88% and 12%, respectively) the effective value is 10% for spinning vs. 100% in the ram direction per spin. In the far coma, where measurement with many hundreds of seconds are available, the spin loss may be accepted by use of long sample integrations. However, in the critical region near the nucleus, ram direction is needed for detection of complex species with short integration times. The mass spectrometers will be canted about 50° to the spin axis in order to maximize the ram orientation per spin.

The plasma probe is spin-scan oriented in configuration 2 if canted at $\sim 50^{\circ}$ to the spin axis. This instrument will use the spinning mode to investigate plasma at different angles including ram direction. Finally, the cosmic dust detector is spin-scan orientated at a 50° angle, also. It can also use spin rotation for ram and off-ram investigations.

Configuration 3-(Despun Platform) - This configuration allows easy access to science pointing in the required directions, but at the penalty of despun complexity. There should be no smear in imaging systems because the instruments are despun. For equator passages, there are no restrictions on pointing at encounter or afterwards. No spacecraft maneuvers are needed during critical

encounter times. Tail passage images can easily be made looking down the tail and at various angles in one plane.

An equatorial passage is assumed in the Earth-spacecraft-Encke plane, and the spacecraft is spinning perpendicular to the plane. Other approaches would require additional gimbals or spacecraft maneuvers.

The mass spectrometers are ram directed for maximum detection and spatial resolution at all encounter modes in Configuration 3. The plasma probe and cosmic dust detectors can also be ram directed for maximum response, or they may be allowed to spin if the platform motor is stepped. The latter mode would be useful for calibrations and spatial direction measurements.

In Configuration 3, the plasma probe will not scan the Sun until ~ 10 to 6 days from RCA depending upon instrument FOV. This sacrifices cruise solar plasma measurements (without spacecraft maneuvers) but it still permits reasonable calibration of solar wind and plasma conditions prior to comet encounter.

Configuration 4 - (Mirror Despun) - This version is similar to Configuration 2 for the optical instruments, but the mirror is not gimbaled and is smaller. Because of the spin axis orientation perpendicular to the 3-body plane (Earth/spacecraft-Encke), there are no restrictions on imaging past the RCA as in Configuration 2. Thus, Configuration 4 is better than Configuration 2 for the IR instrument and post-RCA viewing. Configuration 4 is also targeted for equatorial passages. Visibility is still limited to $\sim 248^\circ$ per revolution due to spacecraft structure. Tail scans are possible at various angles in one plane.

The mass spectrometer is spin-scan operated in Configuration 4, similar to Configuration 2. For the most critical measurements in the inner coma, this spin-scan mode is a degradation of the instrument's potential in the same manner as Configuration 2.

Plasma probe and cosmic dust detectors are spin-scan oriented. Both instruments can benefit from the ram orientation and spin-scan to make spatial measurements in other directions.

Configuration 5 - (All Spin-Scan for Science) - The most important change in this configuration for science is an all spin-scan imaging system. These

imaging systems are light weight, compact and designed to operate in the short integration time of the spinning spacecraft. For spin-scan imaging, two systems were considered: a 395-element array of solid state detectors and a 10-element photomultiplier system (see section V-I). While the resolution appeared comparable to frame systems at close distances, the radiometry study (sec. V-I-5) indicated the comet and nucleus brightness were not high enough to permit good images, until very close distances. These were at E-4 days for the total comet but only a few hours from encounter for the nucleus.

The UV and visual spectrometer (and IR spectrometer flown) are not very effective in the spin-scan mode. The detectors may integrate over several revolutions, but this severely reduces spatial resolution and spectral scan efficiency.

The mass spectrometers are in a spin-scan mode as in Configurations 4 and 2. They thus operate at ~10% of full ram orientation per revolution. At minimum distance, or RCA, such operation may not detect parent molecules.

Plasma probe and cosmic dust detectors are not optimally operated in a spin-scan mode, but they do provide useful data as long as a portion of the spin is in the ram direction. This is true for Configuration 5. Sun viewing by the plasma probe is restricted due to the 3-body plane/Sun angle until about 10 days before comet encounter. This still permits useful Sun viewing before comet entry.

Asteroid viewing is essentially a visual imaging and infrared scanning mission. The above imaging and optical discussions on Configurations 1 through 5 are valid with the comet nucleus being replaced by the asteroids. Such missions do, however, affect comet science return as discussed in the following section.

3. Impact on Comet Science of Asteroid Flyby

There are valid scientific reasons to add asteroid opportunities to an Encke comet mission. Two objectives are: 1) To determine how long asteroids have been in orbit; and 2) To determine whether particulate matter from comets is similar in composition to asteroid surfaces. Both investigations could provide a link that the Apollo asteroids are "dead" nuclei of comets. Such a tie

would be valuable in improving our understanding of solar system evolution - original formation and continuing evolution. It is worthwhile, then, to see what penalties are paid at the comet in order to continue to one or more asteroids.

The impact on Encke science due to asteroid missions can be grouped into three effects: 1) higher velocity at Encke; 2) change in targeting correction at the comet; 3) adjustments to comet science payload. These effects are considered in order.

The increase in relative encounter velocity at Encke goes from ~ 18.3 to 26.3 km/sec for asteroid follow-ons. For most instruments like the UV this only means a loss of 30% in available observation time. Only during the limited time of nucleus search, could this impact be felt. The E-15 minute values would shift to E-10.5 minutes, but this time loss could be compensated in part by an increase in data rate. The instruments most likely to be velocity-dependent are the cosmic dust detector, mass spectrometers, and plasma probe. The cosmic dust detector should be enhanced by the higher velocity impact ionization with no inlet problems anticipated. The plasma probe may need minor electrostatic plate redesign. The mass spectrometers could be affected, if inlet problems develop due to the higher velocity (see Appendix C).

Changes in trajectory orientation at Encke are not critical to science measurement as seen now. A greater tracking curvature at encounter means the spacecraft will not be "oriented" straight down the comet path for as long before, or after encounter. Still, the bow shock, transition region, and contact surface will be traversed. A near 0° angle is not considered that important for instrument operation.

The tail observing time loss is discussed in Section III-B3. The measurement time is decreased by several hours (from nominal value between 9 and 13 hours for the comet) to go to the asteroid. However, the particle and field instruments are designed for fast operation (seconds) and should get meaningful data on a scale of hours. Measurements in the near coma after RCA will provide the foundation for tail structure regardless of tail traversal time.

Finally, the asteroid missions require addition of an IR instrument. It might "replace" the visual spectrometer included in the comet payload. This loss would not be great considering the potential gains at the asteroid by use of the IR instrument. The IR spectrometer can also be used at the comet.

In summary, the potential for asteroid science investigations seems at this time to offset the losses at the comet.

4. Technical Requirements Comparison

All of the spacecraft concepts developed in this study are based on utilization of existing equipment which is primarily from the Pioneer 10 and 11 programs. The communication, electrical power, and distribution, propulsion and data handling subsystems present no unique problems on these missions. Spacecraft thermal control can be accomplished by passive methods.

The key technical issue, common to all of the concepts considered, is the acquisition and tracking of the comet nucleus and the asteroids. This issue concerns the interrelationships between imaging system characteristics (e.g., sensitivity and resolution), imaging system installation, and the collection and processing of data within the attitude control system. Each concept approached the latter aspect differently. Concept 1 achieves camera pointing by precessing the spacecraft. High precession rates, in the very close encounter period, however, could be countered by termination of the imaging sequence before unacceptable build up of slew rate is reached. Much less mass needs to be moved when the despun mirrors of Concepts 2 and 4 are used for pointing the optical instruments. The mirror system would require development. The most complex of the concepts, Concept 3, provides the best platform but introduces a major development task with respect to both mechanical implementation and transfer of signals and data across rotating interfaces. This is in contrast to the simplicity of Concept 5. It is shown in Section V-I, however, that current spin-scan camera technology is not adequate for small body exploration. Further analysis and development of such an instrument would be required.

An attitude control system concept to provide the necessary pointing and stabilization has been described in Section V-D. Although existing

sensors and components might be used in this subsystem, considerable additional study and development will be required to achieve an integrated design.

THIS PAGE BLANK

V. SUBSYSTEM DESIGN

V. SUBSYSTEM DESIGN

Spacecraft design concept number 2 (Earth-pointing with despun mirror) was used as the baseline for analysis of subsystem requirements and selection of subsystem concepts and components. Where significant differences in subsystem implementation occur, they are identified and evaluated.

A. STRUCTURES AND MECHANISMS

1. Primary Structure

The primary structure will be based on an existing spinning spacecraft design since many of its features complement our needs. Figure V-1 shows pictorially the major structural elements.

The structure consists of a large circular honeycomb panel equipment platform, supported by a central cylinder and six diagonal struts and vertical elements. The central cylinder is the load path for all spacecraft inertia loads and is in turn supported by a short adapter (truncated cone) which, along with the Helios adapter, provides the structural interface with the TE364-4 SRM. A conical (truncated) solar array substrate attaches to the equipment compartment structure through 12 struts.

Longitudinal (20g limit induced by TE364-4) and lateral accelerations (60 rpm spin) were determined in order to predict the critical loading conditions on the spacecraft structure for the purpose of estimating structural weights and total spacecraft weights. These were then used for comparison with the Atlas/Centaur/TE364-4 Booster payload capabilities of 335 to 560 kg depending on the mission.

The Helios adapter skirt is used to assemble the spacecraft to the TE364-4 solid rocket motor. The Pioneer 10 adapter is used between the TE364-4 and the Atlas/Centaur Booster. The application of these adapters is shown in Figure V-2

Preliminary strength analysis indicate these selected structural adapters presently may have allowables in excess of the loads they will be subjected to as part of the Encke vehicle.

The Centaur D-1A Payload Fairing has been selected in as much as it was originally designed for the Atlas Centaur booster and requires no design and

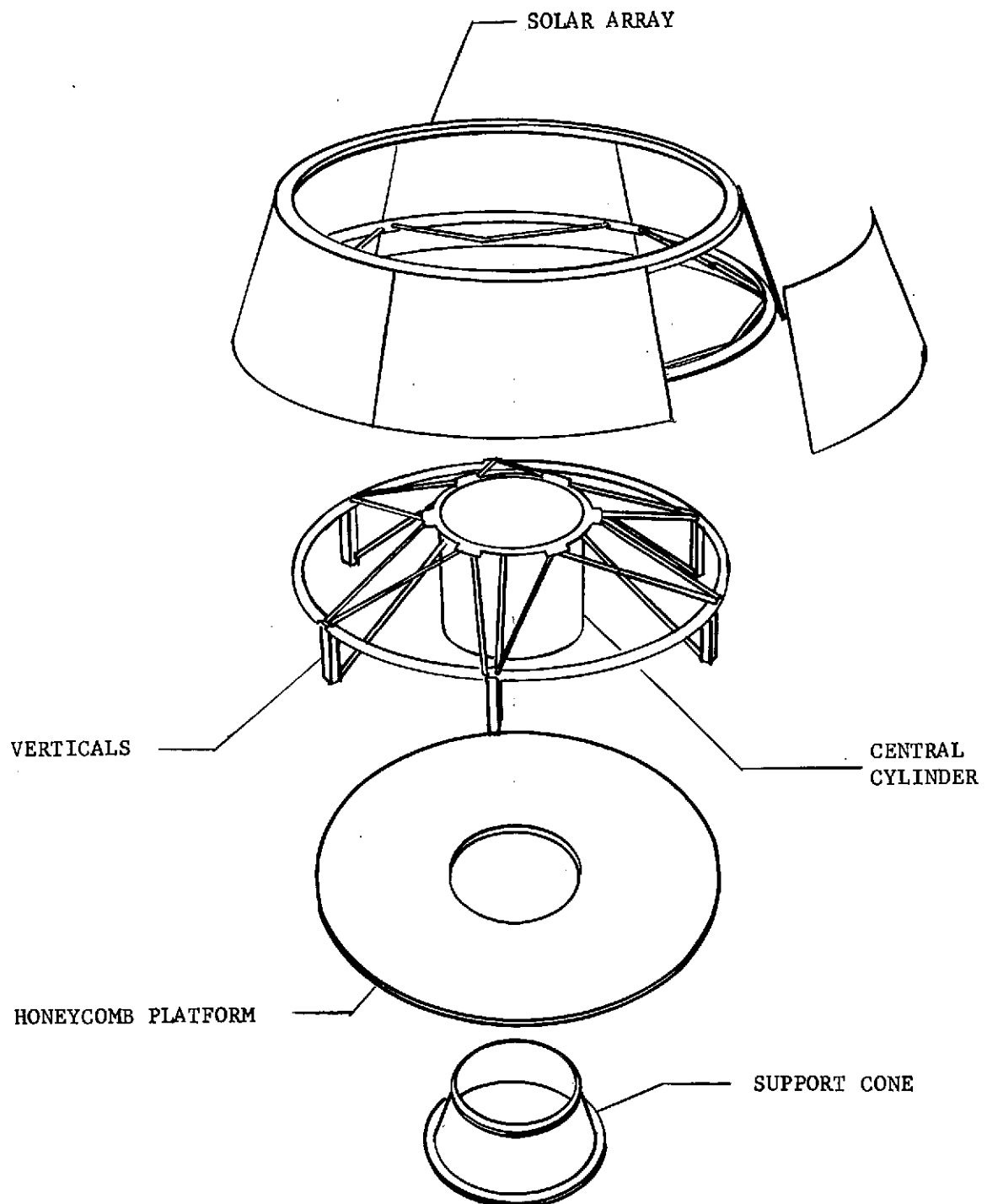


FIGURE V-1 SPACECRAFT PRIMARY STRUCTURE

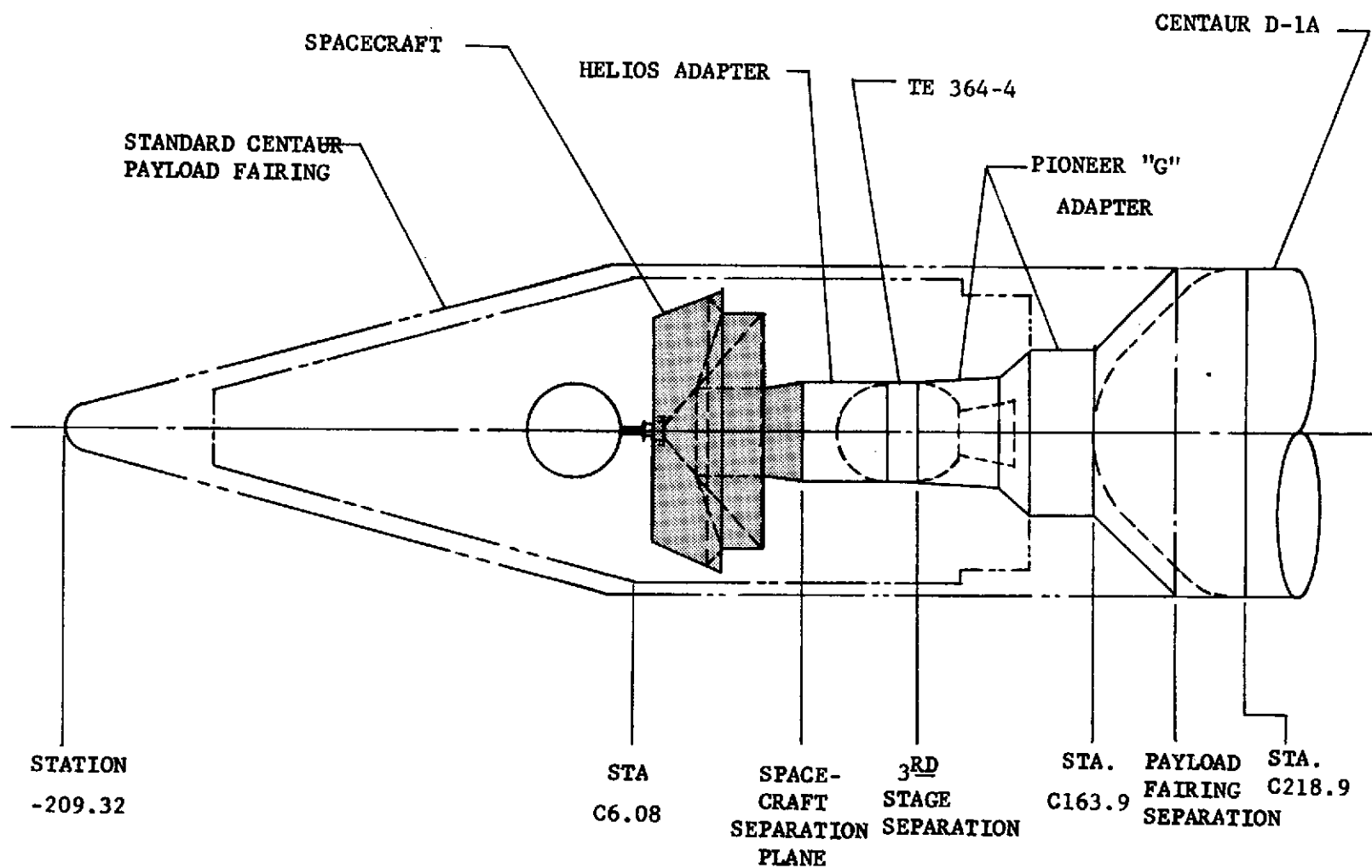


FIGURE V-2 ENCKE SPACECRAFT - BOOST CONFIGURATION

development effort. The internal volume is adequate to accommodate the Encke vehicle.

2. Mechanisms

The various mechanisms required will range from pin pullers and cable cutters, which can be readily purchased, to despin ring devices for the mirror assembly which will be a development item.

No formal product search was performed to determine availability, but we anticipate antenna despin and gimbal mechanisms and magnetometer booms as being presently available.

Small mechanisms used to erect the Langmuir probe, or release and position the plasma wave detector antenna, or the high gain antenna boom (for Concept No. 1) will be designs incorporating springs, pyrotechniques, stepper motors, and snubbers.

The mechanisms for despining and gimbaling the mirror assembly or the despun platform and scan table mechanisms shown on some of the concepts will require development, but are certainly within the present state-of-the-art. Figures V-3 and V-4 further describe our despun platform and despun mirror concepts.

3. Structural Layouts and Equipment Arrangement

Layouts of the five spacecraft concepts are presented in Figures V-5 through V-9. These layouts describe the arrangement of the primary structure and the equipment of the various subsystems for each of the five concepts. Design approaches for the major features of each concept are shown to verify system compatibility.

4. Probe Structure and General Arrangement

Analysis of the Encke coma environment (Appendix C) showed that neither an aerodynamic shape nor a heatshield would be required for the probe. The low particle density of Encke's coma causes no aerodynamic pressures or heating. This simplifies considerably the probe structural design (fig. V-10).

The absence of a heatshield allows external protruding fittings to be used on the probe for interfacing with the spacecraft. In the two-point support

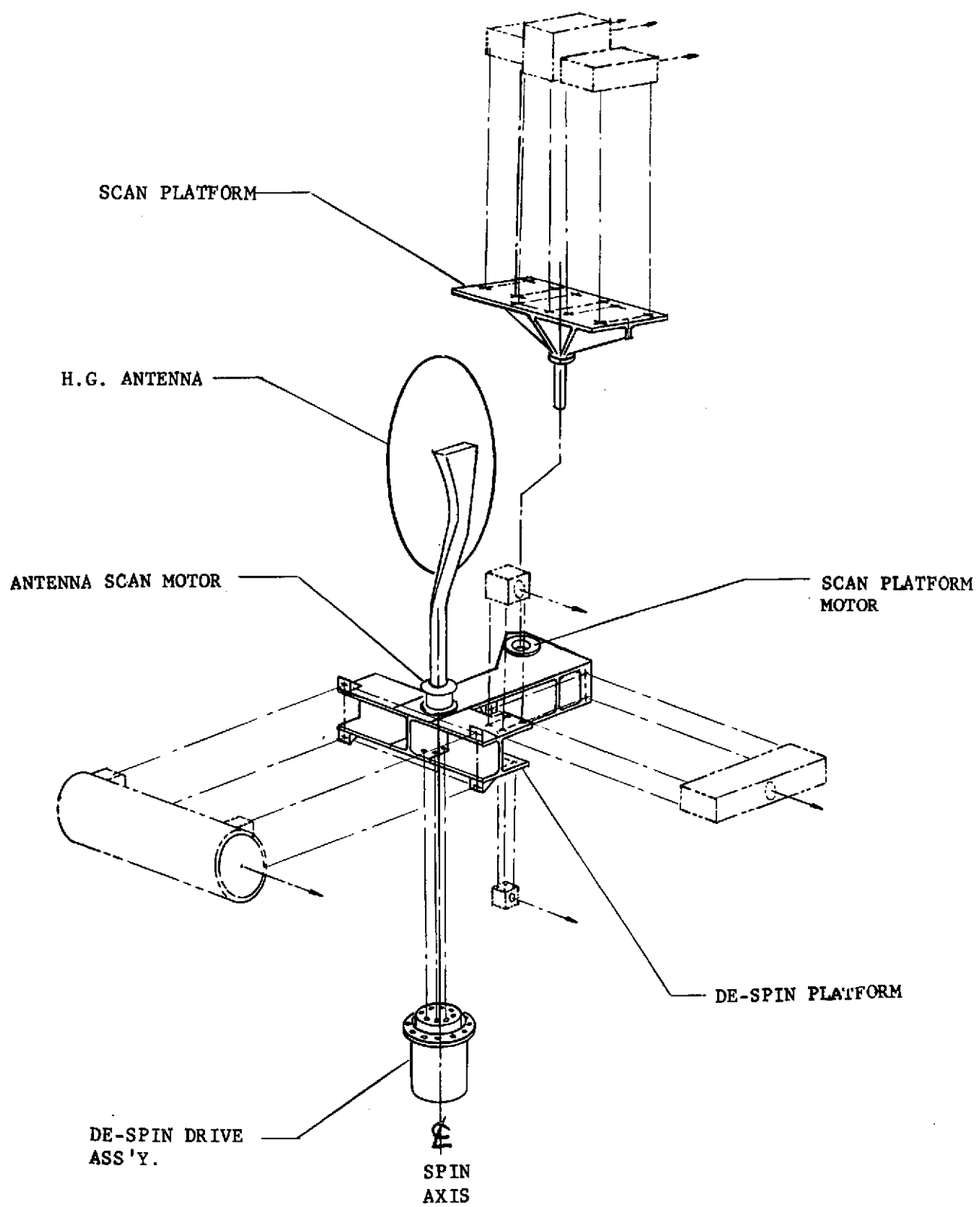


FIGURE V-3 DE-SPIN PLATFORM CONCEPT FOR CONCEPT NO. 3

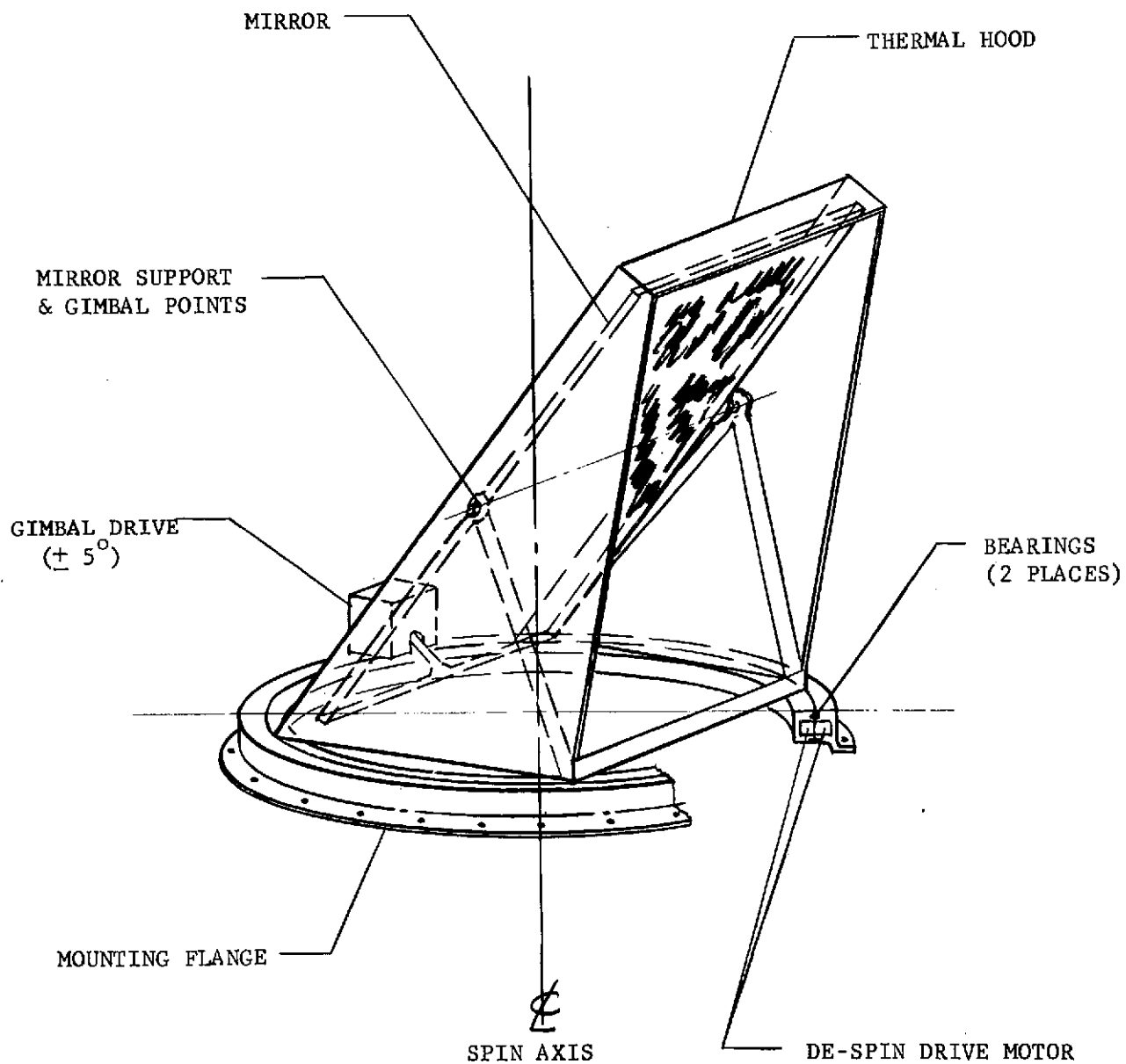


FIGURE V-4 DE-SPIN MIRROR CONCEPT

THIS PAGE BLANK

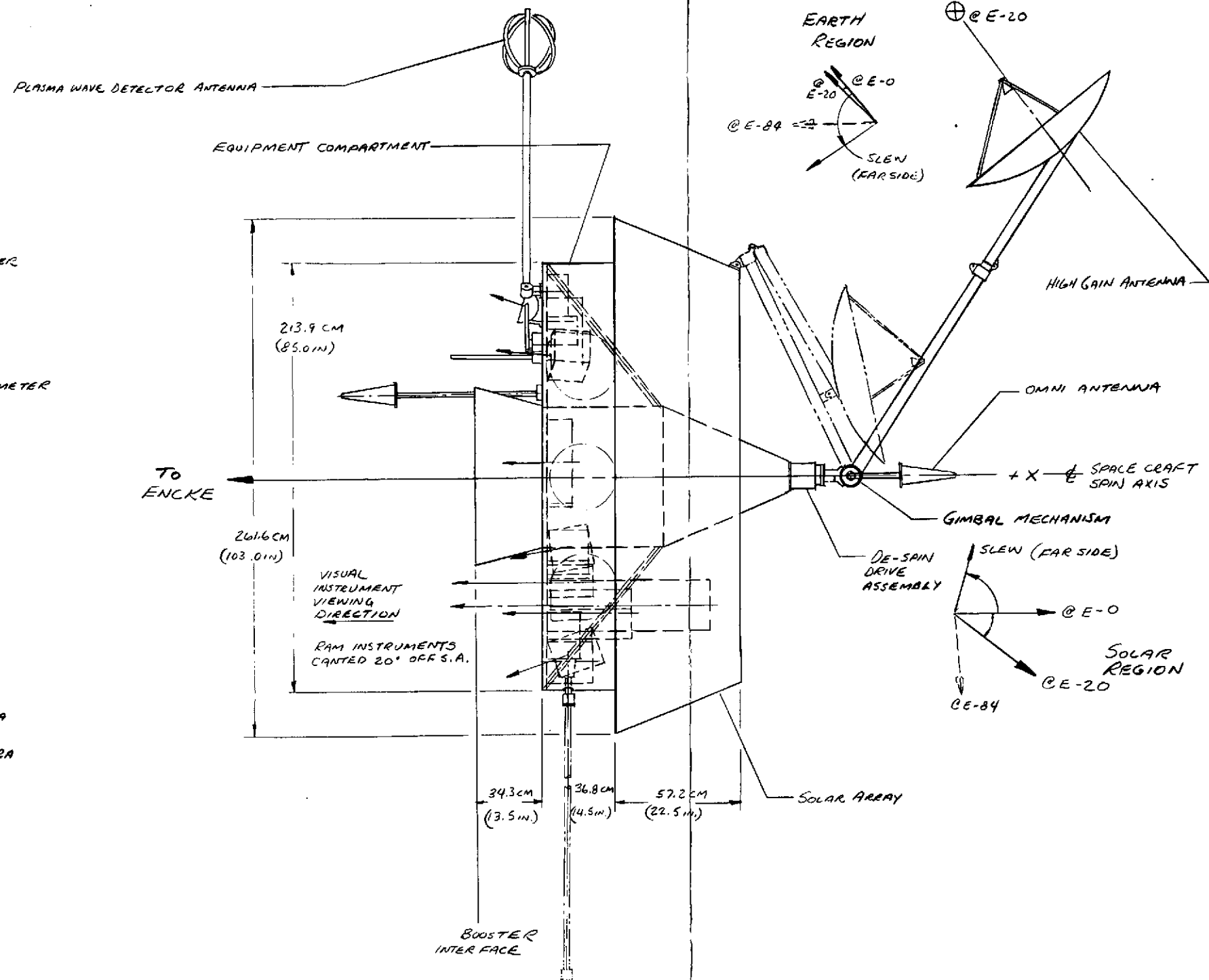
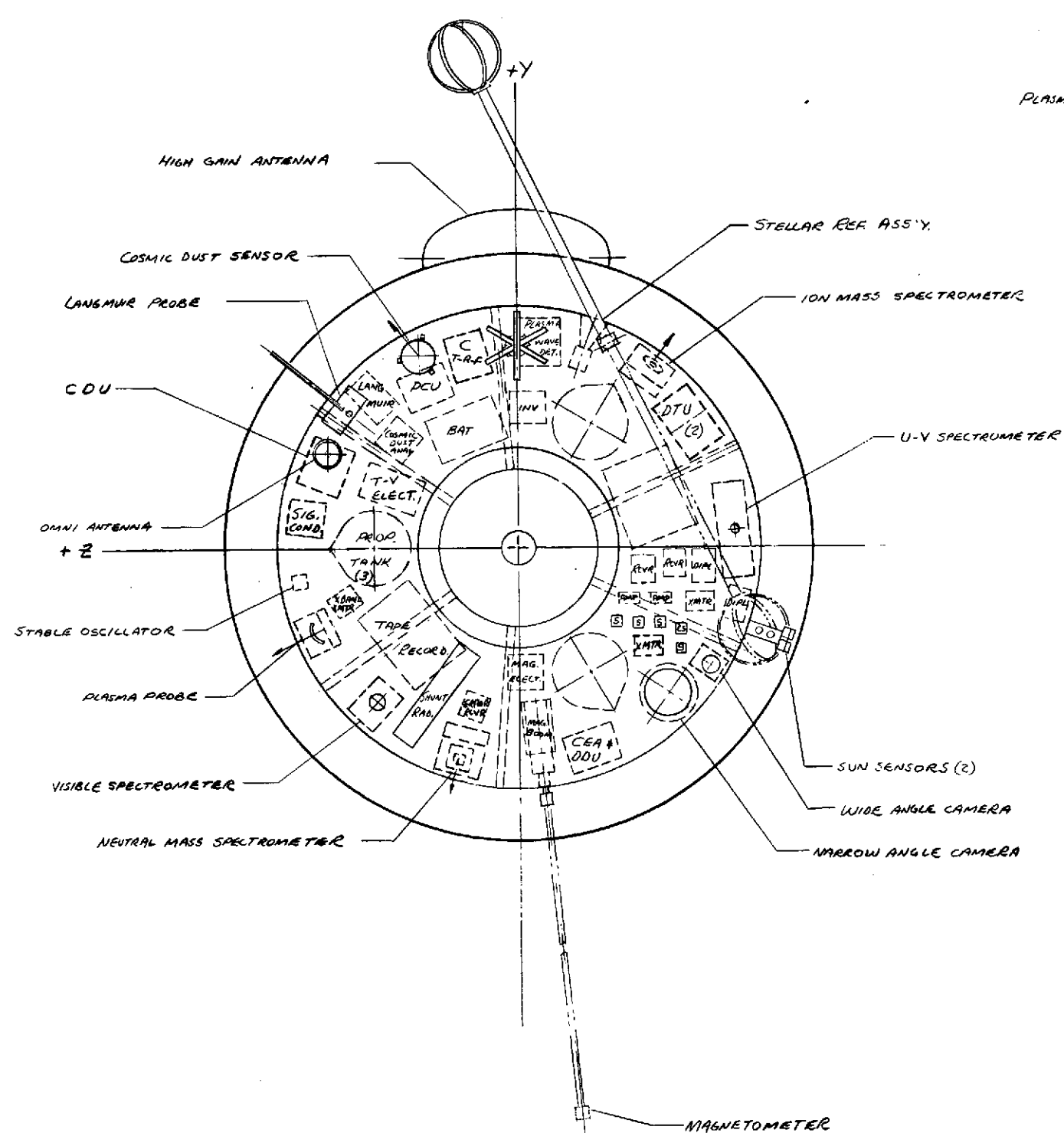
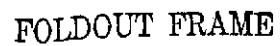


FIGURE V-5 CONCEPT NO. 1: SPIN AXIS POINTS TO ENCKE

V-9/V-10



FOLDOUT FRAME

2

V-11/V-12

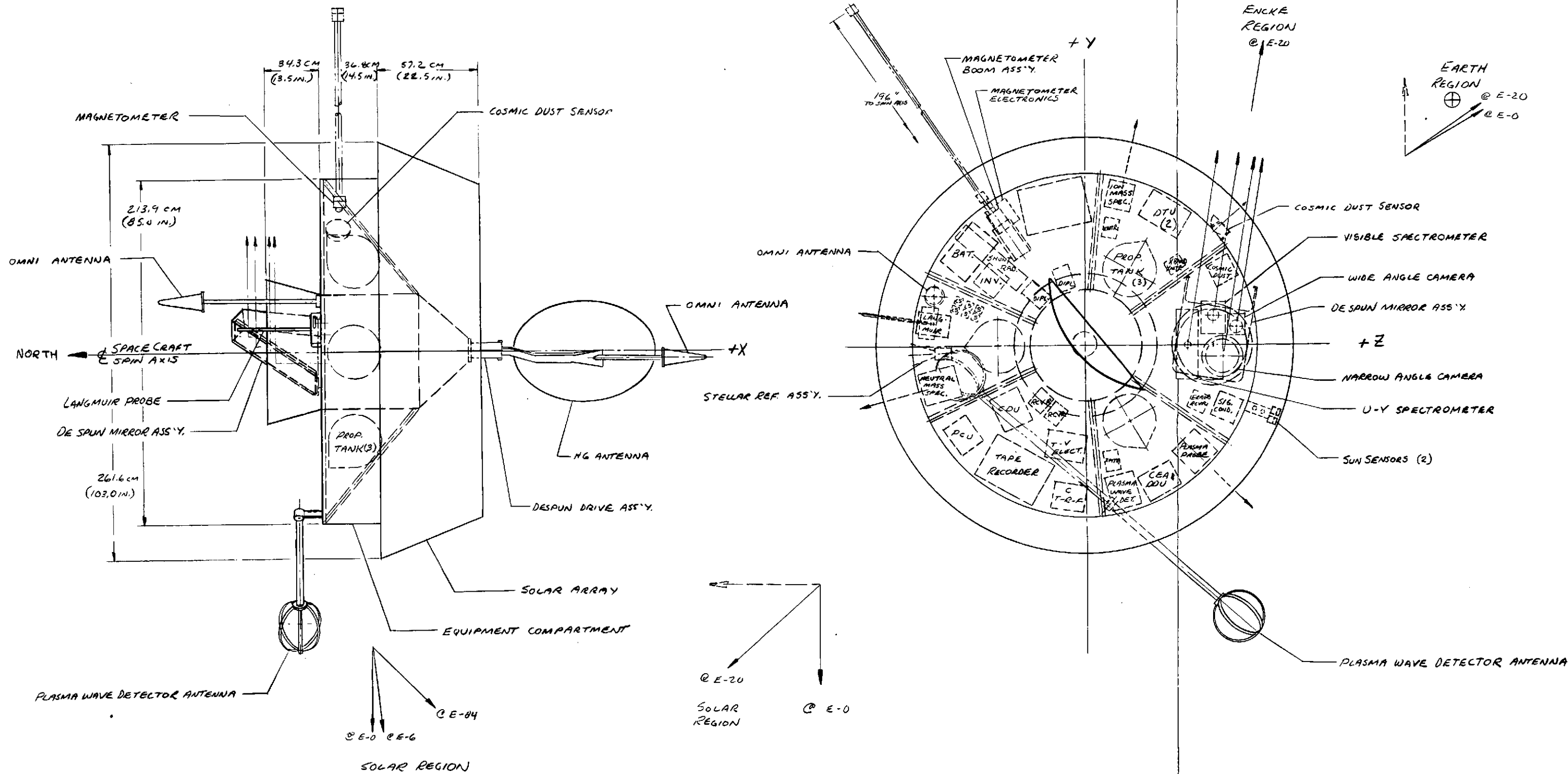
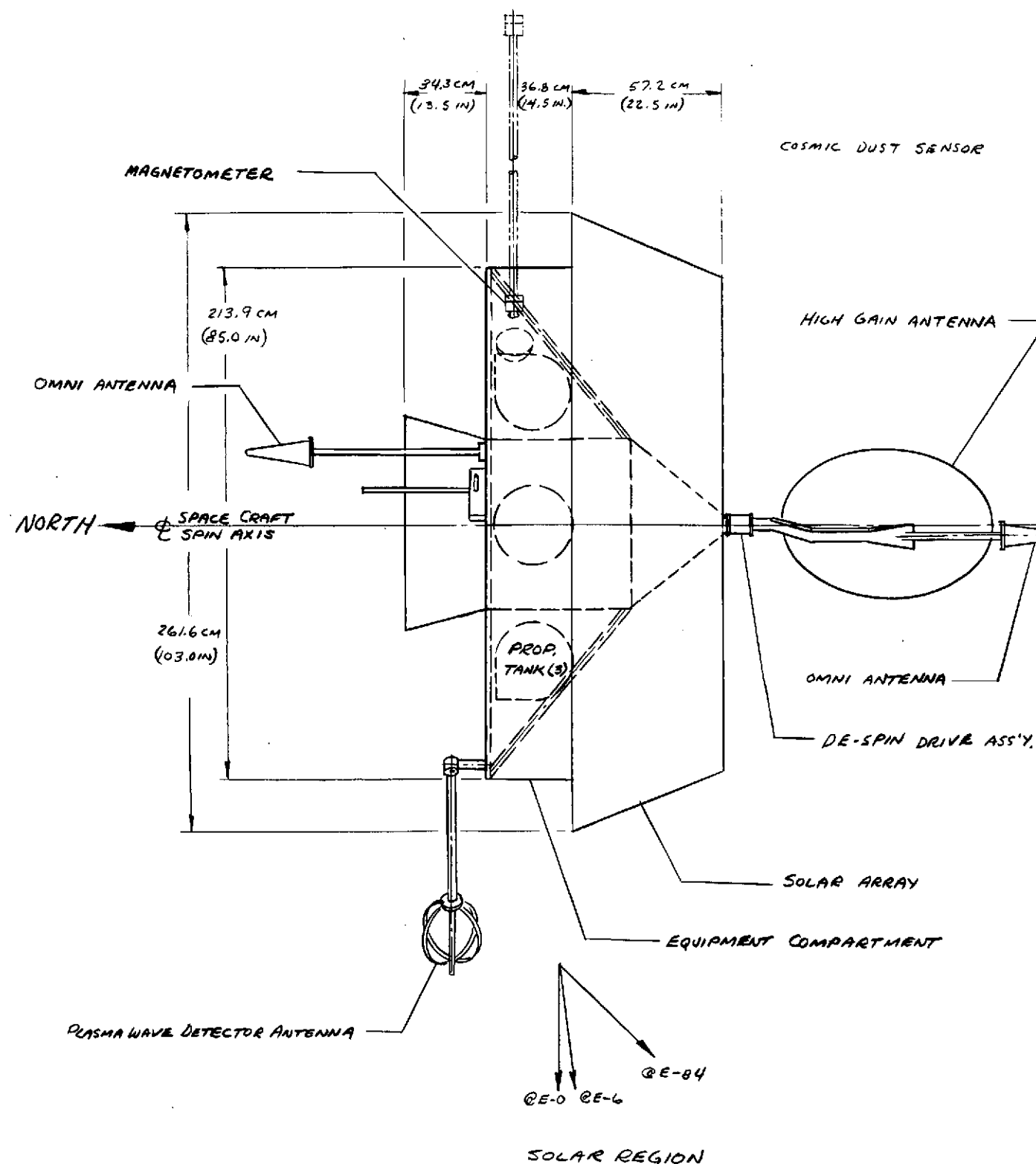


FIGURE V-8 CONCEPT NO. 4: SPIN AXIS PERPENDICULAR TO SPACECRAFT, EARTH, ENCKE PLANE, UTILIZING DESPUN MIRROR

FOLDOUT FRAME 1



FOLDOUT FRAME 2

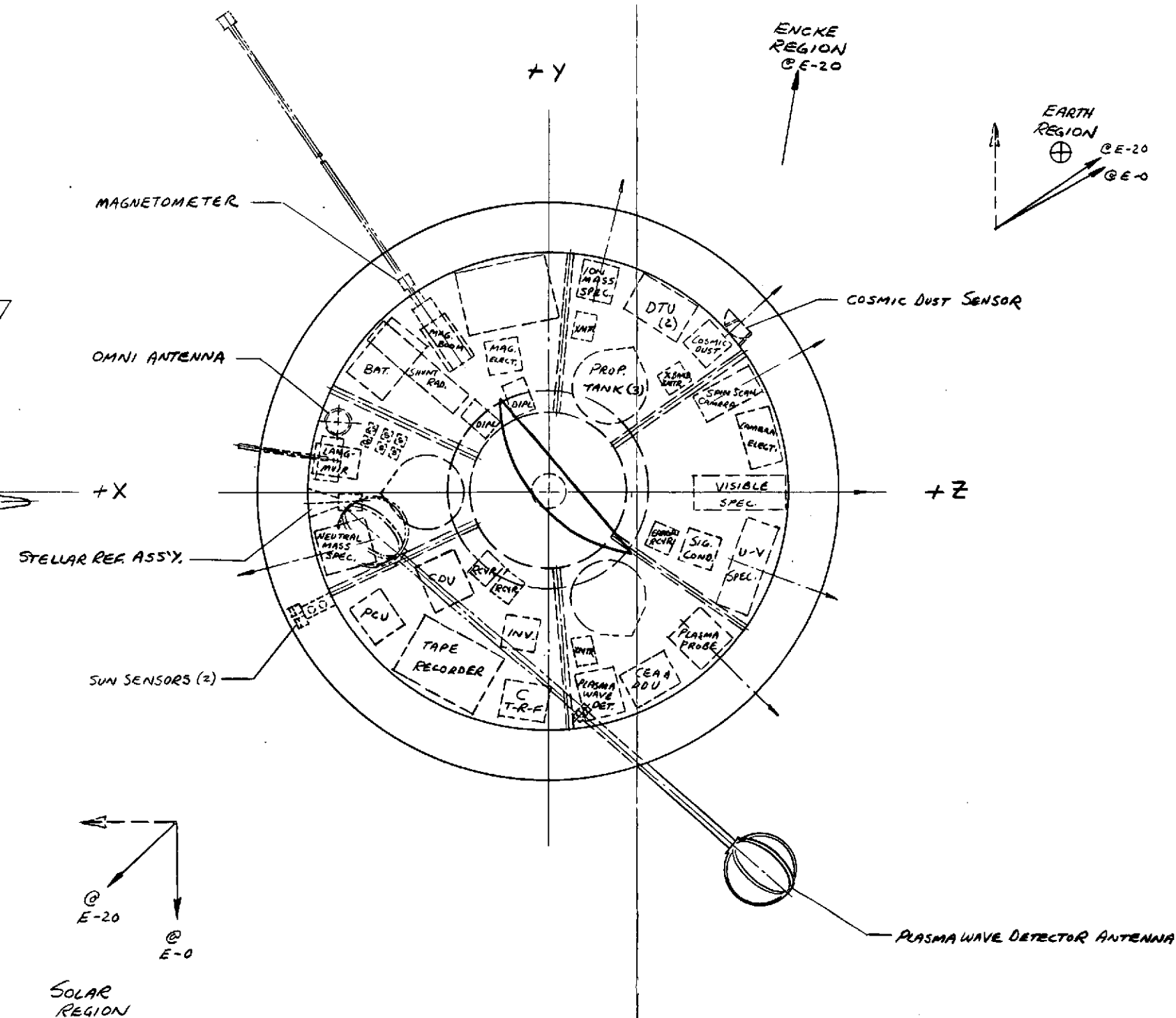


FIGURE V-9 CONCEPT NO. 5: SPIN AXIS PERPENDICULAR TO SPACECRAFT, EARTH, ENCKE PLANE, UTILIZING SPIN-SCAN CAMERA

V-17/V-18

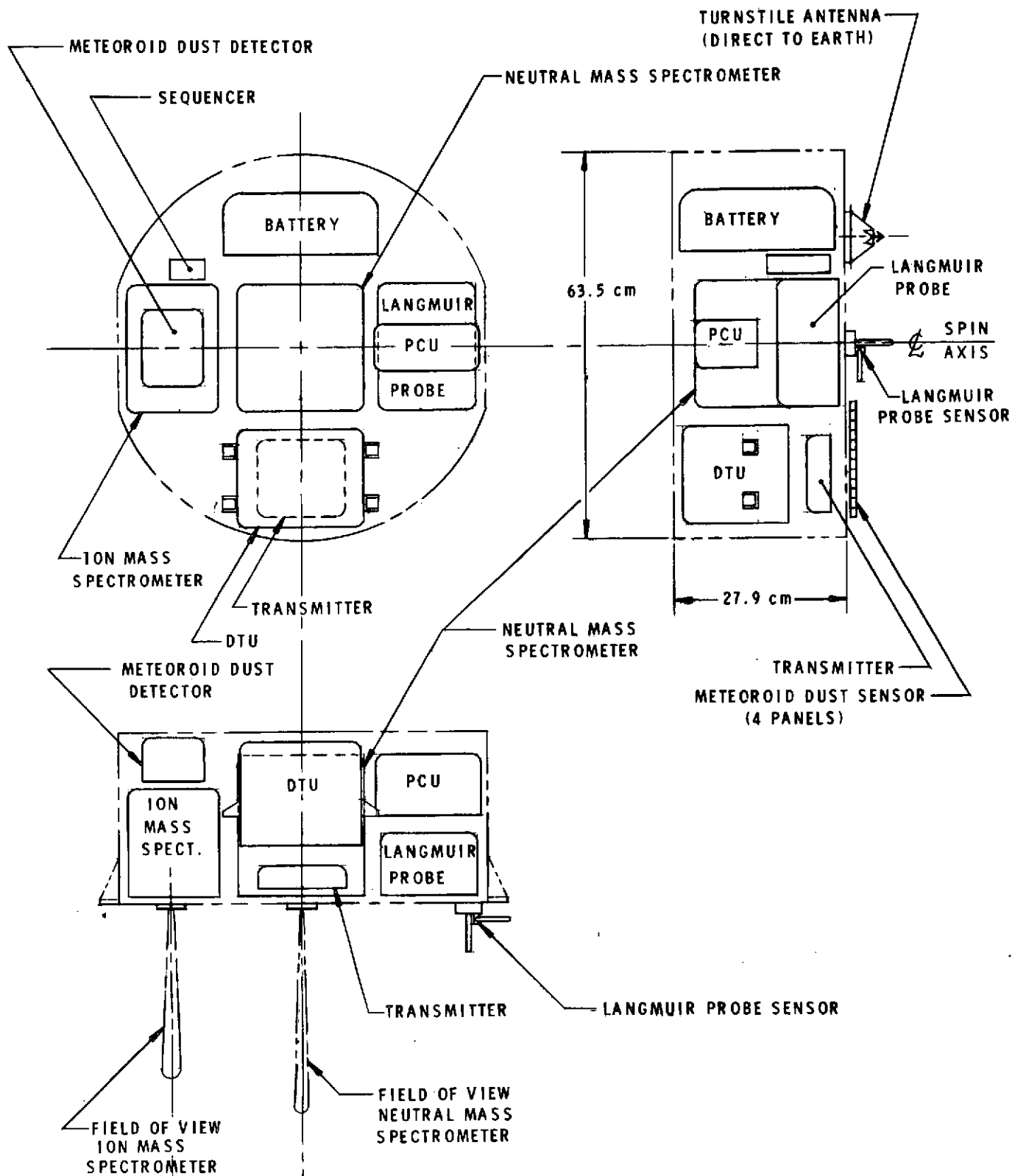


FIGURE V-10 PROBE EQUIPMENT ARRANGEMENT CONCEPT

approach shown, the support points are also separation points.

The probe structure consists of two primary beams and two secondary beams which support all the scientific instruments and other equipment. Fittings placed at the ends of the primary beams are used to pick up the externally mounted separation fittings.

The case is primarily a thermal cover and does not carry primary loads. The leading end and, possibly the sides are filled honeycomb for particle penetration protection. Honeycomb face sheet and core dimensions were based on the particle-damage analysis of Appendix B.

The internal equipment arrangement is shown in Figure V-11. At both of the support points, there are ball lock bolts used for releasing the probe. When the ball lock bolts are ignited, the probe is free and two springs provide the energy to separate the probe.

With the probes centrally located on the spin axis of the spacecraft, the 5 rpm spin rate is imparted to the probe during separation providing it with attitude stability. Just prior to release, a cable cutter will be activated to sever the electrical umbilical cable between the probe and spacecraft. Figure V-12 shows the details of the separation joints.

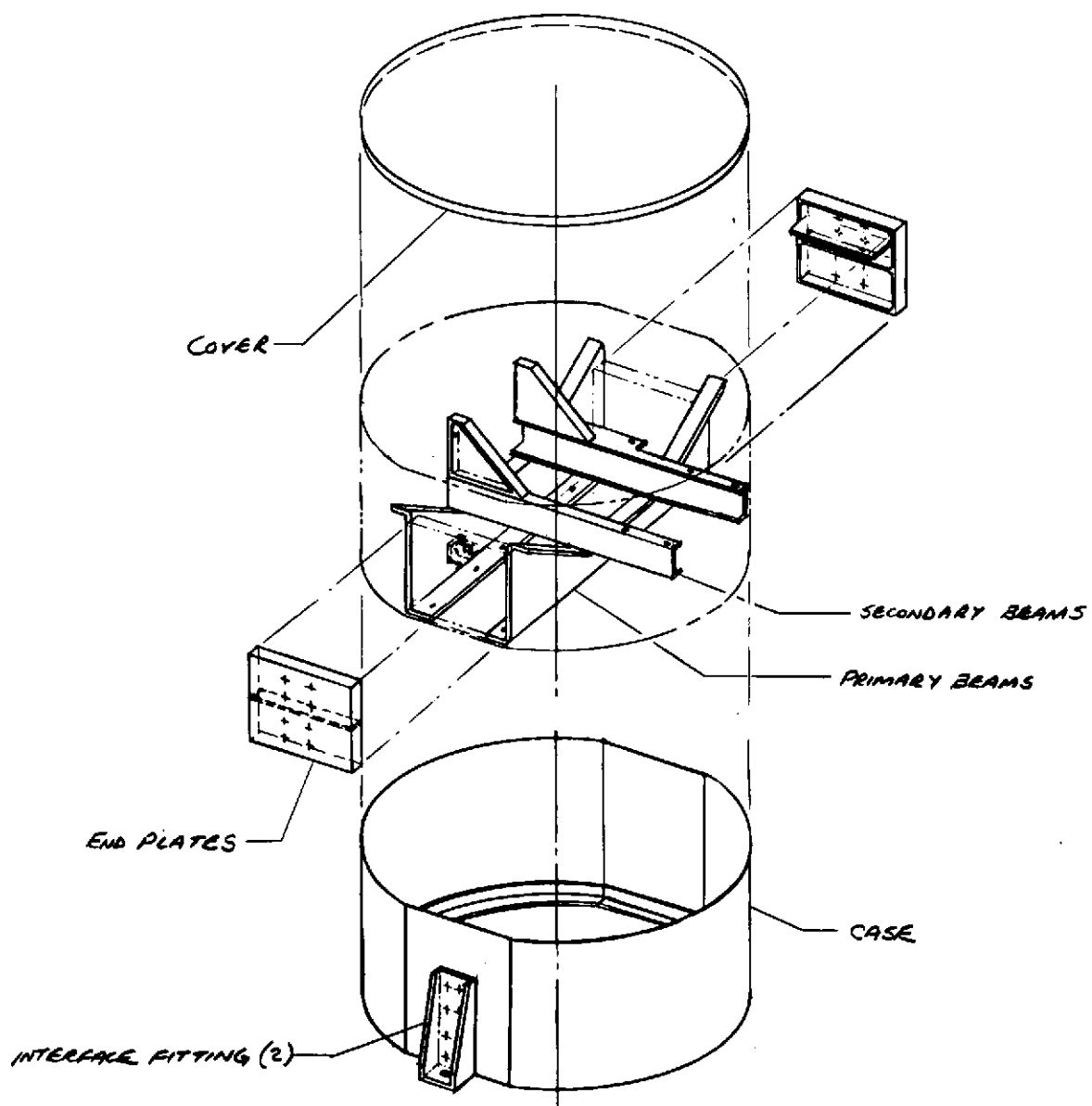


FIGURE V-11

PROBE STRUCTURAL CONFIGURATION CONCEPT

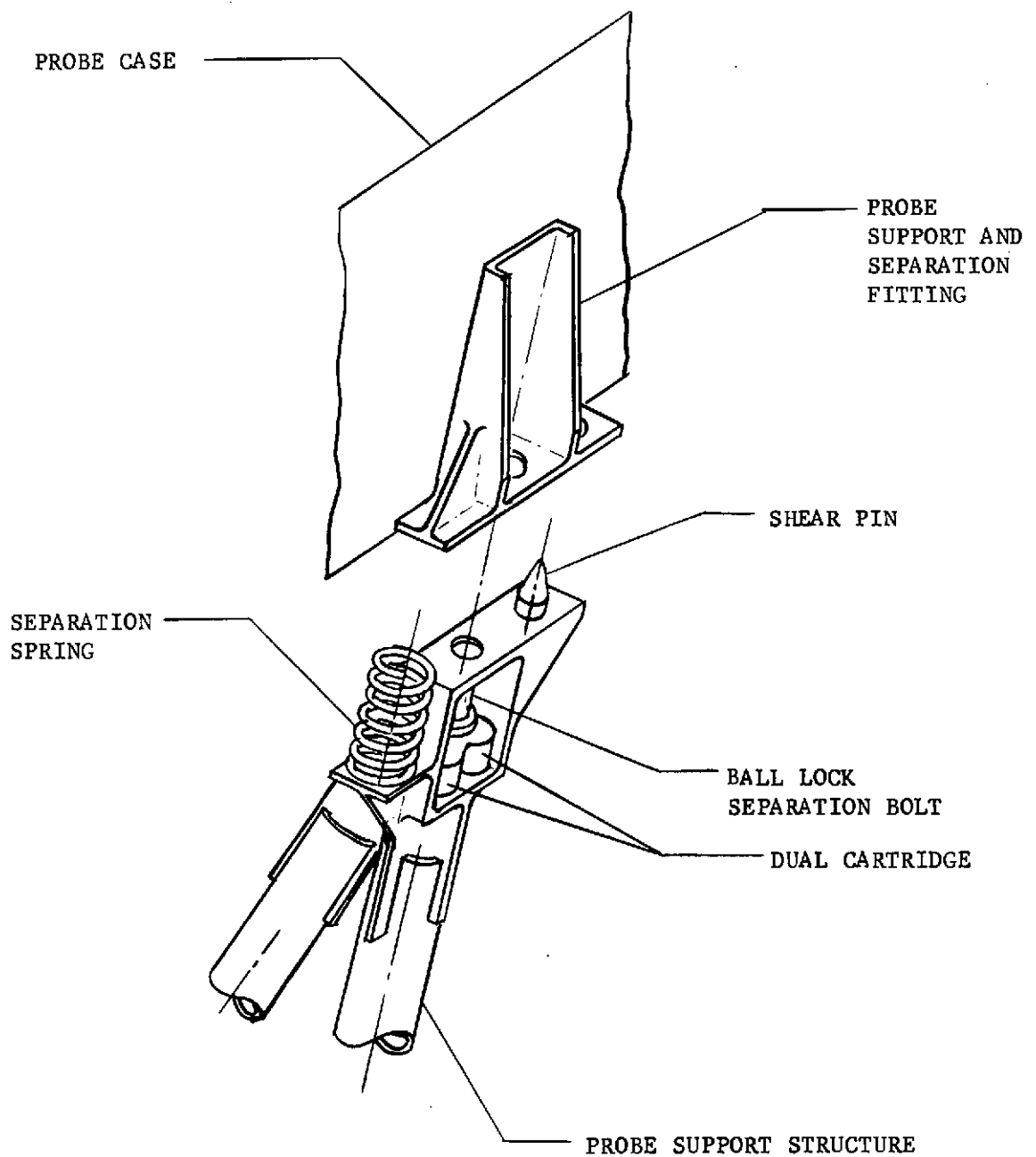


FIGURE V-12 PROBE TO SPACECRAFT SUPPORT AND SEPARATION CONCEPT

B. COMMUNICATIONS

The communications subsystem comprises two command receivers, two digital decoders, two 6 watt S-band transmitters, a single 6 watt X-band transmitter, antennas and a conscan processor as shown in Figures V-13 and V-14. Configurations 1, 3, 4 and 5 each has a single 0.92 meter diameter high gain parabolic reflector and two omni antennas whereas Configuration 2 has, in addition to 2 omni antennas, 2 identical 0.92 meter diameter antennas to provide communications to Earth when either end of the spacecraft spin axis is pointed to Earth. Configurations 3, 4 and 5 have a fanscan antenna which provides, in conjunction with a conscan processor, a signal to the spacecraft for the purpose of aligning the spin axis perpendicular to the spacecraft Earth line. Configuration 2 also has a conscan processor. However, it is used with the offset S-band feed of the 0.92 meter dishes to provide a conscan signal for pointing the spacecraft spin axis to Earth.

The dish antennas of Configurations 1, 3, 4 and 5 also have a capability for automatically tracking the DSN S-band uplink signal so that the antennas can be aligned to Earth for maximum data transfer over the narrow 2.8° half power beam width of the X-band system. This requires a 2 channel direction finding system necessitating the addition of an error channel receiver, an error signal processor and a third RF channel through any rotary joint or despun interface (S-band sum channel, S-band difference channel and X-band telemetry).

During periods when the DSN is providing an uplink and both the spacecraft S-band and X-band transmitters are operating, dual frequency two-way doppler tracking will be available to the ground station.

The S-band communications link will be used to transmit non-imaging science and spacecraft diagnostic data at a 2048 bps rate at encounter with Encke and at a 128 bps rate at the asteroids. The X-band link will be used to transmit imaging science data at a rate of 16,384 bps at Encke and at 2048 bps in the vicinity of the asteroids. Figure V-15 shows the telemetry down-link capability for all antennas at any given communications range. The change in slope at 512 bps represents a shift in modulation index from 1.25 rad to 1.05 rad. Tables V-1 through V-4 are communications design control tables for the S-band and X-band down links at Encke and asteroid encounters. Table V-5

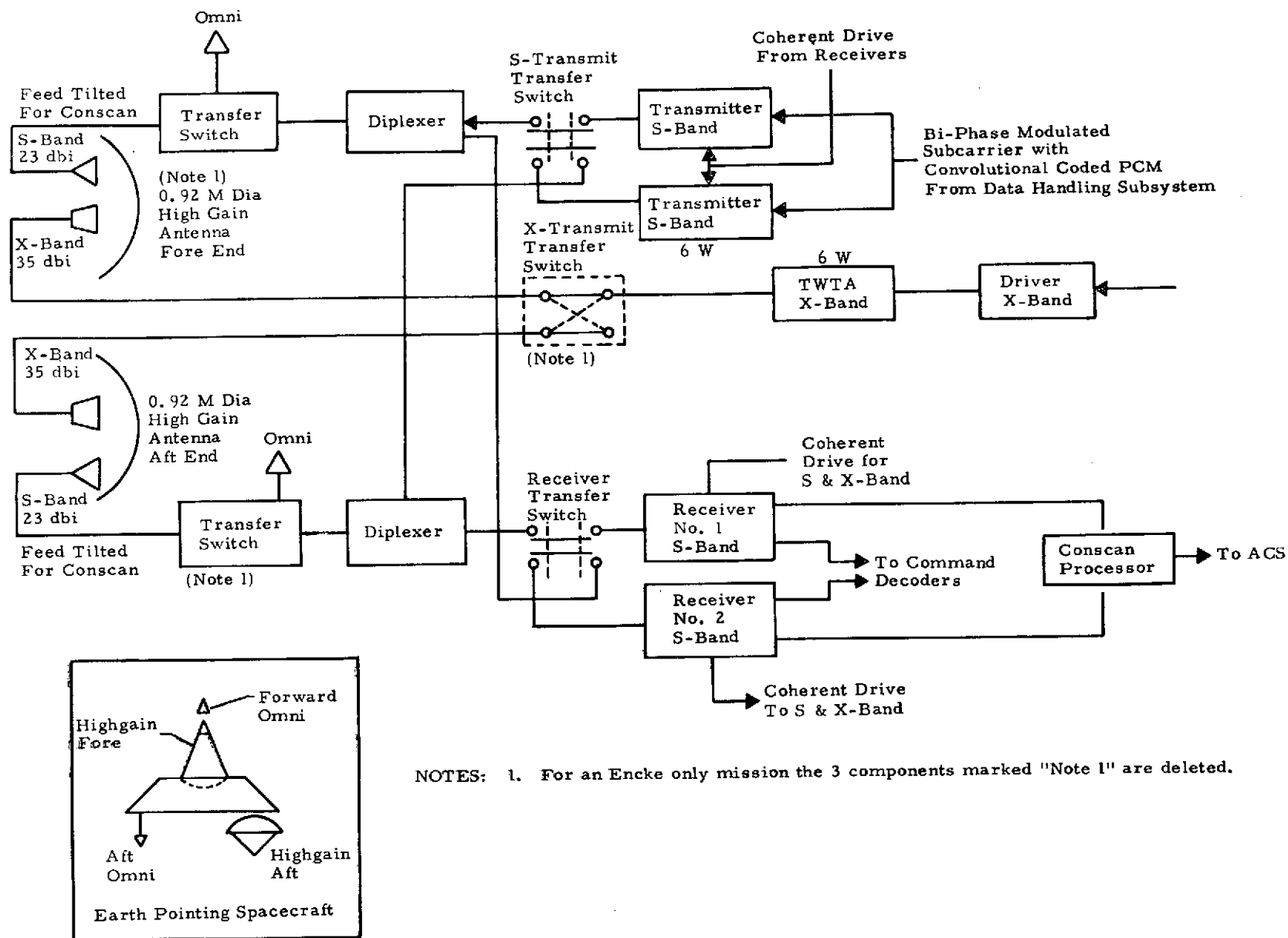


FIGURE V- 13 COMMUNICATIONS BLOCK DIAGRAM - CONFIGURATION 2

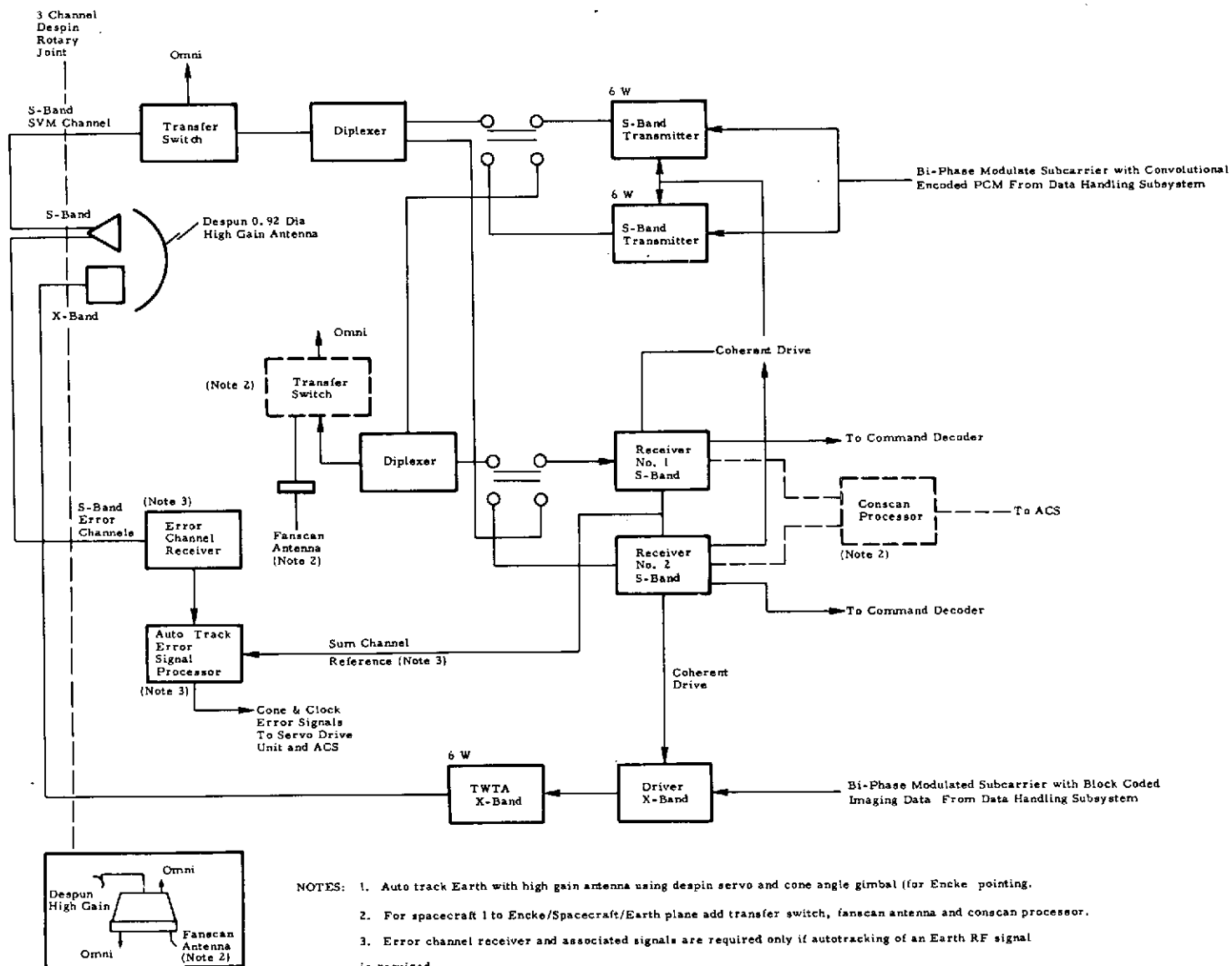


FIGURE V-14 COMMUNICATIONS BLOCK DIAGRAM - CONFIGURATIONS 1, 3, 4 and 5

TABLE V-1 ENCKE ENCOUNTER, 0.57 AU, S-BAND DESIGN CONTROL TABLE

NO.	PARAMETER	NOMINAL	ADVERSE	NOTES
1	FREQUENCY (MHZ)	2300	-	S-BAND
2	RANGE (AU)	0.57	-	END OF MISSION
3	TRANSMITTER POWER (DBM)	37.8	0.4	6 WATTS NOMINAL
4	TRANSMITTER CIRCUIT LOSS (DB)	-1.4	0.1	
5	TRANSMITTER ANTENNA GAIN (DB)	23.0	0.5	0.92 METER (3 FOOT) DISH
6	POINTING LOSS (DB)	-2.8	0.3	CONSCAN LOSS PLUS 0.017 RAD (1 DEG) ATTITUDE ERROR
7	POLARIZATION LOSS (DB)	-0.1	0.1	
8	SPACE LOSS (DB)	-258.2	0	0.57 AU
9	RECEIVER ANTENNA GAIN (DB)	61.6	0.6	64 METERS
10	TOTAL RECEIVED POWER (DBM) (3+4+5+6+7+8+9)	-140.1	0.9	RSS TOLERANCES
11	RECEIVER NOISE SPECTRAL DENSITY (DBM/HZ)	-184.0	0.9	29°K NOMINAL
12	P_T/N_O (DB-HZ) (10-11)	43.9	1.3	RSS TOLERANCES
<u>CARRIER TRACKING PERFORMANCE</u>				
13	CARRIER MODULATION LOSS (DB)	-10.2	2.7	$1.26 \pm 10\%$ RAD
14	THRESHOLD LOOP BANDWIDTH (DB-HZ)	10.3	0.5	$2B_{LO} = 10.8 \pm 10\%$ HZ
15	LOOP SNR (DB) (12+13-14)	23.4	3.0	RSS TOLERANCES
16	REQUIRED LOOP SNR (DB)	15.0	0	RECOMMENDED
17	PERFORMANCE MARGIN (DB) (15-16)	8.4	3.0	RSS TOLERANCES
<u>DATA CHANNEL PERFORMANCE</u>				
18	DATA MODULATION LOSS (DB)	-0.4	0.4	$1.26 \pm 10\%$ RAD
19	DATA BIT RATE (DB-BITS/S)	33.1	0	2048 BITS/S
20	RECEIVER LOSS (DB)	-1.4	0.5	ESTIMATED FROM NASA/ARC DATA
21	E_B/N_O (DB) (12+18-19+20)	9.0	1.5	RSS TOLERANCES
22	REQUIRED E_B/N_O (DB)	3.6	0	10^{-3} FRAME DELETION RATE SEQUENTIAL DECODING
23	PERFORMANCE MARGIN (DB) (21-22)	5.4	1.5	RSS TOLERANCES

TABLE V- 2 ENCKE ENCOUNTER, 0.57 AU, X-BAND DESIGN CONTROL TABLE

NO.	PARAMETER	NOMINAL	ADVERSE	NOTES
1	FREQUENCY (MHZ)	8444	-	X-BAND
2	RANGE (AU)	0.57	-	END OF MISSION
3	TRANSMITTER POWER (DBM)	37.8	0.4	6 WATTS NOMINAL
4	TRANSMITTER CIRCUIT LOSS (DB)	-2.0	0.1	
5	TRANSMITTER ANTENNA GAIN (DB)	35.0	0.5	0.92 METER (3 FOOT) DISH
6	POINTING LOSS (DB)	-3.0	0.3	1.4° POINTING ERROR
7	POLARIZATION AND WEATHER (LOSS)	-0.4	0.1	
8	SPACE LOSS (DB)	-269.5	0	0.57 AU
9	RECEIVER ANTENNA GAIN (DB)	71.6	0.6	64 METERS
10	TOTAL RECEIVED POWER (DBM) (3+4+5+6+7+8+9)	-130.5	0.9	RSS TOLERANCES
11	RECEIVER NOISE SPECTRAL DENSITY (DBM/HZ)	-182.7	0.9	39°K NOMINAL
12	P_T/N_O (DB-HZ) (10-11)	52.2	1.3	RSS TOLERANCES
<u>CARRIER TRACKING PERFORMANCE</u>				
13	CARRIER MODULATION LOSS (DB)	-10.2	2.7	1.26 ± 10% RAD
14	THRESHOLD LOOP BANDWIDTH (DB-HZ)	10.3	0.5	2 B_{LO} = 10.8 ± 10% HZ
15	LOOP SNR (DB) (12+13-14)	31.7	3.0	RSS TOLERANCES
16	REQUIRED LOOP SNR (DB)	15.0	0	RECOMMENDED 810-5
17	PERFORMANCE MARGIN (DB) (15-16)	16.7	3.0	RSS TOLERANCES
<u>DATA CHANNEL PERFORMANCE</u>				
18	DATA MODULATION LOSS (DB)	-0.4	0.4	1.26 ± 10% RAD
19	DATA BIT RATE (DB-BITS/S)	42.1	0	16,384 BITS/S
20	RECEIVER LOSS (DB)	-3.0	0.5	ESTIMATED FROM JPL TM 33-571 & 810-5
21	E_B/N_O (DB) (12+18-19+20)	6.7	1.5	RSS TOLERANCES
22	REQUIRED E_B/N_O (DB)	5.0	0	BLOCK CODING (32,6)
23	PERFORMANCE MARGIN (DB) (21-22)	1.7	1.5	RSS TOLERANCES

TABLE V- 3 TORO, GEOGRAPHOS ENCOUNTER - S-BAND DESIGN CONTROL TABLE

NO.	PARAMETER	NOMINAL	ADVERSE	NOTES
1	FREQUENCY (MHZ)	2300	-	S-BAND
2	RANGE (AU)	1.8	-	END OF MISSION
3	TRANSMITTER POWER (DBM)	37.8	0.4	6 WATTS NOMINAL
4	TRANSMITTER CIRCUIT LOSS (DB)	-1.4	0.1	
5	TRANSMITTER ANTENNA GAIN (DB)	23.0	0.5	0.92 METER (3-FOOT) DISH
6	POINTING LOSS (DB)	-2.8	0.3	CONSCAN LOSS PLUS 0.017 RAD (1 DEG) ATTITUDE ERROR
7	POLARIZATION LOSS (DB)	-0.1	0.1	
8	SPACE LOSS (DB)	-268.2	0	254.32 GIGAMETERS (1.7 AU)
9	RECEIVER ANTENNA GAIN (DB)	61.6	0.6	64 METERS
10	TOTAL RECEIVED POWER (DBM) (3+4+5+6+7+8+9)	-150.1	0.9	RSS TOLERANCES
11	RECEIVER NOISE SPECTRAL DENSITY (DBM/HZ)	-184.0	0.9	29°K NOMINAL
12	P_T/N_O (DB-HZ) (10-11)	33.9	1.3	RSS TOLERANCES
<u>CARRIER TRACKING PERFORMANCE</u>				
13	CARRIER MODULATION LOSS (DB)	-6.1	1.7	$1.05 \pm 10\%$ RAD
14	THRESHOLD LOOP BANDWIDTH (DB-HZ)	10.3	0.5	$2 B_{LO} = 10.8 \pm 10\%$ HZ
15	LOOP SNR (DB) (12+13-14)	17.5	2.4	RSS TOLERANCES
16	REQUIRED LOOP SNR (DB)	12.0	0	RECOMMENDED
17	PERFORMANCE MARGIN (DB) (15-16)	5.5	2.2	RSS TOLERANCES
<u>DATA CHANNEL PERFORMANCE</u>				
18	DATA MODULATION LOSS (DB)	-1.2	0.6	$1.05 \pm 10\%$ RAD
19	DATA BIT RATE (DB-BITS/S)	21.1	0	128 BITS/S
20	RECEIVER LOSS (DB)	-4.8	0.5	ESTIMATED FROM NASA/ARC DATA
21	E_B/N_O (DB) (12+18-19+20)	6.8	1.5	RSS TOLERANCES
22	REQUIRED E_B/N_O (DB)	2.7	0	10^{-3} FRAME DELETION RATE SEQUENTIAL DECODING
23	PERFORMANCE MARGIN (DB) (21-22)	4.1	1.5	RSS TOLERANCES

TABLE V- 4 TORO, GEOGRAPHOS - X-BAND DESIGN CONTROL TABLE

NO.	PARAMETER	NOMINAL	ADVERSE	NOTES
1	FREQUENCY (MHZ)	8444	-	X-BAND
2	RANGE (AU)	1.8	-	END OF MISSION
3	TRANSMITTER POWER (DBM)	37.8	0.4	6 WATTS NOMINAL
4	TRANSMITTER CIRCUIT LOSS (DB)	-2.0	0.1	
5	TRANSMITTER ANTENNA GAIN (DB)	35.0	0.5	0.92 METER (5-FOOT) DISH
6	POINTING LOSS (DB)	-3.0	0.3	1.4°
7	POLARIZATION AND WEATHER LOSS (DB)	-0.4	0.1	
8	SPACE LOSS (DB)	-279.5	0	1.8 AU
9	RECEIVER ANTENNA GAIN (DB)	71.6	0.6	64 METERS
10	TOTAL RECEIVED POWER (DBM) (3+4+5+6+7+8+9)	-140.5	0.9	RSS TOLERANCES
11	RECEIVER NOISE SPECTRAL DENSITY (DBM/HZ)	-182.7	0.9	39°K NOMINAL
12	P_T/N_O (DB-HZ) (10-11)	42.2	1.3	RSS TOLERANCES
<u>CARRIER TRACKING PERFORMANCE</u>				
13	CARRIER MODULATION LOSS (DB)	-10.2	2.7	$1.26 \pm 10\%$ RAD
14	THRESHOLD LOOP BANDWIDTH (DB-HZ)	10.3	0.5	$2 B_{LO} = 10.8 \pm 10\%$ HZ
15	LOOP SNR (DB) (12+13-14)	21.7	3.0	RSS TOLERANCES
16	REQUIRED LOOP SNR (DB)	15.0	0	RECOMMENDED 810-5
17	PERFORMANCE MARGIN (DB) (15-16)	6.7	3.0	RSS TOLERANCES
<u>DATA CHANNEL PERFORMANCE</u>				
18	DATA MODULATION LOSS (DB)	-0.4	0.4	$1.26 \pm 10\%$ RAD
19	DATA BIT RATE (DB-BITS/S)	33.1	0	2048 BITS/S
20	RECEIVER LOSS (DB)	-3.0	0.5	ESTIMATED FROM JPL TM 33-571 & 810-5
21	E_B/N_O (DB) (12+18-19+20)	5.7	1.5	RSS TOLERANCES
22	REQUIRED E_B/N_O (DB)	4.0	0	BLOCK CODING (32,6)
23	PERFORMANCE MARGIN (DB) (21-22)	1.7	1.5	RSS TOLERANCES

TABLE V- 5 UPLINK COMMAND DESIGN CONTROL TABLE, 64 METER NET

NO.	PARAMETERS	NOMINAL	ADVERSE	NOTES
1	FREQUENCY (MHZ)	2115	-	S-BAND
2	RANGE (AU)	1.8	-	
3	TRANSMITTER POWER (DBM)	73.0	0	20 KW
4	TRANSMITTER ANTENNA GAIN (DB)	60.6	0.9	64 METER DSS
5	SPACE LOSS	-267.4	-	
6	RECEIVER ANTENNA GAIN (DB)	-1.0	0.3	OMNI
7	POINTING LOSS (DB)	0	0.2	
8	POLARIZATION LOSS (DB)	-0.5	0.1	
9	RECEIVER CIRCUIT LOSS (DB)	-1.9	0.2	
10	TOTAL RECEIVED POWER (DBM) (3+4+5+6+7+8+9)	-137.2	1.0	
11	RECEIVER NOISE SPECTRAL DENSITY (DBM/HZ)	-169	1.0	$T_{SYS} = 910^{\circ}K$, NF = 6 DB
12	P_T/N_O (DB-HZ) (10-11)	31.8	1.4	
	<u>CARRIER TRACKING PERFORMANCE</u>			
13	CARRIER MODULATION LOSS (DB)	-2.8	0.3	B = 1.09 RAD
14	THRESHOLD LOOP BANDWIDTH (DB-HZ)	13.0	1.0	$2 B_{LO} = 20$ HZ AT 6 DB SNR
15	LOOP SNR (DB) (12+13-14)	16.0	1.8	
16	REQUIRED LOOP SNR = LIMITER LOSS (DB)	6.3	-	LIMITER LOSS = 0.3 DB
17	PERFORMANCE MARGIN (DB) (15-16)	9.7	1.8	RSS TOLERANCES
	<u>COMMAND CHANNEL PERFORMANCE</u>			
18	DATA MODULATION LOSS (DB)	-3.6	0.4	B = 1.09 RAD
19	DATA BIT RATE (DB-BITS/S)	0	-	1 BIT/S
20	RECEIVER LOSS (DB)	-1.1	-	RECEIVER, FILTER, AND LIMITER LOSS
21	E_B/N_O (DB) (12+18-19+20)	27.1	1.5	
22	REQUIRED E_B/N_O (DB)	17.3	1.0	10^{-5} BIT ERROR RATE
23	PERFORMANCE MARGIN	9.8	1.8	RSS TOLERANCES

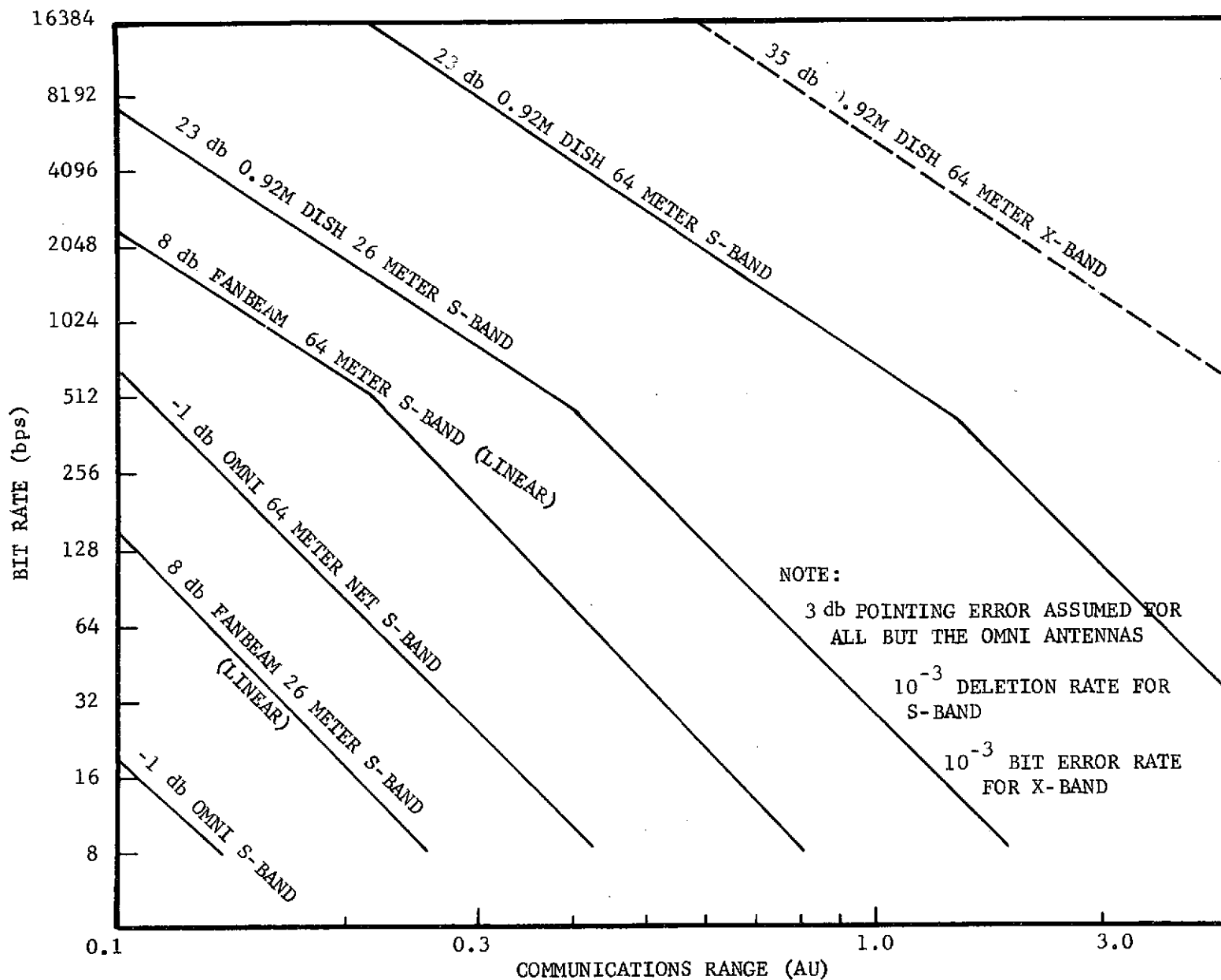


FIGURE V-15 DATA RATE VS RANGE

is a command link table for asteroid encounter range using a blind command into the spacecraft omni antenna.

Tables V-6 and V-7 provide a summary of communications parameters and list of components with weight and power for Configuration 2, an Earth pointing spacecraft.

Tables V-8 and V-9 provide similar data for Configurations 1, 3, 4 and 5 less the fanscan and associated switch and conscan processor. Use of fanscan requires adding the following to Table V-9:

<u>Component</u>	<u>Weight</u>		<u>Power</u> (watts)
	kg	(lb)	
Fanscan Antenna	0.46	1.0	0
S-band Switch	0.46	1.0	Negligible
Conscan Processor	0.36	0.8	1.2

1. Optional High Gain Antenna and Transmitter Implementation

Some of the S-band-only options considered for an Earth pointing spacecraft are shown in Table V-10. However, due to the low bit rates compared to an X-band system and the fact that the selected science configurations required a minimum bit rate of 16,384 bps at Encke, a dual S-band and X-band system was selected. Options for implementing the high data rate link for an Earth pointing spacecraft are shown in Table V-11 for the Encke reference trajectory and the Encke/Geographos/Toro mission. Similar options are available for Configurations 1, 3, 4 and 5 except a single dish is required for these configurations. For Configurations 3, 4 and 5 a despun reflector option is also available as long as the spin axis of the spacecraft is maintained perpendicular to the Earth spacecraft line. Bit rates for a combination of S-band and X-band reflectors plus 6 or 10 watt transmitters are shown in Table V-12. None of the despun reflector configurations were chosen because the bit rates were too low, even with a 10 watt transmitter. However, due to the advantage of not having to provide electrical connections across rotary joints, one should investigate further the possible use of such a system.

2. Communications Hardware

a. Antennas - Conical spiral omni antennas are available from Pioneer 10 and 11 and from the Defense Support Program (DSP). The fanscan antenna can be

TABLE V-6 COMMUNICATIONS FEATURES FOR AN EARTH POINTING SPACECRAFT

<u>CHARACTERISTIC</u>	<u>VALUE</u>
High Gain Antenna(s)	
Size (meters)	0.92
Gain (dB)	
S-band	23
X-band	35
Half Power Beamwidth (deg)	
S-band	10.5
X-band	2.8
Transmitter Power - RF (watts)	
S-band	6
X-band	6
Telemetry Data Rate (bps)	
S-Band High Gain	
Encke	2048 (0.57 AU) 4096 (0.353 AU)
Toro/Geographos	128
X-band High Gain	
Encke	16348 (0.57 AU) 32768 (0.353 AU)
Toro/Geographos	2048
Error Control Encoding	
S-band	Convolutional
X-band	*Block
Command Data Rate	1 Bit/Second
Subsystem Weight (kg & lb)	13.1 & 28.7
Subsystem Power (watts)	
S-band	33.5
X-band	28.0
Other Features	S-band Conscan

*NOTE: Block coding was chosen for X-band due to the high data rates.
This is in conformance with JPL 810-5.

TABLE V-7 COMMUNICATIONS COMPONENTS, WEIGHT AND POWER FOR AN EARTH POINTING SPACECRAFT

COMPONENT	ENCKE ONLY MISSION				ENCKE/TORO/GEOGRAPHOS			
	NO. PER S/C	WEIGHT (kg) (lb)		POWER (watts)	NO. PER S/C	WEIGHT (kg) (lb)		POWER (watts)
Receivers S-band	2	2.4	5.2	4.0	2	2.4	5.2	4.0
Transmitter S-band								
Transmitter Driver	2	1.1	2.4	3.0	2	1.1	2.4	3.0
Power Amplifier	2	0.9	2.0	25.0	2	0.9	2.0	25.0
Diplexer S-band	2	2.0	4.3	0	2	2.0	4.3	0
Switch S-band	3	1.4	3.0	0	4	1.8	4.0	0
Switch X-band	0	0	0	0	1	0.4	1.0	0
Forward Omni	1	0.4	0.9	0	1	0.4	0.9	0
Aft Omni	1	0.4	0.9	0	1	0.4	0.9	0
Fore High Gain Antenna	0	0	0	0	1	3.2	7.0	0
Aft High Gain Antenna	1	3.2	7.0	0	1	3.2	7.0	0
X-band Driver	1	0.5	1.2	3.0	1	0.5	1.2	3.0
X-band TWTA	1	0.4	1.0	25.0	1	0.4	1.0	25.0
Conscan Processor	1	0.4	0.8	1.2	1	0.4	0.8	1.2
TOTAL		13.1	28.7	61.2		17.1	37.7	61.2

TABLE V-8 MAJOR COMMUNICATIONS SUBSYSTEM CHARACTERISTICS FOR ALL SPACECRAFT CONFIGURATIONS EXCEPT NUMBER 2.

<u>CHARACTERISTIC</u>	<u>VALUE</u>
High Gain Antenna	
Size (meters)	0.92
Gain (dB)	
S-band	23
X-band	35
Half Power Beamwidth	
S-band	10.5
X-band	2.8
Transmitter Power - RF (watts)	
S-band	6
X-band	6
Telemetry Data Rate	
S-band High Gain	
Encke	2048 (0.57 AU) 4096 (0.353 AU)
Toro/Geographos	128 (1.8 AU)
X-band High Gain	
Encke	16384 (0.57 AU) 32768 (0.353 AU)
Toro/Geographos	2048 (1.8 AU)
Error Control Encoding	
S-band	Convolutional
X-band	Block
Command Data Rate	1 Bit/Second
Subsystem Weight (kg & lb)	12.7 & 27.9 - (No Autotrack) 14.3 & 31.5 - (With Autotrack)
Subsystem Power (watts)	
S-band	32 - (No Autotrack) 35 - (With Autotrack)
X-band	28
Other Features	Earth Autotracking Antenna

TABLE V-9 COMMUNICATIONS COMPONENTS, WEIGHT AND POWER FOR ALL SPACECRAFT CONFIGURATIONS EXCEPT NUMBER 2.

AUTOTRACK, NO AUTOTRACK OPTIONS COMPONENT	NO AUTOTRACKING ANTENNA				WITH AUTOTRACKING ANTENNA			
	NO. PER S/C	WEIGHT (kg) (lb)		POWER (watts)	NO. PER S/C	WEIGHT (kg) (lb)		POWER (watts)
Receivers S-band	2	2.4	5.2	4.0	2	2.4	5.2	4.0
Error Channel Receiver	0	0	0	0	1	1.2	2.6	2.0
Transmitter S-band								
Transmitter Driver	2	1.1	2.4	3.0	2	1.1	2.4	3.0
Power Amplifier	2	0.9	2.0	25.0	2	0.9	2.0	25.0
Diplexer S-band	2	2.0	4.3	0	2	2.0	4.3	0
Switch S-band	3	1.4	3.0	Nom.	3	1.4	3.0	Nom.
Forward Omni Antenna	1	0.4	0.9	0	1	0.4	0.9	0
Aft Omni Antenna	1	0.4	0.9	0	1	0.4	0.9	0
Despun High Gain Antenna	1	3.2	7.0	*	1	3.2	7.0	*
X-band Driver	1	0.5	1.2	3.0	1	0.5	1.2	3.0
X-band TWTA	1	0.4	1.0	25.0	1	0.4	1.0	25.0
Autotrack Error Signal Processor	0	0	0	0	1	0.4	1.0	1.0
TOTAL		12.7	27.9	60.0		14.3	31.5	63.0
* Servo Drive Part of Attitude Control Subsystem								

TABLE V-10 TELEMETRY OPTIONS FOR A S-BAND ONLY CAPABILITY CONSIDERED FOR AN EARTH POINTING SPACECRAFT CONFIGURATION 2.

Earth Pointing Spacecraft (S-band only)

Encke Only Mission (0.57 AU Range)

<u>Option</u>		<u>Bit Rate</u>	<u>Body</u>	<u>Conscan</u>
1	3' Dish and 10 W S-Band	4096	Encke	No
2	3' Dish and 6 W S-Band	2048	Encke	No
3	2.5' Dish and 10 W S-Band	2048	Encke	No
4	2.5' Dish and 6 W S-Band	1024	Encke	No
5	2' Dish and 10 W S-Band	2048	Encke	No
6	2' Dish and 6 W S-Band	1024	Encke	No

Encke, Toro, Geographos (0.353, 1.8 and 1.8 AU Ranges)

<u>Option</u>		<u>Bit Rate</u>	<u>Body</u>	<u>Conscan</u>
1	Aft End 3' Dish and 10 W S-Band	8192	Encke	No
	Fore End 5' Dish and 10 W S-Band	1024	Toro/Geo	Yes
2	Aft End 2.5' Dish and 10 W S-Band	4096	Encke	No
	Fore End 5' Dish and 10 W S-Band	1024	Toro/Geo	Yes
3	Aft End 2' Dish and 10 W S-Band	4096	Encke	No
	Fore End 5' Dish and 10 W S-Band	1024	Toro/Geo	Yes
4	Aft End 3' Dish and 10 W S-Band	8192	Encke	No
	Fore End 3' Dish and 10 W S-Band	256	Toro/Geo	Yes
5	Aft End 2.5' Dish and 10 W S-Band	4096	Encke	No
	Fore End 3.0' Dish and 10 W S-Band	256	Toro/Geo	Yes
6	Aft End 2.0' Dish and 10 W S-Band	4096	Encke	No
	Fore End 3.0' Dish and 10 W S-Band	256	Toro/Geo	Yes

TABLE V- 11 DUAL S-BAND AND X-BAND TELEMETRY OPTIONS CONSIDERED FOR AN EARTH POINTING SPACECRAFT

Earth Pointing Spacecraft (S-Band and X-Band)

Encke Reference Trajectory (0.57 AU Range)

<u>Option</u>		<u>Bit Rate</u>	<u>Body</u>
1	3' Dish and 10 W X-Band	32768	Encke
	3' Dish and 10 W X-Band	4096	Encke
2	3' Dish and 10 W X-Band	32768	Encke
	3' Dish and 6 W S-Band	2048	Encke
Recommended 3	3' Dish and 6 W X-Band	16384	Encke
	3' Dish and 6 W S-Band	2048	Encke
4	2.5' Dish and 10 W X-Band	16384	Encke
	2.5' Dish and 10 W S-Band	2048	Encke

Encke, Toro, Geographos Trajectory (0.353, 1.8 and 1.8 AU Range, Respectively)

<u>Option</u>		<u>Bit Rate</u>	<u>Body</u>
Recommended 1	3' Aft Dish and 6 W X-Band	32768	Encke
	3' Aft Dish and 6 W S-Band	4096	Encke
	3' Fore Dish and 6 W X-Band	2048	Toro/Geo
	3' Fore Dish and 6 W S-Band	128	Toro/Geo
	2' Aft Dish and 6 W X-Band	16384	Encke
	2' Aft Dish and 6 W X-Band	2048	Encke
2	3' Fore Dish and 6 W X-Band	2048	Toro/Geo
	3' Fore Dish and 6 W X-Band	128	Toro/Geo
	2' Aft Dish and 10 W X-Band	32768	Encke
	2' Aft Dish and 10 W S-Band	4096	Encke
	3' Fore Dish and 10 W X-Band	2048	Toro/Geo
	3' Fore Dish and 10 W X-Band	256	Toro/Geo

TABLE V-12 SPACECRAFT SPIN AXIS PERPENDICULAR TO EARTH SPACECRAFT PLANE
(S-BAND OR S-BAND AND X-BAND).

Note: For this spacecraft attitude we have all the options of antenna size and transmitter power available that are available for the Encke Pointing Spacecraft case plus the following additional options related to despinning an antenna reflector

Encke Only Mission (0.57 AU Range)

<u>Despun Reflector Options</u>		<u>Bit Rate</u>	<u>Body</u>
1	22.5 dbi Reflector and 6 W S-Band	2048	Encke
2	22.5 dbi Reflector and 10 W S-Band	2048	Encke
3	22.5 dbi Reflector and 6 W S-Band	2048	Encke
	27.0 dbi Reflector and 6 W X-Band	2048	Encke
4	22.5 dbi Reflector and 10 W S-Band	2048	Encke
	27.0 dbi Reflector and 10 W X-Band	4096	Encke

Encke, Toro, Geographos (0.353, 1.8 and 1.8 AU)

<u>Despun Reflector Options</u>		<u>Bit Rate</u>	<u>Body</u>
1	22.5 dbi Reflector and 6 W S-Band	4096	Encke
		128	Toro/Geo
2	22.5 dbi Reflector and 10 W S-Band	8192	Encke
		256	Toro/Geo
3	22.5 dbi Reflector and 6 W S-Band	4096	Encke
		128	Toro/Geo
	27.0 dbi Reflector and 6 W X-Band	4096	Encke
		128	Toro/Geo
4	22.5 dbi Reflector and 10 W S-Band	8192	Encke
		256	Toro/Geo
	27.0 dbi Reflector and 10 W X-Band	16384	Encke
		256	Toro/Geo

NOTE: These data are based on Helios type colinear mounted S and X-Band feed and reflectors. The S Band feed is made up of 10 colinear slot dipole arrays. The feed dimensions are 0.61 M high by 0.05 M diameter with a 0.6 M high parabolic reflector measuring 1.1 M across the open face. The X Band feed is 0.15 M high by 0.15 M diameter and contains 8 slots. The X-Band reflector is 0.15 M high by 0.4 M across the open face.

shortened Pioneer 6 through 9 Franklin array with a peak gain of 7.5 dbi, linear polarization and half power beam width of 12 degrees. The pancake shaped beam will be tilted 3.5 degrees for a 1 dB fanscan crossover.

The 0.92 meter dish is similar in construction to the designs flown on Defense Satellite Communications System Phase II (DSCS II) spacecraft of aluminum honeycomb construction with fiberglass face sheets and vacuum deposited aluminum reflecting surface. The circular polarization feeds for S band Earth pointing conscan arrangement and X-band channel are separate 13 element and 9 element log periodic cross dipole feeds giving 23 and 35 dbi gains.

For the auto tracking S-band feed application a 4 arm conical spiral feed can be utilized with a 2 channel DF system. A separate X-band feed is required for the X-band link.

b. Diplexers and Switches - Pioneer 10 and 11 diplexer and RF switches can be used as low cost qualified components for these applications.

c. Transponder (S-band Receiver/Transmitter Driver) - Viking lander transponders by Philco Ford modified to give conscan AGC output and X-band drive are proposed for all configurations. Motorola also is in a position to provide S-band transponders and X-band drive. TRW is also a possible source of such units.

d. S-band Power Amplifiers - Solid state S-band power amplifiers are available from microwave Semiconductor Corporation, Philco Ford and others. These units are state-of-art, but require space qualification.

e. X-band Driver - An X-band driver is required to provide modulation and drive for the TWTA. Either modification of the S-band driver to also supply X-band, or a new design X-band modulator driver would be required.

f. X-band TWTA - Watkins-Johnson & Hughes are potential sources for the X-band TWTA. Watkins-Johnson WJ 391-2 TWT is an example of a tube suitable for this application.

g. Error Channel Receiver - The error channel receiver should exhibit the same phase and amplitude characteristics as the sum channel for a good autotracking system. Presumably a modification of the receiver portion of an S-band transponder could be accomplished to provide this function.

h. Error Channel Signal Processor - This unit must compare the phase and amplitude of the sum and difference channels of the S-band tracking system to generate the error signals. It could be combined with the error channel receiver in a common chassis.

i. Conscan Processor - The conscan processor is a flight-proven unmodified Pioneer 10 and 11 unit used with the offset feed of the conscan dish. It estimates the phase and amplitude of the signal embedded in noise produced by antenna pattern distortion or other sources. Phase angle determines the precession thruster firing while amplitude terminates the conscan when the vehicle is Earth pointing within the dead zone about the spin axis. The processor requires an accurate spin reference which is supplied by the sun sensor. The conscan processor design can also be used with a fanscan antenna because it rejects even harmonics of the spin frequency. If the spin axis is offset from the plane normal to the Earth line, the AGC signal from the receiver will contain a component at the spin frequency whose amplitude is a function of the pointing error.

j. Rotary Joints All the configurations studied with the exception of the Earth-pointing spacecraft, (Configuration 2) and the despun reflector configurations will require the transmission of RF signals across rotary joints unless one mounts receivers and transmitters on the despun platform. Both Sage and Philco Ford have developed multichannel S-band and X-band rotary joints, but until a suitable one has been flight proven the design risk is relatively high.

C. PROBE COMMUNICATIONS

A communication link between a probe (targeted to Encke) and the spacecraft or, alternatively, directly from the probe to Earth is required to return data to Earth. A probe data transmission rate of 128 bps is desired; however, a 64 bps rate was also investigated for comparison purposes.

Included in the primary factors to be considered in sizing the communications links for this application are communications range and antenna aspect angles for the probe and spacecraft relay antennas. These vary with the separation and spacecraft delta velocity as shown in Figure III-14 for the selected technique. A maximum range of 7774 km and a probe-to-spacecraft antenna aspect angle of 40° have been selected as the most promising for the relay geometry. A range of 0.57 AU results for the probe to Earth direct link for an Encke only mission while a range of 0.353 AU is experienced for an Encke, Geographos, Toro trajectory. Spacecraft relay antenna aspect angle varies with the basic pointing philosophy associated with the spacecraft spin axis such as Earth pointing, Encke pointing, or spin axis perpendicular to the orbit plane. Because of the variation of spacecraft antenna aspect angle with the spacecraft attitude philosophy, the basic link treatment will be in terms of the sum of transmit and receive antenna gains and transmitter power in dBW where dBW is dB referenced to a 1W source and zero dB antenna gain. These data will then be applied to each spacecraft attitude to determine antenna gain and transmitter power requirements.

Other parameters such as frequency and modulation considered in the design of the probe communications link are shown in Table V-13.

Relay Link Calculations - Two modulation systems (wideband FSK and Coherent PSK/PM) will be investigated for this application. A wideband FSK relay link compared to a coherent PSK/PM link has the advantage that no frequency searching is required. The disadvantage is that at any given frequency higher power is required. Two frequencies will be considered, 380 MHz and 1700 MHz, which correspond respectively to the Viking '75 relay link and a C-band frequency allocation for space application. Table V-14 shows the link calculations for an uncoded wide band FSK link at 64 bps and 128 BPS at the two radio frequencies resulting in a total required probe Effective

TABLE V-13 PROBE COMMUNICATIONS LINK PARAMETERS

- o Frequency
 - Relay Link
 - 400 MHz
 - 1700 MHz
 - Direct Link
 - 2295 MHz
- o Modulation
 - Wideband Binary FSK
 - Coherent PSK/PM
- o Error Control Coding
 - Uncoded only for relay links
 - Convolutional coding only for direct to Earth link
- o Antenna Types
 - Spacecraft
 - Conical Helix
 - Turnstile Over Cone
 - Turnstile
 - Probe
 - Turnstile Over Cone
 - Flat Plate Antenna
- o Transmitter Power
 - 20 Watts RF or Less
- o Bit Rates
 - 64 or 128 bps

TABLE V-14 RELAY LINK CALCULATIONS, WIDE BAND FSK

7774 km RANGE

LOSSES		380 MHz		1700 MHz	
Transmit Circuit Loss		- 1.0 dB		- 1.0 dB	
Space Loss (7774 km)		- 162.3 dB		- 174.9 dB	
Polarization Loss		- 1.0 dB		- 1.0 dB	
Receive Circuit Loss		- 1.5 dB		- 1.5 dB	
TOTAL		- 165.8 dB		- 178.4 dB	
REQUIRED SIGNAL/ N_0	FOR	64 bps	128 bps	64 bps	128 bps
E_b/N_0 (10,000 Hz Freq. Uncertainty)		18.1 dB	16.9 dB	18.1 dB	16.9 dB
Bit Rate		18.1 dB	21.1 dB	18.1 dB	21.1 dB
Assumed Margin		3.0 dB	3.0 dB	3.0 dB	3.0 dB
		39.2 dB	41.0 dB	39.2 dB	41.0 dB
NOISE POWER DENSITY (1310°)		- 199.2 dBW (4 dBNF & 150° ANT)		- 197.4 dBW (6 dBNF & 150° ANT)	
REQUIRED SIGNAL (dBW)		-156.2 dBWi	-154.4 dBWi	-154.4 dBWi	-152.4 dBWi
REQUIRED EIRP	dBW	+ 5.8 dBW	+ 7.6 dBW	+20.2 dBW	+22.2 dBW
+ RECEIVE ANT GAIN					

Isotropic Radiated Power (EIRP) plus spacecraft antenna gain of 5.8 dBWi at 380 MHz and 128 bps. In this case, EIRP is the sum of transmitter power in dBW and antenna gain in dBi, where i is isotropic. At 1700 MHz, 20.2 dBWi is required for 64 bps and 22.2 dBWi for 128 bps. Clearly, 380 MHz is the better frequency from an EIRP standpoint. A 10 kHz total frequency uncertainty due to Doppler shift and oscillation stability was assumed for each link and the E_b/N_o was chosen for a bit error probability of 1 part in 10^3 considering the ratio of filter bandwidth (ahead of the detectors) to bit rate.

Calculations for a coherent PSK/PM relay link at 1700 MHz are shown in Table V-15 for the two bit rates. A probe EIRP plus spacecraft antenna gain of 13.9 dBWi and 16 dBWi are required for bit rates of 64 and 128 bps respectively using an uncoded system and a 20 Hz threshold loop bandwidth for the receiver. Thus approximately 6.3 dB is saved by use of PSK/PM over Wideband FSK at 1700 MHz. A comparison of the gain requirements for these 3 links shows that the 380 MHz wide band FSK link requires the least gain due to the inverse frequency ratio squared space loss and use of PSK/PM at 380 MHz would further reduce the gain requirements, however, frequency search and antenna dimensions (the latter are roughly proportional to frequency) must also be considered before one selects a final configuration.

Performing a frequency search followed by the phase tracking of the carrier and subcarrier as required for PSK/PM was considered so undesirable for the 380 MHz link (due to the low transmitter power required for Wideband FSK at 380 MHz) that no further consideration is given to PSK/PM at 380 MHz. The other 3 options are now investigated for the various spacecraft configurations (spin orientations).

Probe Relay Link to an Earth Pointing Spacecraft - For an Earth pointing spacecraft and a probe to spacecraft relay link, the probe antenna aspect angle is 40 degrees and the spacecraft antenna aspect angle from Table V-16 is 22.9° for the reference Encke mission and about 20° for the Encke, Toro, Geographos mission. Available gain from typical 1700 MHz antennas scaled from a proposal Pioneer probe antenna are shown below. The 380 MHz antenna gains are based on the Viking Orbiter 75 spacecraft relay antenna, Figure V-16, and a newly developed flat plate probe antenna concept developed by Langly, NASA (ref. V-1a). Size and weight for the latter are estimated as shown in Figure V-17.

TABLE V-15 RELAY LINK CALCULATIONS, COHERENT PSK/PM
7774 km RANGE, 1700 MHz, UNCODED

LOSSES

TRANSMIT CIRCUIT LOSS	1.0 dB
SPACE LOSS (7774 km 1700 MHz)	174.9 dB
POLARIZATION LOSS	1.0 dB
RECEIVE CIRCUIT LOSS	1.5 dB
	<hr/>
	-178.4 dB

NOISE POWER DENSITY (1310°K) -197.4 dBW

REQUIRED SIGNAL/ N_o FOR 128 bps 64 bps

CARRIER

MODULATION LOSS (dB)	6.5	4.4
ADDITIONAL LOSSES (dB)	1.0	1.0
THRESHOLD LOOP BW (dB)	13.0	13.0
REQUIRED SNR (dB)	11.0	11.0
MARGIN ALLOWANCE (dB)	3.5	3.5
	<hr/>	<hr/>
	35.0 dB	32.9 dB

DATA

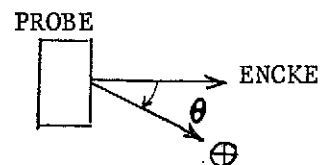
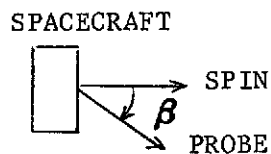
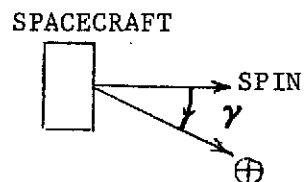
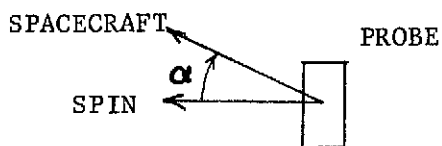
MODULATION LOSS (dB)	1.1	2.0
ADDITIONAL LOSSES (dB)	3.0	3.0
BIT RATE (dB)	21.1	18.1
E_b/N_o (dB) ($P_e=10^{-3}$)	6.8	6.8
MARGIN (dB)	3.0	3.0
	<hr/>	<hr/>
	35.0 dB	32.9 dB

REQUIRE SIGNAL LEVEL -158.6 dBW -160.7 dBW

REQUIRED EIRP DBW i 16.0 dBW i 13.9 dBW i
+ RECEIVE ANT GAIN

TABLE V-16 RANGES AND ANTENNA ASPECT ANGLES FOR
PROBE RELAY AND PROBE DIRECT LINKS

SPACECRAFT ATTITUDE OPTION	TIME FROM PROBE ENTERING COMA	β		α	γ		θ		RANGE RELAY LINK (KM)	RANGE TO EARTH (AU)	
	(MINUTES)	(DEG)		(DEG)	(DEG)		(DEG)			(AU)	
		*	**		*	**	*	**		*	**
SPIN AXIS	-10	30	40	40	46	56	52.8	60	7756	0.57	0.353
TO ENCKE	- 5	25			45				7760		
	0	20	20		43	53			7763		
	5	10			41				7767		
	10	5	0		37				7770		
	15	0			30	40			7774		
SPIN AXIS	-10	22.9	20	40	0	0	52.8	60	Same	0.57	0.353
TO	to										
EARTH	+15										
SPIN AXIS	-10	90	90	40	110	125	52.8	60	Same	0.57	0.353
⊥ TO SPACE-	to										
CRAFT ORBIT	+15										
PLANE											



NOTE:

* FOR ENCKE REFERENCE TRAJECTORY

** FOR ENCKE, TORO, GEOGRAPHOS TRAJECTORY

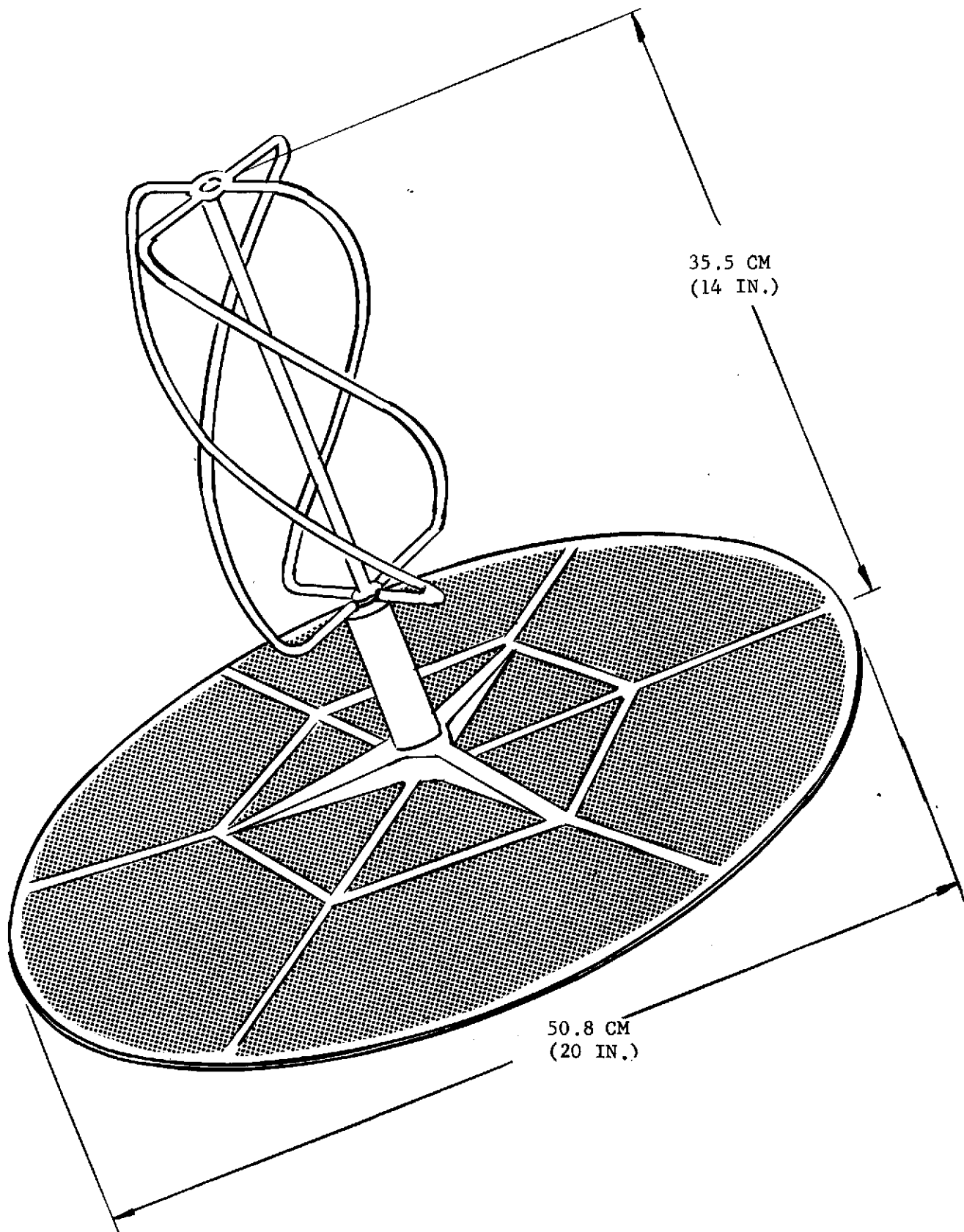
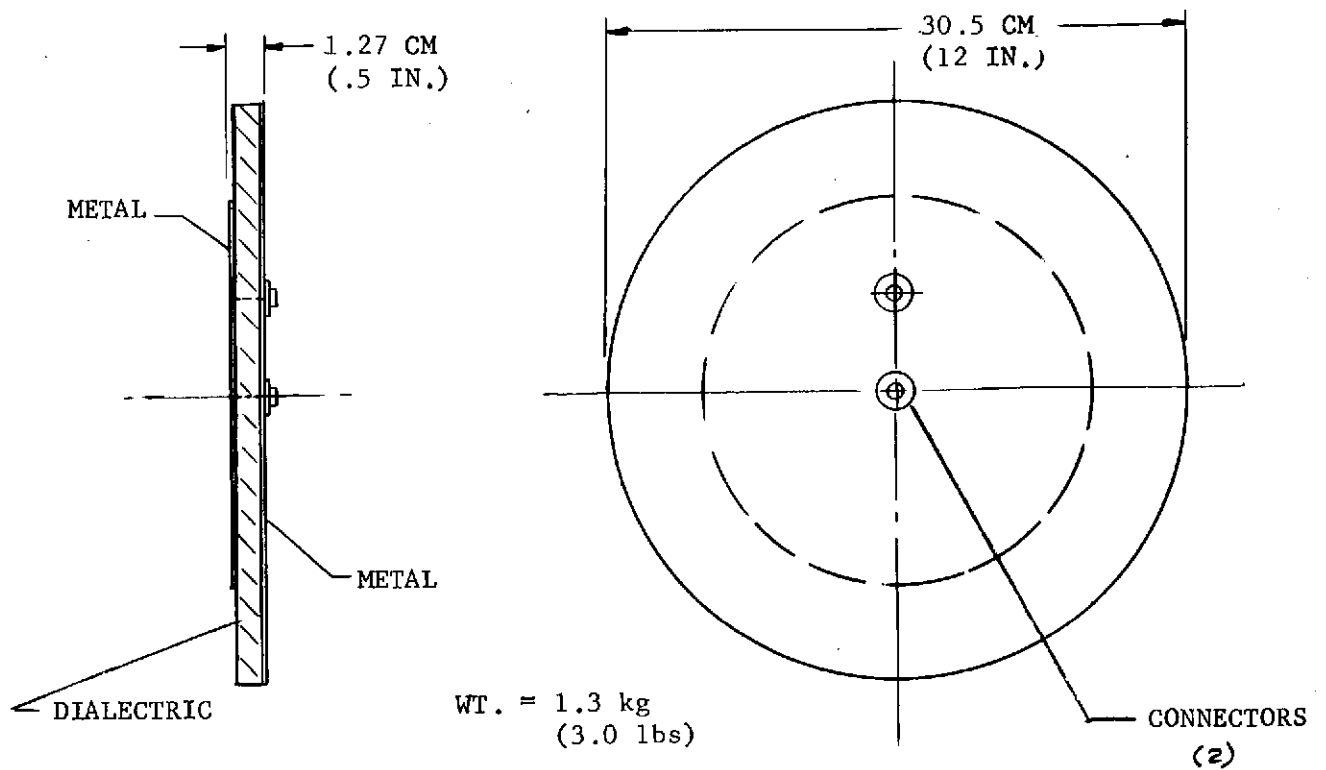


FIGURE V-16 380 MHZ VIKING '75 ORBITER RELAY ANTENNA (ref. V-1b)



NOTE: This is based on the report of a Langley Research Center development and is a rather gross approximation of size and weight.

FIGURE V-17 PROBE FLAT PLATE ANTENNA OUTLINE DIMENSIONS

	1700 MHz	380 MHz
Probe antenna gain at 40°	3.5	3.5
Spacecraft antenna gain at 22.5°	4.5	2.5
Total antenna gain (dBi)	8.0	6.0

Subtracting the total antenna gain from the total gain requirements for 64 bps computed above we have the required transmitter power for 64 bps =

	dBW	Watts
380 MHz Wideband FSK (5.8 dBWi - 6 dBi)	-0.2	0.95
1700 MHz Wideband FSK (20.2 dBW - 8 dBi)	+12.2	16.6
1700 MHz coherent PSK/PM (13.9 dBW - 8dBi)	+ 5.9	3.9

Required transmitter power for 128 bps	dBW	Watts
380 MHz Wideband FSK (7.6 dBWi - 6.0 DBi)	+1.6	1.45
1700 MHz Wideband FSK (22.2 dBWi - 8.0 DBi)	+14.5	28.2
1700 MHz Coherent PSK/PM (16.0 dBWi - 8 dBi)	+ 8.0	6.3

Any of the three approaches considered above are feasible, however, the 1700 MHz wideband FSK requires excessive power for a 128 bps rate and should be ruled out. For completeness, Tables V-17, V-18, and V-19 show size, weight, and power for the three relay link approaches providing a bit rate of 128 bps.

Probe Relay Link to an Encke Pointing Spacecraft - There is one basic difference in relay link requirements for an Encke pointing spacecraft as opposed to an Earth pointing Spacecraft, that is, the spacecraft relay antenna aspect angle changes by 30 to 40° as spacecraft attitude is changed to keep the spin axis pointed to Encke. The net result of this requirement is changing effective spacecraft antenna gain as a function of time and a requirement to increase probe transmitter power to compensate for the reduced antenna gain. The spacecraft antenna aspect angle from Table V-16 changes over a range of 40° to 0° during the transmission period. Taking the worst case of 40° gives a spacecraft antenna gain of 3.5 dBi at 1700 MHz for the turnstile over cone and 2.0 dBi for the Viking orbiter 380 MHz antenna. These effective gains amount to 1.0 dB reduction in spacecraft antenna gain for the 1700 MHz links and 0.5 dB for the 380 MHz link. The required probe transmitter powers for the 3 cases for 64 and 128 bps are as given below:

TABLE V-17 380 MHz WIDEBAND FSK COMMUNICATIONS EQUIPMENT FOR PROBE TO SPACECRAFT RELAY LINK

<u>PROBE EQUIPMENT</u>	<u>SIZE</u>	<u>WEIGHT</u>		<u>POWER</u>	<u>COMMENTS</u>
		(kg)	(lb)	(watts)	
Antenna	12 Dia. x 0.5 in. thick 30.5 dia x 1.27 cm thick	1.36	3.0	-	Flat plate OMNI new item
Transmitter (1.5 watts)	5 x 5.5 x 1.4 in. 12.7 x 14 x 3.65 cm	0.91	2.0	6	Modified Teledyne TK-2400 Series
TOTAL		2.27	5.0	6	
<u>SPACECRAFT EQUIPMENT</u>					
Relay Antenna	20 in. dia. ground plane 14 x 4 in. element	1.27	2.8	-	Viking Orbiter Relay Antenna
Relay Receiver & Bit Synchronizer	4.2 x 4.75 x 2.75 in. 10.7 x 12.0 x 7.0 cm	1.8	4.0	3	New item (use basic Viking Orbiter design)
TOTAL		3.07	6.8	3	

NOTES:

1. 128 bps Data Rate
2. 6.0 dBi assumed for sum of probe and spacecraft antenna effective gains.
3. Viking Lander transmitter and Viking Orbiter receiver unsuitable for use on this mission due to excessive size, weight, and bit rate capability.
4. Flat plate OMNI based on Langley Research Center development.

TABLE V-18 1700 MHz WIDEBAND FSK COMMUNICATIONS EQUIPMENT FOR PROBE TO SPACECRAFT RELAY LINK

<u>PROBE EQUIPMENT</u>	<u>SIZE</u>	<u>WEIGHT</u>		<u>POWER</u> (watts)	<u>COMMENTS</u>
		(kg)	(lb)		
Antenna	6.15 dia x 2.9 in 15.6 dia x 7.3 cm	0.32	0.7	-	Turnstile over cone - scaled for 1700 MHz
Transmitter (28 watts)	5 x 5.5 x 1.4 in 12.7 x 14 x 3.65 cm.	1.13	2.5	120.0	Teledyne TR-2400 modified
Stable Oscillator	2.25 x 2.25 x 2.3 in. 5.72 x 5.72 x 5.54 cm	0.34	0.8	2.3	Proposed Pioneer Probe
TOTAL		1.79	4.0	122.3	
<u>SPACECRAFT EQUIPMENT</u>					
Relay Antenna (Note 3)	5.5 dia base x 13.4 cm high 14 dia base x 34 cm high	0.7	1.5	-	Conical helix scaled from Advanced Pioneer Omni
Relay Receiver & Bit Synchronizer	4.2 x 4.75 x 2.75 in 10.7 x 12 x 7.0 cm	1.18	2.6	3.0	New design
TOTAL		1.88	4.1	3.0	

NOTES:

1. 128 bps data rate.
2. Transmitter size based on 8 dBi sum of effective antenna gains.
3. Relay antenna can be identical to probe antenna.

TABLE V-19
1700 mHz COHERENT PSK/PM COMMUNICATIONS EQUIPMENT FOR PROBE TO SPACECRAFT RELAY LINK -
128 bps

<u>PROBE EQUIPMENT</u>	<u>SIZE</u>	<u>WEIGHT</u>		<u>POWER</u>	<u>COMMENTS</u>
		(kg)	(lb)	(watts)	
Antenna	6.15 dia x 2.9 in. 15.6 dia x 7.3 cm	0.32	0.7	-	Turnstile over cone scaled from proposed Pioneer Probe
Transmitter (6.3 W)	5 x 5.5 x 1.4 in. 12.7 x 14 x 3.65 cm	1.13	2.5	31.5	Advanced Pioneer modified for 1700 mHz
Stable Oscillator	2.25 x 2.25 x 2.3 in. 5.72 x 5.72 x 5.54 cm	0.34	0.8	2.3	Proposed Pioneer Probe Unit
TOTAL		1.79	4.0	33.8	
<u>SPACECRAFT EQUIPMENT</u>					
Relay Antenna (Note 3)	5.5 dia x 13.4 in. 14 dia x 34 cm	0.7	1.5	-	Scaled from Advanced Pioneer Spacecraft Omni
Relay Receiver	4.2 x 4.75 x 1.75 in 10.7 x 12 x 4.45 cm	1.18	2.6	3.0	Based on Advanced Pioneer Spacecraft
Subcarrier Demod & Bit Synchronizer	4.2 x 4.75 x 1.75 in 10.7 x 12 x 4.45 cm	0.46	1.0	1.5	Estimate
TOTAL		2.34	5.1	4.5	

NOTES:

1. 128 bps Data Rate. 2.8 dBi sum of effective antenna gains assumed.
3. Relay antenna can be identical to probe antenna.

Required Probe transmitter RF Power - Encke Pointing Spacecraft

	64 bps		128 bps	
	<u>dBW</u>	<u>Watts</u>	<u>dBW</u>	<u>Watts</u>
380 MHz Wideband FSK	+ 0.3	1.1	+ 2.1	1.62
1700 MHz Wideband FSK	+13.2	21.0	+15.5	35.5
1700 MHz Coherent PSK/PM	+ 6.9	4.9	+ 9.0	8.0

Again, the 1700 MHz wideband FSK link requires excessive power and is eliminated from consideration.

Probe Relay Link to a Spacecraft Spinning Perpendicular to its Orbit Plane -

For a relay link between a probe and a spacecraft spinning perpendicular to its orbit plane, the spacecraft relay antenna aspect angle will be essentially 90° to the spin axis. This will result in a spacecraft relay antenna gain of the order of - 1 dBi for example for a 380 MHz turnstile or a 1700 MHz conical helix. Higher gain antennas giving pancake type patterns could be employed for the 1700 MHz links (similar to the Pioneer spacecraft Franklin array); however, for this example, it will be assumed that turnstiles or conical helix antennas will be employed.

As compared to the Earth pointing spacecraft case, the reduced spacecraft antenna gain results in a requirement to increase the 1700 MHz link transmitter RF power by 5.5 dB and the 380 MHz link RF power by 3.5 dB. These increases result in the following transmitter RF power requirements.

Required Probe Transmitter RF Power - Spacecraft Perpendicular to Orbit

	64 bps		128 bps	
	<u>dBW</u>	<u>Watts</u>	<u>dBW</u>	<u>Watts</u>
380 MHz Wideband FSK	+ 3.3	2.14	+ 5.1	3.24
1700 MHz Wideband FSK	+17.7	59.0	+20.0	100.0
1700 MHz Coherent PSK/PM	+11.4	13.8	+13.5	22.4

Comparing the RF power for the 3 links for the spacecraft spin axis perpendicular to the orbit plane the 1700 MHz wideband FSK power is unreasonably high and therefore that approach must be eliminated. The 1700 MHz coherent PSK/PM link

TABLE V-20
PROBE LINK CALCULATION - DIRECT TO EARTH

LOSSES

TRANSMIT CIRCUIT LOSSES (dB)	-1.0
RANGE LOSS (2295 MHz) (dB)	-258.1 Range .57 AU (See note 2)
POLARIZATION LOSS (dB)	-0.2
RECEIVING ANTENNA GAIN (dBi)	+61.7
NET LOSS	-197.6 dB
RECEIVE SYSTEM NOISE POWER DENSITY (dBW)	-214.7

REQUIRED S/N_0 CALCULATIONS FOR 64 bps

CARRIER

CARRIER/TOTAL (dB)	-4.0
ADDITIONAL LOSSES (dB)	-0.2
THRESHOLD LOOP BW (dB)	+10.8
REQUIRED SNR (dB)	+10.0 (See note 1)
REQUIRED MARGIN (dB)	+3.5
	+28.5

DATA

DATA/TOTAL (dB)	-2.3
ADDITIONAL LOSSES (dB)	-2.9
DATA BIT RATE (dB)	+18.1 64 BPS (See note 1)
THRESHOLD E_b/N_0 (dB)	+2.2
REQUIRED MARGIN (dBi)	3.0
	28.5
REQUIRED RECEIVE SIGNAL (dBW)	-186.2
REQUIRED TRANSMIT EIRP (dBW)	+11.4 (See notes 1 and 2)

NOTES:

1. For 128 bps add 3 dB as a good approximation (added to carrier for better acquisition).
2. For the Encke reference trajectory, the range is 0.57 AU. For the Encke/Geographos/Toro mission, range 0.353 AU, reduce EIRP by 4.2 dB.

is viable for this spacecraft attitude, but would require a higher gain spacecraft antenna such as a Franklin array to reduce power requirements.

Direct Link to Earth from an Encke Probe - For a direct link to Earth, the spacecraft attitude and probe-to-spacecraft range are independent of the direct link communications. This fact in addition to the deletion of requirements for relay link support equipment on the spacecraft makes a direct link to Earth attractive. Assuming the same type of direct link as proposed for Advanced Pioneer probes (PSK/PM using convolutional encoding) Table V-20 shows the probe EIRP requirements for a 64 bps rate to be +11.4 dBW and for a 128 bps rate, it is assumed this is increased to 14.4 dBW. From Table V-16, the probe antenna aspect angle to Earth is estimated to be 52.8 degrees for the Encke reference trajectory and 60 degrees for the Encke, Geographos, Toro trajectory. For the latter mission, the communications range is only 0.353 AU. Assuming a turnstile over cone antenna as proposed for advanced Pioneer probes, the antenna gain is 2.5 dBi at 52° and 2 dBi at 60°. The resulting transmitter power requirements using the required EIRP and antenna gains are as follows.

Required Transmitter Power for Direct Link to Earth

	PROBE TRANSMITTER POWER	
	dBW	WATTS
o Encke Reference Trajectory		
64 bps (11.4 dBW-2.5 dBi)	8.9	7.75
128 bps (14.4 dBW-2.5 dBi)	11.9	15.5
o Encke, Geographos, Toro Trajectory		
64 bps (9.2 dBW-2.0 dBi)	7.2	5.25
128 bps (12.2 dBW-2.0 dBi)	10.2	10.05

Table V-21 gives the size, weight, and power requirements for a direct S-band link to Earth from an Encke probe.

Probe Relay and Direct Link Hardware - Although the Viking Lander to Orbiter relay link operates at 380 MHz, the only equipment considered suitable for an Encke probe relay link is the Viking orbiter spacecraft relay antenna, Figure V-16. The balance of the equipment is too heavy and large to be suitable

TABLE V-21 2300 MHz DIRECT PROBE TO EARTH LINK COMMUNICATIONS EQUIPMENT

<u>PROBE EQUIPMENT</u>	<u>SIZE</u>	<u>WEIGHT</u>		<u>POWER</u>	<u>COMMENTS</u>
		(kg)	(lb)	(watts)	
ANTENNA	4.5 Dia. X 2.1 in. 11.4 Dia. X 5.34 cm	0.23	0.5	-	Proposed Pioneer Probe Antenna (Turnstile over cone)
TRANSMITTER (15.5 watts RF)	5 X 5.5 X 1.4 in. 12.7 X 14 X 3.65 cm	1.13	2.5	78.0	Assume 20% Efficient
STABLE OSCILLATOR	2.25 X 2.25 X 2.3 in. 5.72 X 5.72 X 5.54 cm	0.34	0.8	2.3	Proposed Pioneer Probe Unit
TOTAL		1.70	3.8	80.3	

- NOTES: 1. 128 bps Data Rate
2. 64 Meter DSN
3. 2.5 dBi Effective Probe Antenna Gain

for this application. For example, the lander antenna is about 39 cm (15 1/2 inches) in diameter and 24.6 cm (9.7 inches) high. The Viking Lander Relay Transmitter size is 11.4 by 15.3 by 26 cm and weighs 4.55 kg. The Viking orbiter relay receiver dimensions have not been obtained, but the receiver requires 2400 Hz primary power. Estimates of suitable hardware size, weight, and power for the Encke mission are given in Table V-17. It appears that this equipment must be developed for this application, but the design can be based on existing technology.

Relay equipment size, weight, and power for the 1700 MHz coherent PSK/PM link are estimated as shown in Tables V-18 and V-19. Although availability of existing hardware is doubtful, it can be designed using state of the art techniques. For example, the Teledyne TR-2400 series of transmitters could be the basic design to be modified for 1700 MHz operation, and Viking S-band receivers could be the basis for a 1700 MHz receiver design. Subcarrier demodulation and bit-synchronizer designs are available from Mariner technology.

Direct link communications hardware can be identical to proposed probe hardware. Size, weight, and power for the direct link communications equipment is given in Table V-21.

Conclusions and Recommendations

- 1) Table V-22 summarizes the antenna gains and transmitter RF power requirements for the various types of relay- and direct-communications links. Table V-23 compares size, weight, and power estimates for the various types of probe communication hardware. From the above data and the fact that the spacecraft is unencumbered by relay link equipment for a direct probe link to Earth, a direct link is the recommended configuration.
- 2) The preferred relay link is a wideband FSK link at 380 MHz since this requires the least power. Accommodation of antennas although a problem at this frequency can be done.
- 3) A spacecraft attitude having its spin axis perpendicular to its orbit plane requires the most power for a relay link due to the lower spacecraft antenna gain available at 90° to the spin axis.

TABLE V-22 ANTENNA GAIN AND REQUIRED PROBE TRANSMITTER RF POWER FOR VARIOUS SPACECRAFT ATTITUDES,
A 40° PROBE ANTENNA ASPECT ANGLE AND 128 bps DATA RATE

TYPE OF LINK	SPACECRAFT ATTITUDE	SPACECRAFT ANTENNA GAIN AND ASPECT ANGLE		PROBE ANTENNA GAIN AT 40° (dBi)	TOTAL ANTENNA GAIN (dBi)	REQUIRED TRANSMITTER RF POWER (watts)
		GAIN (dBi)	ANGLE (Degrees)			
380 MHz Wide Band FSK Relay Link (7774 km Range)	Earth Pointing	2.5	22.5	3.5	6.0	1.45
	Encke Pointing	2.0	40.0	3.5	5.5	1.62
	⊥ to Orbit Plane	-1.0	90.0	3.5	2.5	3.24
1700 MHz Wide Band FSK Relay Link	Earth Pointing	4.5	22.5	3.5	8.0	28.2
	Encke Pointing	3.5	40.0	3.5	7.0	35.5
	⊥ To Orbit Plane	-1.0	90.0	3.5	2.5	100.0
1700 MHz PSK/PM Relay Link	Earth Pointing	4.5	22.5	3.5	8.0	6.3
	Encke Pointing	3.5	40.0	3.5	7.0	8.0
	⊥ To Orbit Plane	-1.0	90.0	3.5	2.5	22.4
2295 MHz PSK/PM Direct Link 0.57 AU	Any Attitude	-	-	2.5 (52°)	2.5	15.5
2295 MHz PSK/PM Direct Link 0.353 AU	Any Attitude	-	-	2.0 (60°)	2.0	10.05

TABLE V-23 COMPARISON OF WEIGHT AND POWER FOR PROBE RELAY WITH EARTH POINTING SPACECRAFT AND FOR
PROBE DIRECT TO EARTH COMMUNICATIONS

	<u>WIDE BAND FSK</u>		<u>COHERENT RELAY</u>	<u>DIRECT TO EARTH</u>
	380 MHz	1700 MHz	1700 MHz, PSK/PM	2295 MHz, PSK/PM
PROBE EQUIPMENT				
Weight kg, (lb)	2.27 (5.0)	1.79 (4.0)	1.79 (4.0)	1.7 (3.8)
Input Power (w)	6.0	122.3	33.8	80.3
Transmitter Output (w)	1.5	28.	6.3	15.5
SPACECRAFT EQUIPMENT				
Weight kg, (lb)	3.07 (6.8)	1.88 (4.1)	2.34 (5.1)	None
Power	3.0	3.0	4.5	None

- NOTES: 1. All links provide 128 bps data rate.
2. The 380 mHz wide band FSK has the most potential for expanding bit rate.

D. ATTITUDE CONTROL

The approach taken in the attitude control subsystem design was to: 1) Select spacecraft Concept No. 2 (the Earth pointer) as a baseline configuration for analysis and definition with the Encke-dedicated mission as the baseline; 2) Identify the requirements and functions of the ACS subsystem for concept No. 2 and define an ACS system that attempts to meet those requirements utilizing flight-proven hardware and methods from Pioneer 10 and 11 and other flight-proven programs; 3) Identify some of the key trades necessary to define the system; 4) Compare the other four spacecraft concepts with Concept No. 2; 5) Identify problem areas and possible follow-on studies required.

1. Attitude Control System Description

a. Functions and Requirements - The operational requirements imposed on the attitude control system for spacecraft Concept No. 2 are:

- o Provide system capable of performing 90 days for Encke and 1.7 years for Encke plus the asteroids during 1980 solar cycle peak.
- o Provide sensors to determine attitude knowledge by ground or on-board processing to within 0.017 radians (1 degree).
 - Inertial orientation of the spin axis
 - Spin angle (roll) reference
 - Relative orientation of gimballed appendages (despun and gimballed mirror)
- o Provide spin speed control
 - Initial despin after TE364-4 separation
 - Nominal spin speed maintenance
 - Spin-up/despin for ΔV maneuvers
- o Provide spacecraft precession system
 - Maintain desired spin axis orientation
 - Reorient the vehicle for velocity corrections and probe deployment
- o Provide signals to time the operation of the RCS thrusters to produce axial or transverse velocity corrections.

- o Provide signals for probe deployment.
- o Maintain spacecraft stability during acquisition, cruise, experiment operation, before and after probe deployment.
- o Provide means to remove spacecraft nutation within a reasonable period.
- o Provide method for acquisition and reacquisition of:
 - Spin axis orientation toward Earth
 - Experiment sensor pointing toward Encke or asteroids
- o Point high gain antenna toward Earth within 0.024 radians (1.4 degrees).
- o Point visual experiment sensors toward Encke or asteroid to within 0.0087 radians (0.5 degrees) fine mode and within 0.087 radians (5 degrees) coarse mode.
- o Maintain spacecraft attitude rate during visual experiment pointing to 10 milliradians/sec. (0.6 degrees/sec.)
- o Maintain probe deployment attitude to 0.017 radians (1.0 degrees)
- o Maintain attitude during ΔV maneuvers to within 0.035 radians (2.0 degrees)

b. System Description - The attitude control system selected for spacecraft concept No. 2 consists of the components listed in Table V-24. A block diagram showing the functional relationship between these components and other subsystems is shown in Figure V-18. As seen from the table, there is maximum usage, where applicable, of flight-proven hardware from Pioneer 10 and 11 or other programs. The reaction control thruster system will be discussed under section V-E, Propulsion.

1) Attitude Determination - Attitude determination of spin axis location and spin angle (roll reference) will be accomplished by the Sun aspect sensor outputs (both Sun aspect and roll reference) and by an RF sensing technique previously used on Pioneer 10 and 11, Conscan.

Doppler modulation and doppler shift (also used on Pioneer 10 and 11) would provide additional sources of attitude determination. Rotation of an offset omni antenna about the spin axis produces a doppler modulation

TABLE V-24 ATTITUDE CONTROL SYSTEM COMPONENTS

<u>COMPONENT</u>	<u>FUNCTION</u>	<u>WEIGHT</u>	<u>POWER</u>	<u>SIZE</u>	<u>USE</u>
Solar Aspect Sensor Assembly	Attitude Determination	0.2 kg	--	5x3x3 cm	Intelsat III
Sun Sensor Electronics		0.5 kg	1.0 W	300 cm ³	Intelsat III
Nutation Damper	Damp. S/C Nutation	2.0 kg	--	U Shape 30 cm.	Spin S/C
Control Electronics Assembly	Data Storage, Sequence Control, Signal Processing, Command Logic, Switch Logic for RCS	2.0 kg	4.0 W	15x20x11 cm.	Pioneer 10 & 11
Despin Drive Assembly (Despin Electronics)	Azimuth-Mirror Assy.	4.5 kg	4.0 W	42 cm.dia.x 8	New
		1.8 kg	1.5 W	2000 cm ³	New
Single Axis Gimbal Assembly (Mirror Elevation Electronics)	Elevation-Mirror	2.0 kg	3.0 W	8 cm.dia.x 8	Solar Array Drives, etc.
		1.2 kg	1.5 W	1500 cm ³	New
Conscan Signal Processor	Attitude Determination	Part of Communications			Pioneer 10 & 11
Spin Period Sector Generator	Measures spin period and generates pulse trains of 1,8,64, & 512 pulses/rev.	Part of Data Handling			Pioneer 10 & 11

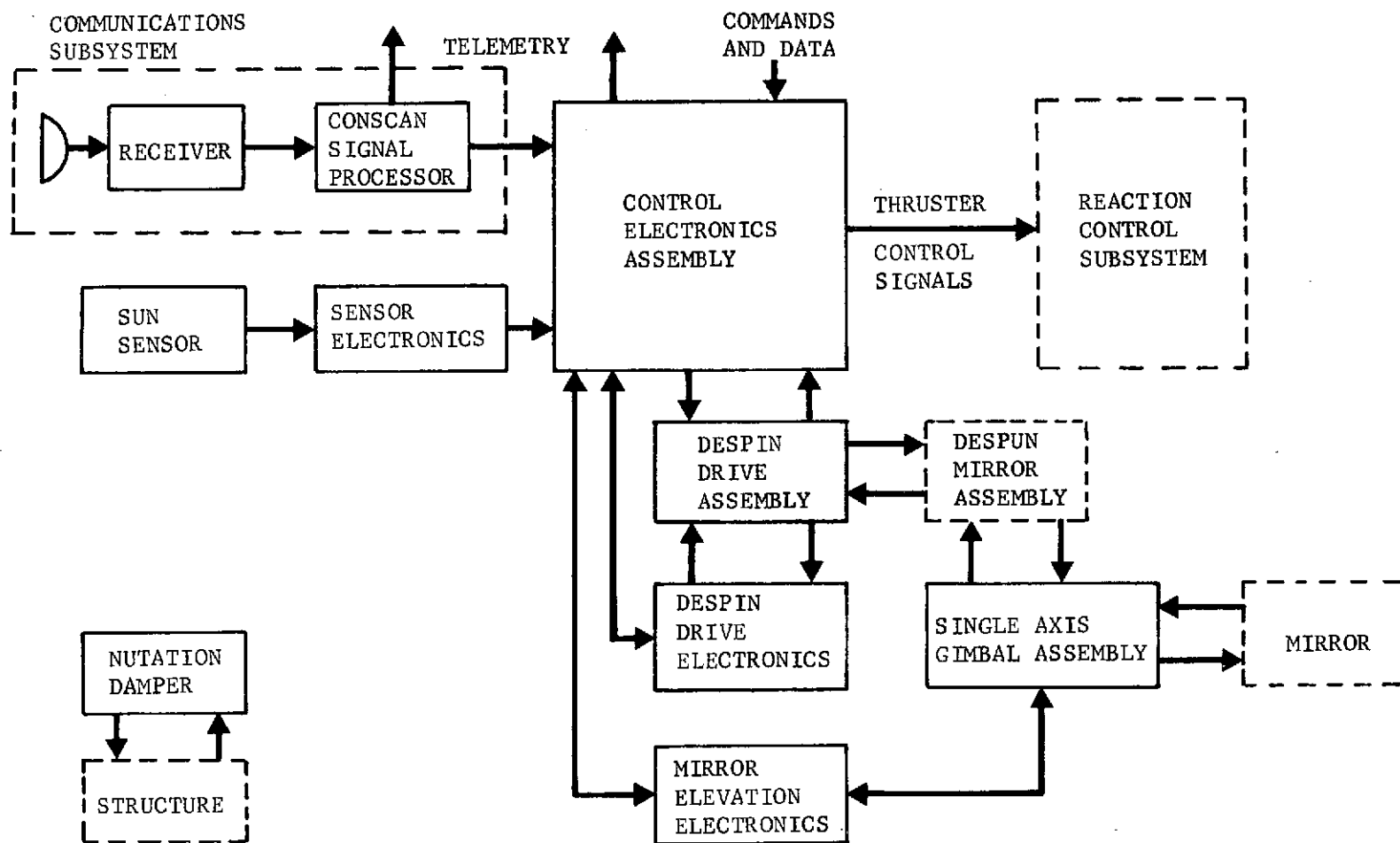


FIGURE V-18. CONCEPT #2 ATTITUDE CONTROL SUBSYSTEM

proportional to $r \sin \theta$ and allows the ground station to estimate θ with good accuracy for θ less than one radian. θ is the angle between the omni antenna axis and the Earth line and r is the offset distance of the omni antenna axis from the spacecraft spin axis.

Doppler shift would be used for attitude determination during ΔV maneuvers. An axial ΔV maneuver produces a doppler shift proportional to $\Delta V \cos \theta$, from which the ground station can estimate θ with good accuracy for θ near 90 degrees.

The imaging system, which will be part of the science payload could also be used as an attitude sensor. Once the despun mirror assembly has been despun, pictures of stars and other celestial bodies could be taken and telemetered to the ground to aid in attitude determination. This operation could also be used to test and to calibrate the imaging system and the despun mirror assembly. Figure V-19 shows Doppler attitude determination accuracies.

2) Spin Axis Acquisition - The spacecraft and TE 364-4 kick motor will be spun to about 60 rpm by Centaur prior to Centaur release. After kick motor firing and kick motor separation, the spacecraft despin thrusters will be fired to reduce the spin rate from 60 rpm down to near the desired 5 rpm. Sun sensor Sun crossings will be processed in the spin period sector generator (Pioneer 10 and 11) to measure the spin speed and will deactivate the spin thruster firings when the proper spin rate is reached. Ground station monitoring and verification (via the omni antenna) of the correctness of the spin rate will be performed before magnetometer boom deployment and the plasma wave detector deployment.

An initial orientation maneuver will then be performed to precess the spin axis from its orientation after injection to an Earth pointing attitude. The initial orientation of the vehicle can be established via injection errors to probably better than 5 degrees so that the initial orientation maneuver can be performed open-loop. The thruster pulses used to precess the spacecraft would be controlled to occur at a constant angle to the plane of the spin axis and the Sun. The basic reference for the angle is the Sun sensor crossing pulse which drives the spin period sector generator.

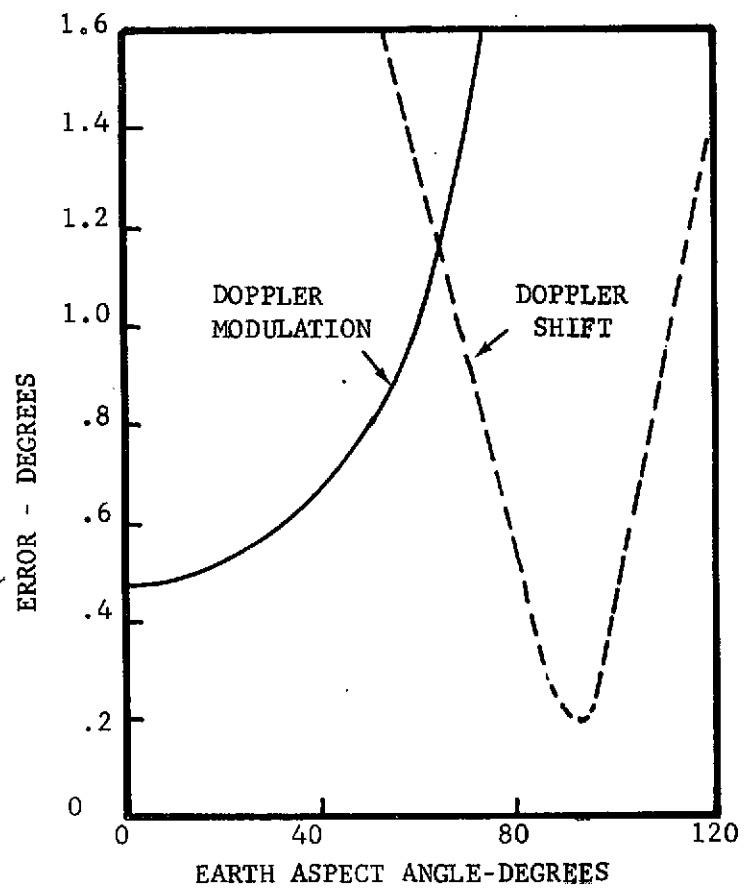


FIGURE V-19. DOPPLER ATTITUDE DETERMINATION ACCURACIES

Conscan can now be used to determine the attitude so that the spin axis can be precessed more accurately in either a closed-loop on-board manner or on an open-loop manner from a known attitude.

During the initial orientation maneuver, a calibration of the precession thrusters could be performed. This calibration maneuver is utilized on Pioneer 10 and 11 and is recommended for usage here to reduce errors associated with future precession maneuvers.

3) Precession Maneuvers - Precession maneuvers would be conducted throughout the mission to maintain the Earth-pointing attitude. These maneuvers would take place every few days depending upon Earth line inertial rate (average about 0.5 degrees/day), environmental torques, and spin speed correction disturbances (very small). Torques due to unbalanced solar radiation pressure would comprise most of the environmental disturbance torque. The solar torque induced attitude drift rate should be less than 0.1 degrees/day.

The Conscan system from Pioneer 10 and 11 would provide a closed loop attitude control system for pointing the spin axis toward the Earth. The closed-loop error signal generated by the offset directional antenna and the spacecraft contains the necessary amplitude and phase information on the pointing angle between the spacecraft spin axis and the Earth signal. Processing of this signal, together with sun crossing pulses provides the necessary timing information for firing the precession thrusters at the appropriate instant in the spin cycle, and for termination of thruster firing when the pointing error is below the specified minimum threshold.

Precession maneuvers will also be required for probe targeting, before ΔV maneuvers to obtain proper ΔV direction and after the ΔV maneuver to return to the desired Earth point orientation. Depending on thruster selection for ΔV and desired ΔV direction, the precession required would range from 0 to 90 degrees. If a solid rocket motor (one type was investigated for asteroid missions) is used for ΔV , the precession angle could be up to 180 degrees. The present and desired attitude would be determined on the ground. The desired thruster pulse width, fire angle (reference from Sun pulse), number of thruster pulses and the enable command would then be sent from the

ground. With the command now stored, the proper precession thruster would be pulsed in synchronism with the spin speed to precess the spin axis.

4) Spin Speed Maintenance - Sun sensor Sun crossings periodically taken over several revolutions will be averaged to determine spin speed so that it can be returned to the desired value.

5) ΔV Maneuvers - For the reference mission, Encke-only, two mid-course ΔV maneuvers are planned. One at launch +5 days of about 15 meter/sec.

A reasonable sequence to reduce angular errors for the ΔV 's would be as follows: 1) Precess to desired orientation; 2) Allow time to damp nutation; 3) Determine attitude and error; 4) Precess to "fine tune;" 5) Allow time to damp nutation; 6) Determine attitude; 7) Perform burn; 8) Damp; 9) Determine attitude; 10) Precess to Earth point orientation. This sequence could imply total on-board attitude determination at large Earth-spacecraft distances because the high gain antenna would no longer be oriented toward the Earth for a high data rate down link. However, the data rate required may be low enough that ground attitude determination could be performed. When the high gain antenna is far off the Earth line, the doppler shift method could be used to determine the attitude.

6) Nutation Damping - A passive type nutation damper chosen from one of the spin type programs should be adequate to reduce the nutational motion in a reasonable period of time. A mercury-filled U-tube which has expanded end-chambers that can be tuned to the spacecraft nutation frequency is suggested. Since the natural frequency of the damper and nutation frequency are both proportional to the spin rate, the damper is self-tuning, i.e., the frequency ratio is independent of spin rate.

7) Despun Mirror Control - The despun mirror will be positioned so as to allow the TV imaging system and radiometer to view Encke and the asteroids. It could also be used to allow the TV imaging system to take pictures of stars and other celestial objects as a back up for attitude determination and for imaging system calibration.

The most obvious way to point and maintain pointing at Encke would be by an onboard autotrack scheme utilizing the TV imaging system as an attitude

sensor. The read out time alone for the TV imaging system is on the order of 42 seconds without including the processing time to identify the coma when far out, or the comet nucleus when close in to the comet. An onboard processing system of this type is probably not available at this time, but its development by 1980 should be possible. However, for the high tracking rates required near Encke and near the asteroids, the processing time of 42 seconds would have to be greatly reduced to provide a sufficient sampling rate to maintain pointing.

Close encounter angular motion for a flyby is given by:

$$\phi = \tan^{-1} \frac{R_{CA}}{D}$$

The planar track rate is given by:

$$\dot{\phi} = \frac{R_{CA} V}{D^2 + R_{CA}^2}$$

where:

ϕ = phase angle

$\dot{\phi}$ = track rate

R_{CA} = closest approach distance

V = relative velocity between spacecraft and target

D = distance from encounter to spacecraft (0 at encounter)

The peak track rate is at encounter and is:

$$\dot{\phi}_{\text{peak}} = \frac{V}{R_{CA}}$$

The peak track rate, picture rate required for an error output every 0.0035 radian (0.20 deg) of motion, and the respective time when tracking would have to be stopped is shown in Table V-25.

A groundbased processing system would further slow down the sample rate because of the communication time involved at these distances (0.5 AU for Earth - Encke). A planet type sensor similar to one used on Mars Mariner or a star sensor could possibly be incorporated to produce the necessary error signals for the despun and gimbaled mirror drive. However, the feasibility of this sensor usage needs to be investigated further.

TABLE V-25 TRACK RATE, PICTURE RATE FOR CLOSE ENCOUNTER

	<u>TRACK CONDITION</u>	<u>REQUIRED PICTURE RATE</u>	<u>PEAK RATE RAD/SEC</u>	<u>STOP TRACK DISTANCE OUT</u>
Encke	Through Encounter	1/sec	3.67×10^{-3}	--
RCA = 5000 km				
V = 18.33 km/sec	Stop 10 minutes out	1/5.6 sec	6.30×10^{-4}	11,000 km
	Stop 30 minutes out	1/42 sec.	8.31×10^{-5}	33,000 km
Geographos	Through Encounter	1/.139 sec.	2.52×10^{-2}	--
RCA = 500 km				
V=12.6 km/sec	Stop 11.5 minutes out	1/42 sec.	8.31×10^{-5}	8692 km
Toro	Through Encounter	1/.230 sec.	1.52×10^{-2}	--
RCA = 500 km				
V = 7.6 km/sec	Stop 14.8 minutes out	1/42 sec.	8.31×10^{-5}	6743 km

Unless an onboard processing system associated with a lower readout time for the imaging system can be developed, or the use of a planet type sensor proves feasible, a programmed function generator type command angle would be used. Periodic picture processing on the ground would be used to update the command angle function and to insure that the target is still in view. For high track rates, loss of target would be a possibility. This needs to be investigated through a more detailed error analysis.

The command angle would be determined from knowledge of spacecraft, Sun, Earth, and assumed target ephemeris information. Sun crossing pulses, a reference pipper pulse and encoder between the spacecraft and despun mirror platform, and a reference pulse and encoder between the despun mirror platform and the gimbaled mirror, would be used to form the feedback loops to insure that the command angle is followed. Essentially, two control systems would be required, one for despin relative to the spacecraft (azimuth) and one for gimbaling the mirror (elevation). Block diagrams of the two systems are shown in Figures V-20 and V-21. Integral control would be provided in the despin control system to minimize errors caused by bearing friction.

8) Despun Mirror Acquisition - After kick motor separation and subsequent spacecraft despin down to 5 rpm and after deployment, the despun mirror assembly will still be spinning with the rest of the spacecraft at 5 rpm relative to inertial space. Any latching mechanism, if required for launch, would now be released. The present spacecraft spin rate value would be put in as a voltage bias in the despin control loop. Sun crossing pulses and the index pulse between the spacecraft and the despun mirror would form the error signal to have the torque motor turn the despun mirror in the opposite direction to the spacecraft spin to obtain a 5 rpm rate relative to the spacecraft and zero rate relative to inertial space. The despun mirror would now be pointing in a known inertial direction relative to the Sun and could be positioned to a known target for testing and calibration purposes.

Comet acquisition begins approximately 20 days before anticipated Encke encounter. With the inertial spin axis orientation known relative to Sun and Earth, the despun mirror would be commanded to the assumed Encke position. The uncertainty of the Encke position will probably be small enough,

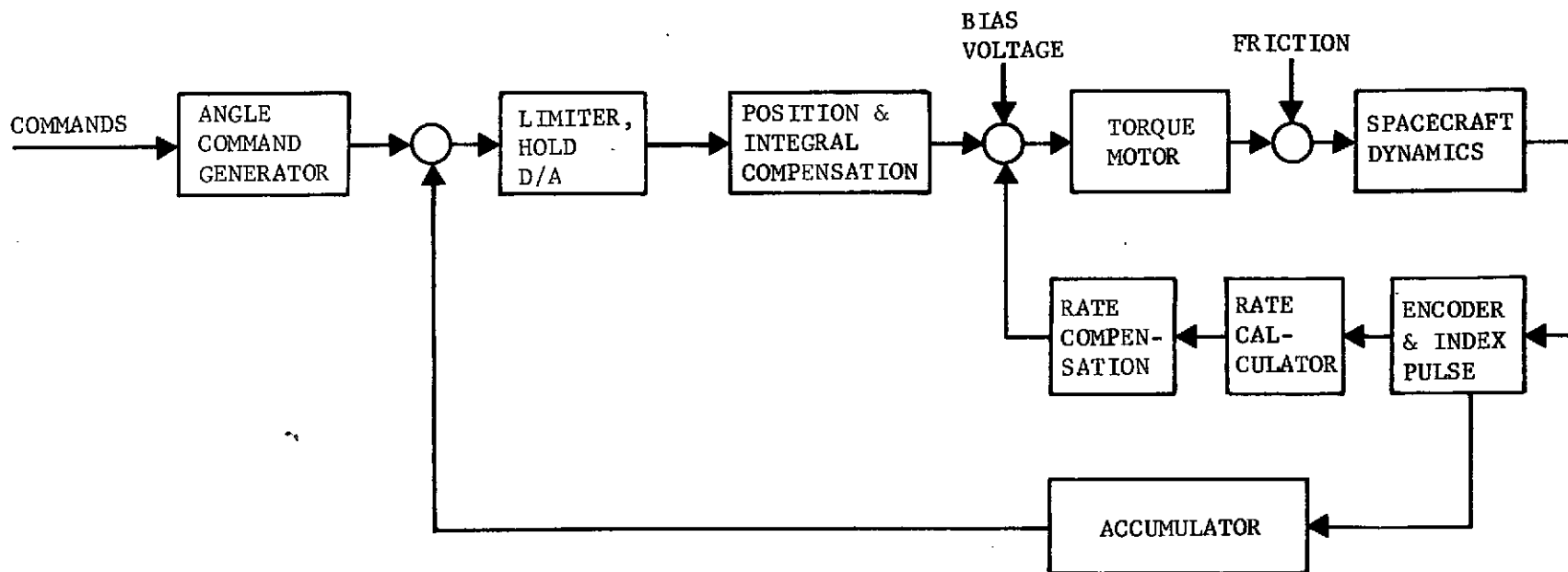


FIGURE V-20. DESPUN MIRROR CONTROL SYSTEM BLOCK DIAGRAM - AZIMUTH

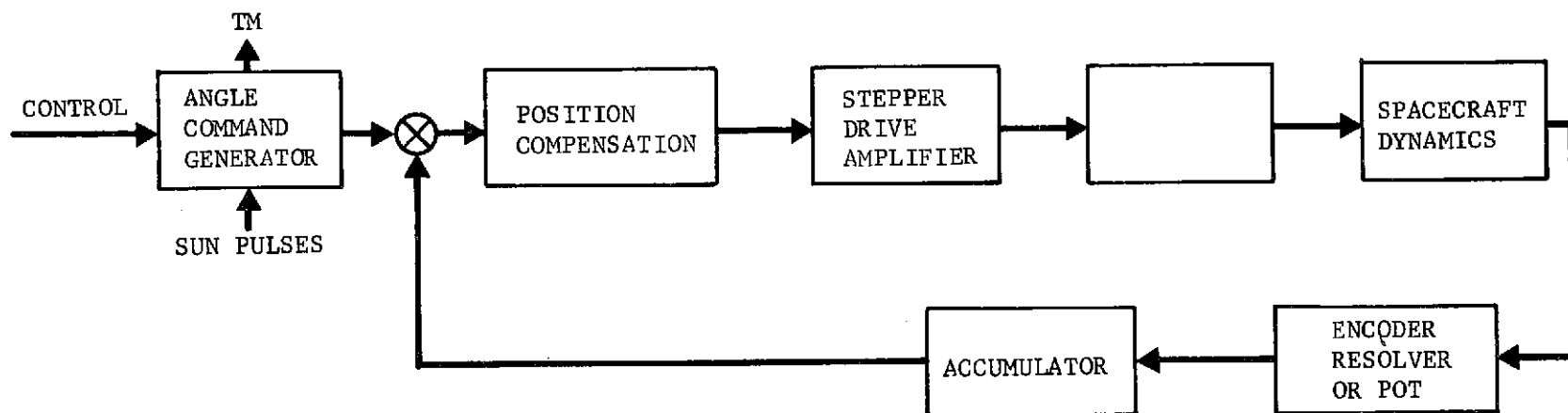


FIGURE V-21. SINGLE AXIS GIMBAL CONTROL SYSTEM BLOCK DIAGRAM

relative to the coma, to use a trial and error procedure to acquire and lock on the coma. Pictures would be taken periodically until the comet is in the field of view of the camera. With the new up-date on Encke position taken into the generation of the angle command, more pictures would be taken until the nucleus is in view. With the nucleus in the field of view, a new command angle profile would be generated to insure that the nucleus stays in the field of view.

As mentioned previously, an onboard processing system with rapid readout of the TV imaging, or an applicable planet type sensor would greatly enhance the ability to acquire and maintain target pointing. Additional study effort should be made in this area.

2. System Performance

a. Attitude Determination - Attitude knowledge of the inertial orientation of the spin axis and the spin angle (roll) reference is required to be within 0.017 radians (1 degree). Obtaining this level of accuracy should be no problem. Attitude determination accuracy, due to the sensor selected, is a function of solar and Earth aspect angles and the Sun-spacecraft-Earth angle. The Sun sensor provides Sun aspect measurements with an accuracy given approximately by the following expression:

$$\theta = K / \sin \alpha_s$$

Where K is the null accuracy of the sensor and α_s is the Sun aspect angle. For a K of 0.0035 radians (0.2 degrees), which is representative of present day Sun sensor capabilities and the history for the Encke only reference mission results in the curve of Figure V-22. The Sun aspect angle is never close to zero or 180 degrees so that adequate Sun information can be obtained during the whole mission.

Since Earth pointing will be maintained during cruise, conscan accuracy will be on the order of 0.5 degrees or less based on Pioneer 10 and 11. The Sun aspect sensor data and conscan method should then produce attitude determination accuracies better than 0.5 degrees.

For the large precession maneuvers, and for ΔV maneuvers, the doppler modulation and doppler shift methods will be used. Expected accuracy as a

function of Earth aspect angle are shown in Figure V-22.

b. Earth Pointing Antenna Accuracy - The error in pointing the high-gain dish must be within 1.4 degrees to maintain maximum data-rate transmission. The spacecraft-Earthline with respect to inertial space changes as a function of time. Solar radiation torques also tend to precess the spin axis. Thus, the high gain antenna pointing accuracy will be a function of how often precession maneuvers are performed to precess the spin axis back to the Earthline. The frequency of these maneuvers, to maintain pointing, should be less than once or twice every few days.

c. ΔV Maneuvers - Until a detailed error analysis can be performed including spin speed uncertainties, thruster misalignments, initial position uncertainties, sensor errors, and c.g. offsets, the angular errors during ΔV maneuvers can only be compared to what values were obtained on Pioneer 10 and 11. Pioneer 10 and 11 angular errors were on the order of one to two degrees. The higher-mass, lower-inertia configuration of this study, compared to Pioneer, could produce larger errors, however 1 or 2 degree error control should still be possible. Thruster calibration performed at the first initial orientation maneuver will help reduce the errors. For large ΔV maneuvers, it could be feasible to divide the ΔV maneuver into segments so that spin speed corrections could be performed and time could be allowed for nutational motion to damp out before the next segment.

d. Experiment Pointing Accuracy - Two requirements exist for experiment pointing. The first is the pointing to keep the target within the field of view of the camera: the second is rate stability when pointing to prevent smear of the camera image.

The field of view for the narrow angle camera is 1.1 x 1.4 degrees which requires that experiment pointing should at least be better than 0.0087 radians (0.5 degrees). Before prime experiment pointing periods, it will be necessary to allow sufficient time for the nutation damper to reduce to a reasonable level (0.1 degrees) any nutational motion due to a prior ΔV or precession maneuver. ΔV or precession maneuvers will not be allowed during the prime experiment pointing periods. Precession maneuvers for high gain

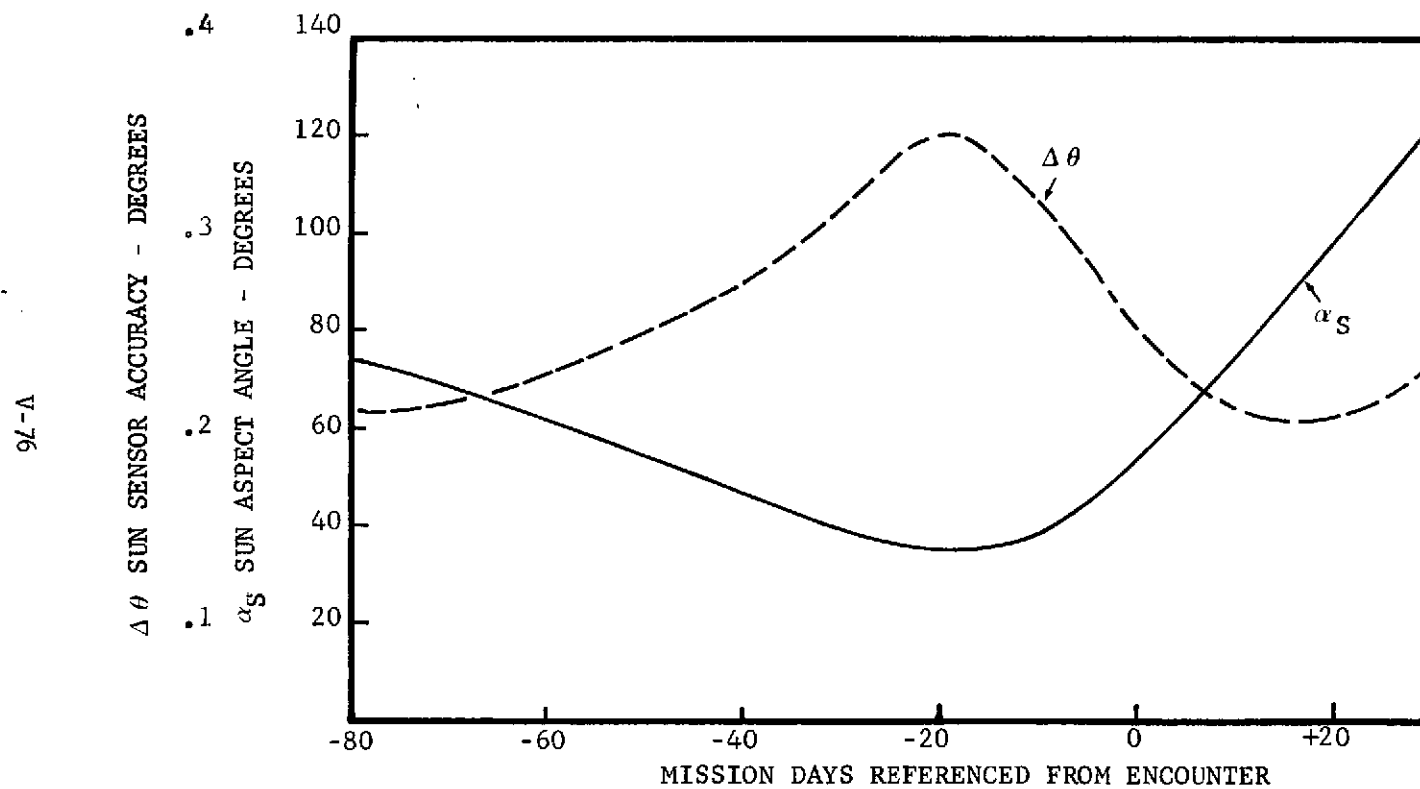


FIGURE V-22. SUN ASPECT ANGLE AND SUN SENSOR ACCURACY
AS A FUNCTION OF MISSION TIME

antenna pointing toward Earth will have been performed beforehand to achieve minimum Earth pointing errors during experiment pointing. Low Earth pointing error implies greater conscan attitude determination accuracy. If the Earth aspect angle is less than one degree, conscan attitude determination accuracy would be ± 0.2 degrees or less.

Each attitude sensor and mission sensor, each thruster, the despin drive assembly, and the mirror must be accurately aligned to the spacecraft and verified after installation in the spacecraft. Static and dynamic balance of the spacecraft will be performed and will need to include probe effects. Propellant usage must be equalized between tanks to reduce possible center of mass shifts. Precautions must also be taken to minimize thermal and vibration effects. Accurate ephemeris data must be available. Encke ephemeris can be updated and improved during experiment operations. Inflight testing and calibrations of the imaging system will reduce the effect of misalignments and scale factor uncertainties. A preliminary error analysis is presented in Table V-26.

The results of the preliminary analysis indicate a pointing error of 0.56 degrees which is reasonably close to the requirement of 0.5 degrees and certainly indicates feasibility. A higher resolution Sun aspect sensor could be used to reduce the error and they are presently available. A star sensor could also improve the accuracy, however, the problem of star availability would have to be investigated first. The mirror servo error is probably the softest parameter and more study is needed in this area to more accurately assess the error in terms of what is achievable as a function of tracking rate.

Unless ground processing methods are available to unscramble the effects of smear, pointing stability must be maintained during the picture exposure time. The exposure time is a function of a target magnitude brightness, and the target relative magnitude is a function of target distance from the spacecraft. Figure V-23 shows the rate stability of pointing required as a function of days from Encke encounter for maintaining less than a one pixel smear during the exposure time for both the wide and narrow field of view cameras.

TABLE V-26. PRELIMINARY EXPERIMENT POINTING ERROR ANALYSIS

ERROR SOURCE	ERROR
Sun Aspect Sensor	
Alignment	0.01 ^o
Accuracy	0.35 ^o
Conscan	
Alignment	0.05 ^o
Accuracy	0.20 ^o
Dynamic Balance	0.10 ^o
Residual Nutation	0.10 ^o
Despin Bearing Alignment	0.01 ^o
Mirror Alignment	0.01 ^o
Solar Torque Disturbance	0.05 ^o
Mirror Servo Errors	0.35 ^o
	<hr/>
RSS TOTAL	= 0.56 ^o
POINTING ERROR	

6L-A

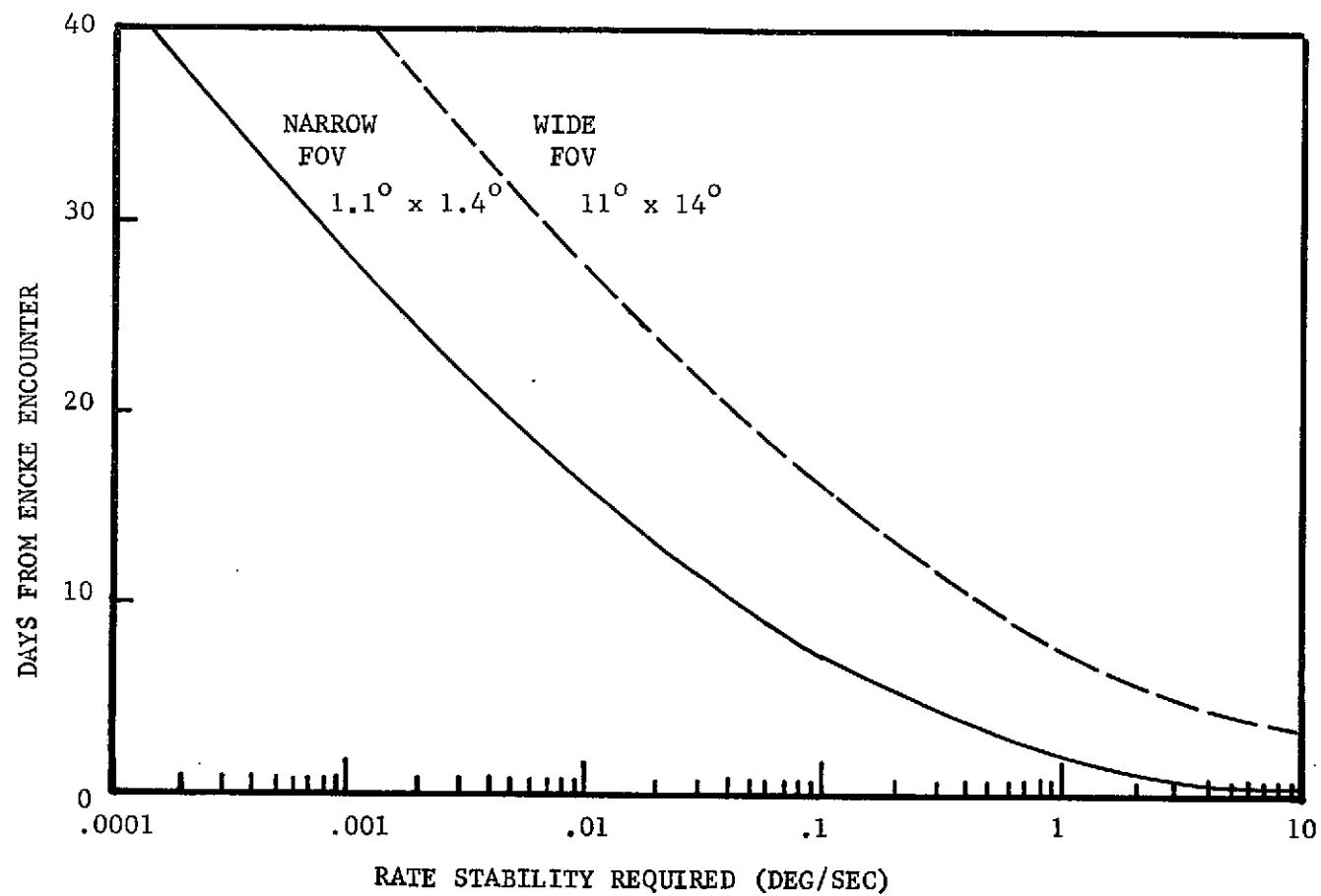


FIGURE V-23. RATE STABILITY REQUIRED VS. TIME FROM ENCKE ENCOUNTER

Due to limitations imposed on the angular travel capability of the mirror assembly provided for concept No. 2, and with the spin axis Earth point constraint, Encke viewing can only occur 20 days from Encke encounter (flyby of nucleus) to day E+0 or Encke encounter. After day E+0, the nucleus will not be in view so that the camera will try to look down the comet tail.

The spacecraft rate stability required at 20 days is 0.0043 deg/second. The ability to obtain this degree of rate stability is highly questionable due to the effects of dynamic unbalance, nutation, mirror control system drive disturbances and inaccuracies, and despin bearing axis misalignments. A quick look at the anticipated rates due to these effects are summarized below.

PRELIMINARY RATE STABILITY ESTIMATE

SOURCE	PEAK RATE (deg/sec)
Dynamic Balance (0.05 - 0.10°)	0.025 - 0.05
Residual Nutation (0.02 - 0.10°)	0.18 - 0.09
Bearing Alignment (0.01°)	0.005
Control System Drive	0.02 - 0.10
<hr/>	
RSS TOTAL	0.037 to 0.14 deg/sec

The above results when compared with Figure V-23, indicate that Encke viewing with less than a one pixel smear will not be possible until from 11 to 6 days out. This constraint needs to be evaluated against mission and science objectives to assess just what is the percentage loss of mission and science objectives.

Because of the preliminary nature of estimates above, a more detailed study to determine what level of rate stability can reasonably be achieved needs to be initiated. However, at the same time, an investigation should be started to see what degree of smear is acceptable (1, 2 or ? pixels) and just what can be accomplished by ground data processing to remove the smear.

3. Spacecraft Concept Comparison

The five spacecraft concepts are all spin stabilized and all five have at least one despun drive assembly required for either a mirror, and antenna, or a sensor platform. Concept 3 could be considered dual-spin, however, all the concepts, because of the despun drive assembly, could be considered dual-spin to some degree. All the concepts share the common problems of acquiring and tracking the target, on-board processing difficulties, and maintaining some level of rate stability as were discussed in Section V-D.2 for Concept 2.

Concepts 3, 4, and 5 with spin axis perpendicular to spacecraft, Earth, and Encke plane, would use a Sun aspect sensor and fanscan (used on Pioneer 10 and 11) for attitude determination. Concept No. 1 would use a Sun aspect sensor, fanscan, and doppler modulation.

Autotrack, using conscan as the attitude sensor, would be a viable contender for controlling the high gain antenna pointing towards the Earth for concepts 1, 3, 4, and 5. The preferred approach, however, due to the additional feeds required through the despun drive assembly for autotrack, would be to use a closed-loop servo system, similar to the one shown in Figure V-20 and driven by a programmed function generator type command angle referenced by the Sun sensor Sun crossing pulses. Sun crossing pulses, data on spacecraft spin axis orientation, plus Sun and Earth position data would be used to specify the command angle. Conscan data or other data signal strength would indicate that the antenna was being pointed properly.

Concept 1, 3, and 4 would be very similar to concept 2 in terms of rate stability requirements. Concept 5 is unique in that a different type of imaging system is used. It has a spun type camera with an exposure time of less than 0.0002 seconds. If only one revolution of the spacecraft is required to obtain a complete picture, the stability rate to prevent the equivalent of one pixel smear is only 30 deg/sec. Concept 5 appears most desirable from an attitude controls standpoint for this reason, and for the reason that it is the least complex.

Concept 1 (spin axis points to Encke) is less desirable for the following reasons: 1) Encke pointing is achieved by precessing the whole spacecraft. Near Encke, relatively high tracking rates are required to maintain pointing for a flyby. The pulse level required to precess would produce excessive nutation unless multiple precession thrusters were added; 2) The errors associated with precessing the vehicle would be greater than slowing a balanced platform; 3) Movement of the high gain antenna causes the center of gravity to move and the inertia properties of the vehicle to change which can result in coning of the vehicle.

Concept 3 requires more degrees of freedom (gimbals) than the other concepts and probably, for this reason, offers more in expected science return. However, due to the size and mass of the despun platform, and its separation distance from the rest of spacecraft, it may be difficult to achieve acceptable inertia ratios for stability (>1.1) without adding considerable ballast to the spinning portion.

4. Conclusions

The feasibility of using a low-cost spinning spacecraft for the Encke-only reference mission has been evaluated on a preliminary basis. The concept, from a controls standpoint, does appear to be feasible. More detailed design of an attitude control system for these missions, however, will require additional trade-off studies on the key problems of target acquisition and tracking. Such studies should consider the interrelationships of imaging system characteristics (e.g., sensitivity and resolution), the capabilities of alternative reference sensors, and the options for processing and using error signal data to achieve required stability.

E. PROPULSION

The propulsion subsystem definition is based primarily upon the configuration with an Earth-pointing spin axis. This basic configuration was analyzed on the basis of requirements imposed on several of the Comet Encke-asteroid missions to identify possible propulsion system problem areas. The propulsion system requirements are identified by mission.

1. Earth-Encke Mission

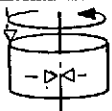
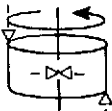
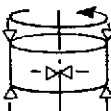
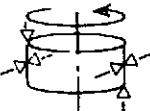
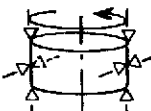
a. Propulsion System Requirements and Definition - The basic Earth-Encke mission requirements are as shown in Table V-27. Assuming a 302 kg (662 pounds) "dry" spacecraft, these ΔV maneuvers require about 32560 N-sec (7320 lb-sec) and 45600 N-sec (10250 lb-sec) of impulse for the spacecraft and the spacecraft with probes respectively. This energy requirement establishes the need for a relatively high performance ΔV system such as a hydrazine monopropellant or bi-propellant system. A gaseous nitrogen system is unattractive because of its high propellant and storage system weight. Bi-propellant systems are also unattractive for systems less than 222,410 N-sec (50,000 lbf-sec) because their weights are equivalent to, or greater than, monopropellant hydrazine systems and their cost and reliability suffer in comparison to hydrazine systems. Additionally, hydrazine monopropellant thrusters can be obtained at low enough thrust levels to provide the necessary attitude control functions.

Attitude control requirements were estimates as shown in Table V-27. Precession was assumed to consist of two 1.57 rad (90°) maneuvers before and after each ΔV maneuver plus 0.87 rad (50°) of precession during cruise. It is assumed that the spacecraft has been spun up to 6.28 rad/sec (60 rpm) by the launch vehicle and is required to be despun to 0.52 rad/sec (5 rpm). The remaining spacecraft functions are accomplished at a spin rate of 5 rpm. The baseline system selected is similar to the Pioneer 10/11 hydrazine system using 1-lbf thrust engine assemblies.

b. System Description - Several thruster configuration options were analyzed and are compared in Table V-28. For the purposes of this study, Configuration E, utilizing eight 4.45 N (1-lbf) nominal thrust engines was selected. The system is shown schematically in Figure V-24. Eight thrusters

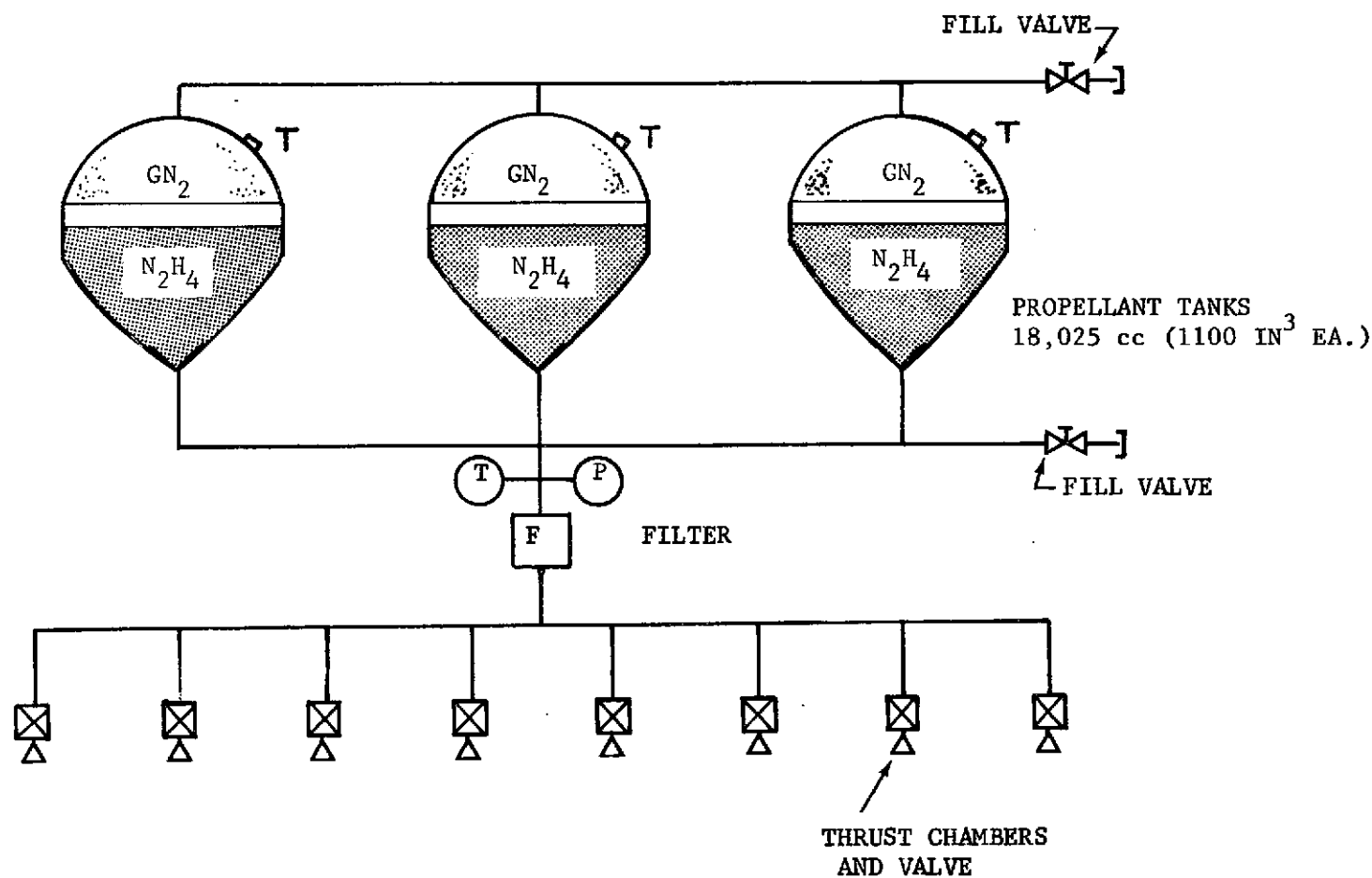
TABLE V-27 SUMMARY OF PROPULSION REQUIREMENTS

REQUIREMENT	SPACECRAFT	SPACECRAFT WITH PROBES
<u>Velocity Increment (ΔV)</u>		
1st Midcourse (max)	101.5 m/s	101.5 m/s
Trim Maneuver (max)	15 m/s	15 m/s
Post Probe Release Maneuver	N/A	45 m/s
Total Maneuvers (max)	116.5 m/s	161.5 m/s
<u>Attitude Control</u>		
Spin Maintenance	370 N-s (83 lb _f -sec)	370 N-s (83 lb _f -sec)
Precession	7.15 rad (410 deg)	10.3 rad (590 deg)
Despin	700 N-s (157 lb _f -sec)	864 N-s (194 lb _f -sec)

CONFIGURATION	 A	 B	 C	 D	 E
NUMBER ENGINES	3	4	6	6	8
PRECESSION SIDE EFFECTS	Add ΔV	None	None	None	None
SPIN JET SIDE EFFECTS	If TC not on CG precession and nutation will occur ΔV Addition	If TC not on CG precession and nutation will occur ΔV Addition	If TC not on CG precession and nutation will occur ΔV Addition	None	None
ΔV ADDITION	Will add spacecraft nutation and precession	Will Add spacecraft nutation and precession	None	Will add spacecraft nutation and precession	Minimal precession ($< 90^\circ$) required for ΔV maneuver
FAILURE MODES	Single failure will fail mission	Single spin jet failure will fail mission	Single spin jet failure will fail mission	Single failure will not fail mission*	Single failure will not fail mission*

* Assuming capability to utilize single jets for ΔV , precession and spin maneuvers is built into spacecraft, and propellant margin to remove errors introduced by failed TC is included.

TABLE V-28 THRUSTER CONFIGURATION OPTIONS



NOTE: EACH THRUST CHAMBER AND VALVE IS ELECTRICALLY HEATED AND THERMOSTATICALLY CONTROLLED

FIGURE V-24 HYDRAZINE REACTION CONTROL SYSTEM SCHEMATIC

are used to minimize cross-coupling during maneuvers and spin maintenance, and to maximize reliability. This thrust chamber configuration offers the most flexibility in that the maneuvers are all performed by thruster couples, thus preventing unnecessary coupling. Additionally, all ΔV maneuvers would be performed by the thrusters whose axes are parallel to the spin axis. ΔV maneuvers could be performed by the spin thrusters, but with losses in performance due to the pulsing activity and losses in efficiency because of the spacecraft rotation.

Configuration D, using six thrusters is an alternate solution for the case where a single engine, whose thrust axis passes through the vehicle center of mass, is used to provide major velocity changes. A single ΔV engine configuration, while it could reduce maneuver times due to the use of larger engines, is more inefficient from a fuel usage standpoint. This is because of the additional precession angles required prior to burn (180° max vs. 90° max). Areas that must be addressed in the final spacecraft design include tradeoffs of engine location with respect to reliability requirements, physical and exhaust-plume interference with other equipment, and required moment arms.

Tankage - The required propellant volume for the spacecraft with and without probes ranges from 12,024 cc (1222 in^3) to 34,544 cc (2108 in^3). In order to maintain the engine inlet pressure range between 3.45×10^6 and $0.93 \times 10^6 \text{ N/m}^2$, for which most of the engines in question are qualified, the tank volume must be from 27,530 to 47,360 cc (1680 to 2890 in^3) minimum. In order to maintain flexibility, the larger volume was chosen with some growth capability included, (10 to 20%). Thus three 18025 cc (1100 in^3) tanks were chosen, which provide 14% margin over the above defined loads. These tanks are used on a present satellite program (Model 777) and are qualified for use with hydrazine.

c. Performance - Pressure blowdown of the system using the tankage described above and estimates of propellant required are shown in Figure V-25. This blowdown profile assumes an isothermal pressure decay. Due to the range of thrust sizing constraints, several assumptions were made and some of the available hardware in the expected thrust range reviewed. The applicable thrust range is of the order of 4.45 to 44.48 N at $3.45 \times 10^6 \text{ N/m}^2$ tank pressure. Typical examples of thrusters are shown in Table V-29. Steady-state thrust as a

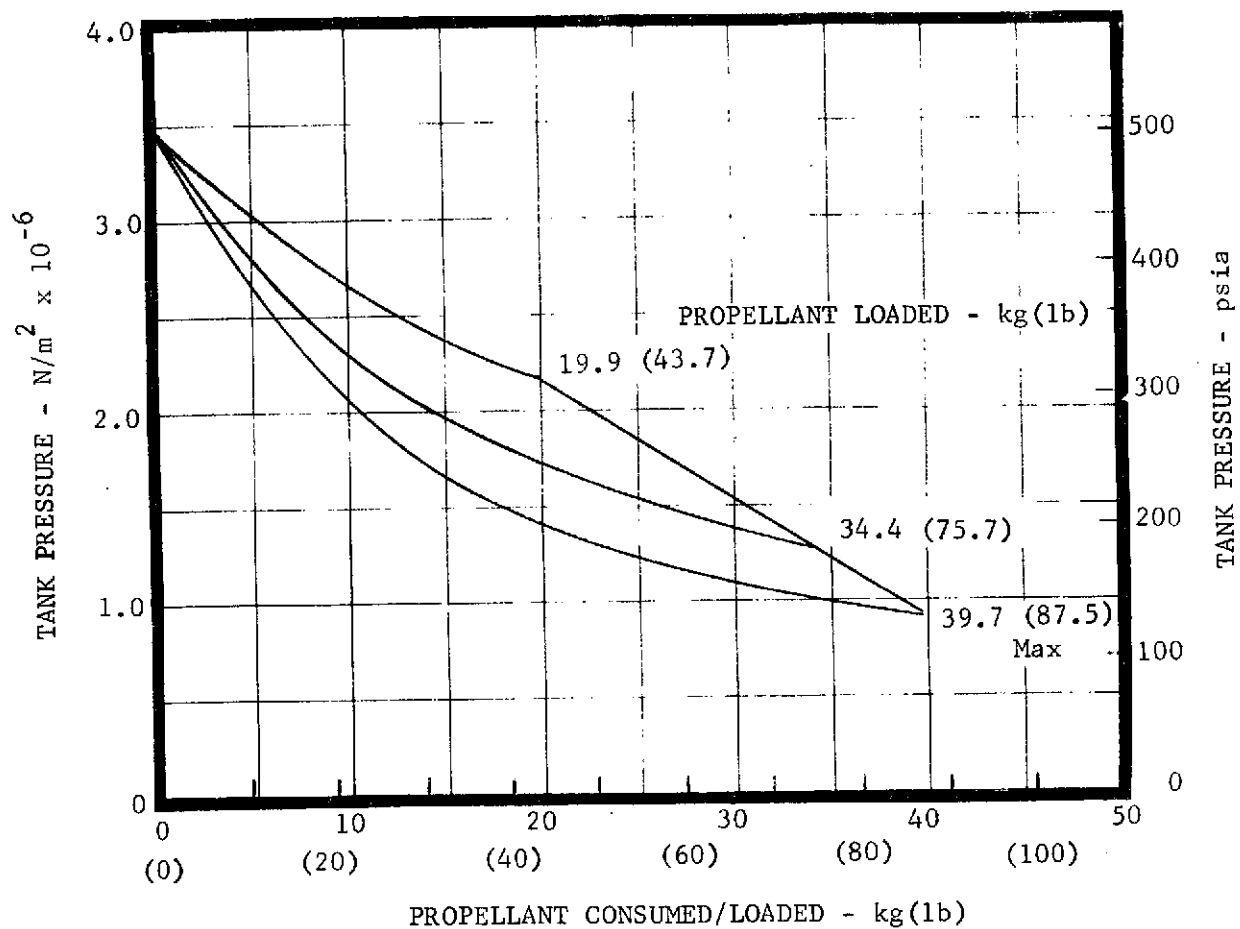


FIGURE V-25 HYDRAXINE TANK BLOW DOWN

TABLE V-29 THREE TYPICAL ROCKET ENGINE ASSEMBLIES

SUPPLIER	TRW	TRW	RRC
. Program	Pioneer 10/11	Intelsat	Viking RCS
. Steady State Thrust @ 3.45×10^6 n/m ²	5.33N (1.2 lb _f)	16N (3.6 lb _f)	39.6N (8.9 lb _f)
. Steady State Specific Impulse @ 3.45×10^6 n/m ²	228 sec	231 sec	231 sec
. Demonstrated Single Burn Time	10,000 sec*	7500 sec	1500 sec*
. Mass	0.27 kg (0.6 lb)	0.27 kg (0.666 lb)	0.73 kg (1.666 lb)
. Valve Configuration	Series Seats Redundant Coils	Series Seats Redundant Coils	Series Valves

* During development testing; qualified to 6500 sec (TRW) and 1210 sec (RRC) respectively.

TABLE V-30 APPROXIMATE BURN TIMES REQUIRED FOR ΔV MANEUVERS
(2 ENGINES FIRING)

MANEUVER	WITHOUT PROBE			WITH PROBE		
	5.3N (1.2 lb _f)	16N (3.5 lb _f)	39.6N (8.9 lb _f)	5.3N (1.2 lb _f)	16N (3.6 lb _f)	39.6N (8.9 lb _f)
101.5 m/s	3285 sec.	1123 sec.	451 sec.	4890 sec.	1690 sec.	679 sec.
15 m/s	549	187	75	931	310	126
45 m/s	-	-	-	3100	1033	416
TOTAL	3834	1310	526	8921	3033	1221

function of the defined pressure blowdown (3.45×10^6 to 0.93×10^6 N/m²) is shown in Figure V-26. The nominal steady state specific impulse as a function of inlet pressure is shown in Figure V-27, for the Pioneer 10/11 engine. This specific impulse is somewhat lower than that given for the higher thrust engines, but for initial system sizing purposes can be considered as typical. Figures V-28 and V-29 show the impulse bit and specific impulse for the Pioneer 10/11 engine firing at a frequency of 0.125 sec on/12.375 sec off. These performance data are not much different (less than a 1% difference) than our baseline duty cycle of 0.125 sec on/11.875 sec off. Each of the three engine configurations shown in Table V-29 is capable of precessing the spacecraft less than a degree per pulse. The 5.3N (1.2 lbf) engines fire a 125 ms pulse at 3.45×10^6 N/m² (500 psia) to precess the spacecraft approximately 0.5 degrees while the 35.6N (8. lbf) engine requires only a 20 ms pulse to obtain a 0.7 degree precession. Impulse bit repeatability is, of course, better for the larger pulse widths. Flexibility of the 5.3N (1.2 lbf) engine can be obtained through the reduction of pulse width to obtain significantly smaller precession angles if required.

ΔV performance of the small engine, however, suffers in that 101.5 mps ΔV would require a burn time of approximately 4890 seconds as compared to 680 sec of the 35.6N (8 lbf) engines (Table V-30). These long burn times are still within the capabilities of the engines however. A preferable approach would be to add two or four of the 5.3N (1.2 lbf) or the 16N (3.6 lbf) engines in the precessional positions to reduce the time required for ΔV maneuvers.

If four of the 5.3N (1.2 lbf) engines were added to the system with the thrust vector of each parallel to the spin axis, this would provide four precessional couples and four ΔV engines in either direction along the spin axis. The longest maneuver time would then be reduced from 4890 seconds to 2445 seconds and the life requirements on the engines considerably reduced.

d. Mass - Table V-31 summarizes the propulsion system component weights and vehicle masses used to compute propellant usage. Table V-31 also shows the propellant usage by basic function.

2. Earth-Encke-Geographos Mission

a. Propulsion System Requirements and Definition - The basic mission

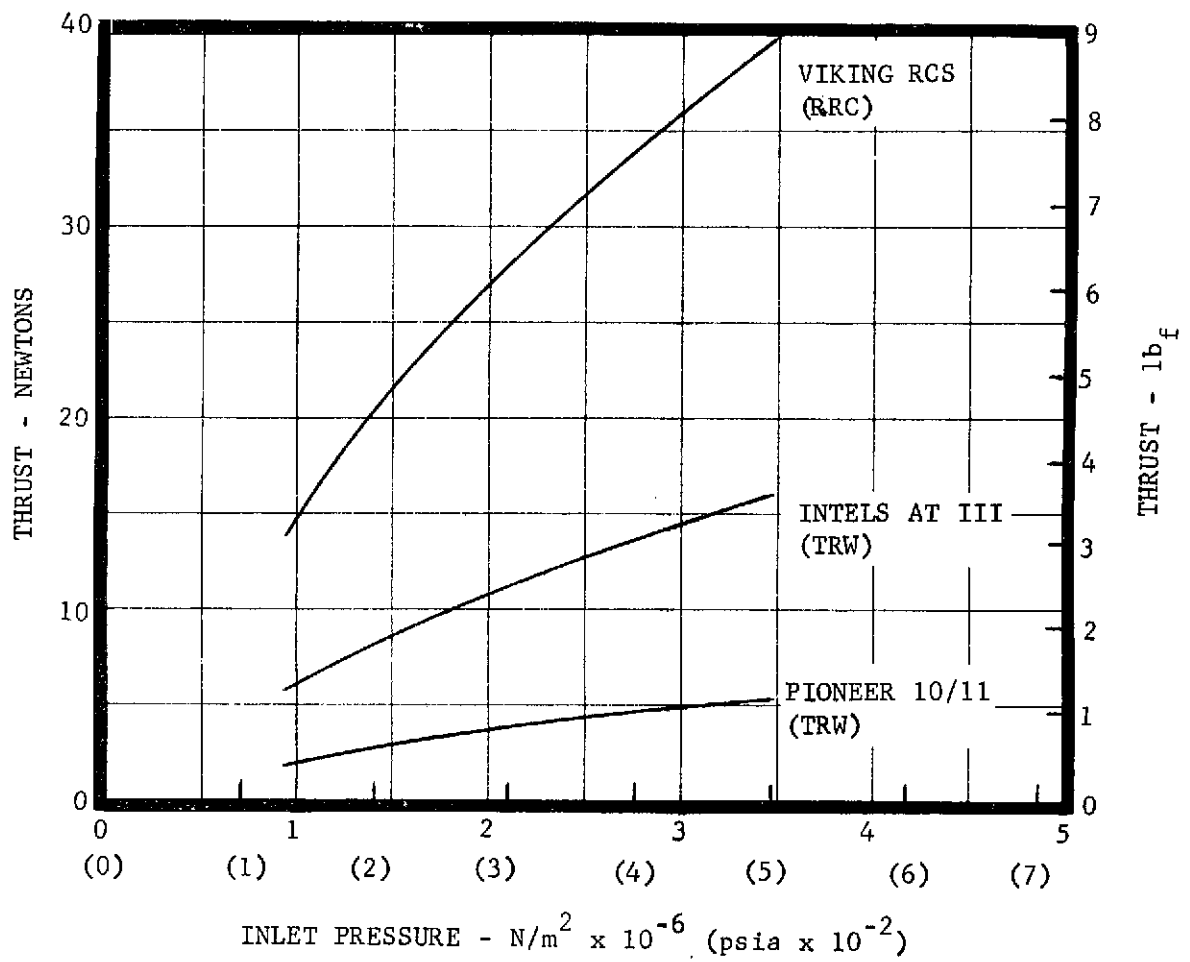


FIGURE V-26 TYPICAL N_2H_4 THRUST PROFILE

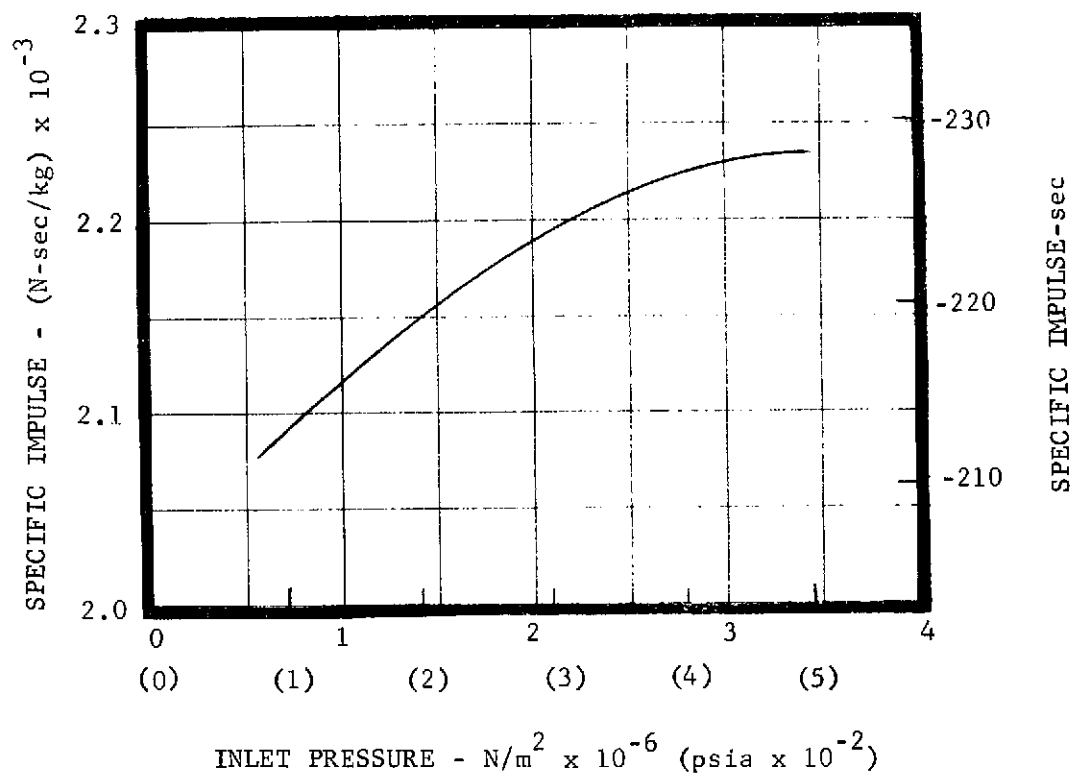


FIGURE V-27 STEADY STATE SPECIFIC IMPULSE FOR PIONEER 10/11 5.3-N THRUSTER.

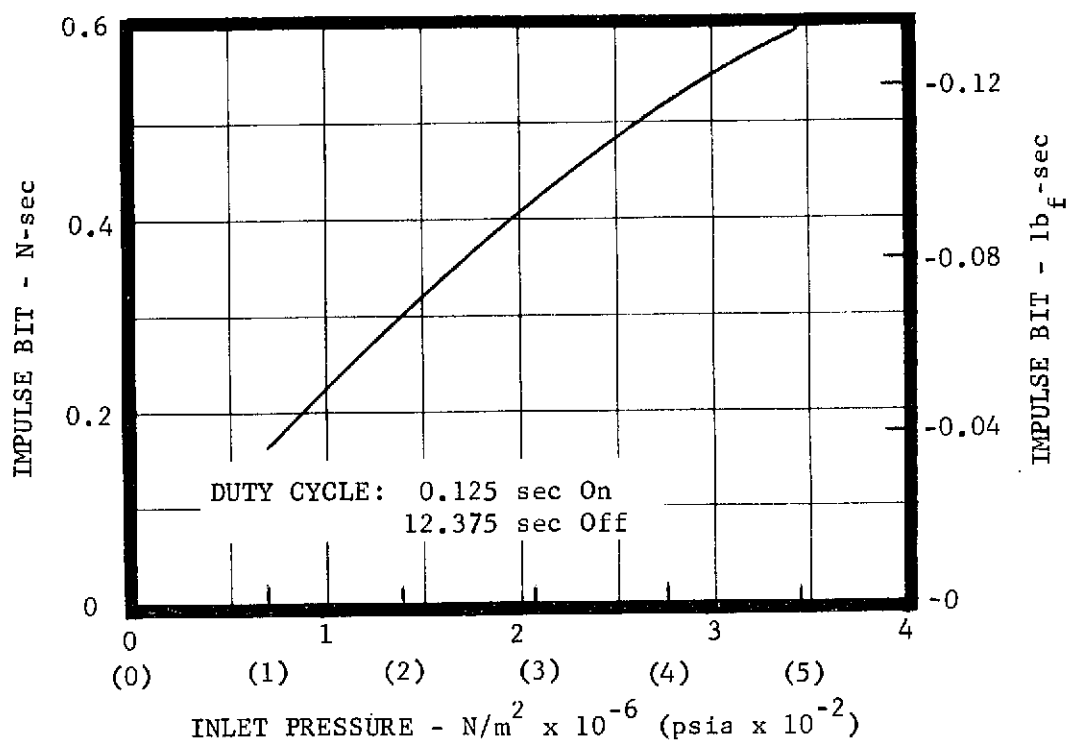


FIGURE V-28 IMPULSE BIT FOR PIONEER 10/11
5.3-N THRUSTER.

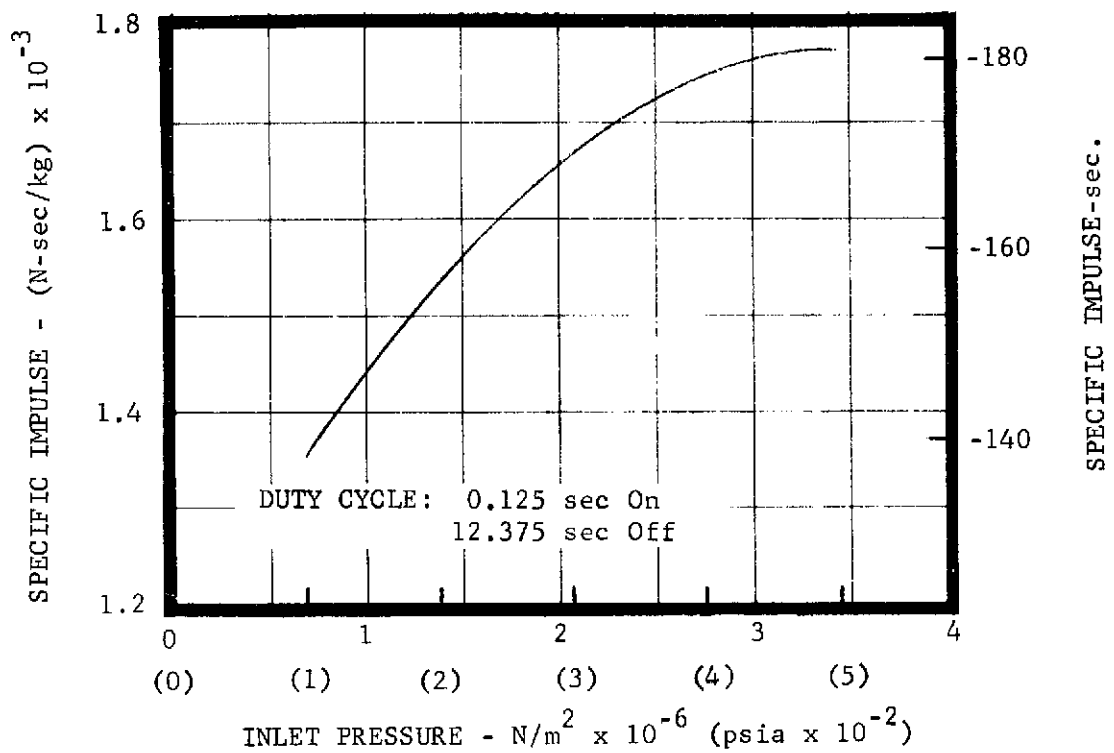


FIGURE V-29 PULSING SPECIFIC IMPULSE FOR PIONEER 10/11 5.3-N THRUSTER.

TABLE V-31
PROPULSION SYSTEM WEIGHT AND PROPELLANT USAGE SUMMARY

	SPACECRAFT WEIGHTS			
	WITHOUT PROBES		WITH PROBES	
	kg	lbm	kg	lbm
Basic Vehicle (less propulsion)	292.2	643.6	375.6	827.4
Propellant Tank (3)	4.8	10.5	4.8	10.5
Rocket Engine Assemblies (8)	2.2	4.8	2.2	4.8
Filter (1)	0.2	0.4	0.2	0.4
Pressure Transducer (1)	0.2	0.4	0.2	0.4
Fill & Drain Valve (1)	0.1	0.2	0.1	0.2
Lines and Fittings	0.8	1.7	0.8	1.7
Total Dry Vehicle	301.0	661.6	383.8	845.4
Pressurant	1.4	3.0	0.8	1.7
Loaded Propellant	19.8	43.7	34.4	75.7
Total Vehicle Mass	322.2	708.3	419.0	922.8
Propellant Usage				
Precession	0.4	0.9	0.5	1.2
ΔV (101.5 mps)	14.3	31.6	18.8	41.3
Precession	1.1	2.5	1.3	2.9
Spin Maintenance	0.2	0.5	0.2	0.5
ΔV (15 mps)	2.0	4.5	2.7	5.9
Precession	0.4	0.9	1.1	2.4
ΔV (45 mps)	-	-	7.9	17.5
Precession	-	-	0.5	1.2
Trapped	1.3	2.8	1.3	2.8
Total Propellant	19.8	43.7	34.4	75.7
Total Impulse Required				
	32560	7320	45600	10250
	N-sec	lb-sec	N-sec	lb-sec

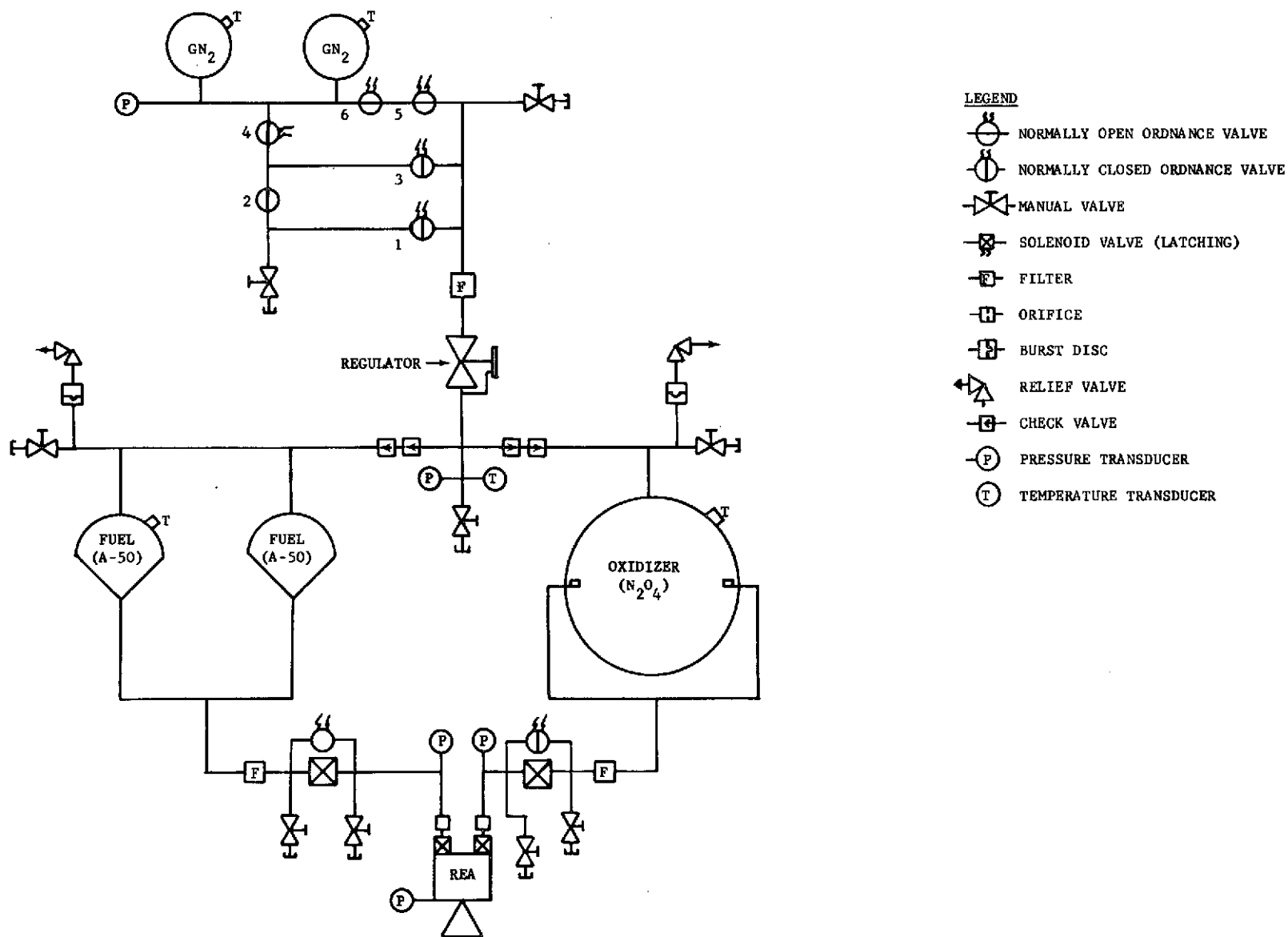
requirements are shown in Table V- 32. Although the total ΔV requirements are approximately twice those of the Encke-only mission, they are still within the range of a hydrazine monopropellant system. However, the system will require larger propellant tanks, and 12 - 5.3N (1.2 lbf) engines will be required to reduce total engine thrusting time as shown in Table V-33. All of the other system conclusions developed for the Encke-mission system are valid. Representative propulsion system mass and propellant usage by basic function for an Encke-Geographos mission are summarized in Table V-34.

3. Earth-Encke-Geographos-Toro Mission

a. Propulsion System Requirements and Definition - The basic Earth-Encke-Geographos-Toro comet-asteroid mission requirements are shown in Table V-35. Some preliminary assumptions were made of the spacecraft weight and inertias to obtain a comparative analysis of the candidate propulsion systems. Again, the basic spacecraft configuration utilizing an Earth-pointing spin axis was used. Because of the large impulse required, three basic propulsion system configurations were compared to determine the best potential system candidates. These systems consist of: 1) the basic hydrazine reaction control system shown in Figure V- 24 in combination with a solid rocket motor (SRM) for the large ΔV maneuver; 2) the basic hydrazine RCS system in combination with a bipropellant ΔV system (fig. V- 30); and 3) a GN_2 RCS system (fig. V-31) in combination with the bipropellant ΔV system. A ground rule used in comparing the systems was that the large ΔV maneuver (837.6 mps) would have to have the spacecraft precessed 3.14 rad (180°) maximum before and after it, and, that each ΔV maneuver performed by the separate ΔV system would be at a spin rate of 6.28 rad/sec (60 rpm) to minimize alignment error impact.

b. Hydrazine RCS-SRM ΔV Systems - The basic hydrazine RCS system (fig. V- 24) was re-sized using representative dry spacecraft weights defined for the basic Earth-Encke mission. The major ΔV maneuver of 837.6 mps was assumed to be performed by a solid rocket motor (SRM), and the remaining ΔV 's performed by the hydrazine system.

Precessional maneuvers were conservatively estimated at 2160 deg (376.5 rad) and the spacecraft was spun-up to 6.28 rad/sec (60 rpm) for only the SRM firing. As in the case of the basic mission, the launch vehicle was assumed to

FIGURE V-30 BI-PROPELLANT ΔV MANEUVER SYSTEM

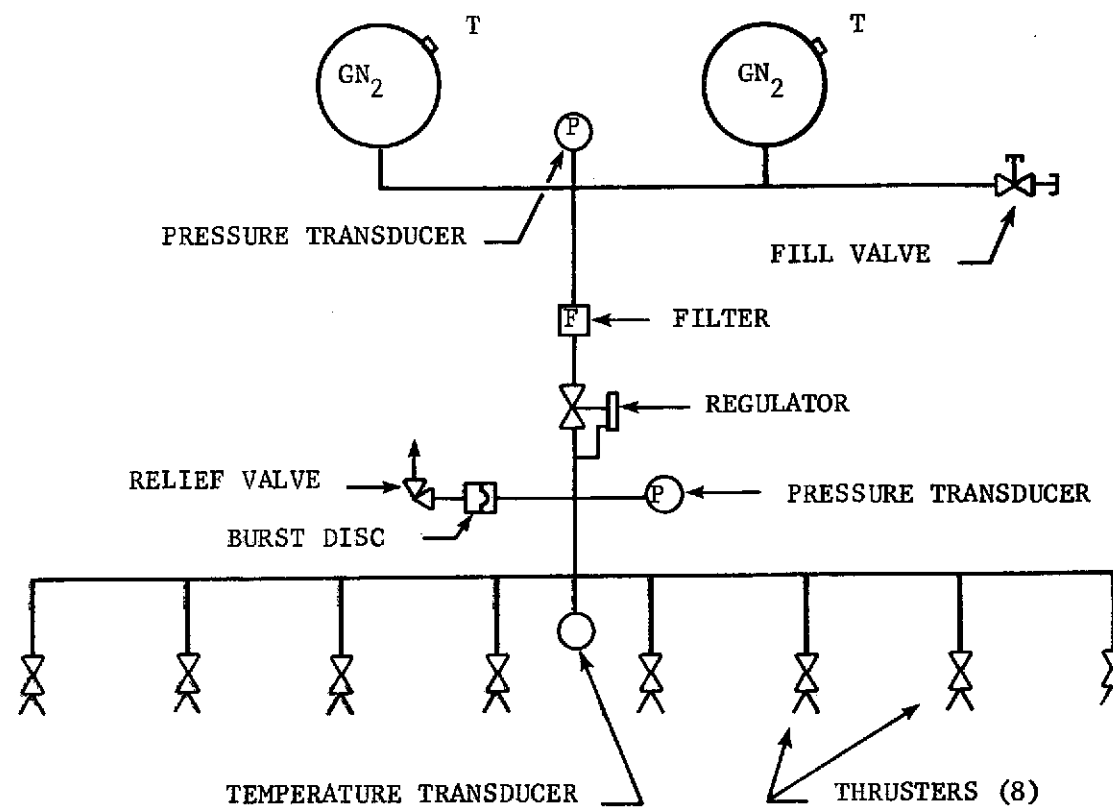
FIGURE V - 31 GN₂ RCS SYSTEM

TABLE V- 32

PROPULSION SYSTEM REQUIREMENTS FOR THE EARTH-ENCKE GEOGRAPHOS I MISSION

<u>FUNCTION</u>		<u>REQUIREMENT</u>
<u>VELOCITY INCREMENTS (ΔV)*</u>		
<u>TIME</u>	<u>IDENTIFICATION</u>	
L+5 days	Midcourse -1 (MC-1)	86.8 mps
L+91	MC-2 (Encounter - 5 days)	11.9
L+297	PMC-1 (E_G -187 days)	130.0
L+307	MC-3 (PMC+10)	2.40
L+479	MC-4 (E_G -5)	8.64
	TOTAL	239.74 mps

* Assuming 99% success criteria

ATTITUDE CONTROL

Spin Maintenance	574 N-sec (166 lbf-sec)
Precession	26.7 rad (1530°)
Spin (Despin maneuver)	783 N-sec (176 lbf-sec)

NOTE: All calculations performed to estimate impulse required or propellant consumption assumed a basic spacecraft weight equal to that used for the basic Comet Encke mission without probes.

TABLE V- 33

APPROXIMATE BURN TIMES REQUIRED FOR ΔV MANEUVERS WITH N_2H_4 SYSTEM

<u>MANEUVER</u>		<u>NUMBER OF 5.3N (1.2 lbf) REA FIRING</u>	
		<u>2</u>	<u>4</u>
MC1	86.8 mps	3448 sec	1724
MC2	11.9	522	261
PMC-1	130	6270	2135
MC3	2.4	134	67
MC4	8.6	484	242
TOTAL		10858	5429

TABLE V-34

PROPULSION SYSTEM WEIGHT AND PROPELLANT USAGE SUMMARY - ENCKE-GEOGRAPHOS I
MISSION

		<u>WITHOUT PROBES</u>	
Basic Vehicle		316.6 kg	(698.0 lb)
Propellant Tank (3)		7.3	(16.2)
Rocket Engine Assemblies (12)		3.3	(7.2)
Filter (1)		.2	(0.4)
Pressure Transducer (1)		.2	(0.4)
Fill and Drain Valve (1)		.1	(0.2)
Lines and Fittings		<u>.8</u>	<u>(1.7)</u>
TOTAL DRY VEHICLE	TOTAL DRY	328.5	(724.1)
Pressurant		1.2	(2.7)
Loaded Propellant		<u>49.2</u>	<u>(108.0)</u>
TOTAL VEHICLE MASS		378.9	(834.8)
<u>Propellant Usage</u>			
AV Maneuvers			
MC-1	86.8 mps	14.5	(31.9)
MC-2	11.9	2.0	(4.3)
PMC-1	130.0	20.0	(44.0)
MC-3	2.4	.4	(0.8)
MC-4	8.64	1.3	(2.9)
		<u>38.2</u>	<u>(83.9)</u>
<u>Attitude Control</u>			
Precession		8.3	(18.2)
Despin and Spin Maintenance		.8	(1.8)
Trapped		1.9	(4.1)
TOTAL PROPELLANT		<u>49.2</u>	<u>(108.0)</u>

TABLE V- 35
PROPULSION SYSTEM REQUIREMENTS FOR THE EARTH-ENCKE-GEOGRAPHOS-TORO MISSION

FUNCTION		REQUIREMENT*
<u>VELOCITY INCREMENTS (ΔV)</u>		
<u>TIME</u>	<u>IDENTIFICATION</u>	
L+5 Days	Midcourse -1 (MC-1)	86.8 mps
L+91	MC 2 (Encounter - 5 days)	11.9
L+29	PMC 1 (Planned Midcourse 1 Encounter with Geographos - 187 days)	122.4
L+307	MC 3 (PMC 1 + 10 days)	2.26
L+480	MC 4 (Geographos Encounter - 5 days)	8.13
L+487	PMC 2 ($E_G + 2$)	837.6
L+497	MC 5 (PMC 2 + 10 days)	15.78
L+617	MC 6 ($E_T - 5$)	6.98
TOTAL		1091.85 mps

* Assuming 99% Success Criteria

ATTITUDE CONTROL*

Spin Maintenance	740 N-sec (166 lb _f -sec)
Precession	37.65 rad (2160°)
Spin (per Spin-up or Despin Manuever)	862 N-sec (194 lb _f)

have spun up the spacecraft initially, therefore requiring the spacecraft to slow its spin rate from 6.28 rad/sec (60 rpm) to 0.52 rad/sec (5 rpm). These maneuvers result in a required system impulse of some 151,300 N-sec (34,000 lbf-sec). Usable propellant required is then 71.3 kg (157.0 lb). The required tankage volume would then be either two 53880 cc (3288 in³) tanks or three 37000 cc (2258 in³) tanks with a 10% propellant margin. Tank diameters would then be two 47 cm (18.5 in) tanks or three 41.3 cm (16.3 in) dia. tanks each weighing approximately 4.54 kg (10 lb) and 5.0 kg (11 lb), respectively. Slightly larger tanks are presently made, but the final tank selection is a function of the final spacecraft design.

The RCS engine selection is the same as for the basic mission. Burn time requirements are the only parameter significantly affected by this particular propulsion system selection. As can be seen in Table V-36, these parameters are quite large. Again, as mentioned above, the use of four additional engines, of any of the three thrust levels shown, would significantly reduce the maneuver times. This approach is recommended both from the standpoint of reducing ΔV maneuver times to an acceptable range and from the standpoint of reducing the engine life and single burn requirements to their demonstrated levels, particularly in the case of the 5.3N (1.2 lbf) thruster.

TABLE V-36

APPROXIMATE RCS BURN TIMES REQUIRED FOR ΔV MANEUVERS
(2 ENGINES FIRING) WITH N₂H₄ RCS/SRM ΔV SYSTEM COMBINATION

ΔV MANEUVER		THRUST LEVEL		
		5.3N(1.2 lbf)	16N(3.6 lbf)	39.6N(8.9 lbf)
MC1	86.8 mps	5039 sec	1735 sec	1697 sec
MC2	11.9 mps	815	277	111
PMC1	122.4 mps	10759	3586	1445
MC3	2.26 mps	200	67	27
MC4	8.13 mps	743	246	100
MC5	15.78 mps	1107	363	147
MC6	6.98	495	163	66
TOTAL		19158	6437	2593

The major ΔV maneuver would, in this concept, be provided by a solid rocket motor. The motor design characteristics assumed are:

- o Required total impulse - 350,500 N-s (78,800 lb-sec)
- o Average thrust level 13,345 N to 17,793 N (3000 to 4000 lbf)
- o Average specific impulse - 284 sec
- o Mass fraction (mass of usable propellant/total mass)- 0.86
- o ΔV maneuver time - 19.7 sec to 26.2 sec
- o Length - 114.3 cm (45 in) max
- o Diameter - 71.1 cm (28 in) max
- o SRM's in this general impulse/thrust/size class are available
 - o Aerojet SYM-2 - 386,500 N-s (86,900 lbf-sec)
 - o Thiokol TE-M-521 - 318,477 N-s (71,500 lbf-sec)

c. Hydrazine RCS - Bipropellant ΔV System - The basic hydrazine RCS system remains as described above, with a few differences:

- o The bipropellant system will be used to perform three ΔV maneuvers; MC-1 at 80.8 mps, PMC 1 at 122.4 mps and PMC 2 at 837.6 mps.
- o The hydrazine RCS will spin and despin the spacecraft to 6.28 rad/sec (60 rpm) for each of the three bipropellant system ΔV maneuvers.
- o Only 8 thrusters are required to provide the RCS ΔV maneuver capability, total engine burn times are given in Table V-37
- o Total impulse and propellant required is much less; required total impulse is 43600 N-sec (9800 lb/sec) usable propellant is 23.7 kg (52.3 lb).
- o Propellant tankage defined for basic Encke mission can be used for this mission with 59% margin or growth potential.

TABLE V-37

APPROXIMATE RCS BURN TIMES REQUIRED FOR ΔV MANEUVERS (2 ENGINES FIRING)
WITH N_2H_4 RCS/BIPROPELLANT SYSTEM COMBINATION

ΔV MANEUVER	THRUST LEVEL		
	5.3N(1.2 lb _f)	16N(3.6 lb _f)	39.6N(8.9 lb _f)
MC2 11.9 mps	623 sec	212 sec	85 sec
MC3 2.26 mps	123	42	17
MC4 8.13 mps	461	159	64
MC5 15.78 mps	735	248	100
MC6 6.98 mps	339	113	616
TOTAL	2281	774	312

A storable bipropellant ΔV maneuver system was selected for this study because of the long term space storage requirements of the mission. The most prevalent Earth-storable bipropellants in use today are the nitrogen tetroxide/Aerazine 50 (50% UDMH/50% N_2H_4) and nitrogen tetroxide/MMH propellant combinations. The nitrogen tetroxide/A-50 combination was chosen for this study due to its slightly higher performance characteristics. The baseline system characteristics are summarized below.

- o System total impulse is 455,840 N-sec (101,700 lb-sec)
- o System schematic is as shown in Figure V-30.
- o System on-off firing flexibility allows each ΔV maneuver to be performed incrementally if desired.
- o Ordnance and latching solenoid valve configurations allow positive system pressurant and propellant sealing between maneuvers.
- o System will perform 3 ΔV maneuvers.
- o ΔV maneuver times are :
 - 837.6 mps (779 sec burn time)
 - 122.4 mps (136 sec burn time)
 - 86.8 mps (102 sec burn time)

- o Mixture ratio is 1.6
- o Single oxidizer tank is mounted on vehicle centerline (spin axis) with propellant pickup in tank outer diameter. Requires new 75380 cc (4600 in³) propellant tank.
- o Two 37,690 cc (2300 in³) fuel tanks mounted in spacecraft structure within environmentally controlled area (under thermal blankets). Requires new tanks.
- o Two 6555 cc (400 in³) GN₂ tanks mounted in spacecraft structure. Existing psi pressurant tanks can be used, designed for HEOS-A, operating pressure $25.0 \times 10^6 \text{ N/m}^2$ (3620 psia)
- o Gas (GN₂) stored at $17.0 \times 10^6 \text{ N/m}^2$ (2460 psia)
- o Pressurant regulated to $1.2 \times 10^6 \text{ N/m}^2$ (170 psia)
- o Engine is Marquardt R-4D engine
 - o Thrust - 445 N (100 lbf)
 - o Mass Ratio - 1.6
 - o Specific Impulse - 290 sec (min)
 - o Weight - 2.22 kg (4.9 lb)
 - o Length - 34.0 cm (13.4 in) max
 - o Overall Dia. - 16.5 cm (6.5 in) max

In addition to the nitrogen tetroxide/A-50 bi-propellant system, a brief examination was made of a space storable system to determine potential gains resulting from the increased I_{sp} . This system was based upon a fluorine/hydrazine system studied during the recent Martin Marietta Corporation Venus Orbiter Mapper contract (ref. V-1c) and was examined only in sufficient detail to develop approximate weight data.

While JPL has fired a 2670N (600 lb) thrust fluorine/hydrazine engine, the (445N) thrust class engine required for this application would be a new development, and while the JPL tankage and valving was classed as flight-type, refinements would be necessary.

The following is a summary of the parameters used for this system:

Engine Thrust	444.5 N (100-lbf)
ISP	3677.5 N-sec/kg (375 sec.)

Oxidizer: flourine

Density 1506 kg/m³ (94 lb/ft³)

Tankage - Aluminum

Fuel: hydrazine

Density 1001 kg/m³ (62.5 lb/ft³)

Pressurant: helium

It was found that a launch weight saving of 30-35 kg would be possible on the combined Encke-Geographos-Toro mission. However, this is not sufficient improvement to permit the installation of probes on Configurations 1-4 for this mission.

d. GN₂ - RCS - Bipropellant ΔV System - This configuration replaces the basic hydrazine RCS with a cold gas - GN₂ system. Because of the limited impulse capability of GN₂ systems, none of the ΔV maneuvers were assumed to be performed by the GN₂ system. The GN₂ system did, however, have the additional task of spinning the spacecraft 6.28 rad/sec (to 60 rpm) for each ΔV maneuver. System characteristics are:

- o Total impulse required - 34,500 N-sec⁴ (7756 lbf-sec)
- o System configuration per Figure V-31
- o GN₂ stored at 20.7×10^6 N/m² (3000 psia)
- o 2 GN₂ 127,490 cc (7780 in³) storage tanks required
- o Regulated system to 2.1×10^6 N/m² (300 psia)
- o 8 GN₂ thrusters 4.4 N (1-lbf)
- o Specific Impulse = 70 sec

The basic bi-propellant system described above was again used for this analysis. System characteristics that are different than those shown above are as follows:

- o System to perform eight ΔV maneuvers
- o Two each of normally open and normally closed ordnance valves must be added to gas storage section of system for sealing.

- o Oxidizer tank is 97500 cc (5950 in³)
- o 2 fuel tanks are each 48750 cc (2975 in³)

3. Preferred Propulsion System

The three RCS/maneuver-propulsion systems described above were compared on the basis of the key parameters, state-of-the-art, weight, flexibility, and performance, (Table V-38). An attempt was made to keep the systems simple, yet provide maximum reliability for the missions involved. The comparison shows that from a mass and performance standpoint, the hydrazine/SRM and hydrazine/bipropellant systems are almost equivalent and much lighter than the GN₂ /bipropellant system (Table V-39). Both of these systems can perform the mission with the vehicle as defined for this tradeoff. The hydrazine/SRM system would need 4 additional (total of 12) thrusters to obtain reasonable maneuver times and remain within the engine life restraints. The hydrazine/bipropellant system is lighter than the hydrazine/SRM system, however, its reliability would not be as good and its recurring and nonrecurring costs would be higher. Tradeoffs performed in the final design would have to be performed that included cost and reliability factors to determine which system is preferable. Based on system and mission flexibility, mission growth potential, weight and performance however, the hydrazine/bipropellant system appears superior to the other two combinations.

4. Conclusions

Based on the analyses performed , the following conclusions may be formed:

- o The propulsion system best suited to perform the basic comet Encke mission as defined herein is a blowdown hydrazine system, as shown in Figure V- 24.
 - Tank volume should be 54080 cc (3300 in³) to allow impulse required for the vehicle with and without probes.
 - 8 engines in the 5.3 N (1.2 lbf) thrust range, four spin engines and eight ΔV /precession engines.
 - Total impulse required for the vehicle without probes is in the 33400 N-sec (7500 lbf-sec) category while with probes it is in the 48900 N-sec (11000 lbf-sec) category.

TABLE V-38

RCS/MANEUVER SYSTEM COMPARISON

<u>PARAMETER</u>	<u>N₂H₄/SRM</u>	<u>N₂H₄/BIPROP.</u>	<u>GN₂/BIPROP.</u>
Dry Vehicle Mass	348 kg (767 lb)	340 kg (748 lb)	414 kg (911 lb)
Loaded Vehicle Mass	550 kg (1211 lb)	532 kg (1171 lb)	690 kg (1518 lb)
State of Art	yes	yes	yes
Flexibility			
Growth Cap.	N ₂ H ₄ - Good SRM - Fixed after impulse fixed	Good	GN ₂ : Yes but at high weight penalty Biprop. yes
Incremental ΔV Capability	yes, except for SRM	Yes	Yes
No. of System Components	Al ₂ H ₄ : 20 SRM: 1 + Igniter	N ₂ H ₄ : 16 Biprop: 43	GN ₂ : 18 Biprop: 47

TABLE V-39 RCS/MANEUVER SYSTEM WEIGHT COMPARISON

SYSTEM	<u>N₂H₄/SRM</u>		<u>N₂H₄/BIPROP.</u>		<u>GN₂/BIPROP.</u>	
	RCS	ΔV	RCS	ΔV	RCS	ΔV
Propulsion System						
Type	N ₂ H ₄	SRM	N ₂ H ₄	Biprop.	GN ₂	Biprop.
Basic Vehicle Mass (kg)	309.5		309.5		309.5	
Propellant Tankage (kg)	13.6	-	4.8	7.1	75.4	11.1
Pressurant Tankage (kg)	-	-	-	5.5	-	5.5
Engine Wt. (kg)	3.3	20.2	2.2	2.2	1.1	2.2
Miscellaneous Hardware (kg)	1.2	-	1.2	6.8	2.5	7.8
Total Dry Vehicle (kg)	347.8		339.3		415.5	
Pressurant (kg)	1.4	-	1.8	2.5	-	3.1
Loaded Propellant (kg)	74.0	125.9	24.9	162.8	60.1	212.1
Total Vehicle Mass (kg)	549.1		531.3		690.8	
Propellant Usage (kg)						
ΔV Maneuvers						
MC-1 - 86.8 mps	21.0		-	15.9		20.5
MC-2 - 11.9	2.8		2.7	-		2.7
PMC-1 - 122.4	27.9		-	21.4		27.1
MC-3 - 2.26	0.5		0.5			0.5
MC-4 - 8.13	1.8		1.8			1.7
PMC-2 - 837.6	-	125.9	-	121.9		151.8
MC-5 - 15.78	2.5		2.5			2.4
MC-6 - 6.98	1.1		1.1			1.0
Total - 1091.9 mps	57.6	125.9	8.6	159.2	-0-	207.7
Attitude Control						
Spin Maintenance	0.5	-	0.5	-	1.1	-
Spin & Despin	1.2	-	2.3	-	20.1	-
Precession	12.2	-	12.2		29.1	-
Total	13.9		15.0		50.3	
Trapped Propellant	2.5		1.3	3.6	9.8	4.4
TOTAL PROPELLANT (kg)	74.0	125.9	24.9	162.8	60.1	212.1

- o The recommended propulsion system for the Comet Encke-asteroid missions is a hydrazine-bipropellant combination.
- Hydrazine system is same as on basic Encke mission
 - o Impulse requirement for Encke-Geographos-Toro mission, about 44500 N-sec (10000 lbf-sec)
- Bipropellant Nitrogen-Tetroxide/Aerozine-50 ΔV Maneuver System
 - o 445 N (100 lbf) engine
 - o Perform large >50 mps maneuvers
 - o Regulated system with positive consumable sealing
 - o Required impulse for Encke-Geographos-Toro Mission about 454,000 N-s (102,000 lbf-sec)

F. ELECTRICAL POWER

1. Spacecraft Power Subsystem

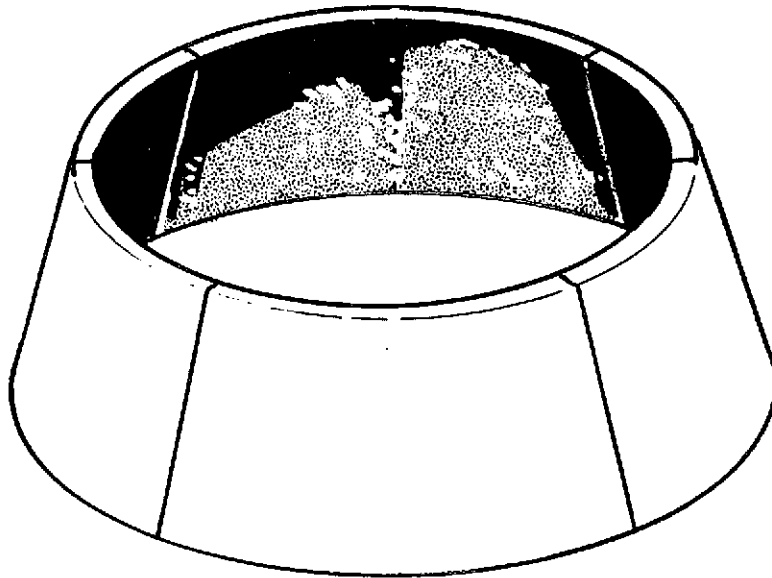
The electrical power subsystem consists of the solar array, power controls, power conditioning, and battery. Command and telemetry provisions are included. Since a spinning vehicle is used, solar cells are mounted on the external surface of a structural truncated cone so that a constant electrical output is produced during the vehicle's rotational spin. The angle of the truncated cone is fixed at 0.39 rad (22.5 deg.) in order to obtain a minimum variation in power output as the spin axis angle changes its relationship with the Sun line during the course of the mission. Details of the makeup of the solar array are given in Figure V-32. Radiation damage resulting from solar flares in the cruise mode was estimated to be 5.6 percent. To this was added 6 percent for degradation associated with application of coverglasses, installation and mismatch. Output was computed by determination of single cell output from solar cell data (ref.V-1d) under intensity and temperature conditions at specific points in the mission. Then, using the aspect ratio corresponding to the spin axis direction and the array and degradation factors, current-voltage plots were made and power available at 28-volt output determined.

The arrangement of the equipment making up the subsystem is shown in Figure V-33. Voltage control is provided by a shunt regulator operating at 28 Vdc \pm 2 percent.

A 16-cell, 8 ampere-hour, high-energy-duration nickel-cadmium battery is provided to augment the solar array in carrying peak loads. It is maintained by a charger located in the power control unit. Maximum charge voltage is limited to 24 volts. When power is required, a discharge regulator boosts the output of the battery to 28 volts. The various utilization voltages, other than 28 Vdc, required by the subsystems are provided from a central transformer rectifier filter supplied by an inverter.

Array power availability as compared to the required power for various mission phases is shown in Table V-40.

During periods where the solar array power level is below that required by the spacecraft, the battery will be paralleled with the solar array output to



CONE ANGLE	22.5 DEG.
SOLAR CELL	2 OHM-CM, 2x2x0.025 CM
COVERGLASS	2x2x0.015 CM
NO. OF CELLS	9504
NO. CELLS IN PARALLEL	108
NO. CELLS IN SERIES	88
NO. PANELS	6

FIGURE V- 32 SOLAR ARRAY CONFIGURATION

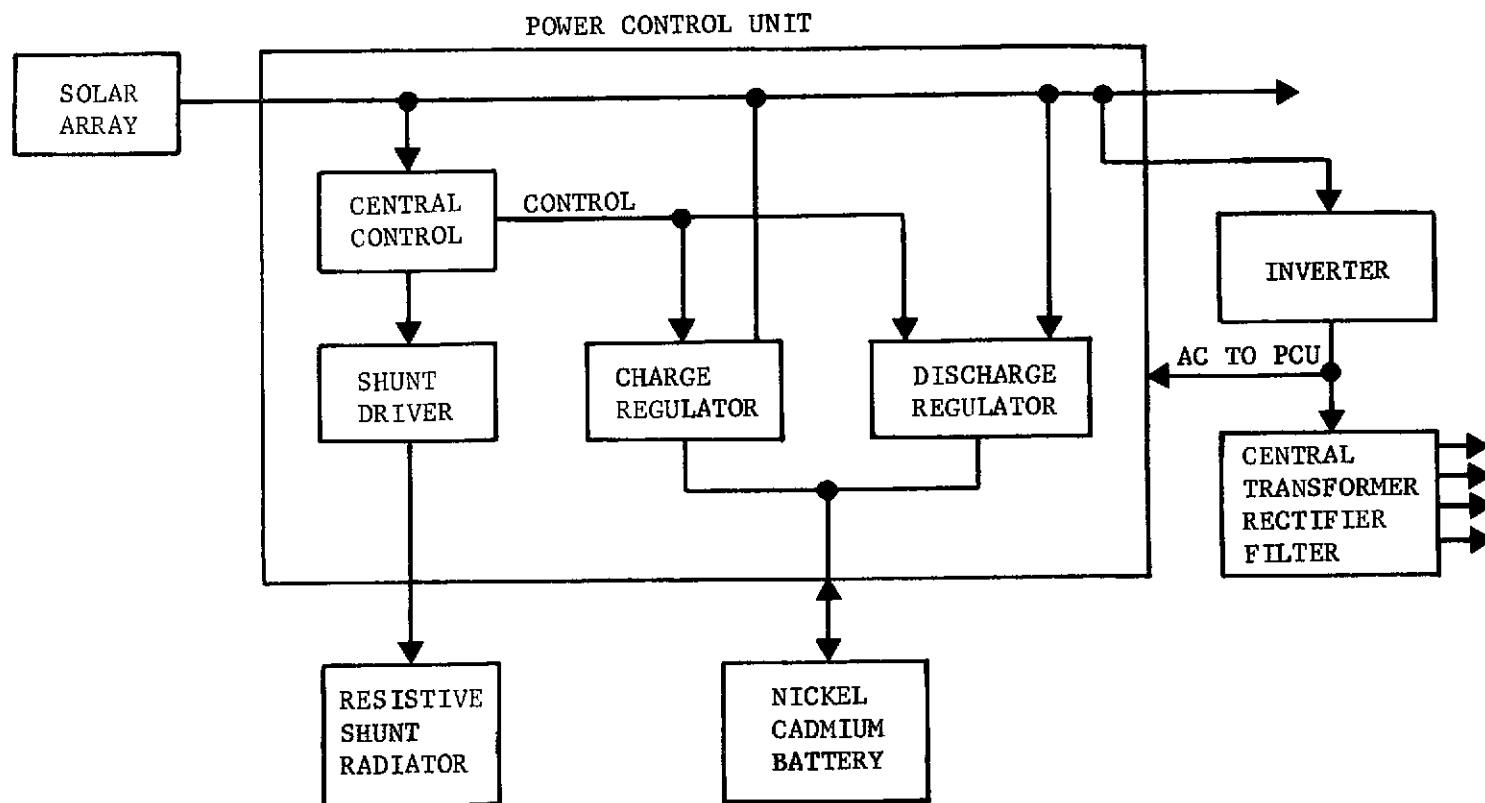


FIGURE V-33
POWER SUBSYSTEM BLOCK DIAGRAM

TABLE V-40 POWER PROFILE SUMMARY (ENCKE-GEOGRAPHOS-TORO MISSION)

EVENT	POWER REQ'D(W)	POWER AVAIL.(W)	POWER MARGIN(W)
T_0 - T_0 + 90 min. Launch Phase	35.0	Batt-No S/A pwr	--
T_0 + 90 min. \Rightarrow T_0 + 2 hrs. S/C Separation & Deployment	63.0	Batt-No S/A pwr	
T_0 + 2 hrs. S/C Orientation & Sun Acquisition	81.2	123.0	+41.8
T_0 + 5 Days - First Mid-course Correction Maneuver	81.2	123.0	+41.8
T_0 + 6 Days - T_0 + 76 Days I/P Cruise Science	117.9	123.0	+ 5.1
T_0 + 76 Days - T_0 + 90 Days Targeting Maneuvers	198.8	227.0	+28.2
T_0 + 90 Days - T_0 + 96 Days Close Approach Science	202.0	227.0	+25.0
T_0 + 94 Days Probe Separation	202.0	232.0	+30.0
T_0 + 96 Days (E_0 - 1.5 hrs - E_0) Encke Encounter Science	253.1	235.0	-18.1*
T_0 + 96 Days - T_0 + 98 Days Tail Observations	203.0	235.0	+32.0
T_0 + 98 Days - T_0 + 116 Days Far Tail Observations	150.6	239.0	+88.4
T_0 + 116 Days - T_0 + 622 Days I/P Cruise Science	104.6	262.0	+157.4
T_0 + 200 Days ΔV Burn - To Asteroids	104.6	148.0	+43.4
T_0 + 389 Days Geographos Encounter	200.7	176.0	-24.7*
T_0 + 390 Days Midcourse Maneuver	122.5	176.0	+53.5
T_0 + 622 Days Toro Encounter	200.7	186.0	-14.7*
T_0 + 623 Days Data Dump	158.0	186.0	+28.0

* Solar Power Deficit Supplied by Battery.

provide necessary operating margin. The Encke/asteroid mission represents a worst-case condition for solar power. The heliocentric distance at which the spacecraft encounters Encke is 0.75 AU. For the reference mission (Encke only) the distance is 0.53 AU. For the combined mission, the solar array provides 235 watts at encounter, and for the reference mission, the power available is approximately 370 watts. There is sufficient combined power (solar array plus battery) for any of the proposed missions.

2. Probe Electrical Power and Sequencing Subsystem

Subsequent to release of the probe from the spacecraft, the event timer will be started by closure of the parallel redundant separation switches. The event timer will count down for a period of 46 hours, assuming a separation of the probe two days before encounter with the nucleus. At this time, the event timer will apply power to the sequencer. The event timer will include provisions for adjusting its count-down to compensate for variation in deployment time. This feature provides greater flexibility in the selection of probe deployment time. Execution of a ground command will be required to select a count down duration less than the 46-hour nominal, count down times of one day, 12 hours, and 6 hours will be furnished.

Upon receipt of a signal from the event timer, the sequencer will in turn apply power to the probe equipments in a serial fashion. This provision is made to reduce transients and high current surges on the power bus.

The electrical subsystem will be composed of an AgZn battery and a power control unit (PCU). The battery has been selected to provide a maximum of 246 W-hr capacity. The battery rating was derated by 30%, providing a 172 W-hr level. Figure V- 34 shows the power usage as a function of time for both a 246 W-hr and a 172 W-hr capacity. In both cases, two hours of pre-encounter science and a minimum, of one hour for tail observations can be obtained from the proposed battery.

The PCU will include the event timer and sequencer circuitry, a DC/DC converter as a secondary power source, and the necessary power control and transfer circuitry.

The probe will operate from an unregulated primary power bus. Primary

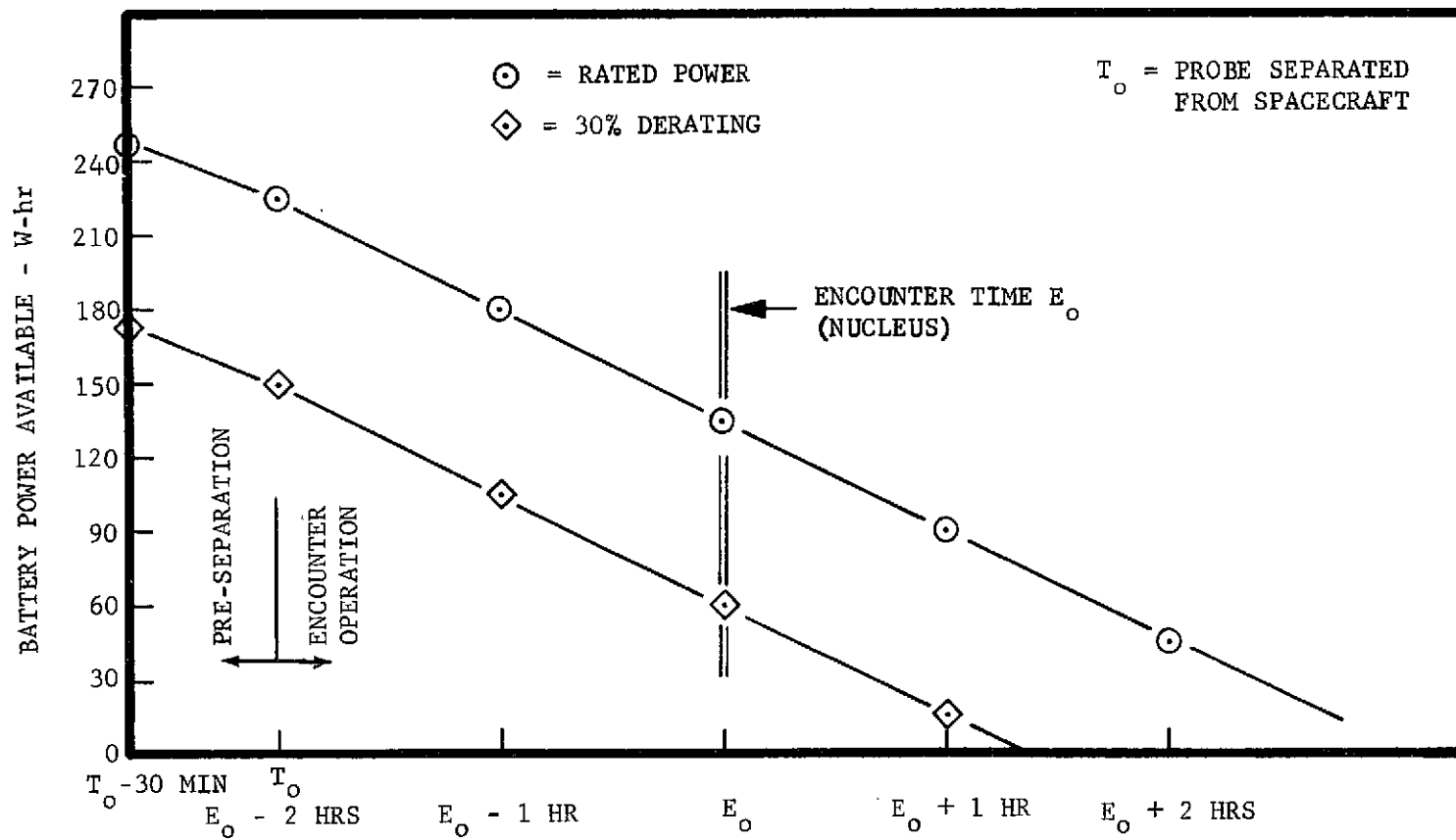


FIGURE V- 34 PROBE POWER USAGE

power will be referenced to a single point ground. Current limiting provisions will be incorporated into the primary power input lines to each of the using equipments. No fuses will be used in the probe power distribution circuitry.

Figure V-35 is a block diagram of the proposed configuration, Table V-41 defines the sequence of major events involving the probe. Table V-42 defines the power requirements for probe equipment.

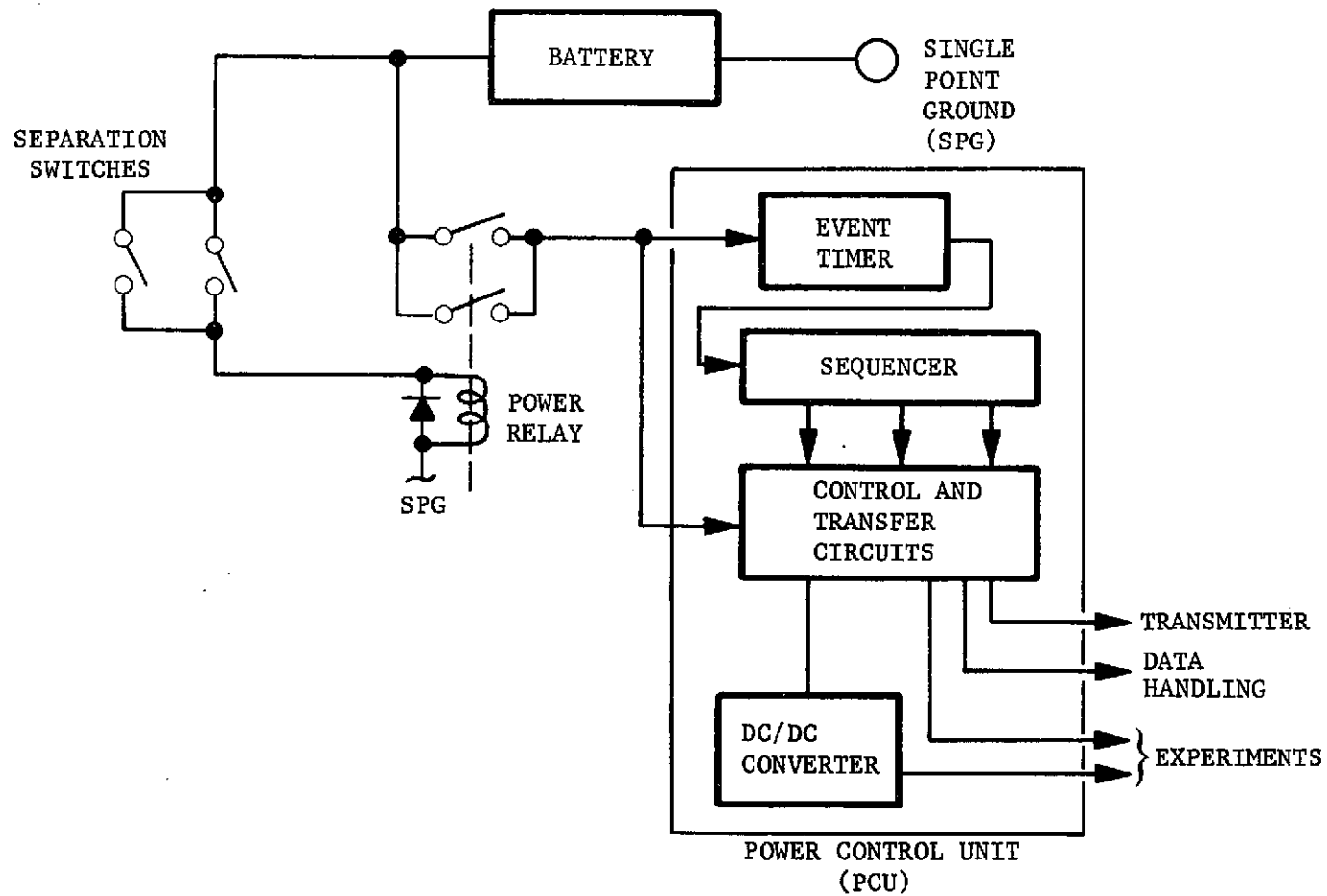


FIGURE V-35 PROBE POWER SUBSYSTEM

TABLE V-41 PROBE SEQUENCE OF EVENTS

T_0 - 30 min.

Pre-separation Checkout and Calibration.

(Note: The battery is used as the source of power for on-board checkout. This will reduce the load on the spacecraft bus during the close approach period.)

T_0 - (Separation) - Start event timer (set timer count-down time)

E_0 - 2 hrs. - Initiate Sequencer - Apply power to Communications, Data Handling, Science Payload

TABLE V-42 PROBE EQUIPMENT POWER REQUIREMENTS

UNIT	POWER (W)
Power Control Unit (internal losses)	5.0
Communications	8.0
Data Handling	4.7
Science Payload	
Ion Mass Spectrometer	4.0
Neutral Mass Spectrometer	14.0
Langmuir Probe	2.0
Micrometeorite Detector	1.0
	<hr/>
TOTAL	36.7
Thermal and Line Losses 20%	7.5
	<hr/>
TOTAL	44.2

G. THERMAL CONTROL

The spacecraft is thermally compartmentized with multilayer insulation blankets into a solar array compartment and an equipment compartment.

For an assumed electrical power level of 250 watts in the equipment compartment, approximately seven square feet of louvers are required on the external side of the platform. The louvers do not receive direct solar radiation and are space viewing in order to maintain the compartment temperature at between 5°C and 30°C. Figure V-36 shows a concept for the location of multilayer blankets, shields, and louvers.

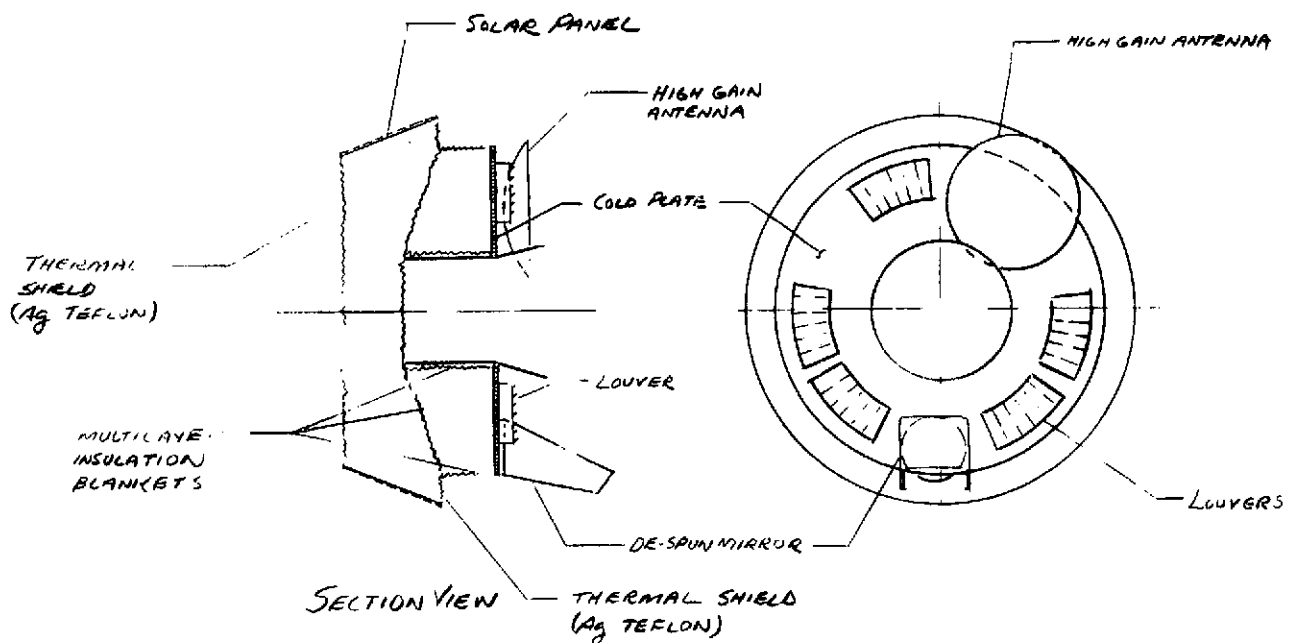


FIGURE V-36 THERMAL CONTROL CONCEPT

The solar array compartment is designed to emit the absorbed solar energy through the forward end. At an encounter radius of 0.52 AU, the solar array temperature is estimated to be about 127°C. This temperature was estimated for the case of direct illumination of the array face as shown by the following preliminary analysis (see Figure V-37).

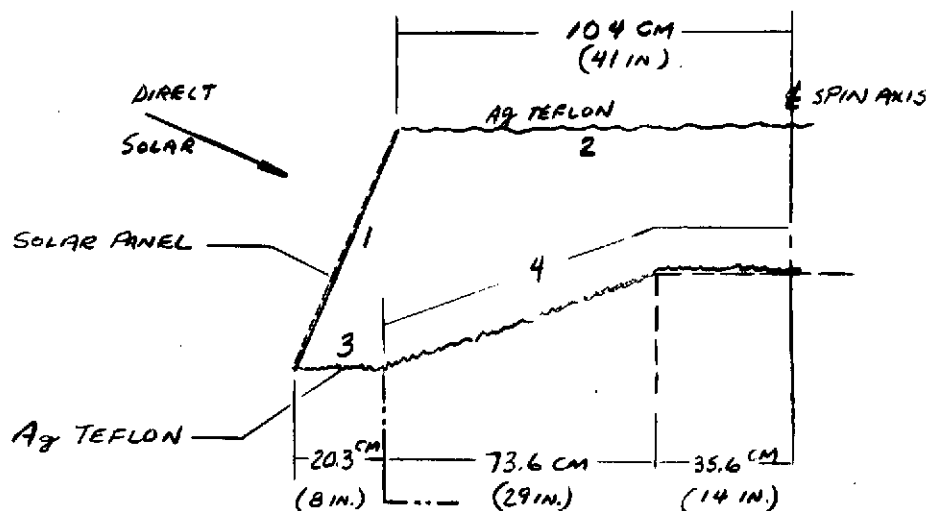


FIGURE V-37 THERMAL ANALYSIS DIAGRAM

The energy balance on surfaces 1, 2 and 3 is given by:

$$\text{Surface 1: } S\alpha_1 A_{p1}/\sigma + (A_1 \overline{f}_{12})(T_2^4 - T_1^4) + (A_1 \overline{f}_{13})(T_3^4 - T_1^4) - \epsilon_1 A_1 T_1^4 = 0$$

$$\text{Surface 2: } S\alpha_2 A_{p2}/\sigma + (A_1 \overline{f}_{12})(T_1^4 - T_2^4) + (A_2 \overline{f}_{23})(T_3^4 - T_2^4) - \epsilon_2 A_2 T_2^4 = 0$$

$$\text{Surface 3: } S\alpha_3 A_{p3}/\sigma + (A_1 \overline{f}_{13})(T_1^4 - T_3^4) + (A_2 \overline{f}_{23})(T_2^4 - T_3^4) - \epsilon_3 A_3 T_3^4 = 0$$

where $S = 29250 \text{ W/m}^2$ (Solar Flux @ 0.52 AU)

$\sigma = 5.6696 \times 10^{-8} \text{ W/(m}^2 \text{ } ^\circ\text{K}^4)$ (Boltzmann Radiation Constant)

Based on the surface properties of Table V-43, the estimated radiation exchange factors are: $A_1 \overline{f}_{12} = 14.2$, $A_1 \overline{f}_{13} = 6.8$, and $A_2 \overline{f}_{23} = 2.8$. The resulting surface temperatures are:

$$T_1 = 400^\circ\text{K} (127^\circ\text{C})$$

$$T_2 = 360^\circ\text{K} (87^\circ\text{C})$$

$$T_3 = 322^\circ\text{K} (49^\circ\text{C})$$

TABLE V- 43 SURFACE PROPERTIES

	SURFACE			
	1	2	3	4
Total Area, A, m ²	4.27	3.40	1.44	3.95
Solar Projected Area, m ²	1.49	1.67	0	0
(Absorptivity) α	0.80	0.18	-	-
(Emissivity) ϵ	0.80	0.66	0.66	0
(Reflectivity) ρ	0.20	0.34	0.34	1.0

For Concept number 2, with the externally despun mirror, a temperature level in the neighborhood of -130°C with a temperature gradient along the length between the rotating bearing and the outer tip can be expected. Such a temperature level does not appear to be a problem, and heaters to equalize the temperature gradient could be provided for approximately 20 watts of electrical power.

For the concept where some of the instruments are mounted on the despun platform, remote from the equipment compartment, it will be necessary to control the temperatures in an isolated compartment and to maintain a range of -10° to 15°C. Thermal control will be achieved with equipment power dissipation, absorbed solar radiation, and thermostatically-controlled electrical heaters.

Although temperature control of the externally-mounted coma probe has not been investigated, it would also be treated as an isolated compartment while still on the spacecraft. Thermal control of the probes installed at the lower (boat-tail) end of the structural central cylinder (see Figure IV- 7) presents fewer problems than for the cases where the probe is installed in the solar array compartment. In the latter case, the probe is at the hot end of the spacecraft. Detailed thermal analysis will be required to assess the impact of the solar orientation profile on the probe as well as the interaction between the probe and the solar array compartment.

Thermal control techniques which will be considered in this analysis include solar reflecting shades and shields, surface coatings, multilayer insulation blankets and thermal conduction standoffs in the support structure.

H. DATA HANDLING

1. Spacecraft Data Subsystem - The data handling subsystem has been based primarily on the Pioneer 10/11 subsystem with modifications dictated by the requirements of this mission. The subsystem is essentially two operationally independent branches; (1) - a lower data rate section for processing the non-imaging science and spacecraft performance data, and (2) - a section to exclusively process the data from the television imaging system. Block diagrams for the above are shown in Figures V-38A and V-38B.

The low data rate section consists of a Digital Telemetry Unit (DTU), a Data Storage Unit (DSU), and a Signal Conditioner. This section has the capability of processing data at rates of 128, 256, 1024 and 2048 bits per second. The low rate system will use convolutional coding, with a bi-phase carrier modulating the S-band transmitter (Section V-B).

The high data rate section will be utilized to telemeter the television picture data stored in a tape recorder. These data will be block coded, bi-phase modulated and transmitted using the X-band transmitter. A separate DTU (No. 2) will be required to process these data. The data transmission rates for this section are; 16,384 bits per second at the comet, and 2048 bits per second at the asteroids.

It is proposed that the DTU's (1 and 2) will be designed to provide 8 bit quantization accuracy in order to be consistent with imaging and other science requirements. As in the case of the Pioneer DTU's, each DTU will be internally redundant for all mission critical functions. No single failure will result in the loss of mission critical data, or the loss of the redundant element. Further, appropriate input and output buffering provisions will be included to protect against failures resulting in short circuits referenced to ground potential or a common input or output line.

Provisions for connecting the imaging science data to the low rate telemetry link, in event of failure of the X-band link, will be furnished. The coupling of X-band data to the S-band system will be accomplished by execution of a command from the ground station. Some loss of non-imaging science data may occur during play back of the imaging data.

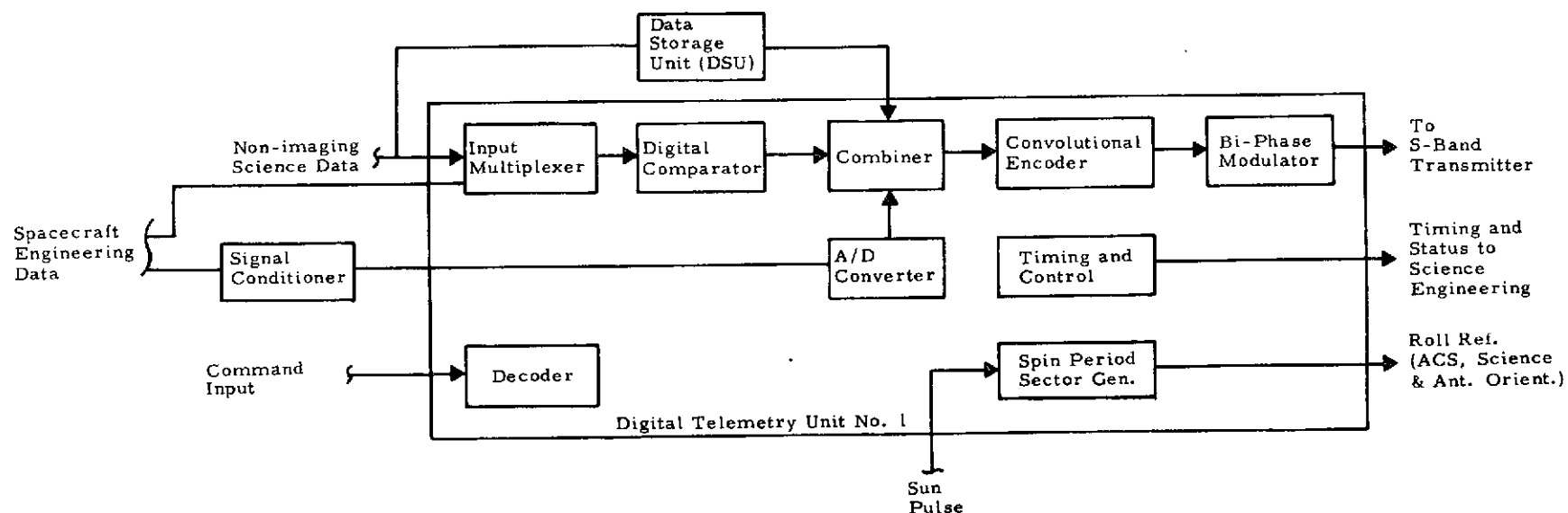
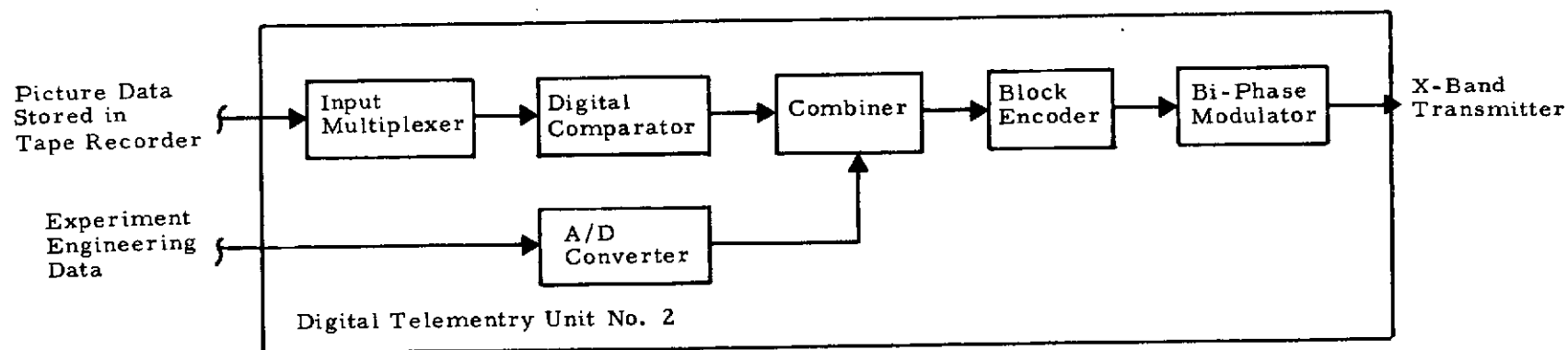


FIGURE V-38A NON-IMAGING SCIENCE AND SPACECRAFT ENGINEERING DATA



Single Format
2 Bit Rates at 16, 384 bps, at 2048 bps

FIGURE V-38B IMAGING SCIENCE DATA

It is proposed that the imaging data from the cameras be stored in a tape recorder comparable to that previously used on MM71.

This recorder has a storage capacity of 1.8×10^8 bits. It must be recognized that this recorder has a relatively small storage capacity, and as a result of this, will require frequent play back during the close-approach and encounter phases of the mission. With 5.25×10^6 bits per picture, approximately 30 pictures could be stored in the recorder. At encounter, the X-band telemetry link has a transmission rate of 16,384 bits per second, with a full tape approximately 3.0 hours would be required to read-out the tape. The long read out time requires the tape to be read out when it is only partially filled in order to obtain maximum science return. This mode of operation requires careful control of the picture storage and playback sequence. A stored program will be used to sequence the taking of pictures, the time between pictures, and read-out of the stored data in the recorder. Command access to the program sequencer will be provided to override the stored program, or to isolate and remove operational problems.

A similar mode of operation is anticipated during encounter with the asteroids. A stored program, unique to the asteroid mission, will be provided.

No provisions have been included in the spacecraft data system to process information from the coma probe subsequent to its release from the spacecraft.

Information regarding probe status, battery condition, experiment calibration, etc. will be provided through use of a special format during probe pre-separation checkout and conditioning.

Table V-44 is a tabulation of expected mass, volume, and power required for this subsystem.

TABLE V-44 DATA SYSTEM COMPONENT CHARACTERISTICS

<u>UNIT</u>	<u>MASS (kg)</u>	<u>POWER (W)</u>	<u>SOURCE</u>
DTU (1 & 2)	3.1	4.7	Pioneer
DSU	1.0	1.0	Pioneer
SIGNAL CONDITIONER	0.25	0.0	Pioneer
TAPE RECORDER	10.9	REC. 22.0	MM'71
		PB 18.0	

A spin period sector generator, as currently used in Pioneer 10/11 has been included in DTU No. 1 to provide precise measurement of the spacecraft's rotation rate. For spin rates between 4.7 and 6.0 rpm, the percentile error is 0.002%, and at 60 rpm the error is 0.01%. The primary sources of error are sun pulse jitter, and the telemetry quantization errors.

2. Probe Data System - The probe data handling subsystem uses a Digital Telemetry Unit (DTU) to process probe science and engineering data. The DTU is the 3.1 kg/4.7 watt unit incorporated in advanced Pioneer mission studies.

Two data rates will be provided, the low bit rate will be 64 bits per second, with 128 bits per second as the high rate. As is described in the Communication Subsystem section (V-B), will be transmitted at 380 MHz, will be frequency shift keyed, and use convolution encoding.

Tentative science and engineering data allocations are shown below:

Science	80 bps
Engineering	32 bps
Telemetry Status and Synchronization	16 bps
<hr/>	
TOTAL	128 bps

The above table is based on a 16 word format, with 8 bits per word, giving a frame size of 128 bits.

At a 128 bps transmission rate, one frame would be transmitted per second, and half a frame per second transmitted at the low data rate.

Data will be transmitted directly to the ground station rather than to the spacecraft, thereby reducing the complexity of the spacecraft system.

I. SCIENCE INSTRUMENTS

In Chapter II, the selection of science instruments was made in order to perform meaningful science at the comet and asteroids. The baseline payload selected fulfilled the scientific objectives and was consistent with the comet/asteroid observables. A brief rationale was given also for selection of instruments that were typical and were available from previous missions.

In this section, science requirements that influence spacecraft configurations and mission design are given, and typical science instruments are defined further. Imaging and non-imaging requirements in the form of timelines are given for the comet/asteroids. These science timelines were used to determine the mission sequence of events, power and data levels, pointing, communications loads, and other spacecraft subsystems requirements. Graphs used in developing the imaging and spectrometer timelines are included. Two instruments are then given special study for operation at the comet/asteroids: imaging and mass spectrometers.

An imaging radiometer study indicates vidicons are expected to perform better than a solid state spin-scan system because of light limitations at the targets. The mass spectrometers will work in a spinning mode, but not as efficiently as they would if oriented in the "ram" (i.e., relative velocity) direction. Scoops to increase efficiency in a spinning mode do not appear feasible.

Finally, the section concludes with recommendations that several instruments be given technology development emphasis in order to better match instrument capability with the specific requirements of comet/asteroid missions.

1. Instrument Descriptions

Instruments selected are those representative for the measurements defined for these missions. The instruments used on the noted spacecraft are the closest flight or proposed experiments that could be found. With the exception of three instruments discussed in Section V-I-7, little or no modifications are anticipated.

a. Visible Spectrometer (OGO-F)

Instrument Description - The instrument selected for this mission is a multi-channel, narrow-band, interference-filter spectrometer. Filter selection will be based on data previously obtained from ground based observations of Encke.

Performance Characteristics - Spectral range and bandwidth for typical filters are shown below:

<u>Radical</u>	<u>Wavelength Å</u>	<u>Bandwidth</u>
CN	3883, 4216	$\pm 10 \text{ Å}$
C ₂	4738, 5160, 5640	$\pm 10 \text{ Å}$
C ₃	4050	$\pm 10 \text{ Å}$
CO ₂	4550	$\pm 10 \text{ Å}$
CO ⁺	4000	$\pm 10 \text{ Å}$
N ₂ ⁺	3910	$\pm 10 \text{ Å}$
NH ₂	6300	$\pm 10 \text{ Å}$

Interfaces

Electrical

Power 3 watts

Mechanical

Size (cm) 15.0 x 20.5 x 42.0

Volume (cm³) 1.29×10^4

Mass (kg) 3.5

b. Infrared Spectrometer (Mariner Mars '71 Instrument)

Instrument Description - In order to obtain precise measurement of the thermal emissions of the asteroids, and, secondarily, in order to measure the coma and nucleus, an interferometer spectrometer has been chosen for this mission. The instrument can also measure low-energy molecular transitions in the vicinity of the nucleus. The spectral region to be studied lies between 5 μm and 36 μm , assuming blackbody temperatures ranging from 80°K to 600°K.

High-resolution spectrometers using many discrete detectors have been flown; however, the interferometer-type instrument on MM'71 (IRIS-M) offers even greater resolution. The size and mass of the IRIS-M is comparable to other

typical multiple-detector instruments.

An additional advantage of the selected experiment is its ability to compress the data from the interferograms prior to their transmittal to the ground station.

Performance Characteristics

Spectral Range 5 μm to 36 μm
Number of Samples per Interferogram 4096
Optical Path Difference (cm) 0.85
Mirror Displacement During Interferograms (cm) 0.42
Mirror Scan Rate (cm sec⁻¹) 0.023
Aperture Area (cm²) 15
Field of View (degree) 4.7×10^{-3}
Read-out Rate (sec) 18

Interfaces

Electrical

Power (watts) 20

Mechanical

Size (cm) 25.4 x 30.5 x 50.8

Volume (cm³) 3.94×10^4

Mass (kg) 13.5

c. Television System (Mariner Mars '71 Imaging System)

Instrument Description - This instrument consists of wide-angle (WA) camera, a narrow-angle (NA) camera, and their associated electronics assemblies.

Experiment Objectives - The camera system will be used to observe cometary features such as the coma size, structure, luminosity, the nucleus size, shape, albedo, and perhaps rotation rate. At the asteroid, observations will be made of the size, shape, and surface morphology.

Performance Characteristics

	<u>WA Camera</u>	<u>NA Camera</u>
Focal Length	5 cm	50 cm
Focal Ratio	f/4.0	f/2.35
Shutter Speed (ms)	3 to 6144	3 to 6144

	<u>WA Camera</u>	<u>NA Camera</u>
Angular Field of View	$11^{\circ} \times 14^{\circ}$	$1.1^{\circ} \times 1.4^{\circ}$
Number of Vidicon		
Reseau Marks	111	111
Pixels/Line	832	832
Scan Lines/Frame	700	700
Bits/Pixel	9	9
Bits/Picture	5.25×10^6	5.25×10^6

Interfaces

Electrical

Power: Continuous (Cruise) 20 watts

Imaging Mode 41 watts total (NA active WA standby)

33 watts total (WA active, NA standby)

Telemetry:

Picture data - These data are stored in the tape recorder and are transmitted exclusively with the X-band down link. An A/D converter with 8-bit accuracy has been provided to handle the experiment engineering data. Maximum transmission rate = 16,384 bps.

Commands:

Power On-Off

Backup command

Capability has been provided to override automatically programmed operations in the camera system.

Mechanical

Mass (total system) 24.5 kg

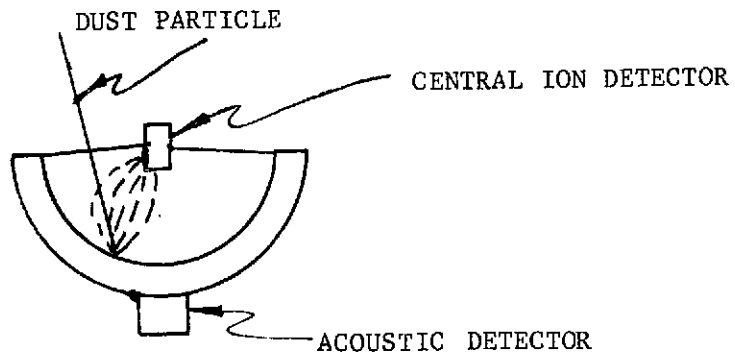
Dimensions (cm): WA camera: $22.9 \times 12.7 \times 10.2$

NA camera: $81.3 \times 25.4 \times 25.4$

Electronics: $15.25 \times 35.6 \times 16.67$

d. Cosmic Dust Analyzer (Grand Tour Proposal - S. Auer-Max Planck Inst.)

Instrument Description - This instrument consists of an acoustic momentum sensor and an impact-ionization analyzer. The impact-ionization analyzer, which is essentially a mass spectrometer capable of measuring the ionized plasma produced as a result of collision between the particle and sensor detection surface, is shown below.



Performance Characteristics - This instrument has not been flown. An instrument design of this type was proposed for Grand Tour. The data tabulated below are estimates only:

Mass Range	10^{-7} to 10^{-13} grams
Field of View	60°
Velocity Resolution	$\pm 10\%$
Mass Resolution	$\pm 30\%$

Interfaces

Electrical

Power 1 watt

Mechanical

Size (cm) 15.0 x 15.0 x 7.5

Mass (kg) 2.0

e. Triaxial Flux-gate Magnetometer (Apollo Particles-and-Fields Subsatellite)

Instrument Description - The experiment consists of a triaxial fluxgate sensor mounted on an extendable boom, approximately 5 meters long, and an internally mounted electronics package.

Performance Characteristics

Dynamic Range

Low Range ± 25 gamma

High Range ± 100 gamma

Sensitivity 0.1 gamma

Readout Accuracy ± 0.25 gamma

Interfaces

Electrical

Power 5.7 watts

Telemetry 24 bps

Mechanical

Size (cm)

Sensor 7.62 x 7.62 x 7.62

Electronics 15.25 x 15.25 x 5.0

Mass (kg) 2.8

f. Plasma Probe (Pioneer 9 - Modified)

Instrument Description - This experiment is an electrostatic analyzer using channeltron multipliers as the detection element.

Performance Characteristics

Energy Range: 5.0 eV to 70 keV

Dynamic Range: 3×10^5 counts/sec

Accuracy: 4% - 10%

Scan Time (each energy level) 5 sec.

Resolution: The energy range above will be resolved into 16 discrete energy bands.

Interfaces

Electrical

Power 5.0 watts

Telemetry (56 bps)

Mechanical

Size (cm) 15.0 x 17.5 x 20.0

Mass (kg) 5.0

g. Plasma Wave Detector (OGO-E)

Instrument Description - This instrument is composed of an extendable boom to which are attached multiple dipole antennas mounted normal to the boom's longitudinal axis, and a triaxial inductor-search-coil system. The dipole-antenna configuration is used to measure VLF electric field oscillations over a frequency range of 10 Hz to 200 kHz. Magnetic field oscillations will be examined over a frequency range of 560 Hz to 70 kHz. A boom-mounted pre-amplifier unit and an internally mounted electronics unit complete the experiment.

Performance Characteristics

Spatial Response

E field 10 Hz - 200 kHz

B field 560 Hz - 70 kHz

Measurement Range

Delta E: 1 μ V/m to 20 mV/m

Delta B: 1 milligamma to 1 gamma

Sensitivity

E field < 1 μ V

B field < 1 milligamma

Interfaces

Electrical

Power 5 watts

Telemetry 56 bps

Mechanical

Size:

Antenna:

Boom: 150 cm long

Dipole: (extended) 30 cm

Coil System Diameter: 30 cm

Preamplifier Unit (cm):

12.7 x 5.0 x 5.0

Electronics (cm):

10.0 x 19.0 x 21.5

Mass (kg): 5.5

h. Neutral Mass Spectrometer (OGO-F)

Instrument Description - This instrument is a quadrupole neutral-particle spectrometer. The sensor system is composed of a knife-edged aperture, an enclosed thermionic ion source, a mass filter, and a photomultiplier collector. Two operational modes are provided in this experiment: a sweeping mode and a stepped mode. In the stepped mode, mass scans at discrete levels may be made over long intervals. In the sweeping mode, sequential scans are made of the mass ranges tabulated below:

1.1 to 2.0 AMU

2.2 to 4.0 AMU

4.0 to 9.0 AMU

9.0 to 16.0 AMU

16.0 to 28.0 AMU

18.0 to 32.0 AMU

25.0 to 45.0 AMU

In the sweeping mode, one operational cycle is completed every 20 seconds.

Performance Characteristics

Mass Range 1.0 - 45.0 AMU

Accuracy $\pm 4\%$

Interfaces

Electrical

Power 12 watts

Telemetry (320 bps)

Mechanical

Dimensions (cm) 17.0 x 20.65 x 32.7

Mass (kg) 5.5

i. Ion Mass Spectrometer (OGO-F)

Instrument Description - This instrument is a three-stage Bennett spectrometer. The spectrometer consists of a 4.8 cm (1.9-inch) diameter tube with 16 parallel plane grids mounted normal to the tube axis. This configuration provides three acceleration stages, allowing measurement of ion mass from 1 AMU through 45 AMU.

Performance Characteristics

Mass Ranges

Low Mass 1.0 to 6.0 AMU

High Mass 7.0 to 45 AMU

Response Range 10 to 10^6 ions/cm³

Interfaces

Electrical

Power 4.5 watts

Telemetry 320 bps

Mechanical

Dimensions (cm) 20.3 x 17.5 x 16.0

Mass (kg) 2.6

j. UV Spectrometer (Mariner Venus Mercury '73)

Instrument Description - The instrument consists of a telescope, a scanning Ebert grating, a single photomultiplier detector, and associated electronics.

Experiment Objectives - The instrument shall be used to measure constituents of the cometary atmosphere, Rayleigh scattering and reflected UV

radiation from the nucleus, and absorption lines in the spectral region from 1100 Å to 3400 Å.

Performance Characteristics

Spectral Range

First Order 1900 Å - 3400 Å

Second Order 1100 Å - 1700 Å

Resolution

Second Order 10 Å

Field of View 0.25° x 2.5°

Focal Length 12.5 cm

Focal Ratio f/5

Scan Period 2 seconds

Interfaces

Electrical

Power 2.5 watts

Telemetry

Science Data (320 bps)

Commands

Power-On/Off

Instrument Calibration

Mechanical

Dimensions (cm) 11.4 x 20.3 x 30.5

Weight (kg) 3.6

k. Biaxial Langmuir Probe (OGO-F, Mariner Venus Mercury '73)

Instrument Description - The proposed instrument is based on the configuration previously flown on the OGO-F spacecraft and proposed for Mariner Venus-Mercury 1973. The principal investigators are A.F. Nagy (University of Michigan) and L. H. Brace NASA/GSFC. The instrument consists of two probes positioned perpendicular to one another, and an electronics assembly.

Performance Characteristics

Dynamic Range

N_e 0 to $2 \times 10^5/\text{cm}^3$

T_e 0 to 1.7×10^3 °K

Interfaces

Power 2.5 watts

Mass 1.6 kg

Dimensions (cm)

Electronics pkg: 13.0 x 20.0 x 9.5

Sensor: Probe Length 44.5

Probe Diameter .05

Commands:

Power Switching On-Off

Telemetry:

Data 3-8 bit words

2. Imaging and Non-Imaging Timelines - Comet

Detailed scientific timelines for a comet mission could only be developed after investigator selection, instrument design, and some mission analysis specifications. However, in order to study the feasibility and subsystems requirements of several spinning-spacecraft configurations, it was necessary to formulate a timeline that could be scientifically meaningful. Table V-45 shows a timeline with minimum imaging that is consistent with the scientific goals discussed earlier.

Imaging - The rationale behind the measurement sequences shown in Table V-45 are stated briefly. The numbers chosen are believed representative for a minimal scientific investigation consistent with goals staged below and in Section II. The key goals of the imaging science are to detect the nucleus and, if possible, to obtain spin-rate, anisotropic emission, etc. The nucleus search starts when a 10-km nucleus could just be resolved by the narrow angle camera. At 30 minutes before encounter (E-30 minutes), a 1-km nucleus would have an apparent size equivalent to one pixel. At E-15 minutes, a 1-km object should be resolved with 3-pixel resolution. In the last 15 minutes before

encounter, even a 0.5-km object would have 3-line-pair resolution. The nucleus could be resolved at 5000 km with a maximum resolution of 137 meters/pixel.

Because of uncertainties in the nucleus location and the desire to observe from close to the nucleus as possible, a wide-and narrow-angle camera sequence is shown in Table V-45 for the last two hours before encounter, or approximately that time during which the nucleus has a chance of being resolved by the imaging system.

Coma science is indicated as beginning at E-1 day, which is about when the coma fills the field of view of the narrow-angle camera. At E-6 hours, the wide-angle camera has 100-km resolution and thus can perform good structure-imaging. If the nucleus is not located, or is unresolved, the coma science phase showing the intermediate structure of the coma will be very important. Such information with both wide- and narrow-angle cameras should provide good spatial resolutions of the coma.

For as long as 10 days before encounter, the total comet can be studied with the narrow angle camera with about a 100-x-100-pixel field of view. The comet image will be large enough to show structural details. As the resolution increases to several hundred meters at E-6 days, good-resolution observations of the comet's coma and tail can be made. Tail structure morphology may be studied best during this E-10 to E-6 day period. At E-6 days, the first presence of a deceleration region may be encountered. The shock probably would not be visible directly, but a higher imaging rate is shown when nearing the comet, where some transition region phenomena might be visible.

A final portion of the timeline is concerned with comet detection. It is desired to see the comet as soon as possible for approach navigation and pointing orientation. At about 20 days before encounter, the total comet brightness should be that of a +7-magnitude star and, thus, visible to a vidicon TV system. At these distances, however, the purpose of observations from the spacecraft is to orient the spacecraft and imaging system, because ground-based telescopes will be able to do better imaging.

Other Optics Sequences

UV - The UV sequences are divided into phases similar to those for the TV: far, near, and closest modes. At times near E-10 days, it is desired to look for large halos of hydrogen, atomic oxygen, and OH around the comet. An objective could be to reconstruct an image or draw isophotes of these halos around the comet; therefore, a number of scan directions surrounding the comet will be needed. With instrument sensitivities of about one rayleigh, the number and location of scans shown are thought to be representative. The same neutral halo sequence is shown repeated for closer distances. (See table V-46).

In the near encounter phase at E-6 days, the emphasis probably would shift from imaging to spectral scans for radial gradient information of the UV excited gas species. In this phase, higher spatial resolution would be obtained than that obtainable from ground-based or rocket investigations.

At closest approach, E-2 days and inward, the UV spectrometer would look at the nucleus concurrently with the TV. Clues to photodissociation and energy processes of molecules and radicals from the nucleus would be sought from their respective energy transitions in the UV spectral region.

Finally, in the tail, it would be of value to scan both parallel and perpendicular to the tail and for additional gradient information on UV species. Again, a synchronization with the TV system would be appropriate.

IR - The IR spectrometer sequence would be similar to the UV spectrometer sequence, except for deletion of the far-encounter mode. Energy transitions of certain molecules in the IR region of the spectrum would be investigated near the nucleus (see table V-47).

Attempts would be made to scan the nucleus during the last 2 hours of the mission. In the tail, spectral scans in selected wavelengths could be made to study dust- and gas-absorption mechanisms.

Non-Imaging Science - The remaining instruments are either turned on or increased in sampling rate near the position where a deceleration region is expected for the comet. This distance is not precisely known, but it could be as far as 10^7 km from the nucleus, or 6.25 days from encounter. It is more likely that this deceleration region is only 10^6 km, or less than one day from

TABLE V-45 MINIMUM IMAGING TIMELINE FOR ENCKE

	PHASE	MAJOR OBJECTIVES	FRAMES OR SCANS		TOTAL FRAMES	
			WA	NA	WA	NA
I.	TARGET DETECTION					
	At E-20 days to E-10 days	Search for Encke	4/day	4/day	40	40
		Look for Encke for S/C Orientation and Guidance		2/day	40	60
II.	COMET IMAGING					
	E-10 to E-6 days	Total Comet Morphology & Tail	--	1/4 hrs	40	84
	E-6 to E-10 days	Coma Imaging		1/2 hrs	40	144
III.	COMA SCIENCE					
	E-1 day to E-6 hrs.	Detail Comet Structure	2/hr.	4/hr.	76	216
	E-6 hrs. to E-2 hrs.	Detail Coma Structure	4/hr.	4/hr.	92	232
IV.	NUCLEUS SEARCH					
	E-2 hr. to E-30 min.	Nucleus Resolvable	1/10 min.	1/10 min.	111	241
	E-30 min. to E-15 min.	Nucleus Acquisition	1/min.	1/5 min.	126	244
	E-15 min. to RCA	Nucleus Imaging	1/3 min.	1/3 min.	131	249
V.	TAIL SWEEPS					
	E+15 min.	Photometric Studies	6	6	6	6
	E+30 min.	Down & Angle to Tail Vector	6	6	6	6
	E+2 hr.	Tail Structure Studies	6	6	6	6
	E+4 hr.					
	E+6 hr.					

TABLE V-46 MINIMUM UV TIMELINE FOR ENGKE

	PHASE	MAJOR OBJECTIVES	FRAMES OR SCANS
I.	FAR ENCOUNTER	IMAGE HALOS OF L α , ATOMIC OXYGEN AND OH AROUND COMA	
	E-10d		12 scans of each of 3 lines
	E-8d		12 scans of each of 3 lines
	E-4d		12 scans of each of 3 lines
II.	NEAR ENCOUNTER	SPECTRAL SCANS FOR RADIAL DISTRIBUTION OF GAS SPECIES	
	E-6d		12 scans of each of 3 lines, 2 directions each
	E-4d		12 scans of each of 3 lines, 2 directions each
	E-2d		12 scans of each of 3 lines, 2 directions each
III.	CLOSEST APPROACH	DETAIL COMA SPECTRAL IDENTIFY AND ABUNDANCE MEASUREMENTS	
	E-2 to E-0		Any 4th TV Frame

TABLE V-47

MINIMUM IR TIMELINE FOR ENCKE

<u>PHASE</u>	<u>MAJOR OBJECTIVE</u>	<u>FRAMES OR SCANS</u>
I. <u>NEAR ENCOUNTER</u>		
E-6 d	{ SCAN FOR GAS SPECIES AND SPACIAL DISTRIBUTIONS	12 scans of 6 bands
E-4 d		12 scans of 6 bands
E-2 d		12 scans of 6 bands
II. <u>CLOSEST APPROACH</u>		
E-2h to E-15 m	COMLEX MOLECULE IDENTIFICATION	1 scan every 10 min.
E-15 m to RCA	IR SCANS OF NUCLEUS FOR TEMP & SURFACE DATA	5 scans every 3 min.
III. <u>POST RCA</u>		
E+0 to E+2 hr	SCANS FOR PARTICULATE MATTER	1 scan every 5 min, 2 directions each

TABLE V-48 MINIMUM IMAGING TIMELINE FOR ASTEROIDS

<u>PHASE</u>	<u>MAJOR OBJECTIVE</u>	<u>FIGURES OR SCANS</u>
I. <u>TARGET ACQUISITION</u>		
E-4 d to E-6 h	{ Search for Visibility of Asteroids Tracking and Spacecraft Orientation	1 / 4 h
II. <u>NEAR ENCOUNTER</u>		
E-6 to E-1 h	Photometric Studies	1 / 30 m
III. <u>CLOSE ENCOUNTER</u>		
E-1 h to E-10 m	Resolve Asteroid	1 / 5 m
E-10 to E-0 m	Highest Resolution Imaging	1 / 3 m
IV. <u>POST RCA</u>		
E+0 to E+15 m	Particulate Matter Search	1 / 5 m, at angles to the Radius vector

V-145

encounter, but it would be a great disappointment to miss its detection due to inactive instruments. Therefore, particles-and-fields instruments are increased in sampling rate at E-6 days. If data rates permit, the mass spectrometers can also be activated at this time; however, their main use is for coma science which is predominantly at ± 2 hours around RCA.

These science timelines are used to determine the sequence of events with respect to power levels, pointing, communications loads, and other spacecraft subsystem requirements.

3. Imaging and Non-Imaging Requirements - Asteroids

In contrast to the many observables and energy processes of the comet, the asteroid timeline is aimed primarily at high-resolution TV and IR viewing. Additional instruments will be turned on in a search mode, (i.e., magnetometer, Langmuir probe, UV spectrometer, and particulate detector) during the two-hour period centered at encounter.

Imaging - The timeline in Table V-48 shows the minimal number of images required for acquisition, near encounter, and close encounter. While Toro is slightly larger than Geographos, it is approached from a less favorable phase angle. The result is that the visibility of both asteroids is similar for the purpose of analyzing imaging timelines. Acquisition of the asteroids can occur at ~ 5 days before encounter as ~ 7 magnitude stars. Once acquired, 4 frames a day will aid tracking and asteroid pointing.

Science imaging starts primarily at that position where the asteroid could be resolved by the narrow angle camera, (i.e., 6 hours before encounter for Toro). The prime imaging goal consists not only of detecting (as was the case of the comet), but doing high-resolution imaging. At ~ 1 hour before encounter, the resolution with which the asteroid can be imaged is 1000 meters, and surface morphological imaging can therefore begin. As stated earlier, image goals include observations of, for instance, crater counts, surface stratifications, and regolith material. In the last 10 minutes before encounter, the resolution is tens of meters, so that excellent surface details should be visible.

IR - The IR spectrometer for the asteroid mission will be most useful at relatively close distances, assuming no cooling of the detectors. The time-

line (table V-49) shows three possible phases of IR investigation. First, is the overall IR Bond albedo measurements from 1 day before encounter to 6 hours before encounter. At that time, until about 2 hours before encounter, more detailed reflectance and blockbody temperature scans are attempted. Finally, a limited number of selected molecular absorption bands in the near-IR will be scanned for possible surface-composition information.

While visual imaging is restricted by a dark asteroid during the post-encounter, the IR spectrometer can work effectively. It is suggested that all but the distant albedo measurements be repeated on departure.

There are no a priori reasons to expect particulate matter, magnetic fields, or gas near the asteroids; however, exploration of these phenomena is exciting and is of potentially high value. Therefore, the magnetometer, the Langmuir probe, the UV spectrometer, and the particulate detector will take measurements for 2 hours near asteroid closest approach.

The science timelines are used to determine the sequences of events with respect to power levels, pointing, communication loads, and other spacecraft subsystem requirements.

4. Imaging Graphs

In compiling the comet and asteroid timelines, a number of graphs were constructed. These were based on the Mariner-Mars-1971 wide- and narrow-angle TV-camera systems discussed earlier. The graphs are helpful in understanding encounter geometry, lighting, field-of-view, etc. They could also be used in further timeline refinements.

TABLE V-49 MINIMUM IR TIMELINE FOR ASTEROIDS

<u>PHASE</u>	<u>MAJOR OBJECTIVES</u>	<u>FRAMES OR SCANS</u>
I. <u>FAR ENCOUNTER</u> E-2 d to E-6 h	Bond Albedo Radiometry	1 / 30 m
II. <u>NEAR ENCOUNTER</u> E-6 to E-2 h	Surface Scattering and Radiometry	1 / 15 m
III. <u>CLOSE ENCOUNTER</u> E-2 h to E-0	Surface Composition Spectroscopy	1 / 5 m
IV. <u>POST RCA</u> E+0 to E+30 m E+30 to E+2 h	Surface Spectroscopy Surface Radiometry	1 / 10 m 1 / 30 m

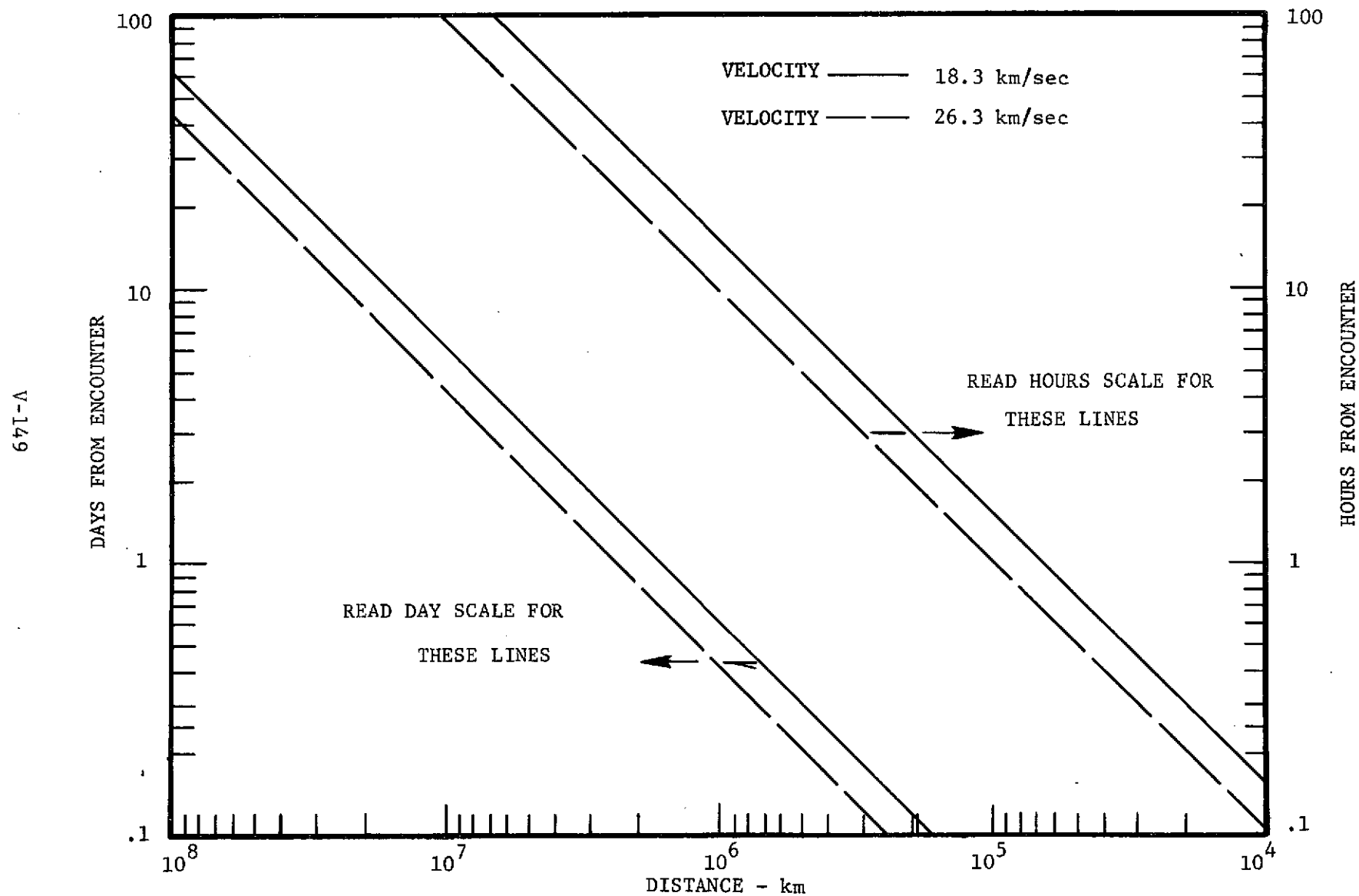


FIGURE V- 39 TRAJECTORY DISTANCE VS. TIME TO COMET RCA

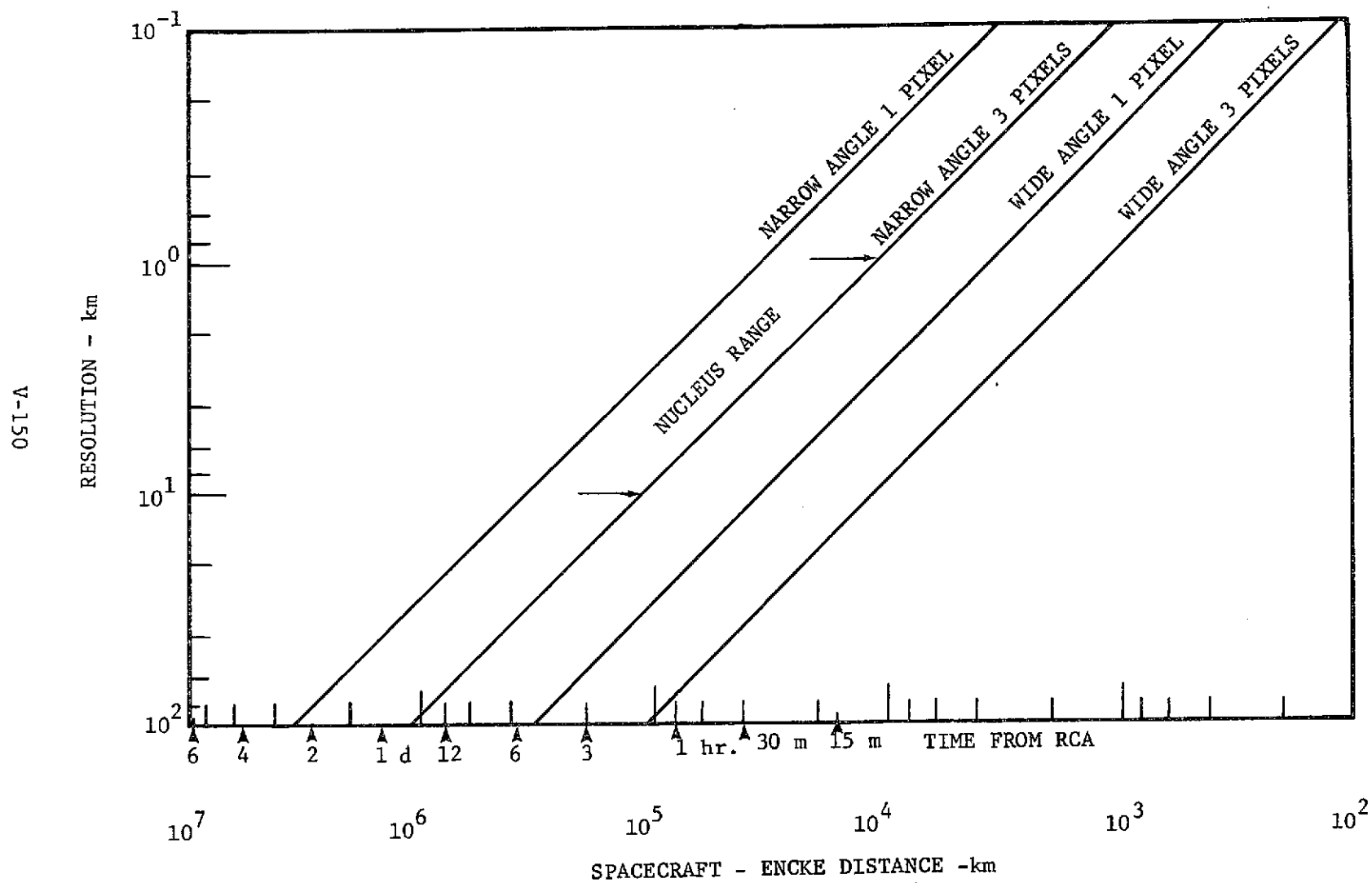


FIGURE V-40 RESOLUTION VS DISTANCE (TIME) FROM ENCKE

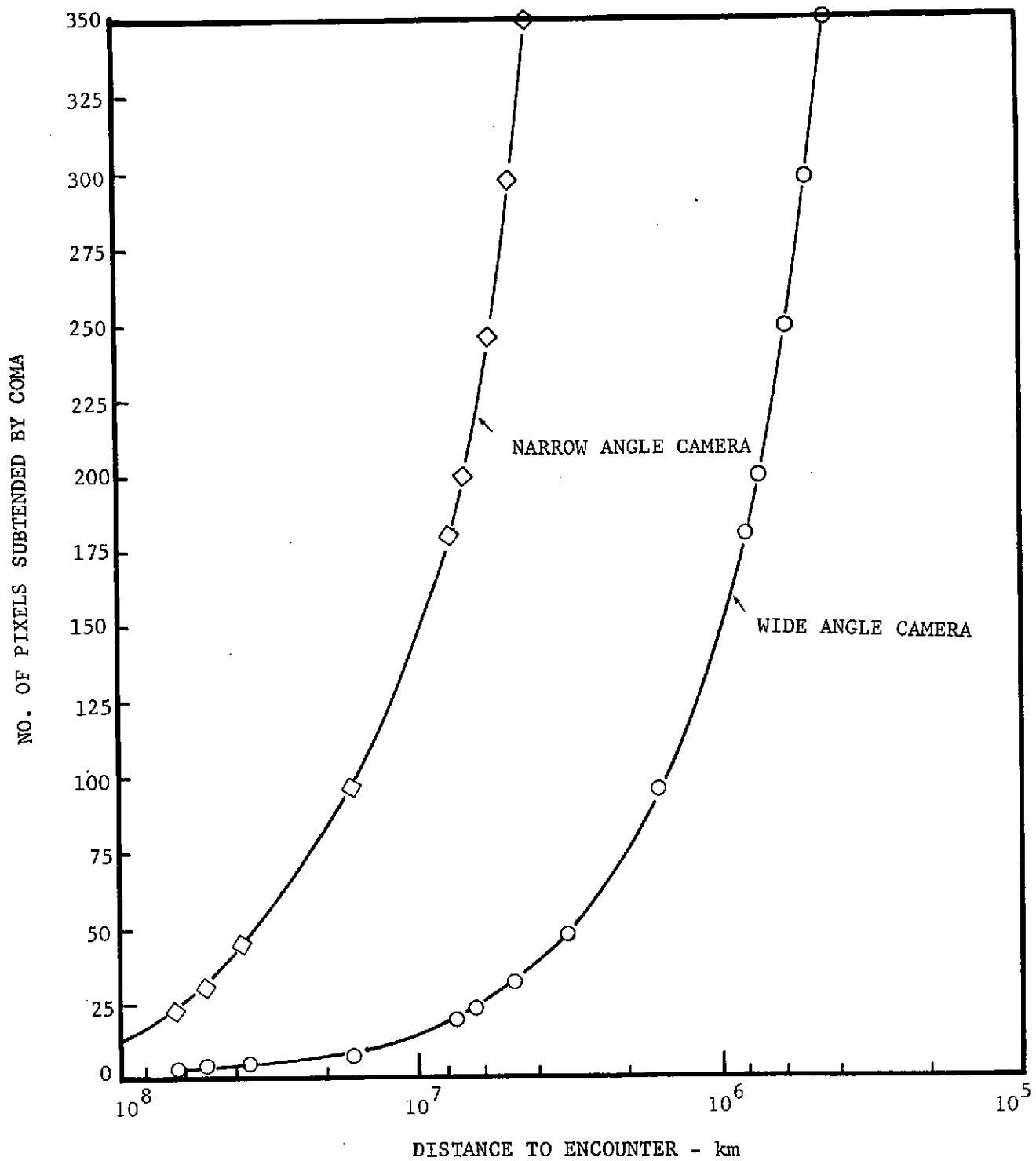


FIGURE V-41 NUMBER OF PIXELS FOR COMA OF ENCKE VS. DISTANCE

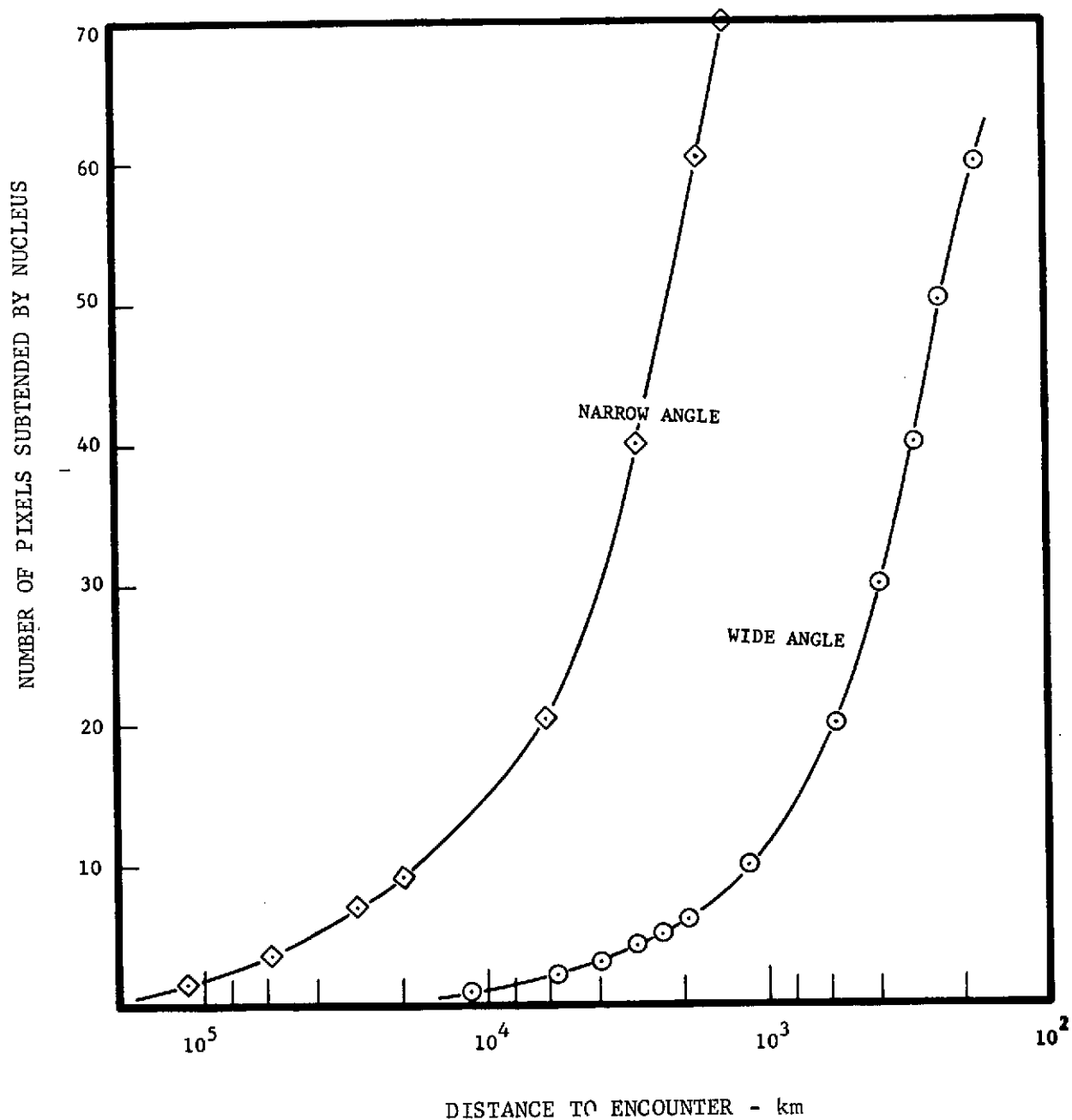


FIGURE V-42 NUMBER OF PIXELS FOR NUCLEUS OF ENCKE VS. DISTANCE

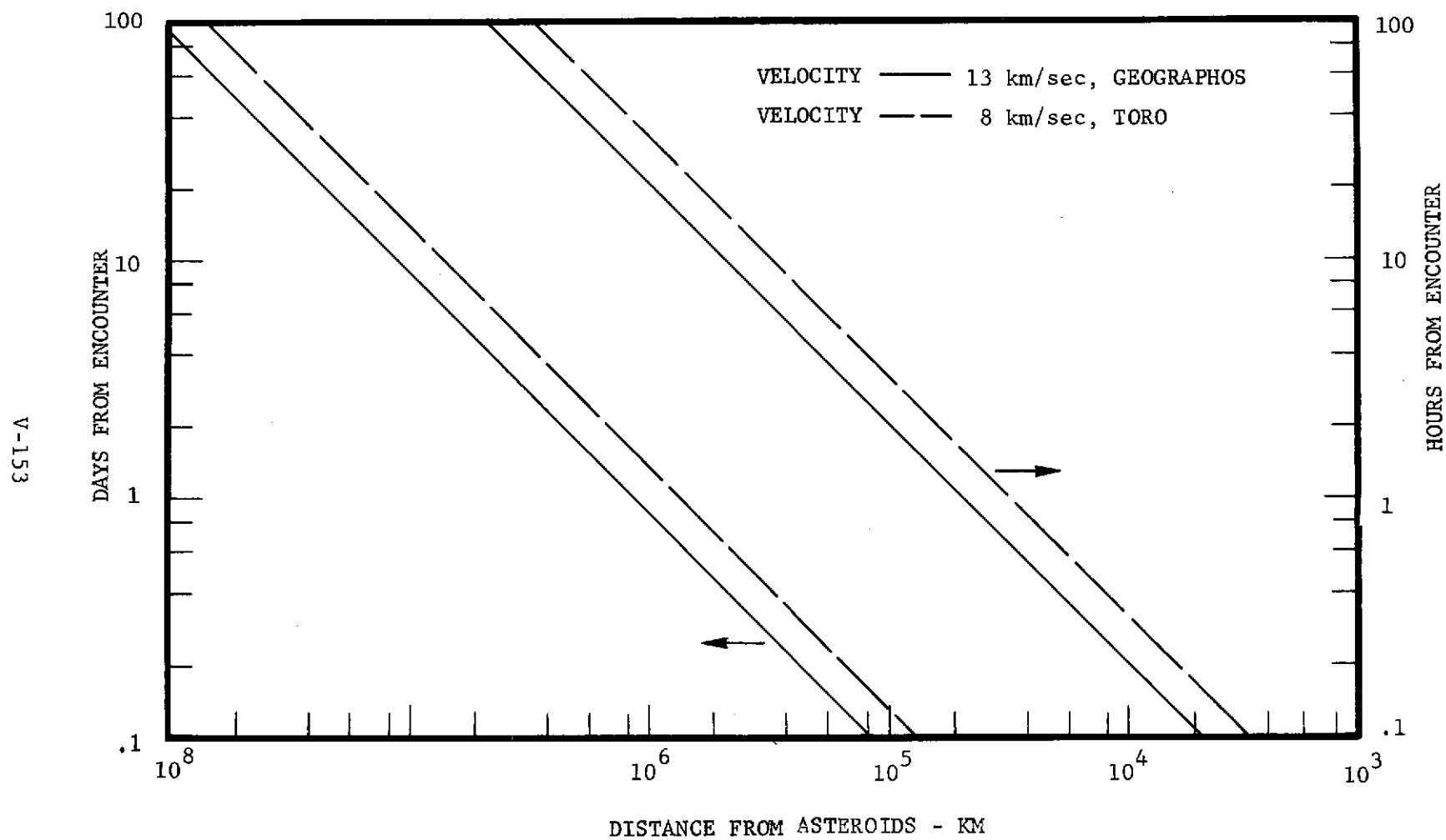


FIGURE V-43 DISTANCE VS. TIME TO ENCOUNTER FOR ASTEROIDS

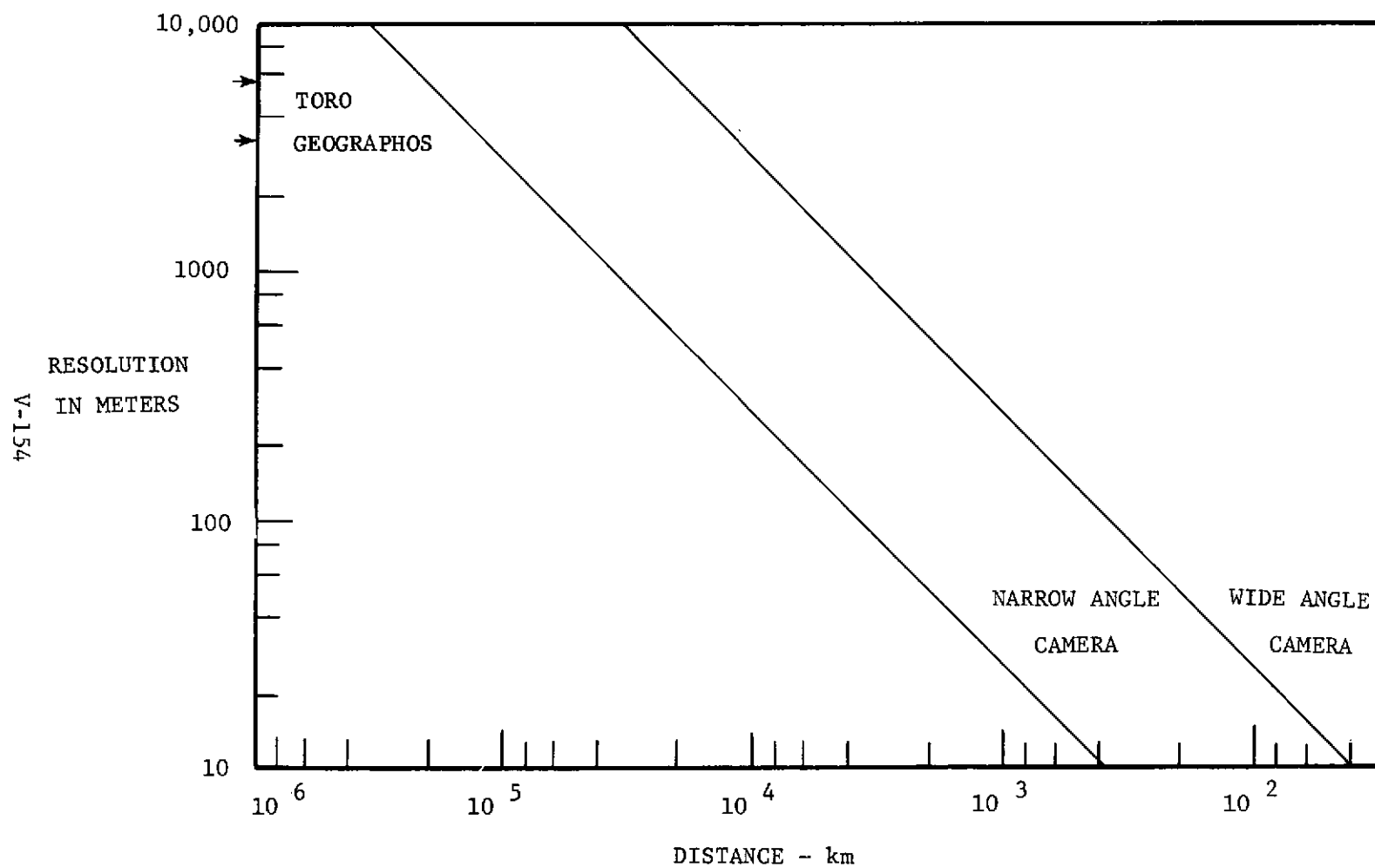


FIGURE V-44 RESOLUTION VS DISTANCE FOR GEOGRAPHOS AND TORO

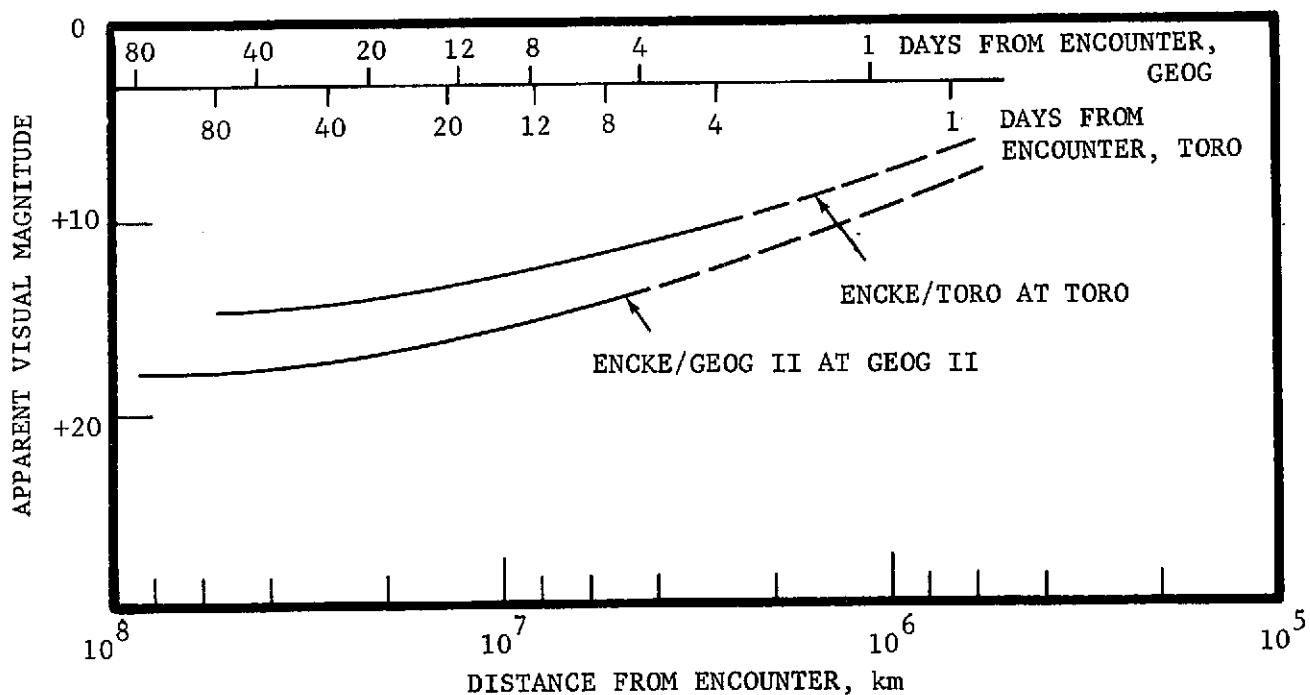
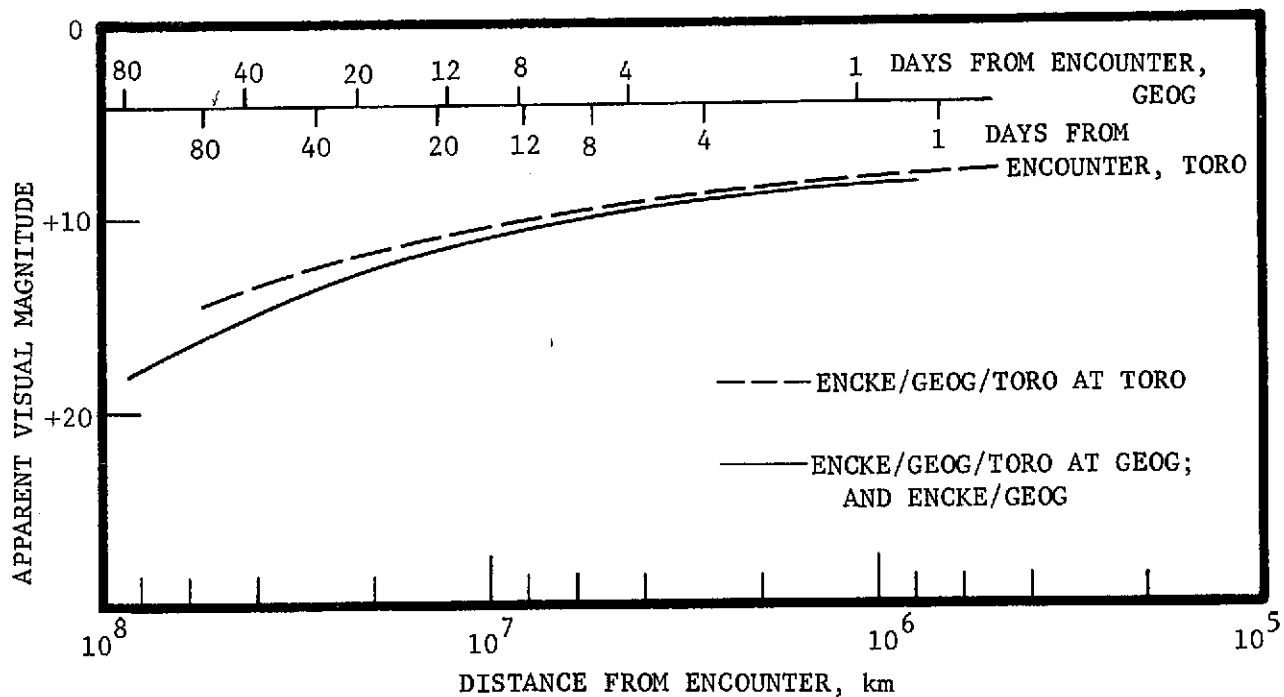


FIGURE V-45 VISUAL MAGNITUDE VS. TIME (DISTANCE) OF GEOGRAPHOS AND TORO

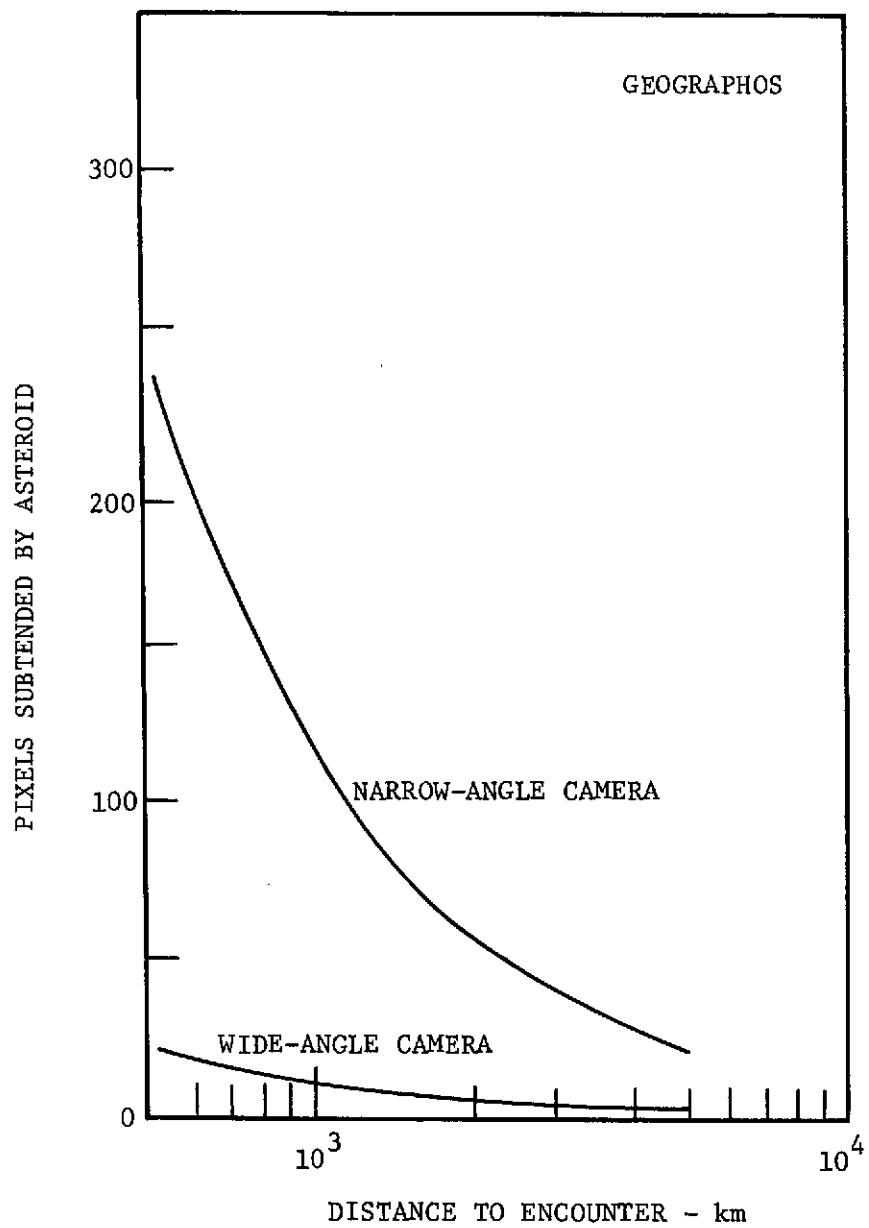


FIGURE V-46 NUMBER OF PIXELS vs DISTANCE FOR GEOGRAPHOS

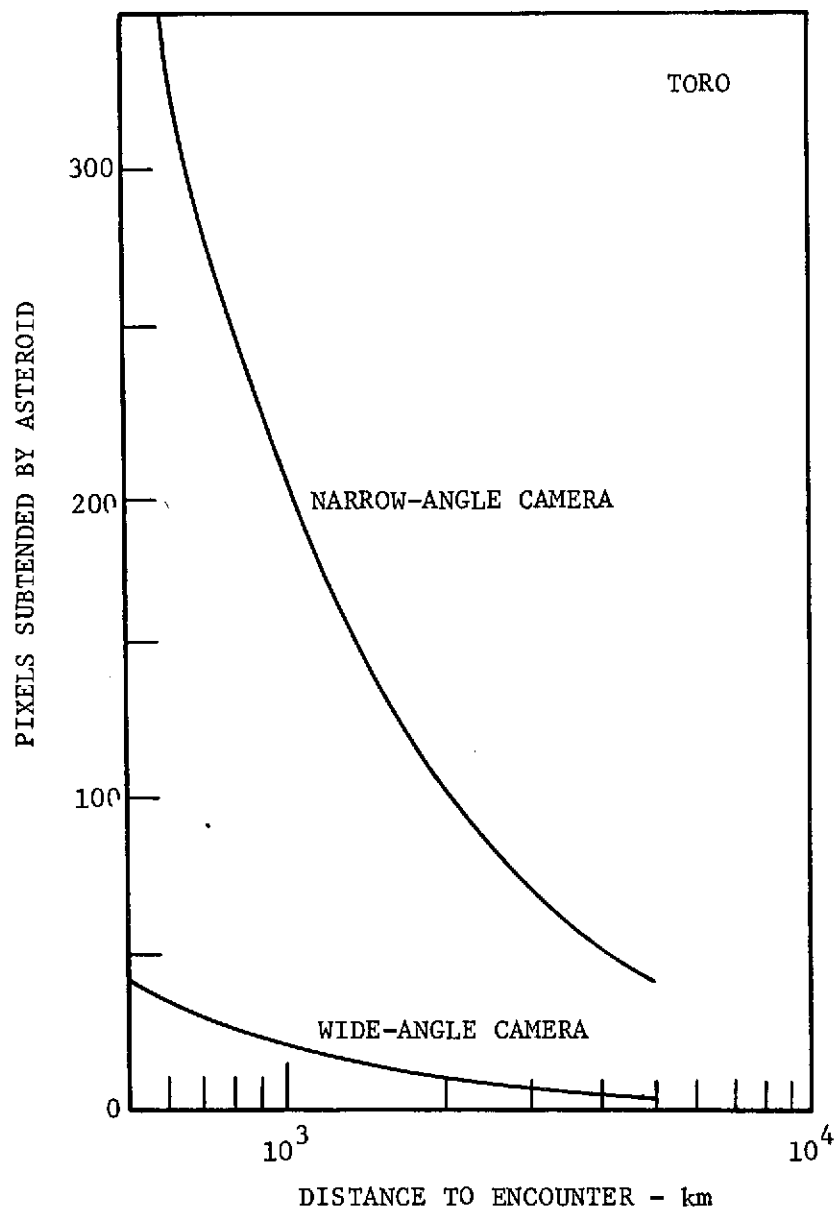


FIGURE V-47 NUMBER OF PIXELS vs DISTANCE FOR TORO

5. Target Visibility from Imaging-Radiometry Study

In imaging a comet or asteroid, it is necessary to apply the photometric equations previously developed to determine when the imaging systems will be sufficiently illuminated to detect the target. In Table V-50, radiometric comparisons are shown between the vidicon and two spin-scan systems. One is a solid state and the other is a miniaturized, photomultiplier (PM) system. Additional details covering the assumptions of signal-to-noise ratio, dark current, etc. can be found following this summary in Table V-50.

The nucleus is bright enough to be seen (i.e., "detected," but not resolved), by the vidicon system with long (i.e., 5-6 sec) exposures as far as 10 days from encounter. A solid state detector system cannot detect the nucleus until several hours before encounter, due to reduced light levels. The PM system could detect the nucleus at E-2.7 days. This will be discussed later.

The coma could be detected with the vidicon 40 days before encounter. The solid state system could not detect the coma until 18 days if all detectors are used, or only 3.2 days before encounter if a single detector is used. The PM system could see the coma at E-23 days.

Once the comet coma is resolved, the problem is no longer the distance at which the comet can be seen; rather, it is how far from the nucleus (radius) can the camera system take images before it must stop because it can no longer see the faint outer coma. Figure V-51 shows these coma visibility radii as a function of spacecraft-to-Encke distance for the camera systems considered. The impact on science return due to imaging instrument choice can be stated simply. With the solid state system analyzed here, all nucleus imaging science would be lost and good resolution of the coma would be possible starting only 3.2 days from encounter as shown in Table V-50.

It is then concluded from this brief radiometry study that the vidicon cameras have greater use and potential success than do present solid state detectors on a comet/asteroid mission. The spin-scan systems have comparable resolution, but will require acquisition sensors prior to their use at a comet. Unless the entire image is acquired on a single revolution, for spin-scan systems, the pointing and underlap are serious near the nucleus, where maximum resolution is desired. If the image is acquired on a single revolution by

TABLE V-50 COMET THRESHOLD POSITION OF VISIBILITY FROM IMAGING-RADIOMETRY STUDY

	COMET		NUCLEUS	
	DISTANCE FROM ENCOUNTER	TIME BEFORE ENCOUNTER	DISTANCE FROM ENCOUNTER	TIME BEFORE ENCOUNTER
	(km)	(days)	(km)	(days)
TV VIDICON	8.7×10^7	40	1.6×10^7	10
MINIATURIZED PM SYSTEM (10, OR FEWER, DETECTORS)	4×10^7	23	4×10^6	2.7
SOLID STATE	3.2×10^7	18*	4×10^5	0.25
	4.7×10^6	3.2 \diamond		

* Adding all detector elements

 \diamond Per detector element

large detector arrays, the light threshold for the outer coma is low and may preclude operation until the spin-scan system is within a few hours of RCA.

The miniaturized PM system was not studied in as much detail as the solid state of vidicon system. From Table V-50, it is seen that the PM system can detect the nucleus 2.7 days before encounter. A detailed design study for comparison of frame vs. spin-scan cameras (both PM and solid state) specifically for the comet, and comet/asteroid missions, is recommended. Photo transistors, photo diodes, and charged couple devices (CCDs) should be included within the solid state detector options. Solid state detectors for the spin-scan concept should also be investigated for ultraviolet and infrared sensing systems.

Further explanation of Table V-50 is given below. It addresses the radiometry for acquisition of Comet Encke. The unresolved comet and the resolved comet will be considered. The unresolved comet is treated as a collimated source (a star), the resolved comet is treated as an extended source. The radiometry involved with collimated sources is different than that for extended sources. For a collimated source, to increase the signal it is necessary to increase the aperture of the optical system. For an extended source, the important parameter is the focal ratio (f/#) of the optical system. Considering the comet as an unresolved point source, the photo-electron signal strength (H), at the detector is:

$$(1) \quad H = N_c A_o \eta_o \eta_e \text{ p.e./sec}$$

where A_o is the unobscured area of the optics = 314 cm^2
 η_o is the optical efficiency = 0.5
 η_e is the quantum efficiency of the detector p.e./photon = 0.2
 N_c is $10^{(6-M_c/2.5)}$ photons/cm²/sec.

The empirical analytic expression for the comet magnitude, M_c , is:

$$(2) \quad M_c = 10.93 + 5 \log \Delta + 3.55 (R^{1.8} - 1)$$

where Δ is the spacecraft - comet distance - AU and

R is the comet - Sun distance - AU

M_c is plotted versus Δ in Figure II-1, (page II-6). Figure V-48 shows the dependence of H on .

For the resolved/extended source, the illumination E at the focal plane (p.e/cm²/sec) can be expressed by:

$$(3) \quad E = \frac{\pi}{4} \frac{B_c}{(f/\#)^2} \eta_o \eta_e$$

where $f/\#$ is the focal ratio of the optical system $\frac{f.l.}{D}$, where $f.l.$ is the focal length and D is the diameter of the aperture.

B_c is comet brightness, where data for B_c was obtained from Table 12 of Reference V-2. In that reference, the slope of the distribution of brightness is seen to be of the form: $B_c = \frac{K}{r}$ where r is the radial distance from the comet nucleus and K is a constant.

We can now normalize this expression $B_c = \frac{K}{r}$. This will be accomplished by equating the irradiance from the extended comet source to the irradiance expected from the comet as a point source at the same comet spacecraft distance.

The expression for the extended source irradiance at the spacecraft is:

$$N'_c = \frac{\bar{B}}{\Delta^2} \pi r_c^2$$

where \bar{B} is defined as the mean brightness, and r_c is the comet radius.

\bar{B} and K are related since:

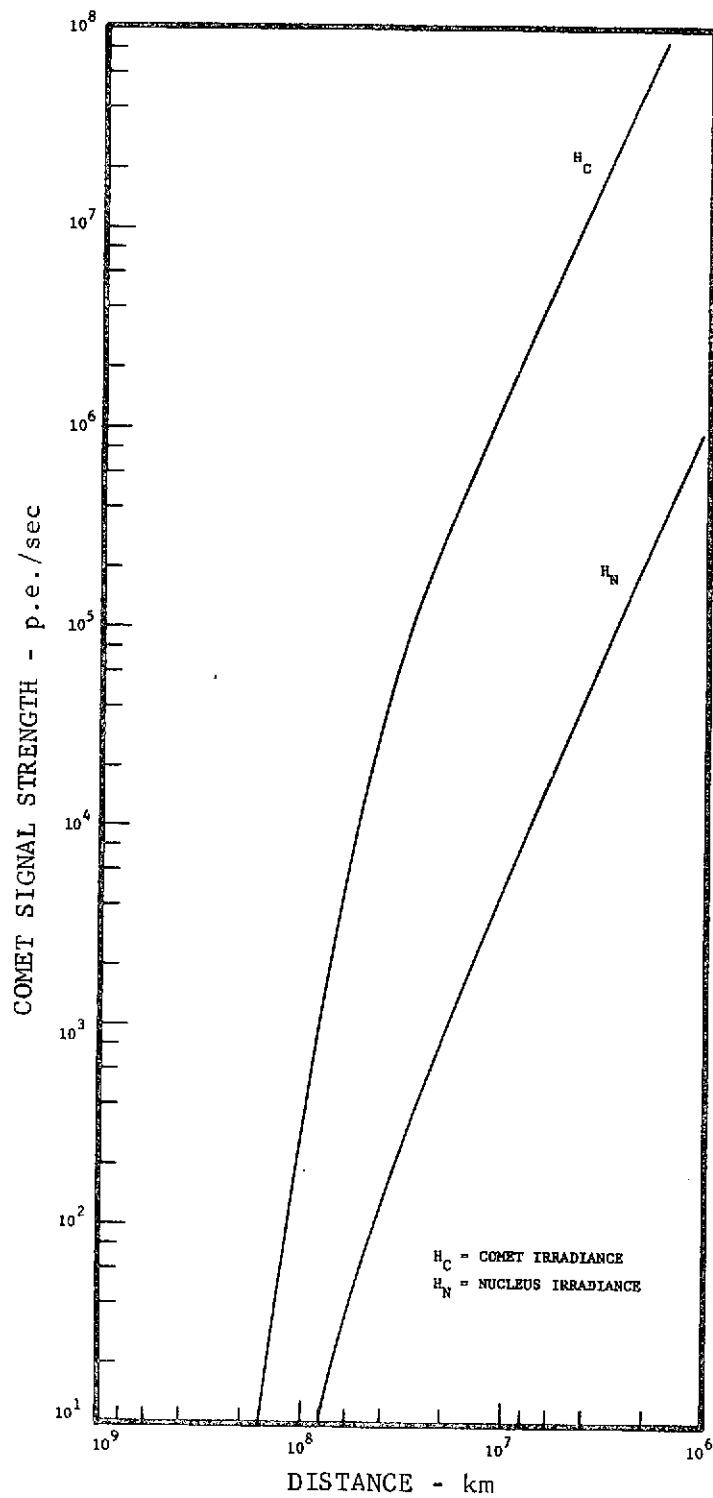


FIGURE V-48 COMET IRRADIANCE VS. SPACECRAFT-TO-ENCKE DISTANCE

$$\pi r^2 \bar{B} = \int_0^{a_0} B dA = 2 \int_0^{r_c} K dr$$

so $K = \frac{r\bar{B}}{2}$, \bar{B} = mean brightness. a_0 is the cross section area of the comet km.

The expression for the irradiance for a point source is:

$$N_c = 10^{(6-M_c/2.5)} \text{ photons/cm}^2/\text{sec.}$$

Equating $N'_c = N_c$, one can solve for \bar{B} , and therefore for K .

With a solution for K , the slope of the curve and ordinate values can be plotted as in Figure V-49. (Only the slope of the curve is from Reference V-2.

In Figure V-49, the brightness of the coma is plotted versus distance from the center of the comet. The brightness is for a distance, $\Delta = 1.8 \times 10^6$ km, where Δ is the distance from the comet to the spacecraft. To obtain the brightness of the comet at any point, and for any distance, Δ , the curve in Figure V-50 can be used. It expresses the ratio of brightness at a distance, Δ , to the brightness at distance, $\Delta = 1.8 \times 10^6$ km. This method gives a true distribution of the brightness for various Δ 's and for various distances, r , from the nucleus. Using this modified B_c , equation (3) can be used to obtain the power per detector:

$$(4) \quad P = E A_d \text{ p.e./sec}$$

where A_d is the detector area (cm^2) and E is the focal plane illumination using the modified B_c and equation (3).

In using this formula, it should be remembered that different parts of the focal plane will have different illumination since the brightness of the coma surface will vary according to $B_c = \frac{K}{r}$.

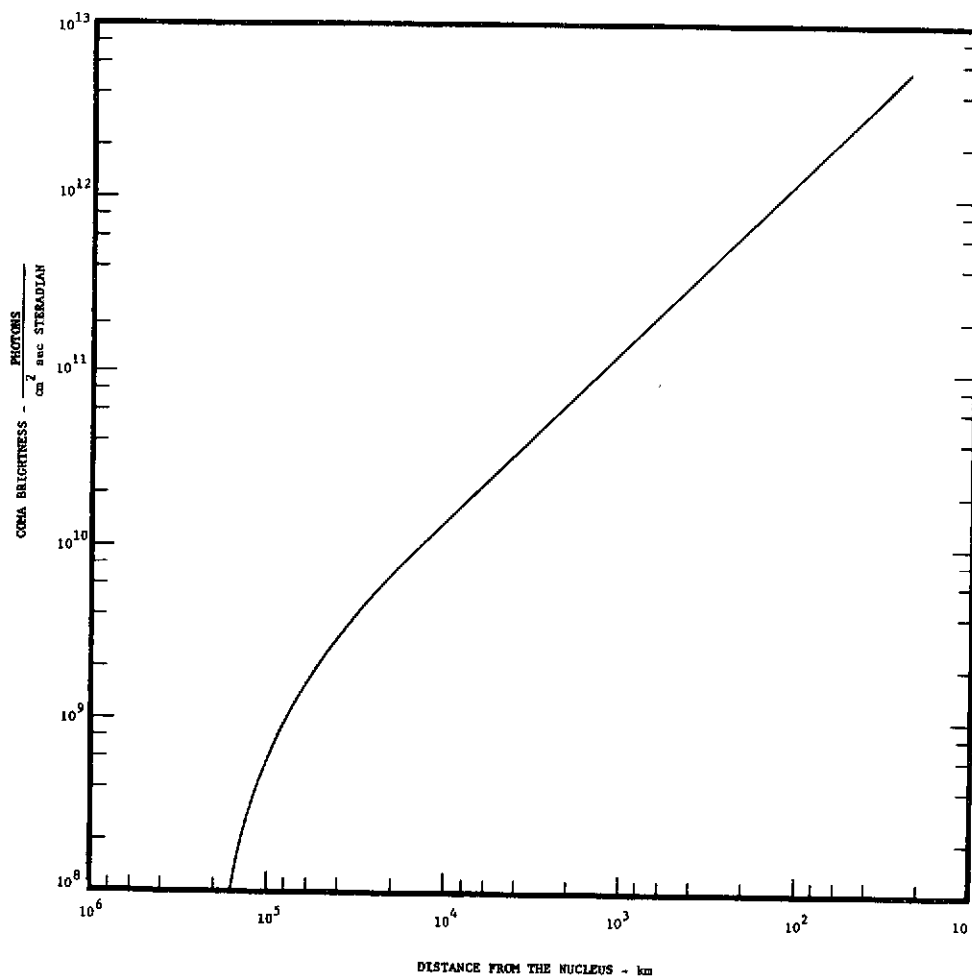


FIGURE V-49 BRIGHTNESS DISTRIBUTION OF COMA VS. DISTANCE FROM THE NUCLEUS
(FOR A SPACECRAFT/ENCKE DISTANCE, Δ , OF 1.8×10^6 km)

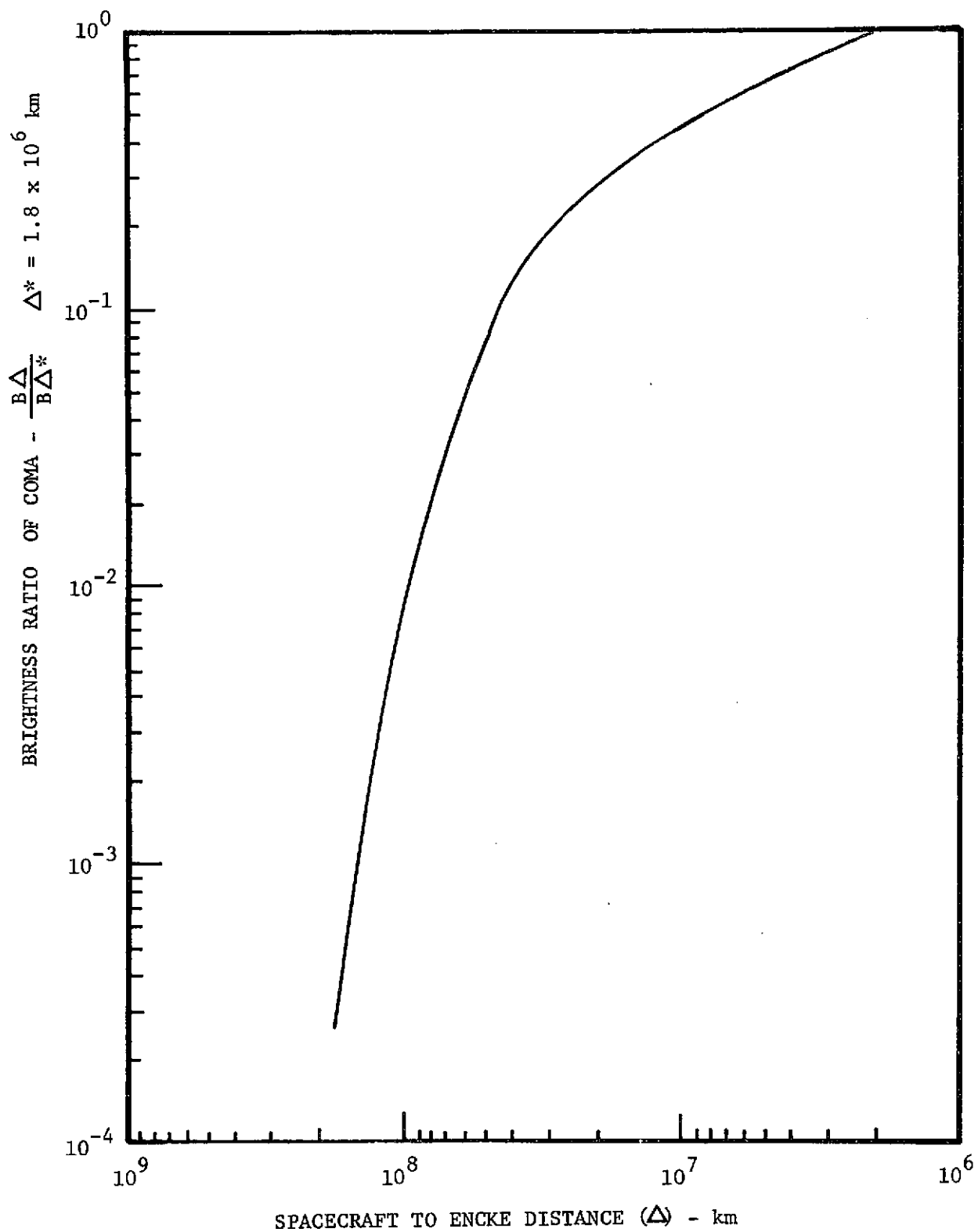


FIGURE V-50 BRIGHTNESS RATIO OF COMA (FOR VARIOUS SPACECRAFT TO ENCKE DISTANCES, Δ)

Detection Systems

The radiometry values, applied to Encke, were discussed in the preceeding section. It is now possible to use there values for specific imaging systems.

The detection systems considered are: 1) Video System (Mariner 71 Vidicon), 2) Photomultiplier Array (10 element system), 3) Solid State Array.

Video System (Vidicon)

The vidicon detection scheme is considered in an image compensation mode, where the frame exposure time can vary from 6 sec. to 10^{-3} sec. The vidicon detector under low light level is dark noise limited. The S/N may be written as:

$$(5) \quad S/N = \frac{S}{(S+N_D^2)^{1/2}}$$

where N_D^2 is the dark noise of the vidicon camera.

Specifically, N_D^2 is:

$$N_D^2 = I_D \times T_P / e$$

where e is electron charge, I_D is the Vidicon dark current, and T_P is the time required to read one pixel.

$$T_P = \frac{T_R}{N_R}$$

where T_R is the time to read one frame and N_R is the number of resolution elements.

For low light levels (i.e., $N_D^2 > S$).

$$S/N \approx \frac{\dot{S} T_F}{(N_D^2)^{1/2}}$$

where $\dot{S} T_F = S$ and \dot{S} is rate of signal electrons (p.e/sec) and T_F is the frame exposure time (sec).

There are two cases under consideration: 1) unresolved, and 2) resolved comet.

1. For the unresolved comet, $\dot{S} = H$, see Equation (1).
2. For the resolved comet, $\dot{S} = P$, see Equation (4).

1. For the unresolved comet and a dark current, I_D , of 0.2×10^{-9} amps and $T_P = 7 \times 10^{-3}$ sec, the H which results for a S/N of 3 is:

$$H_c = \frac{9 \times 10^3}{T_F} = 1.5 \times 10^3 \text{ p.e./sec for } T_F = 6 \text{ sec.}$$

T_F is camera frame exposure time in seconds

The Δ which results in this H_c (see fig. V-48) is 8×10^7 km.

2. For the theoretically resolved comet, we can predict the portion of the coma at a distance from the nucleus that has sufficient S/N to be resolved since the coma brightness is not uniform. This is shown in Figure V-51

The problem of acquiring the nucleus can also be treated in a manner similar to the way the unresolved comet was treated, since the nucleus may be assumed to be a point source for the acquisition distances considered here ($\Delta > 1.8 \times 10^6$ km).

$$H_N = N_N A_o n_o n_e \text{ p.e./sec, (see fig. V-48)}$$

where N_N is defined for the nucleus as N_c was for the coma

$$N_N = 10^{(6-M_N/2.5)} \text{ photons/cm}^2\text{/sec.}$$

The empirical expression for the nucleus magnitude M_N is:

$$M_N = 16.0 + 5 \log \Delta + 5 \log R + 0.03 (\phi)$$

where ϕ is the phase angle in degrees.

For the nucleus and the same conditions as were imposed for the unresolved comet,

$$H_N = \frac{9 \times 10^3}{T_F} = 1.5 \times 10^3 \text{ p.e./sec for } T_F = 6 \text{ sec.}$$

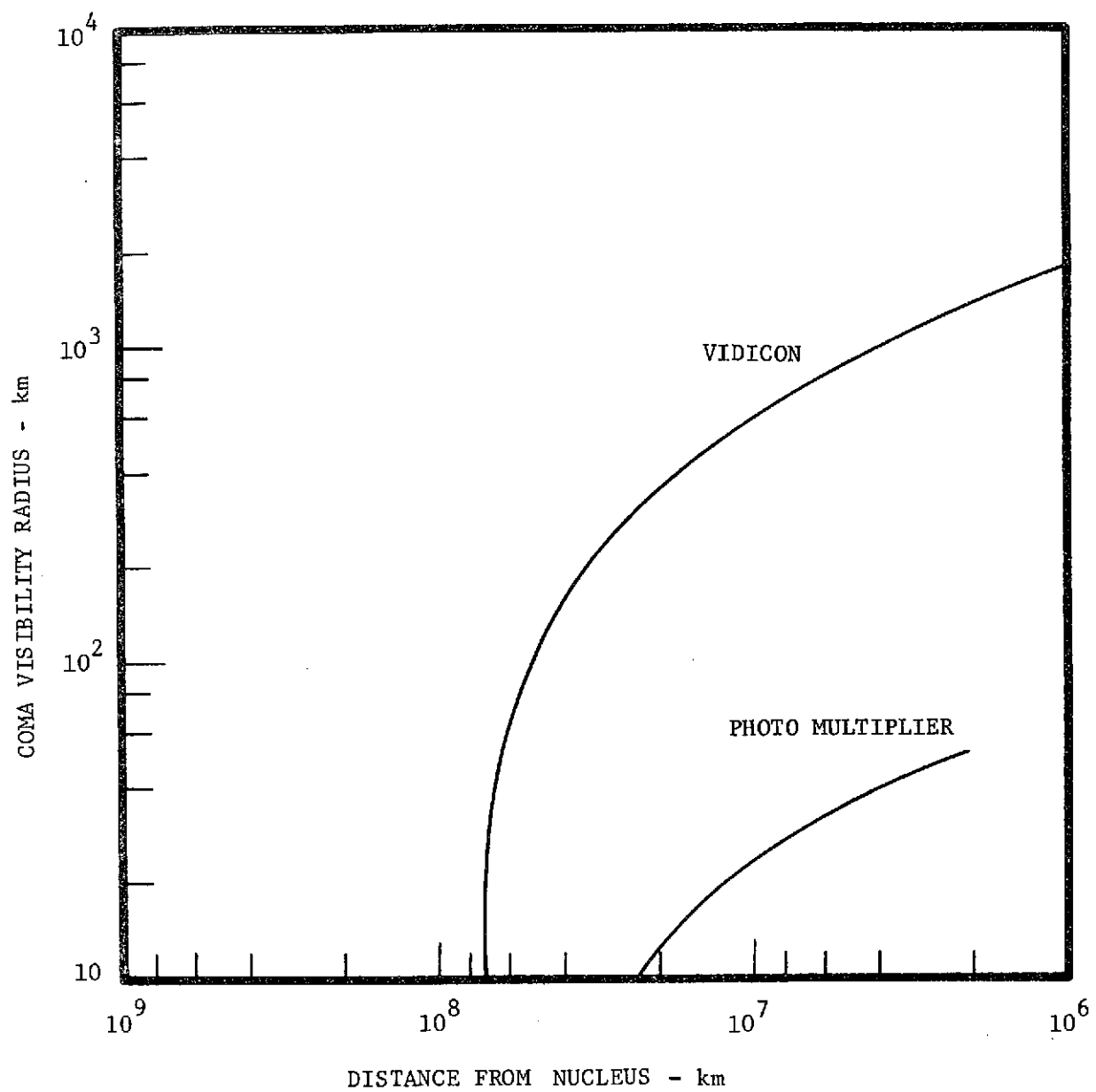


FIGURE V-51 RADIUS OF COMA IMAGING VS. DISTANCE FROM NUCLEUS

The Δ which results in this value of H_N (see fig. V-48) is 1.6×10^7 km.

Photomultiplier Tubes

The use of photomultiplier tubes will be accomplished in the spin scan mode, where the detectors will be on the spinning spacecraft and will scan over the comet at each revolution. The photo-multiplier array is signal noise limited, i.e.:

$$(6) \quad \frac{S}{N} = S^{1/2} = (\dot{S} T_F)^{1/2}$$

$$\text{where } T_F = \frac{\theta}{2 \pi \text{ (r.p.s.)}}$$

$$\theta = 0.1 \times 10^{-3} \text{ rad and r.p.s.} = 1/12, \text{ i.e., 5 rpm.}$$

$$T_F = 2 \times 10^{-4} \text{ sec.}$$

For a $S/N = 3$:

$$\dot{S} = H_c = 4.5 \times 10^4 \text{ p.e./sec, } \Delta = 4 \times 10^7 \text{ km, Figure V-48}$$

$$\text{For the nucleus } \Delta = 4 \times 10^6 \text{ km., Figure V-48.}$$

Note that this is for one image per revolution; if many images are added together, the threshold range would increase. This summing of images is possible as long as the image of the comet does not move more than ~ 0.1 MRAD per revolution.

For the resolved coma, one can again plot the resolvable portion of the comet for various distances, Δ . This has been done in Figure V-51.

The Solid State Array

The solid-state detectors array is also used in a spin scan mode, analogous to the photomultiplier detection scheme.

For these detectors, the S/N is given by:

$$(7) \quad S/N = \frac{S}{(N_D^2 + S)^{1/2}}$$

For photo-transistors used in Reference V-6, N_D is a constant dark noise number of electrons primarily induced by read-out and is independent of integration time. $N_D \approx 660$ photo electrons. (ref. V-6)

$$S/N = \frac{S}{N_D} = \frac{S}{660 \text{ p.e.}}$$

$$(8) \quad S/N = \frac{\dot{S} T_F}{N_D} \quad \text{where } T_F = 2 \times 10^{-4} \text{ sec.}$$

For a signal to noise ratio of 3 and using Figure V-48, and $\dot{S}=H$, $\Delta = 4.7 \times 10^6$ km for the comet acquisition.

Since we do not require spatial resolution for acquisition, we can sum the signals from all the detectors and can increase our integration time to be the time to scan the comet. The linear array is perpendicular to the scan direction. In this case, $T_F = 1.2 \times 10^{-3}$ sec., which is an approximate scan time for the acquisition distances considered.

$$(9) \quad S/N = \frac{\dot{S} T_F \sqrt{N}}{N_D}, \text{ where } N \text{ is the total number of detectors } = 400.$$

Then, $\Delta \approx 3.2 \times 10^7$ km (using fig. V-48).

This increase results since integration time was increased and the signal from all the detectors was summed. That is, all the light from the coma impinging on the focal plane was integrated.

The detection distance for nucleus acquisition, using a S/N of 3 and using equation 8, is found to be, $\Delta = 4 \times 10^5$ km. This distance corresponds to only 6 hours before encounter.

6. Mass-Spectrometer Requirements

Because of the importance of mass-spectrometer measurements, several calculations were made to assess their operational effectiveness. As already stated in the timeline section, the neutral and ion mass spectrometer are primarily for coma investigations and would be activated ~ 1 hour prior to encounter.

If the mass spectrometers are not oriented in the ram, or relative-velocity-vector, direction, measurements are degraded. Still, these instruments can accept flow with $\pm 20^\circ$ half angles. The actual effectiveness depends on inlet design, flow velocities, and molecules or species sought. However, a brief dwell-time calculation for 40° acceptance angle indicates that a completely-spinning-instrument installation degrades the instruments by $\sim 89\%$ (e.g., they are 11% as effective per revolution as they would be in the ram direction.) But the mission may permit many revolutions to be used, (e.g., in the outer coma). So a final decision on spin vs. ram direction requires careful study with a specific reference trajectory. Reference V-3 contains detailed discussion of mass-spectrometer designs and gas/spacecraft-surface interactions.

From a brief study using typical number densities for a 5000-km RCA, it does not appear that the spinning instrument could be improved by trying to scoop, or channel, the species at the high velocities encountered. The following tables (V-51 and V-52) show that the kinetic energies of the molecules are greater than both their ionization potentials and their dissociation energies at the velocities encountered, 18.3 to 26.3 km/sec. This indicates that the species could be dissociated/ionized, or would tend to recombine on impacting any static scoop or surface.

Table V-53 indicates that a magnetic deflection scheme to prevent particles from impacting the sides of some scoop is also not feasible. The magnetic fields are too great for typical turning radii of about 7.62 cm (3 inches).

Finally, the effectiveness of the instruments for both detection and spatial resolution will depend on the number densities of molecules and species encountered. Table V-54 shows the increase in sensitivity for detecting water molecules as the spacecraft approaches the nucleus. In addition, if a number

TABLE V-51 KINETIC ENERGY OF SPECIES (ev)

SPECIES	MOLECULAR WEIGHT	KINETIC ENERGY (eV)	
		VELOCITY (18.3 km/sec)	VELOCITY (26 km/sec)
H ₂ O	18.015	31.26	63.11
OH ⁻	17.007	29.51	59.58
H ⁺	1.008	1.75	3.53
O	16.000	27.76	56.05
CN ⁻	26.018	45.15	91.14
C ₂	24.022	41.69	84.15
C ₃	36.033	62.53	126.22
CH	13.019	22.59	45.61
NH ₂	16.023	27.80	56.13
NH	15.015	26.06	52.60

TABLE V-52 DISSOCIATION ENERGIES AND IONIZATION POTENTIALS OF SPECIES

SPECIES	<u>DISSOCIATION ENERGIES</u> ¹ (ev)	<u>IONIZATION POTENTIAL</u> ² (volts)
H ₂ O		12.6
OH ⁻	4.35	
O		13.61
CN ⁻	7.6	
C ₂	3.6	12.0
C ₃		12.6
CH	3.47	11.13
NH ₂		11.4
NH	3.8	13.10

1. Herzberg, G. Spectra of Diatomic Molecules, Van Nostrand Co. 1961
2. Handbook of Chem. and Phys., Chem. Rubber Co., 1969-1970.

TABLE V-53 MAGNETIC FIELD STRENGTH TO TURN SPECIES 90° THROUGH 7.12 CM RADIUS

SPECIES	MOL. WT.	MASS	MAGNETIC FIELD, B (Gauss)
H^+	1.008	1.67×10^{-27}	35.6
H_2O	18.015	2.99×10^{-26}	638
C_3^+	36.033	5.98×10^{-26}	1,275

Where $B = \frac{mv}{rq}$

B = field in weber/m² (1 weber/m² = 10^4 gauss)

m = mass in kg

v = vel. in m/sec = 26,000 m/sec

r = radius in meters - 0.0762 m

q = charge in coulombs - 1.6×10^{-19} coul.

TABLE V-54 SENSITIVITY OF MASS SPECTROMETER FOR DETECTING WATER MOLECULES

DISTANCE FROM NUCLEUS (km)	GAS DENSITY, n_i (molecules/sec)	PRESSURE (Newton/meter ²)	MASS SPECTROMETER SENSITIVITY (counts/sec)
50,000	1×10^4	5.02×10^{-8}	2.26×10^4
10,000	3.16×10^6	1.59×10^{-5}	7.1×10^6
5,000	3.16×10^7	1.59×10^{-4}	7.1×10^7
1,000	1×10^9	5.02×10^{-3}	2.26×10^9
500	4.5×10^9	2.27×10^{-2}	1.02×10^{10}
100	1.41×10^{11}	7.07×10^{-1}	3.18×10^{11}

$$\text{Dynamic Pressure} = 8.30 \times 10^{-16} n_i M V^2, \text{N/m}^2 \quad (\text{ref. V-5})$$

Where: n_i = gas density, molecules/cc

$V = 18.3 \text{ km/sec}$

$M = 18 \text{ (i.e., H}_2\text{O)}$

$$\text{Sensitivity} = (4.5 \times 10^{11}) \times (\text{Dynamic Pressure})$$

Where sensitivity $7.5 \times 10^{-8} \text{ amperes/(N/m}^2\text{)}$ which is $\sim 4.5 \times 10^{11} \frac{\text{ions-m}^2}{\text{sec-n}}$

like 10^6 to 10^8 counts were required to detect tenuous species (ref. V-2), Table V-54 indicates that the instruments are likely to work at 5000 km without long integrations. At 1000 km, the sensitivity is better by 1 1/2 orders of magnitude and very good measurements would be expected. Charles E. Giffin, at JPL (ref. V-5), pointed out the pressure approach to mass spectrometer sensitivity and the equation in Table V-54.

7. Instrument Development Requirements

The following instruments: TV, UV spectrometer, visual spectrometer, plasma probe, plasma wave detector, magnetometer, and Langmuir probes are instruments that will require little modification for a comet mission. Minor changes of range, sample frequencies, or sensitivity are anticipated. Those other instruments requiring instrument development are discussed here.

Neutral and Ion Mass Spectrometer - Several mass spectrometers are in development for planetary missions, but none have yet operated at velocities near 20 km/sec. For a comet mission, the molecules and radicals are extremely tenuous (more so than typical planetary atmosphere entries). Techniques for long-time collection, of comet specific species, need to be incorporated into instrument design.

The Yerkes group calls out several types of mass spectrometers, and a detailed trade study might lead to designs other than the free-molecular approach used here. Even with this approach, the spectrometer inlets must be carefully designed to produce a sample which can be satisfactorily related to the undisturbed ambient atmosphere. Phenomena, such as impact dissociation, impact ionization, secondary electron ejection, and vehicle induced interference effects must all be considered in the design of an instrument inlet. Reference V-3 discusses these problems in more detail, but we believe that in spite of good progress in this area, development work remains for a comet oriented mission.

IR Spectrometer - IR devices have not been strongly recommended for the comet mission. The off-the-shelf instruments, often require detector cooling, are slow in scan operation, and tend to be large in size, weight, and power. Yet, the potential value for good IR science on asteroids and comets is great,

and new instrument designs for comet missions should be studied.

Cosmic Dust Analyzer - The cosmic dust analyzer is a very important instrument for a comet mission because in situ dust particle composition cannot be measured in any other way on a flyby mission. Information on comet composition may be a way of tying together asteroid surfaces (by IR measurements) with comet particles.

In theory, the fast flyby velocities aid in ionization of particles, but there are problems with spectral scan rates, with ambiguity of chemical species detected, and with inlet design so that ionization does not occur before hitting a detector plate.

J. MASS PROPERTIES

Detailed mass estimates of the Earth-pointing spacecraft configuration (Concept number 2) were prepared and center-of-gravity and inertia data needed for the attitude control system analysis were developed. Mass estimates relied heavily on Pioneer 10/11 and advanced Pioneer study data. Structure estimates are based upon similar designs suitably modified to account for Atlas/Centaur/TE364-4 launch loads and additional equipment carried. Equipment mounting and electrical cabling were estimated on the basis of statistical data from existing designs. A contingency factor of 10% was used to allow for unforeseen design complications. There is sufficient historical data to show that a factor of this magnitude is adequate when a practical weight control program is conducted during design. It should be emphasized that this is a design contingency factor and not a growth factor useable for additional science or subsystems.

The baseline detail mass statement is given in Table V-58. Mass data for the other four Encke-only configurations were developed as modifications to this baseline with appropriate changes to the RCS propellant load. Mass estimates for the Encke coma probe, as shown in Table V-59, were developed using background information from other current probe studies.

Estimates for combined-mission spacecraft were made and accounted for 1) The additional propulsion required for trajectory maneuvers after Encke encounter; and 2) Replacement of the visual spectrometer by the IR instrument in the science payload (see Chapter II). Propellant quantities were based upon representative data shown in Section V-E (Propulsion) modified for the mass of each spacecraft. Table V-60 is a comparison of the five configuration concepts for the mission options considered feasible. The Encke-only and the combined Encke/Geographos mission mass estimates are shown for both probe and no-probe configurations. The Encke-Geographos mission was accomplished using RCS propulsion only, while an additional bi-propellant system was required for the Encke-Geographos-Toro mission. In this case, the major course-change maneuvers are performed by the bi-propellant system and the RCS performs the others as described in Section V-E. It should be noted that the Encke-Geographos-Toro mission results are given only for the no-probe configurations. Launch vehicle capability on this mission is a 560-kilogram injected mass (Chapter III). As

Table V-55 Baseline Detail Mass Statement
Concept No. 2

	<u>Mass (kg)</u>	<u>Weight (pounds)</u>	
Structure	84.4		186.1
Basic Structure	74.8	164.9	
Equipment Support	9.6	21.2	
Mechanisms	15.1		33.3
Magnetometer Boom	4.2	9.3	
Plasma Wave Boom	1.8	4.0	
Mirror Spin System	9.1	20.0	
Thermal Control	15.2		33.5
Insulation	8.3	18.4	
Closures	1.9	4.1	
Louvers (0.465 m ²)	2.9	6.5	
Misc. Thermal Devices	2.1	4.5	
Propulsion (RCS)	9.3		20.4
Tanks	5.9	12.9	
Thrusters (8)	2.2	4.8	
Lines & Valves	1.2	2.7	
Power	41.8		92.2
Solar Panels	19.5	43.0	
Battery	3.2	7.0	
Power Control Unit	6.4	14.0	
Transformer Rectifier	6.0	13.3	
Inverter	2.3	5.1	
Distribution Unit	4.4	9.8	
Communications	14.1		31.0
Receivers (2)	2.4	5.2	
Transmitter Drivers (2)	1.1	2.4	
Power Amplifiers (2)	.9	2.0	
X-Band Transmitter	1.1	2.4	
Error Channel Rec.	2.3	5.2	
Con Scan Processor	.4	.8	
Low Gain Antenna (2)	.5	1.0	
Hi Gain Antenna	1.6	3.5	
Antenna Sys. Plumbing	3.8	8.5	
Data Handling	18.4		40.5
Digital TM Unit (2)	6.2	13.6	
Tape Recorder	10.9	24.2	
Digital Decoder Unit	.8	1.7	
Signal Conditioner	.5	1.0	
Attitude Control G&C	5.1		11.2
Control Electronics	2.4	5.4	
Sun Sensors	.5	1.0	
Nutation Damper	2.2	4.8	

Table V- 55 Baseline Detail Weight Statement
Concept No. 2 (cont.)

	<u>Mass (kg)</u>	<u>Weight (pounds)</u>
Cabling (11% of 267)	13.6	30.0
Science	55.4	122.0
Television Imaging	23.4	51.6
Plasma Wave Experiment	5.5	12.1
Langmuir Probe	1.6	3.5
Plasma Probe	5.0	11.0
Neutral Mass Spectrometer	5.5	12.1
Ion Mass Spectrometer	2.5	5.5
Visible Spectrometer	3.5	7.7
UV Spectrometer	3.6	7.9
Magnetometer	2.8	6.2
Cosmic Dust Analyzer	2.0	4.4
Ballast	4.5	10.0
Contingency 10%	<u>27.7</u>	<u>61.0</u>
Spacecraft Dry	304.6	671.2
Residuals	2.6	5.7
N ₂ Gas	1.3	2.9
Propellant	1.3	2.8
Spacecraft Burnout	<u>307.2</u>	<u>676.9</u>
ACS Propellant	<u>18.8</u>	<u>41.5</u>
Launch	326.0	718.4

Table V-56 Coma Probe Detail Mass Statement

	<u>Mass (kg)</u>	<u>Weight (Pounds)</u>
Structure	10.1	22.3
Thermal Control	1.3	2.9
Insulation	.8	1.9
Phase Change Material	.5	1.0
Power	7.5	16.6
Battery	4.7	10.4
Power Control Unit	2.8	6.2
Communications	1.9	4.2
S-Band Transmitter	1.2	2.7
Antenna	.2	.5
Antenna Plumbing	.5	1.0
Data Handling	3.6	7.8
Digital Telemetry Unit	3.1	6.8
Sequencer	.5	1.0
Cabling	2.0	4.5
Science	11.0	24.2
Ion Mass Spectrometer	2.5	5.5
Neutral Mass Spectrometer	5.5	12.1
Langmuir Probe	1.0	2.2
Cosmic Dust Detector	2.0	4.4
Contingency 10%	<u>3.7</u>	<u>8.2</u>
Total Probe	41.1	90.7
Probe Attachment	<u>3.8</u>	<u>8.3</u>
Probe Installation	44.9	99.0

Table V-57 Spacecraft Mass Data Comparison

	<u>Encke Only</u>		<u>Combined E-G</u>		<u>Combined E-G-T</u>	
	<u>No Probe</u>	<u>1 Probe</u>	<u>No Probe</u>	<u>1 Probe</u>	<u>No Probe</u>	
					<u>Bi-Prop.</u>	<u>Sp. Storable</u>
Concept (1)	331.6 kg (731.1 lb)	387.5 (854.4)	369.6 (814.8)	431.5 (951.2)	569.4 (1255.3)	535.4 (1180.4)
Concept (2)	326.0 (718.4)	381.5 (841.0)	365.4 (805.6)	423.6 (933.8)	561.0 (1236.9)	527.7 (1163.4)
Concept (3)	358.0 (789.2)	414.6 (914.0)	397.2 (875.8)	455.1 (1003.3)	608.5 (1341.5)	575.6 (1268.9)
Concept (4)	332.2 (732.3)	388.1 (855.6)	370.2 (816.1)	432.0 (952.4)	570.3 (1257.3)	536.0 (1181.8)
Concept (5)	298.5 (658.1)	353.4 (779.2)	333.7 (735.7)	393.8 (868.1)	515.4 (1136.3)	488.6 (1077.2)

shown in Table V-60, only Concepts 2 and 5 are within this constraint when the nitrogen tetroxide/Aerozine-50 propulsion system is used. However, Concepts 1 and 4 are less than two percent above this constraint, and design refinements or science modifications could yield acceptable weights. A brief examination was made of a space-storable fluorine/hydrazine system to determine whether spacecraft mass could be reduced sufficiently to allow addition of a probe on the Encke-Geographos-Toro mission. Only Concept 5 (with probe) would be compatible with launch vehicle performance on this mission. Based on the no-probe masses shown, Concepts 1, 2, and 4 would have with-probe masses of the order of 600 kg, and Concept 3 would be about 650 kilograms.

Extensive spacecraft redesign would be necessary to bring these design concepts (with probe) within weight limits or substantial reductions would have to be made in the science instrument complement.

THIS PAGE BLANK

VI. CONCLUSIONS AND RECOMMENDATIONS

VI. CONCLUSIONS AND RECOMMENDATIONS

Two general conclusions were reached as a result of this study:

- Ballistically-launched, spin-stabilized spacecraft can feasibly support a broad-based instrument complement for the effective accomplishment of scientific goals in the exploration of comets and asteroids.
- A number of Encke pre-perihelion, fast-flyby mission options during the 1980 apparition are feasible for consideration by the scientific community and NASA program planners.

The Atlas/Centaur/TE364-4 launch vehicle provides the capability to perform the following missions with spacecraft incorporating a high degree of current technology:

- Encke-Dedicated Flyby - No Probe
 - Unique opportunity to combine coma and nucleus observations with 9-13½ hours of tail observation.
 - Shortest mission time (3 months).
 - Ground-based navigation probably adequate.
- Encke-Dedicated - With Probe
 - Tail observation time reduced to ~5 hours - still adequate for science objectives.
 - Coma observations to within at least 500 km of nucleus with probe are feasible.
 - On-board navigation required for best probe targeting.
- Encke-Geographos - With or Without Probe
 - Tail observation time about 1 hour - acceptable
 - Relative velocity at Encke increases from 18.3 to 26.3 km/sec.
 - Excess launch-vehicle capability. (550 kg vs 400-450 kg for spacecraft with probe).
 - On-board navigation required for targeting at Encke (probe) and asteroid.
 - Mission maneuvers performed by RCS

- Encke-Geographos-Toro - Without Probe

- Tail observation time about 1 hour - acceptable.
- Triple-target opportunity
- On-board navigation required
- Main propulsion system added for major maneuvers

The Encke-Geographos-Toro mission with a probe at Encke can be considered only if space-storable propulsion is used to perform the major course-change maneuvers. Of the configurations studied, only the lightest-weight concept (No. 5) incorporating spin-scan imaging could meet launch vehicle constraints. It was concluded, however, that existing-technology cameras of this type were not adequate.

The key technical issue, common to all of the concepts considered, is the acquisition and tracking of the comet nucleus and the asteroids. This issue concerns the interrelationships between imaging system characteristics (e.g., sensitivity and resolution), imaging system installation, and the collection and processing of data within the attitude control system. Each concept approached the latter aspect differently. It is recommended that a comprehensive study of these interrelationships be made to determine the preferred concept for implementation in detailed spacecraft design.

A concerted effort is needed between now and 1980 (and during the mission) to improve Earth-based ephemeris knowledge of Comet Encke and the target asteroids. Preliminary analysis indicates that on-board navigation capability can provide adequate data for final probe targeting at Encke and spacecraft targeting at the asteroids. However, it is recommended that a detailed navigation analysis of the Encke/asteroid missions to define specific sensor requirements and mission operations procedures be made.

Three scientific instrument categories require development for specific application to comet/asteroid missions. These are the neutral and ion mass spectrometers, the cosmic dust analyzer, and the IR spectrometer.

REFERENCES

REFERENCES

- II-1 Romer, E., "The Dimensions of Cometary Nuclei," Mem. Soc. Roy. des Sci. de Liege, 12, 23, 1966.
- II-2 Marsden, B. G., "Comets and Nongravitational Forces, II," Astron. J., 75, 1970.
- II-3 Sekanina, Z., "Total Gas Concentration in Atmosphere of the Short-Period Comets and Impulsive Forces Upon Their Nuclei," Astron. J., 74, 944, 1969.
- II-4 Senanian, Z., "Dynamical and Evolutionary Aspects of Gradual Deactivation and Disintegration of Short-Period Comets," Astron. J., 74, 1223, 1969.
- II-5 Marsden, Brian G., IAU Circular No. 2547, "Periodic Comet Encke," June 19, 1973.
- II-6 TRW Systems Group, Study of a Comet Rendezvous Mission, Tech. Report No. 72-87, May 1972.
- II-7 Mendis, D. A., Holzer, T. E., and Axford, W. I., "Neutral Hydrogen in Cometary Comas," Astro. and Space Sci., 15, 313, 1972.
- II-8 Sekanina, Z., Private Conversation, 1973.
- II-9 Delsemme, A. H., and Miller, D. C., "Physico-Chemical Phenomena in Comets - II, Gas Adsorption in the Snows of the Nucleus," Planet. Space Sci. 18, 717, 1970.
- II-10 Marsden, B. G., and Sekanina, Z., "Comets and Nongravitational Forces, IV," Astron. J., 76, 1135, 1971.
- II-11 Taylor, F. W., A Model of the Physical Properties of Comet Encke, Jet Propulsion Lab, Tech. Report 3-21590, 1973.
- II-12 Biermann, L., Brosowski, B., and Schmidt, H. U., "The Interaction of the Solar Wind with a Comet," Sol. Phys., 1, 254, 1967.
- II-13 Wurm, K., "The Physics of Comets," in The Moon, Meteorites, and Comets, ed. B. M. Middlehurst, and G. P. Kuiper, Univ. of Chic. Press. 1963.
- II-14 Yerkes Observatory, Proceedings of the Cometary Science Working Group, IITRI Publication, 1971.
- II-15 Vanysek, Valdimir, "Structure of Comets," Endeavor, 31, 60-66, 1972.
- II-16 Dunlap, J. L., "Minor Planets and Related Objects. XV. Asteroid (1620) Geographos," Preprint submitted to Astron. J., 20 August 1973.

- II-17 Chapman, Clark, R., and Salisbury, John W., "Comparisons of Meteorite and Asteroid Spectral Reflectivities," Icarus, 19, 507-522, 1973.
- II-18 Swings, D., "Le Spectre de la Comete d' Encke," Ann. Astrophysics, 124-136, 1948
- II-19 Whipple, F. L., "Problems of the Cometary Nucleus," Astron. J., 66, 375-380, 1961.
- II-20 Whipple, F. L., "A Comet Model I, "The Acceleration of Comet Encke," Astrophysics J., 3, 375-394, 1950.
- II-21 Marsden, B.G., "Comets and Nongravitational Forces, II," Astron. J. 74, 720, 1969.
- II-22 Wetherill, G. W., Cometary Versus Asteroidal Origin of Chondrite Meteorites, in Physical Properties of the Minor Planets, Proceedings of the 12th I.A.U. Colloquium, T. Gehrels, ed., 1971.
- II-23 Brandt, J. C., "The Physics of Comet Tails," Ann. Rev. of Astron. and Astrophys., 6, 267-286, 1968.
- II-24 Delsemme, A. H., "Vers un Modelle Physico-Chemique du Noyon Cometaire," Mem. Roy des Sci, de Liege, 12, 77, 1966.
- II-25 Delsemme, A. H., and Miller, D. C., "Physico-Chemical Phenomena in Comets - III, The Continuum of Comet Burnham (1960 II)," Planet. Space Sci., 19, 1229, 1971.
- II-26 Delsemme, A. H., and Wenger, A., Physico-Chemical Phenomena in Comets-I, Experimental Study of Snows in a Cometary Environment," Planetary Space Sci., 18, 709, 1970.
- II-27 Marsden, B. G., "Comets and Nongravitational Forces," Astron. J., 73, 367, 1968.
- II-28 Whipple, F. L., and Douglas-Hamilton, D. H., "Brightness Changes in Periodic Comets," Mem. Soc. Roy. des Sci. de Liege, 12, 469, 1965.
- II-29 Vsekhsvyatskii, S. K., "Physical Characteristics of Comets," NASA TT F-80, Office of Technical Services OTS 62-11031, 1964.
- II-30 Levin, B. J., "Are Gases Evaporated or Desorbed from Cometary Nuclei?," Mem. Soc. Roy des Sci. de Liege, 12, 65, 1966.
- II-31 Delsemme, A. H., "Comets: Production Mechanisms of Hydroxyl and Hydrogen Halos," Science, 172, 1126, 1971
- II-32 Biermann, L., "Comets and Their Interaction with the Solar Wind," Quart. J. Roy. Astron. Soc. 12, 417, 1971.

- II-33 Wetherill, G. W., and Williams, J. G., "Evolution of the Apollo Asteroids as Sources of Stone Meteorites," J. Geophysical Res., 73, 635-648, 1967.
- II-34 Hamid, S, and Whipple, F. L., "On the Origin of the Taurid Meteors," Astron. J., 55, 185-186, 1950.
- II-35 Swings, P. and Haser, L., Atlas of Representative Cometary Spectra, Univ. of Liege, Tech. Rept., 1955.
- II-36 Probstein, R. F., "Problems of Hydrodynamics and Continuum Mechanics," Soc. of Industrial and Applied Mechanics, Phil. Pa., 1968.
- II-37 O'Dell, C. R., "Emission-Band and Continuum Photometry of Comet Burnham, 1959K," Pub. Astron. Soc. of the Pacific, 73, 35, 1961.
- II-38 Goldberg, R. A., and Aikin, A. C., "Comet Encke: Meteor Metallic Ion Identification by Mass Spectrometer," Science, 180, 294-296, 1973.
- II-39 Sekanina, Z., "A Model for the Nucleus of Encke's Comet," IAU Symposium, No. 45, Springer-Verlag, N.Y., 301-307, 1972.
- II-40 Jackson, W. M., and Dunn, B. "Collisional Processes in the Inner Coma," Mem. Soc. Roy des Sci. de Liege, 12, 133, 1965.
- II-41 Matson, D. L. "Infrared Observations of Asteroids," in Physical Studies of Mirror Planets, Proceedings of the 12th IAU Colloquium, ed., T. Gehrels, NASA SP-267, 41, 1971.
- II-42 Frye, William E., Infrared Optical Sensing of the Asteroids, in Proceedings of the 9th Inter. Symp. on Space Tech. and Sci., 1077-1086, Tokyo, 1971.
- II-43 Forward, Robert L., Pilcher, L. S., and Norwood, V. T. "Asteroid Belt Investigation Using Small, Spin-Stabilized Fly-by Probes" in Use of Space Systems for Planetary Geology and Geophysics, Vol. 17, Am. Astronautical Soc. Publication, 327-346, 1968.
- II-44 Marsden, Brian G., IAU Circular No. 2446, "Periodic Comet Encke," Sept. 25, 1972.
- II-45 Marsden, Brian G., IAU Circular No. 2435, "Periodic Comet Encke (1970 I)," (1970 I)," August 22, 1972.
- II-46 Marsden, Brian G., IAU Circular No. 2276, "Periodic Comet Encke," Sept. 4, 1970.
- II-47 Atkins, K. L., and Moor, J. W., "Cometary Exploration: A Case for Encke," AIAA Paper No. 73-596, 1973.

- II-48 Mendis, D. A., "Some Recent Development in Cometary Physics," AIAA Paper No. 73-549, 1973.
- II-49 Chapman, Clark R., and Salisbury, John W., "Comparisons of Meteorite and Asteroid Spectral Reflectivities," Icarus, 19, 507-522, 1973.
- II-50 Chapman, Clark R., McCord, Thomas B., and Pieters, Carle, "Minor Planets and Related Objects. X. Spectrophotometric Study of the Composition of (1685) Toro," Astron. J., 78, 502-505, 1973.
- II-51 Johnson, Torrence V., and Matson, Dennis L., "Minor Planets and Related Objects. XI. 0.4-0.8 μ m Spectrophotometer of (1685) Toro," Astron. J., 78, 505-507, 1973.
- II-52 Goldstein, R. M., Holdridge, D. B., and Lieske, J. H., "Minor Planets and Related Objects. XII. Radar Observations of (1685) Toro," Astron. J. 78, 508-509, 1973.
- II-53 Williams, J. G., and Wetherill, G. W., "Minor Planets and Related Objects. XIII. Long-Term Orbital Evaluation of (1685) Toro," Astron. J., 78, 510-515, 1973.
- II-54 Arrhenius, G., Alfven, H., and Fitzgerald, R., Asteroid and Comet Exploration, NASA CR-2291, 1973.
- II-55 JPL, Mission to a Comet: Preliminary Scientific Objectives and Experiments for use in Advanced Missions Studies, TM 33-297, 1967.
- II-56 NASA, Comets and Asteroids: A Strategy for Exploration, Report of the Comet and Asteroid Mission Study Panel, NASA TMX-64677, 1972.
- II-57 Chapman, C. R., and Stone, C.A., Asteroid Selection for Mission Opportunities, IIT Res. Inst., TM No. P-42 with Appendix Asteroid Data Sheets, 1972.
- II-58 Gehrels, T., "Photometry of Asteroids," in Surfaces and Interiors of Planets and Satellites, ed. A. Dollfus, Academic Press, N.Y. 1970.
- II-59 Klopp, D., Orbital Imagery for Planetary Exploration, Vol. IV, Imaging Sensor System Scaling Laws, IIT Res. Inst. for NASA, Ames, 1969.
- II-60 Chapman, Clark R., Surface Properties of Asteroids, Ph.D. Thesis, MIT., 1972.
- II-61 Wetherill, George W., "Solar System Sources of Meteorites and Large Meteoroids," Preprint, 1973.
- II-62 Abate, John E., "Star Tracking and Scanning Systems; Their Performance and Parametric Design," IEEE Transactions on Aerospace and Navigational Electronics, 171-181, Sept. 1963.

- II-63 JPL, d'Arrest Comet Mission Study, 760-66, 1971.
- II-64 Niehoff, John C., "An Assessment of Comet and Asteroid Missions," American Astron. Soc. AAS-71-104, 1971.
- II-65 JPL, A Mission Analysis Study of Comet Rendezvous and Asteroid Docking, 760-71, 1972.
- II-66 Friedlander, Alan L. and Welds, William C., Comet Rendezvous Mission Study, IIT Research Inst. Report No. M-28. For NASA Contract No. NAS-2144, 1971.
- II-67 O'Dell, C. R., "Nature of Particulate Matter in Comets as Determined from Infrared Observations," Astrophys. J., 166, 675-681, 1971.
- II-68 Delsemme, A. H., and Swings, P. Ann of Astrophysics, Vol. 15, 1952.
- III-1 NASA, Launch Vehicle Estimating Factors for Advance Mission Planning, NHB7100.5B, 1973 Edition.
- III-2 P. Hong, Internal Memorandum, 'Brian Marsden on Comet/Asteroid Ephemeris Errors', Martin Marietta Corporation, 23 May 1973.
- III-3 E. G. Howard, Martin Marietta Corporation Communication with Dr. Elizabeth Romer, on Encke Observations, 1 August 1973.
- III-4 J. J. Krasovec, First Midcourse ΔV Requirements for New Delta 2914 Injection Covariance Matrice, Internal Memo., MMC, 24 July 1972.
- III-5 J. W. Underwood, Preliminary Comets and Asteroids Navigation Analysis for an Extended Mission to Encke, Geographos, and Toro, Internal Memorandum, Martin Marietta Corporation, 16 Aug. 1973.
- III-6 A. Satin, Comet Ephemeris Accuracies with On-Board Optical Sensor, Internal Memorandum, Martin Marietta Corp., 21 August 1973.
- III-7 Ondrasik, et. al, An Analysis of Outer Planet NAV System, AIAA Paper No. 72-926, September 1972.
- V-1a Howell, J. Q., and Crosswell, W. F., "A Disc Antenna for the Viking Lander," Handout at Viking Design Review by NASA/LRC Personnel, 1973
- V-1b Anon., "Critical Design Review for Viking Orbiter 1975 Antenna Subsystems - Visual Aid Package Volume II," March, 1973.
- V-1c A Study of an Orbital Radar Mapping Mission to Venus, Martin Marietta Corporation for NASA/Ames, NASA CR-114640, CR-114641, and CR-114642, September, 1973.

- V-1d JPL Technical Memo 33-473, Measured Performance of Silicon Solar Assemblies for Use at High Solar Intensities., 15 March 1971
- V-2 Taylor, F. W., Michaux, C. M., and Newburn, R. L., A Model of the Physical Properties of Comet Encke, JPL, TR 37-1590, 1973.
- V-3 Jupiter Turbopause Probe Gas Physics Environment and Instrument Response Study, Martin Marietta Corporation for NASA-Goddard, MCR-71-142, 1971.
- V-4 French, J. B., Reid, N. M., Nier, A. O., and Hayden, J. L., "Molecular Beam Simulation of Planetary Atmospheric Entry - Some Recent Results," C.A.S.I. Transactions, 5, 77-82, 1972.
- V-5 Giffin, Charles E. JPL, Private discussions on Sensitivity of Neutral Mass Spectrometers, 1973.
- V-6 Hieatt, J., TRW, Private Communication on Solid State Spin Scan Imaging, 1973.
- V-7 Mendis, D. A., "Some Recent Development in Cometary Physics," AIAA Paper No. 73-549, 1973.
- V-8 Frye, William E., "Infrared Optical Sensing of the Asteroids," in Proceedings of the 9th Inter. Symp. on Space Tech. & Sci., 1077-1086, Tokyo, 1971
- V-9 Probst, R. F., "Problems of Hydrodynamics and **Continuum Mechanics**," Soc. of Industrial and Applied Mechanics, Phil. Pa., 1968.
- V-10 Wurm, K. "The Physics of Comets," in The Moon, Meteorites and Comets, ed. B. M. Middlehurst, and G. P. Kuiper, Univ. of Chic. Press. 1963.
- V-11 Frye, William E. Infrared Optical Sensing of the Asteroids, in Proceedings of the 9th Inter. Symp. on Space Tech. and Sci., 1077-1086, Tokyo, 1971.
- V-12 Forward, Robert L., Pilcher, L. L., and Norwood, V. T., "Asteroid Belt Investigation Using Small, Spin-Stabilized Fly-by Probes," in Use of Space Systems for Planetary Geology and Geophysics, Vol. 17, Am. Astronautical Soc. Publication, 327-346, 1968.
- V-13 Tomasko, Martin, "Spin Scan Imaging Capabilities, **Grigg-Skjellerup Flyby**," Informal Memo to NASA-Ames, 1973.
- V-14 Yerkes Observatory, Proceedings of the Cometary Science Working Group, IITRI Publication, 1971.
- V-15 Arrhenius, G., Alfven, H., and Fitzgerald, R., Asteroid and Comet Exploration, NASA CR-2291, 1973.

- V-16 NASA, Comets and Asteroids: A Strategy for Exploration, Report of the Comet and Asteroid Mission Study Panel, NASA TMX-64677, 1972.
- V-17 Klopp, D., Orbital Imagery for Planetary Exploration, Vol. IV, Imaging Sensor System Scaling Laws, IIT Res. Inst. for NASA, Ames, 1969.
- V-18 Lavery, Norman P., "The Comparative Performance of Electron Tube Photodetectors in Terrestrial and Space Navigation Systems," IEEE Transactions on Aerospace and Navigational Electronics, 194, 1963
- V-19 Abate, John E., "Star Tracking and Scanning Systems; Their Performance and Parametric Design," IEEE Transactions on Aerospace and Navigational Electronics, 171-181, Sept. 1963.
- V-20 Lefferdo, J. M., Edquist, C. T., and Steel, P. C., "Gas Dynamics Environment of High Altitude Jovian Entry," AIAA Paper No. 72-203, 1972.

APPENDIX A

APPENDIX A

A. PRIOR CONTRACTOR STUDY EFFORT

The data included in this section of the Appendix is a summary of the Martin Marietta Corporation effort prior to receiving this study contract. The study effort was conducted in late 1972 and early 1973, and considers possible ballistic fast flyby mission options associated with the 1980 perihelion passage of Comet Encke. The data presented should be considered as typical. Data given in the main body of the report should be used in preference, when specific answers are desired in overlapping areas.

1. Background

Probably the most desirable comet mission in the 1980's is comet Halley in 1986. Because of the extremely high approach speeds, which are due to the combined effect of its eccentricity (75 year period) and its retrograde motion, energy requirements for rendezvous or a slow flyby are very high. Fast flybys are also possible but none of the above options would be considered without a precursor mission to a short period comet.

One of these precursor missions which has been studied at Martin Marietta Corporation is Comet Encke, which has also been suggested as desirable for study by the "Comet and Asteroid Panel" (ref. A-1).

Comet Encke is, of course, also very interesting for its own sake as a subject of scientific investigation. It has been observed at most of its apparitions since its discovery in the late 18th century and has well known elements. It is also possible that it may lose all of its volatile substances before the end of this century, which tends to make it a unique object to investigate before this occurs. This would permit later missions to make useful comparisons between the comet in its active and passive states.

The 1980 mission to Encke was selected for investigation. This is probably the earliest mission which would be attempted and is also desirable since it occurs near a maximum of solar activity. Furthermore, this mission should be soon enough to influence the Halley mission design.

For further understanding of the various Encke 80 mission options,

Martin Marietta Corporation has generated fast flyby mission characteristics over a wide range of launch energies and arrival conditons. Combined Encke/Asteroid missions, which were also recommended by the previously mentioned panel, have been investigated. Earth return options, which could also have application to a Halley mission, are also discussed in this section.

2. 1980 Mission Options

Considerable effort by many organizations has been devoted to assessment of missions to Comet Encke. Most of the recent investigations have emphasized the related and progressive modes of slow flyby, rendezvous, docking and sample return. This class of missions is characterized by launch from the comet descending node and involves long ballistic flight times (on the order of the comet period) and large in-flight propulsion maneuvers (see fig. A-1). Spacecraft employing electric propulsion could reduce trip time by a factor of about 2 and are, therefore, attractive for such mission modes.

Less attention has been directed to the fast flyby mode and assessment of techniques to maximize science return. As a contribution to improved understanding of early comet exploration options, Martin Marietta Corporation has conducted a study of the fast flyby mission mode for the 1980 apparition of Encke. The primary impetus for this approach was the compatibility with programmed launch vehicles and conventional spacecraft technologies. In addition, timely experience with the fast flyby mode could prove valuable to implementation of a practical Halley/86 mission.

Results of the investigation are summarized in this section of the Appendix. As shown, a variety of options are available to the mission planner. In particular, the possibilities of returning physical data to earth for laboratory analysis and extending the mission to include asteroid flybys offer considerable enhancement for an Encke flyby mission.

Treatment of the Encke/80 trajectory characteristics for ascending node launches has been of a broad parametric nature to provide perspective for option comparisons. Data are presented in Figure A-2 for launch energies up to $120 \text{ km}^2/\text{sec}^2$ to encompass the capabilities of launch vehicles programmed for 1980 availability.

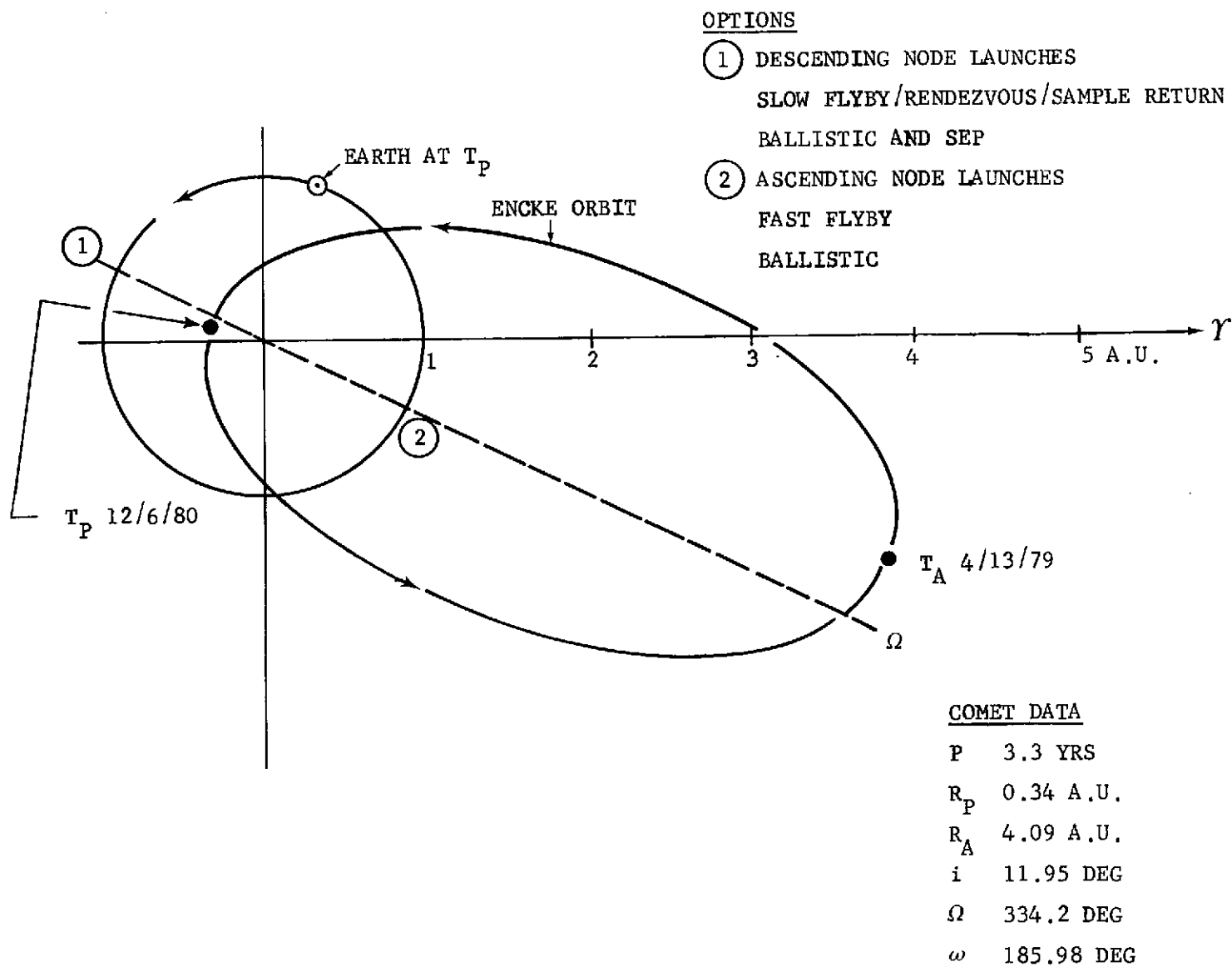


FIGURE A-1 1980 COMET ENCKE MISSION CLASSES

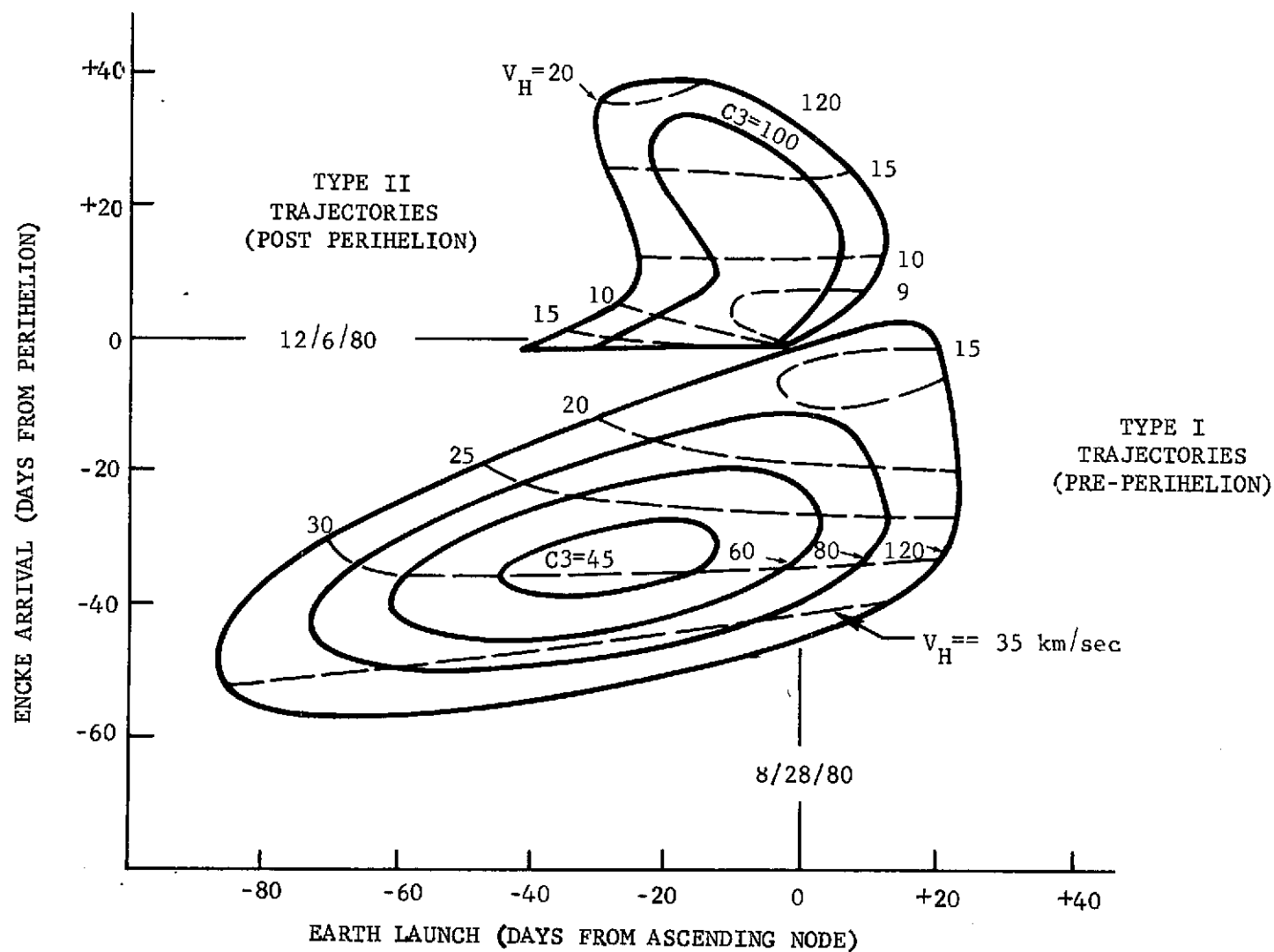


FIGURE A-2 ENCKE/80 FAST FLYBY CHARACTERISTICS

Due to the near-alignment of the line of nodes and the line of apsides exhibited by Encke, the Type I/Type II trajectory distinction essentially corresponds to encounter before and after comet perihelion, respectively. Both cases are of general interest but especially significant for Encke in view of the unique activity cycle. Pre-perihelion encounters offer the science observables characteristic of an active comet while greatly reduced activity after perihelion passage should permit improved observation of the nucleus.

As shown by the chart, post-perihelion encounters are more restricted by launch energy considerations but are benefitted by reduced relative velocities at flyby. This sort of tradeoff is basic to mission option selection and illustrates the value of broad parametric treatment.

Encounters near perihelion can produce relative velocities as low as 6.5 km/sec. However, the Encke activity level at this condition is transitory and Earth launch periods are severely restricted.

Launch when Earth is at the comet ascending node produces flyby in the comet orbit plane. Non-nodal launches correspond to non-coplanar encounter conditions which may prove useful or detrimental to science observations.

Encounter with Encke occurs a few months after launch with Earth in position to receive real-time and recorded data. Additional options representing subsets of the launch/arrival date matrix offer opportunities for returning the spacecraft to Earth after extra solar revolutions, without significant propulsive maneuvers.

This option may be of value if Earth laboratory analysis of dust specimens and film recorded data are sufficiently superior to the capabilities of on-board instruments and data handling systems. If employed, Earth return could enhance the science value of the fast flyby mode through information normally associated with the difficult sample return mission.

As shown on Figure A-3, pre-perihelion Encke encounters are compatible with Earth return in 1 to 3 years. For example, a nodal launch arriving at Encke about 20 days before perihelion corresponds to a reasonable combination of launch energy and relative velocity at flyby. This mission can be targeted over a wide launch period to produce a spacecraft orbit period of $2/3$ of an

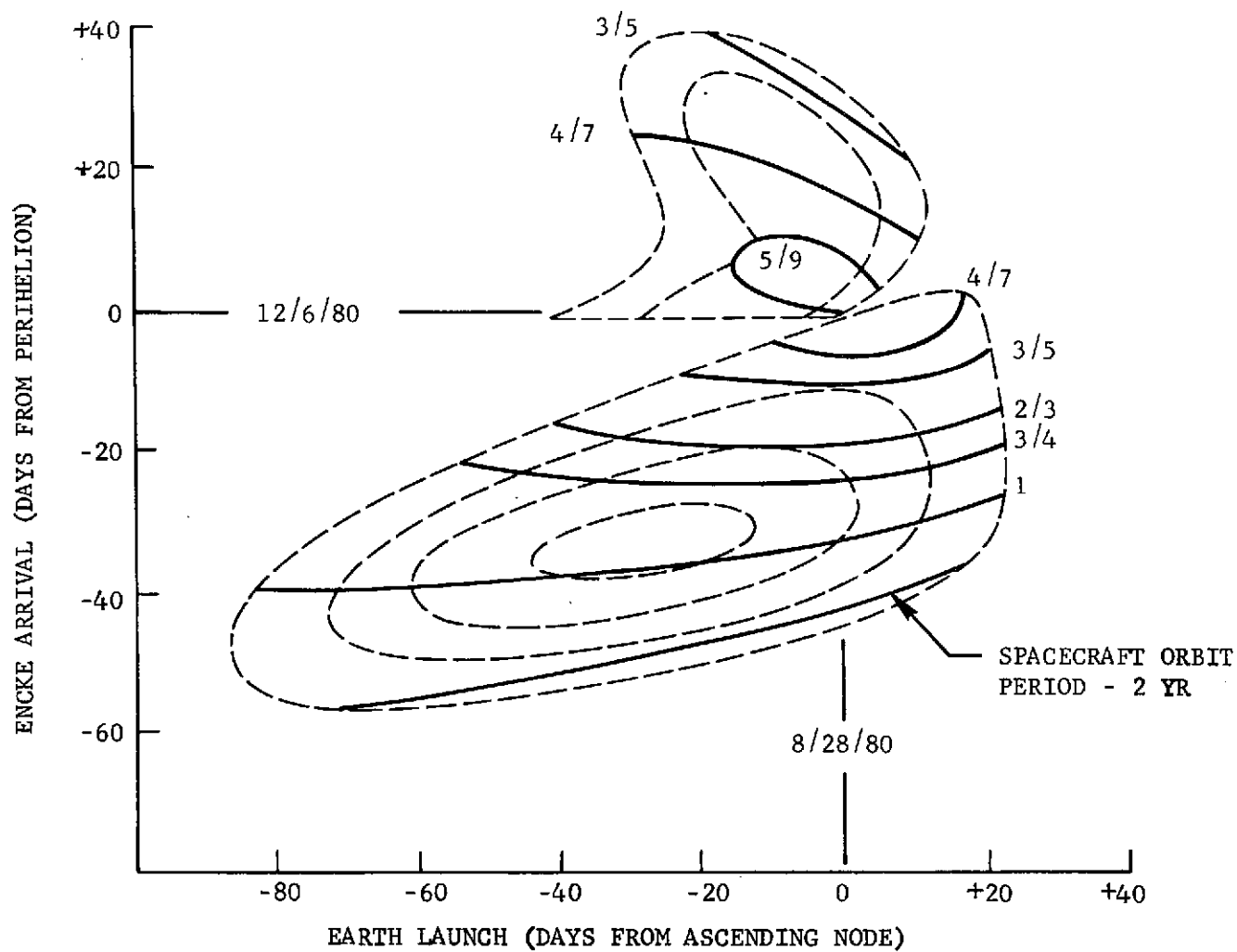


FIGURE A-3 ENCKE/80 FLYBY, RETURN TO EARTH OPTIONS

Earth year which will result in re-encounter with Earth in 2 years after 3 complete solar revolutions of the spacecraft.

Pre-perihelion Encke encounters involve coma and tail activity for which science evaluation may be improved by return of physical data. Conversely, the post-perihelion Encke condition is expected to be less active and more compatible with on-board data processing. Also, since the shortest Earth return trip time compatible with this mode is 4 years, the Earth return option does not appear attractive.

3. Typical Mission Characteristics

Heliocentric flight profiles are typified in Figure A-4 for each basic type of Encke flyby. Data are tabulated to illustrate the differences in launch energy requirements and the relative velocity at target encounter.

Earth tracking conditions at flyby are indicated. Both cases appear to be compatible with prompt return of RF data.

Pre-perihelion Encke encounters occur at about 0.6 AU and, for consideration of extended spacecraft operation, further descend to about 0.5 AU. The trajectories for post-perihelion encounter approach the sun about as close as does the comet (0.35 AU) and flyby occurs inside 0.5 AU.

Large scale relative motion is presented in Figure A-5 for both basic mission types with respect to a moving, rotating coordinate system based on the target comet. Significant differences in geometry during approach and flyby are apparent.

Pre-perihelion encounter is typified by approach from the solar direction producing an essentially longitudinal flyby of the extended comet. In contrast, post-perihelion encounters approach from the anti-sun direction which is detrimental to target acquisition. However, the long period of near proximity should facilitate acquisition as well as offer observation of the expected comet activity transition in the vicinity of perihelion.

A small scale schematic of pre-perihelion flyby geometry (fig. A-6) illustrates the encounter options available to mission science planners. For example, a trajectory targeted for free Earth return and constrained to pene-

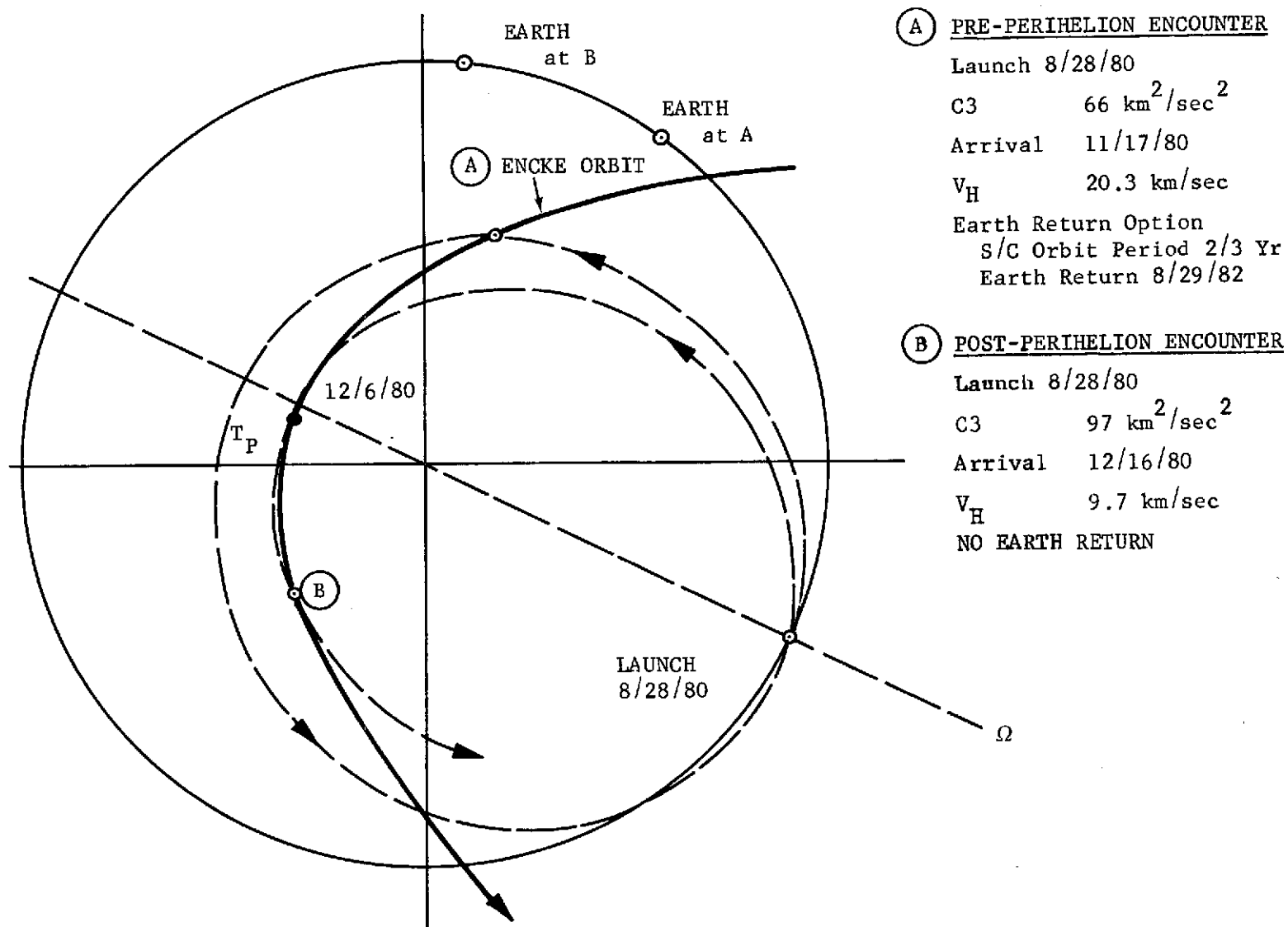


FIGURE A-4 TYPICAL ENCOUNTER TRAJECTORIES

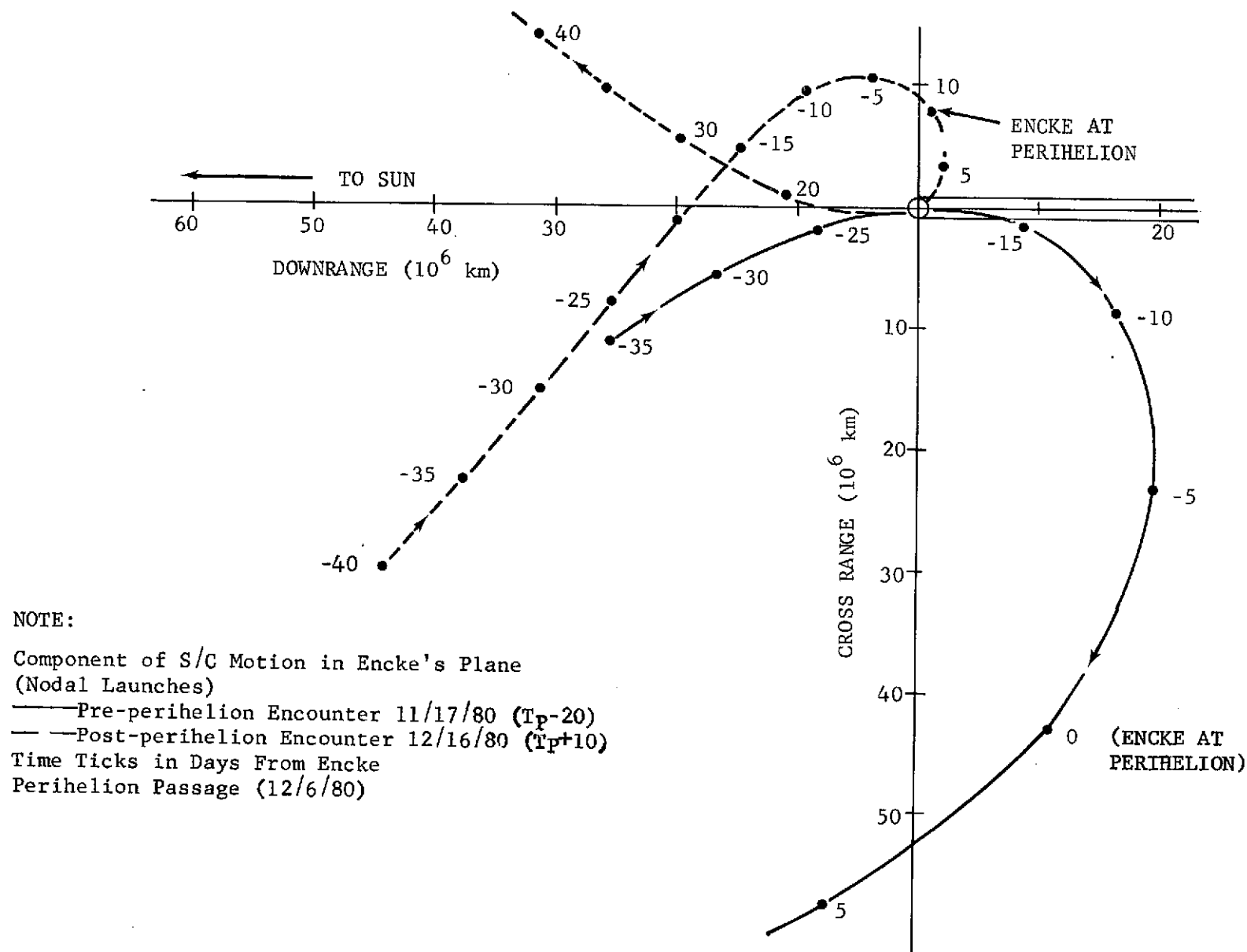
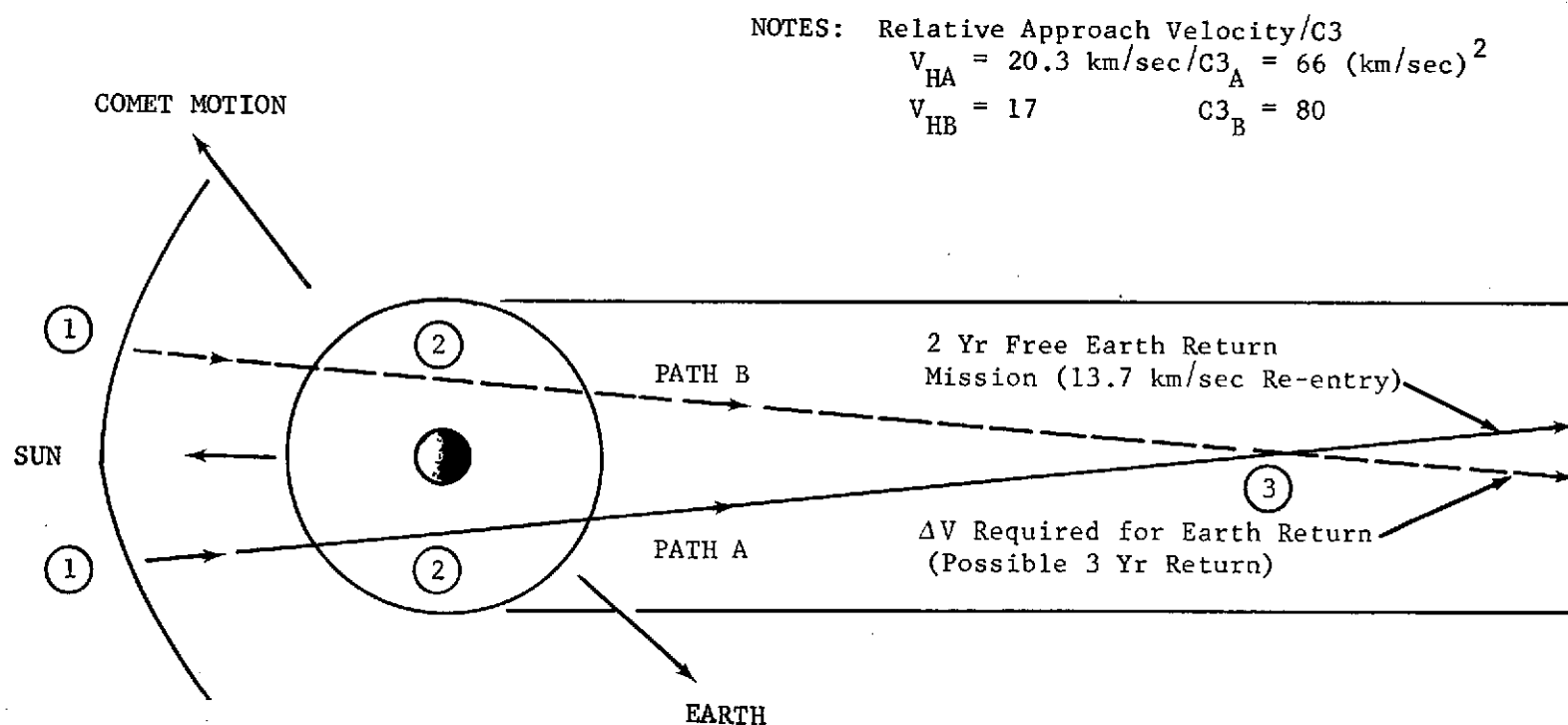


FIGURE A-5 RELATIVE MOTION FOR TYPICAL ENCOUNTERS



TYPICAL SCIENCE EVENTS

- ① Approach Spectrography, Imaging, Bow Shock Penetration
- ② Coma Specimen Collection
 RF Occultation Through Coma
 Separate Probe for Deep Coma Penetration (Optional)
- ③ Solar Transit Spectrography, Imaging
 Tail Specimen Collection
 RF Occultation Through Tail

FIGURE A-6 PRE-PERHELION ENCOUNTER FLYBY GEOMETRY OPTIONS

trate both coma and tail passes on the Earth side of the comet. A comparable path permitting greater RF attenuation involves higher launch energy (but reduced flyby velocity) and interacts adversely with Earth return prospects. The options include the intermediate case of parallel passage.

The extent of the Encke coma at encounter is expected to be about 20,000 km radius. As depicted on the figure, closest approach will probably be limited to about half this distance by spacecraft survival considerations. A feasible method of obtaining information nearer the nucleus would involve a separate instrumented probe deployed from and monitored by the flyby spacecraft.

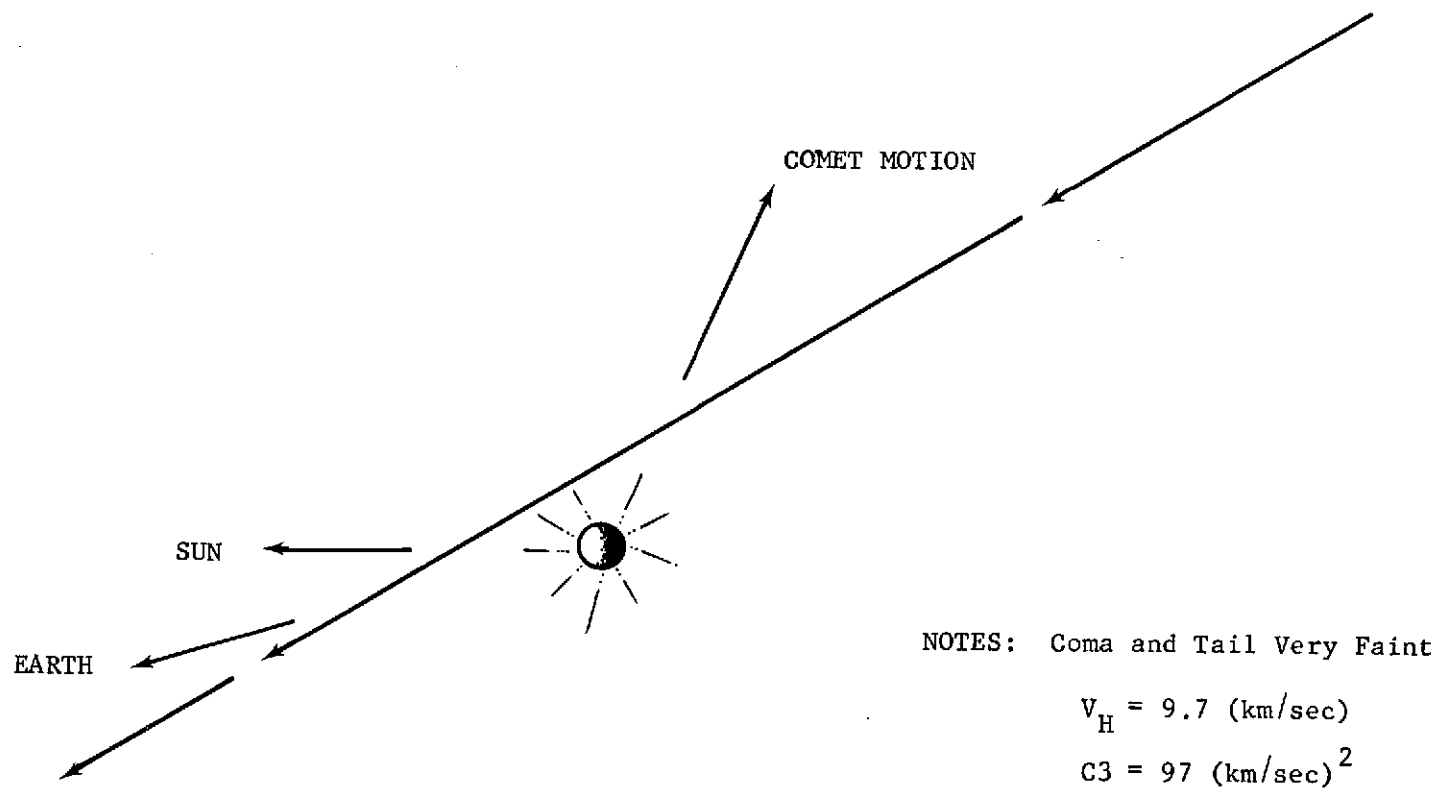
Typical science observables, including those appropriate for the Earth return mode, are presented. It is expected that the low dust content of Encke will permit filtered imaging of the nucleus during approach and flyby. However, as a backup, targeting to produce a transit of the nucleus across the solar disc is an interesting option. In the case of an opaque inner coma, multi-spectral imaging of the transit event could provide resolution of clues to size and nature of the nucleus. The observables may be sufficiently subtle to benefit from film photography and return to Earth. Another reason for considering the transit technique is the potential application to a comet Halley flyby mission.

The unique activity cycle of Encke offers the prospect of superior nucleus observation during the post-perihelion phase, as depicted in Figure A-7. While still close to the sun and intensely illuminated, such details as surface irregularities and rotation rate may be discernable.

Due to the relative predictability of the Encke orbit and the diminished comet activity, close approach distances are possible. Limitations are probably similar to those of asteroid flyby missions and center on such matters as acquisition and motion compensation for the imaging system.

4. Combined Comet/Asteroid Missions

Space mission planning to explore the small bodies of the solar system is complicated by the large number of potential targets and the meager state of current knowledge. Properly, the initial missions should generate planning



SCIENCE OBJECTIVES (NUCLEUS EMPHASIS)

Physical Shape
Rotation Rate
Surface Details, Outgassing
Albedo
Temperature

FIGURE A-7 POST-PERHELION ENCOUNTER FLYBY GEOMETRY

information to provide for the foundation of more extensive investigation. The value of early missions can be substantially enhanced if ancillary objectives can be economically combined with a dedicated primary target. In view of this fact, considerable recent effort has been devoted to identification of opportunities to study multiple bodies with a single mission. Many such missions have been defined. In particular, combinations of comets with belt asteroids have been shown to be possible.

An effort to identify secondary targets compatible with the subject fast flyby Encke missions was undertaken. Prospects were essentially limited to the four cataloged asteroids which pass inside the orbit of Earth. Of these, Geographos and Toro exhibit orbit geometries and time phasing consistent with Encke/80, as shown in Figure A-8.

Opportunities to achieve asteroid flybys subsequent to Encke flyby are presented in the context of Encke flyby requirements (fig. A-9). Only pre-perihelion Encke encounters have been shown to be compatible with such combined missions.

Preliminary data are presented for post-Encke encounter with Geographos at both orbit intersections. Due to different geometry of the Toro orbit, only a single flyby option is practical.

The three single asteroid opportunities and the double asteroid opportunity span a large Earth launch interval and correspond to reasonable launch energies and comet flyby velocities. Primary requirements imposed on the spacecraft design are increased propulsion capability and extended lifetime.

For reference, the 3/4 year spacecraft period line is displayed. This is indicative of the prospects that Earth return may be retained as a practical option for combined missions. Assessment of maneuver requirements for such cases is not being pursued at this time.

Additional information pertaining to asteroid flyby conditions is presented in Table A-1. As shown, flight durations are considerably greater than the 3-5 months required for simple Encke missions.

Relative velocities at flyby are appreciably lower than the corresponding Encke encounters. This is fortunate due to the closer permissible approach

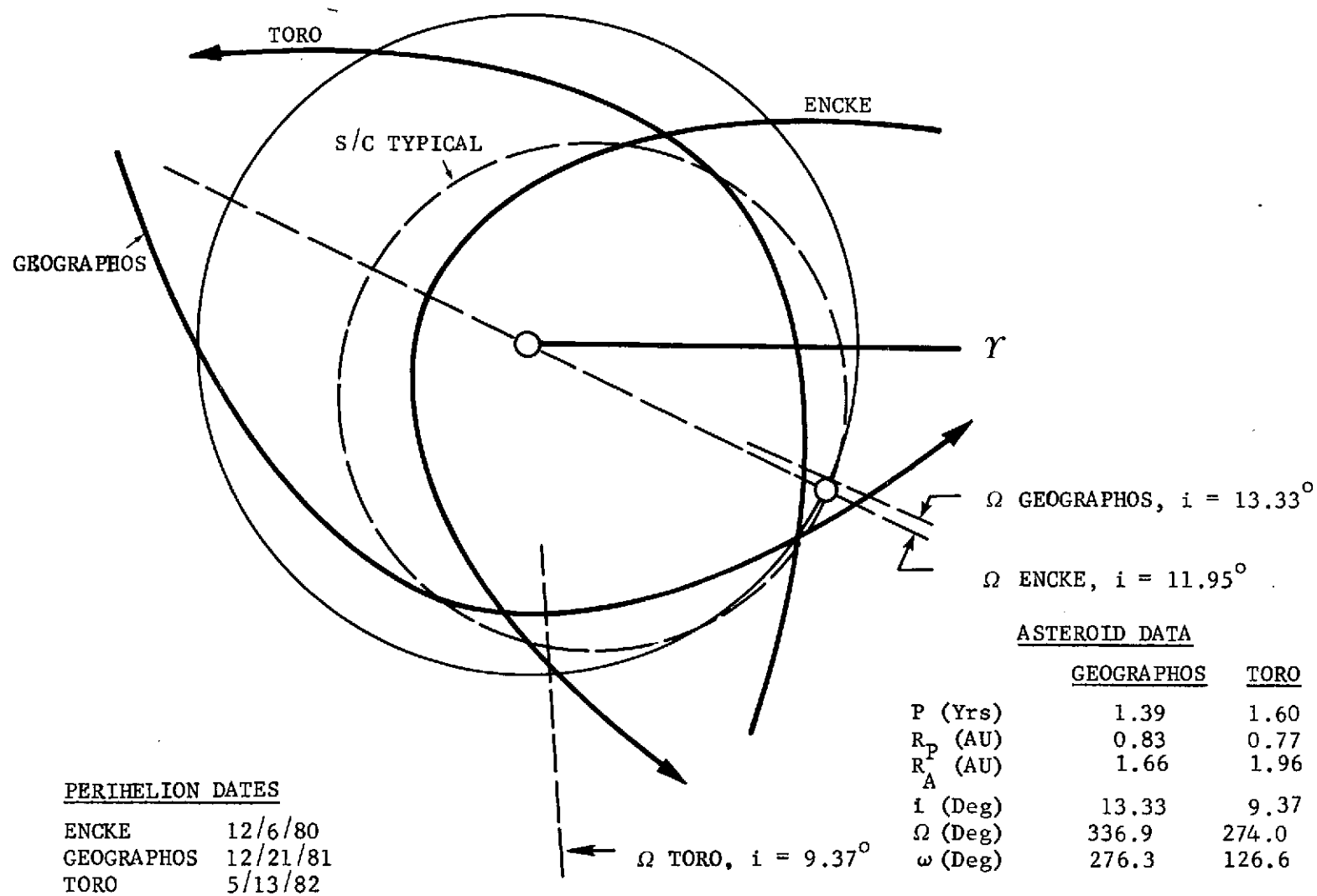


FIGURE A-8- ASTEROID FLYBY CANDIDATES

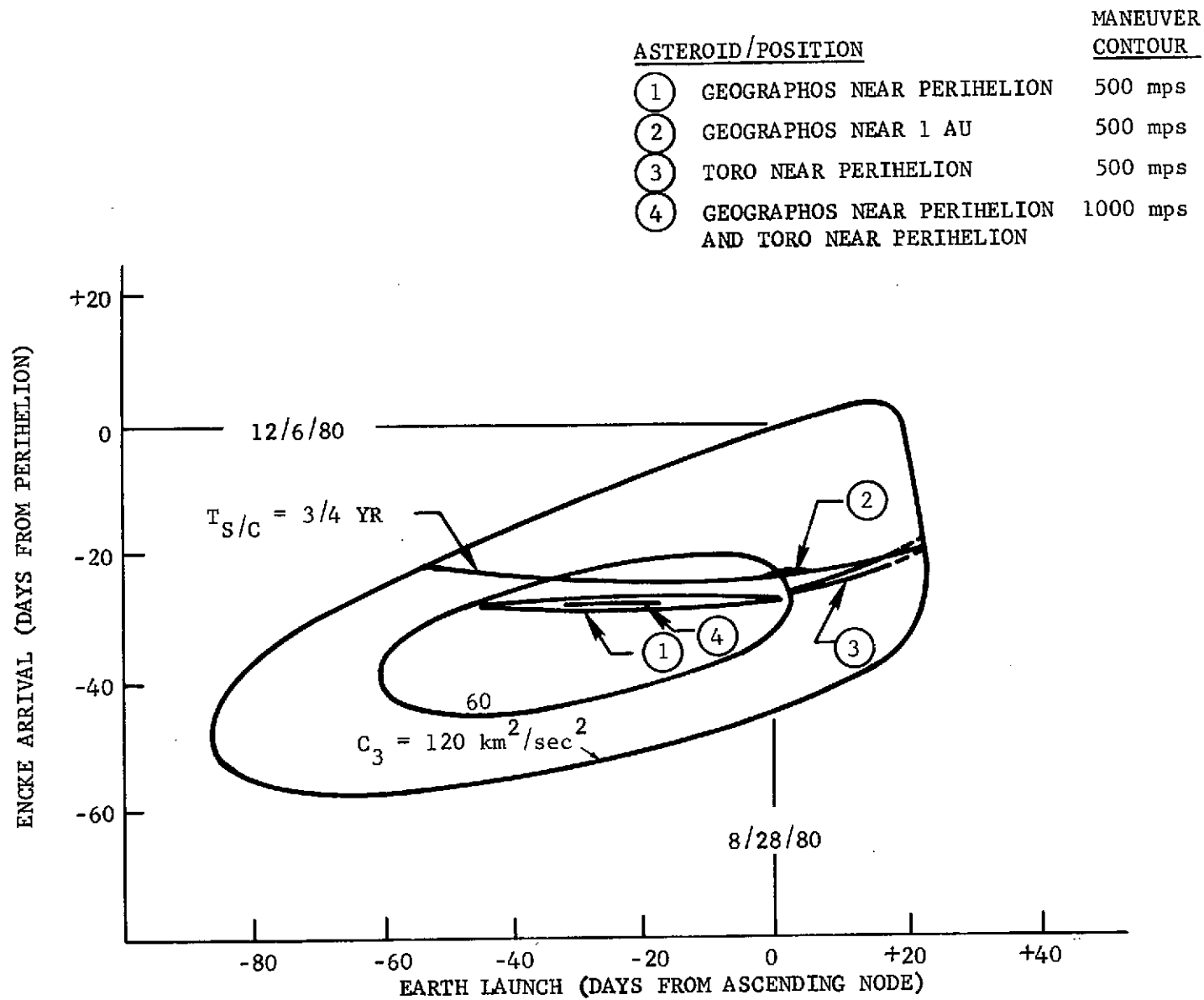


FIGURE A-9 COMBINED MISSION CHARACTERISTICS

TABLE A-1 ASTEROID FLYBY CHARACTERISTICS

<u>ASTEROID/ENCOUNTER POSITION</u>	<u>POST-ENCKE MANEUVER REQUIREMENTS</u>	<u>ENCOUNTER CONDITIONS</u>			
		<u>SPACECRAFT REVS</u>	<u>TIME FROM LAUNCH</u>	<u>RELATIVE VELOCITY</u>	<u>PHASE ANGLE</u>
GEOGRAPHOS NEAR PERIHELION	500 mps	1 3/4	480 d	12-13 km/sec	90 ⁻ deg
GEOGRAPHOS NEAR 1 AU	500	2	540	13-14	90 ⁺
TORO NEAR PERIHELION	500	2 1/4	610	11-18	90 ⁺
GEOGRAPHOS NEAR PERIHELION AND TORO NEAR PERIHELION	250 to	1 3/4 to	480 to	12 1/2 to	90 ⁻ to
	Geog.	Geog.	Geog.	Geog.	Geog.
	750 to	+ 1/2 to	+140 to	7 1/2 to	90 ⁺ to
	Toro	Toro	Toro	Toro	Toro
<hr/> 1000 TOTAL		<hr/> 620 TOTAL			

distances and the nature of the observables.

Phase angles at approach have not been calculated. The tabulated data are indications derived from inspection of the heliocentric geometries and are only intended to classify cases as more or less than half phase at acquisition.

5. Mission Option Summary

A matrix of the simple and compound mission options previously discussed is presented in Table A-2. Evaluation of maneuver requirements for retargeting to Earth after flyby of one or two asteroids has not been evaluated. In the case of pre-perihelion Encke encounter without asteroid objectives, it is assumed that launch/arrival conditions permitting "free return" to Earth would be selected.

Preliminary efforts to identify asteroid opportunities for combination with a post-perihelion Encke mission have not been successful. Also, no Earth return option is shown for this Encke case due to the long trip times and the expected adequacy of on-board data processing.

TABLE A-2 MISSION OPTION SUMMARY

<u>ENCKE FLYBY</u>	<u>NO ASTEROID FLYBY</u>	<u>GEOGRAPHOS FLYBY</u>	<u>TORO FLYBY</u>	<u>GEOGRAPHOS AND TORO FLYBY</u>
PRE-PERIELION ENCOUNTER				
NO PROBE OR R/V	X	X	X	X
PROBE ONLY	X	X	X	X
R/V ONLY	X	#	#	#
PROBE AND R/V	X	#	#	#
POST-PERIELION ENCOUNTER				
	X			

NOTE:

- X = Option Analyzed
= Option Not Analyzed

APPENDIX A REFERENCES

- A-1 NASA, Comets and Asteroids: A Strategy for Exploration,
Report of the Comet and Asteroid Mission Study Panel, NASA
TMS-64677, May 1972.

APPENDIX B

APPENDIX B

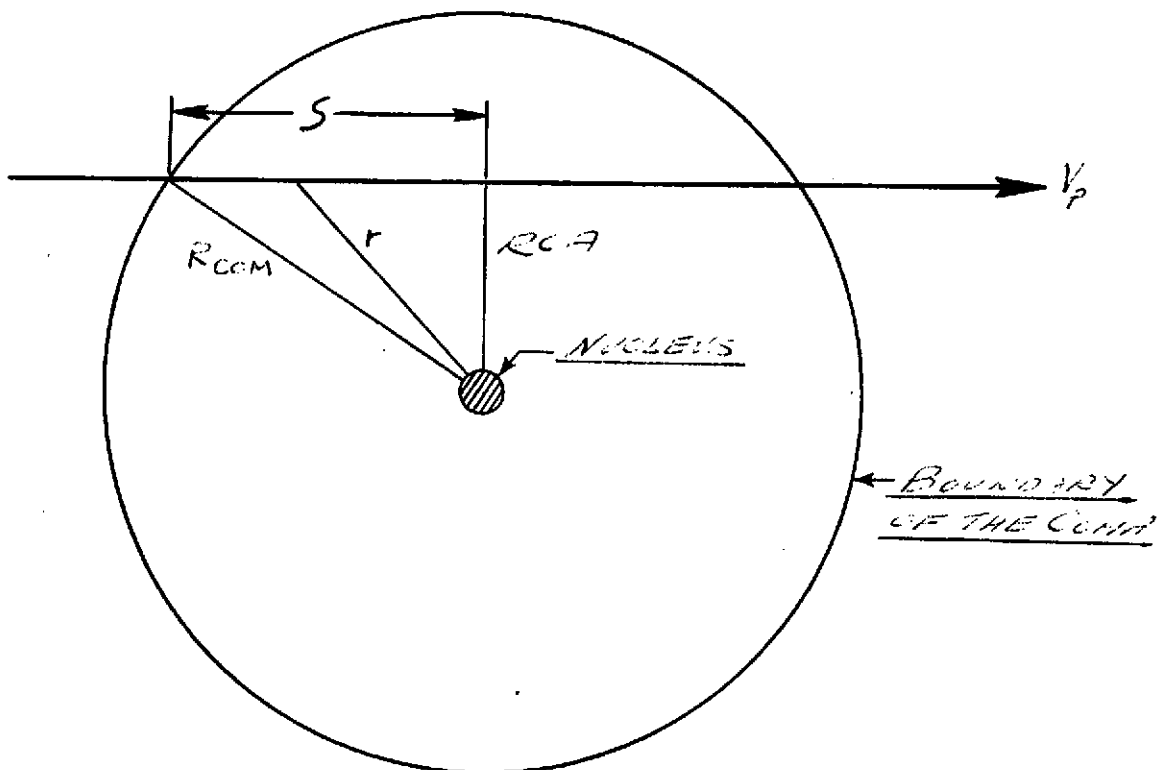
COMET PARTICULATE MATTER MODEL AND SPACECRAFT SURVIVABILITY

In Chapter II, the distance of closest approach was selected to be 5000 km, primarily in order to keep spacecraft survivability high, with large uncertainties in comet dust models. It is desirable for imaging and mass-spectrometer measurements to have a minimal R_{CA} , while the survival probability varies directly with the R_{CA} .

In this appendix, a computer model is explained which permits a simulated fly-through of the comet's dust environment. The model, comet-environment parameters, and survival results for the spacecraft and probe are explained.

Computer Model - A computer model has been developed to facilitate studies of the hazard to nearby spacecraft due to particulate matter emitted by a comet. The elements of this model are described below.

Because of its relatively low mass, a comet would be expected to perturb the trajectory of a spacecraft only very slightly as it flies-by. Consequently, the trajectory within the coma of the comet has been assumed to be linear. The resulting geometrical situation is sketched below.



V_P = the velocity of the spacecraft, constant, kilometers/second.

R_{CA} = radius of closest approach to the nucleus, kilometers.

R_{COM} = radius of the coma, 20,000 kilometers.

The trajectory history is calculated during the time required to traverse the distance S , i.e., half the chord of the spherical region assumed to contain the coma. When the spacecraft impacts the nucleus, the history terminates at impact. When the spacecraft passes the nucleus, the integrated particle flux is doubled to account for passage through the entire coma. The duration of the trajectory is calculated as follows:

$$S = \sqrt{R_{COM}^2 - R_{CA}^2} \quad \text{kilometers}$$

$$T = \frac{S}{V_P} \quad \text{seconds}$$

The distance from the center of the nucleus to the spacecraft is:

$$r = \sqrt{R_{CA}^2 + (S - V_P t)^2} \quad \text{kilometers}$$

where, t is time from entry of the coma.

Particle Environment Due to Emission from the Nucleus - The particle environment within the coma is assumed to be due to the steady emission of matter from the nucleus. In this model, the particles are emitted at a constant total mass rate and constant velocity and isotropically. Consequently, the particle density at any location is inversely proportional to the square of the distance from the center of the nucleus. Accordingly, the particle density near the surface of the nucleus is as follows:

$$D_{SURF} = \frac{\dot{m}_E}{4\pi R_N^2 V_E} \quad \text{grams/meter}^3$$

where, \dot{m}_E = mass emission rate (60,000 grams/sec. assumed)

R_N = radius of the nucleus (1,600 meters. assumed)

V_E = emission velocity (300 meters/sec. assumed)

Note that the density is directly proportional to the mass emission rate, \dot{m}_E , and inversely proportional to the emission velocity, V_E . The significance of the mass emission rate is obvious, the more material emitted by the nucleus, the greater the density. It is not so obvious, but physically reasonable, that the more rapidly this material passes through a unit volume of space, the fewer the particles that are present at any instant.

The characteristic mass versus number integral spectrum is inferred to be consistent with the cometary particle spectrum for all interplanetary space defined in Reference B-1. In the model we discussing here, the slope of the spectrum and the range of particle mass are identical to those of the reference. The resulting equation for the particle density is:

$$\log_{10} D = \log_{10} A - 1.213 \log_{10} m, \quad (m_1=10^{-6}) \leq m \leq (m_2=10^2)$$

where: m = particle mass, grams

A = a constant relating emission from the comet nucleus to the density equation.

The constant, A , is calculated as follows:

$$D = Am^{-1.213}$$

The density integrated over the entire range of particle masses is the the particle density at the surface of the nucleus. Therefore:

$$\int_{m_1}^{m_2} D dm = D_{SURF}$$

which leads to:

$$A = \frac{-0.213 \dot{m}_E}{4 \pi R_N^2 V_E \left[m_2^{-0.213} - m_1^{-0.213} \right]}$$

The particle flux at any distance, r , from the nucleus is, finally:

$$\log_{10} F = \log A - 1.213 \log_{10} m + \log_{10} V_P - 2 \log_{10} (r / R_N) \quad (B-1)$$

Resistance to Penetration of the Spacecraft Structure - The following equation from Reference B-1 has been used to calculate the penetrating mass at the ballistic limit of the spacecraft structure.

$$m_B = \frac{\ell^3 \rho^2 C_1^2}{(4.25)^3 \rho_P V_P^2}$$

where, ℓ = single sheet thickness,

ρ = density of the structural material, 2.75 grams/cm³ assumed
(Aluminum)

C_1 = speed of sound in the material, 6.25 kilometers/sec assumed

ρ_P = density of the cometary particle, 0.5 grams/cm³ assumed

V_P = Velocity of the spacecraft relative to the cometary particles.

This mass is the minimum required to penetrate the structure. If the structure includes a meteoroid bumper or two thicknesses ℓ_1 and ℓ_2 , the thickness to be used in the equation for m_B above is:

$$\ell = \frac{\ell_1 + \ell_2}{K}$$

where K is an effectiveness factor derived from Reference B-2, and is a function of the spacing between the bumper and the inner structure.

Probability of No Penetrations of the Spacecraft - The probability of no penetrations is calculated from the Poisson expression,

$$P(0) = e^{-N}$$

where, $N = C \cdot A_s \cdot T \cdot F(m_B)$, number of penetrations during exposure to the environment and,

C = constant relating the mission duration and the type of mission.

If the spacecraft impacts the nucleus, there is only an inbound trajectory only and $C=1$. If the spacecraft flies by, there is an inbound and outbound trajectory and $C=2$.

A_s = the largest area projected of the spacecraft exposed to mass particle environment, in meters².

Note: The exposed area must be adjusted to account for the orientation of the spacecraft with respect to the particle environment. If the vehicle is spinning, only 1/4 of the entire surface area will be exposed. Even if the vehicle does not spin, when the particle flux is directional, as in the case of radial emission from the nucleus, only the part of the vehicle facing the oncoming particles is exposed. Note the possibility of no penetration is zero for $m < m_B$ but it is calculated according to the Poisson equation above for $m > m_B$. T = time of flight from entry of the coma to termination of either impact or closest approach.

$F(m_B)$ = particle flux of mass, m_B (Ballistic limit) or greater. The flux is a function of position and is integrated along the trajectory.

The results of calculations using this model are discussed next in this report. It should be noted, however, that there are several conservative assumptions in this model. First, the probability of no penetrations used to define survivability is based on the exposed area of the spacecraft. Actually, the vulnerable area is only that which, if penetrated, could lead to failure. Our concern is primarily with electronic equipment. Penetration of a black box containing such equipment could cause destruction of a device, such as a transistor, or disruption of a circuit, either by breaking of wires or through removal of insulation resulting in shorting due to contact of 2 or more wires. Considering typical packaging densities in spacecraft, only some fraction of

the total area actually is vulnerable, and therefore the probability of no penetrations calculated by this model is too low if used as a survival number. Another element of conservatism is due to not including the thickness of the black boxes in the materials protecting the spacecraft. If this effect were included, the probability of no penetrations would also be higher.

Finally, the model assumes that all particles have the same velocity relative to the spacecraft. Actually, for radial emission, the particles would have a higher relative velocity as the spacecraft enters the coma and a lower relative velocity as the spacecraft leaves. This would also affect the probability of no penetrations. It is suggested that refinements be made in the future to include these and other effects that have not been considered in this first approach to the study. Techniques such as those discussed in Reference B-5 would be appropriate as the definition of the spacecraft is pursued to greater depth.

Particulate Flux - Some results are plotted in Figures B-1, and B-2, using equation (B-1). For reference, the comet particle range anticipated is between 10^{-6} and 10^{+2} grams. The most "harmful" (i.e., penetrating particles) are probably those with masses near 5×10^{-4} grams (i.e., 10^{-5} to 10^{-3}).

Spacecraft Survivability - A number of runs were made using the particulate model, comet environment, and various spacecraft materials. The area used for the spacecraft was 3.2 m^2 (a diameter of 2.14 meter minus a 0.71-meter-diameter inner circle for the spacecraft frontal area. For the probe, the area was 0.3 m^2 (effective diameter of 0.62 meters) for the frontal end. A number of aluminum thicknesses were considered, both single and double plate with filled spacing. The result was that to provide effective shielding with minimal weight, a 18-mil., aluminum double plate with 1-inch separation filled with polyurethane at 0.032 gm/cm^3 was sufficient.

Tables B-1 to B-4 summarize a survival story for spacecraft and probe at various distances from the nucleus for both comet-only missions (18.3-km/sec flyby velocity) and comet/asteroid missions (26.3 km/sec. flyby velocity).

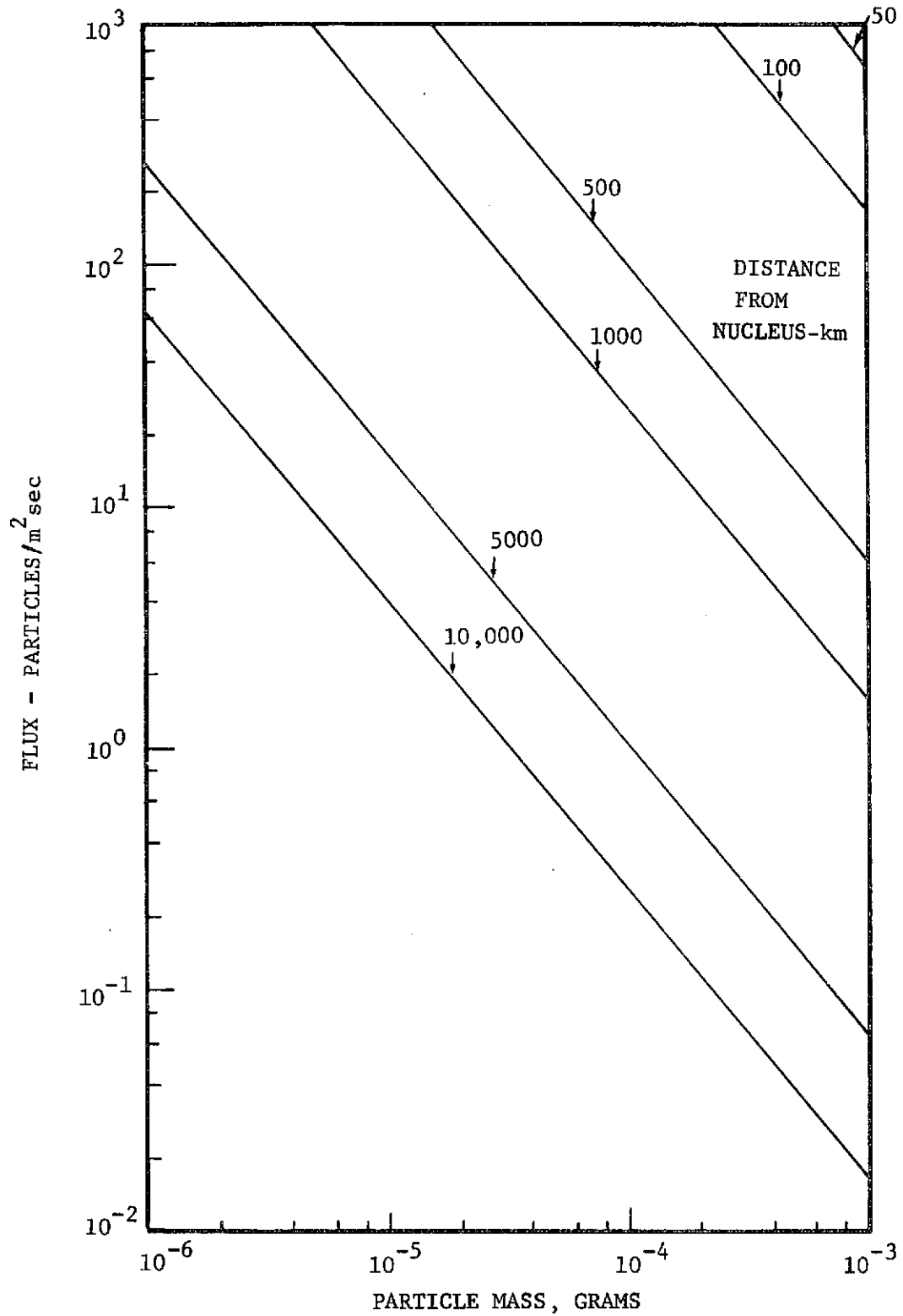


FIGURE B-1 ENCKE PARTICLE FLUX VS DISTANCE FROM NUCLEUS

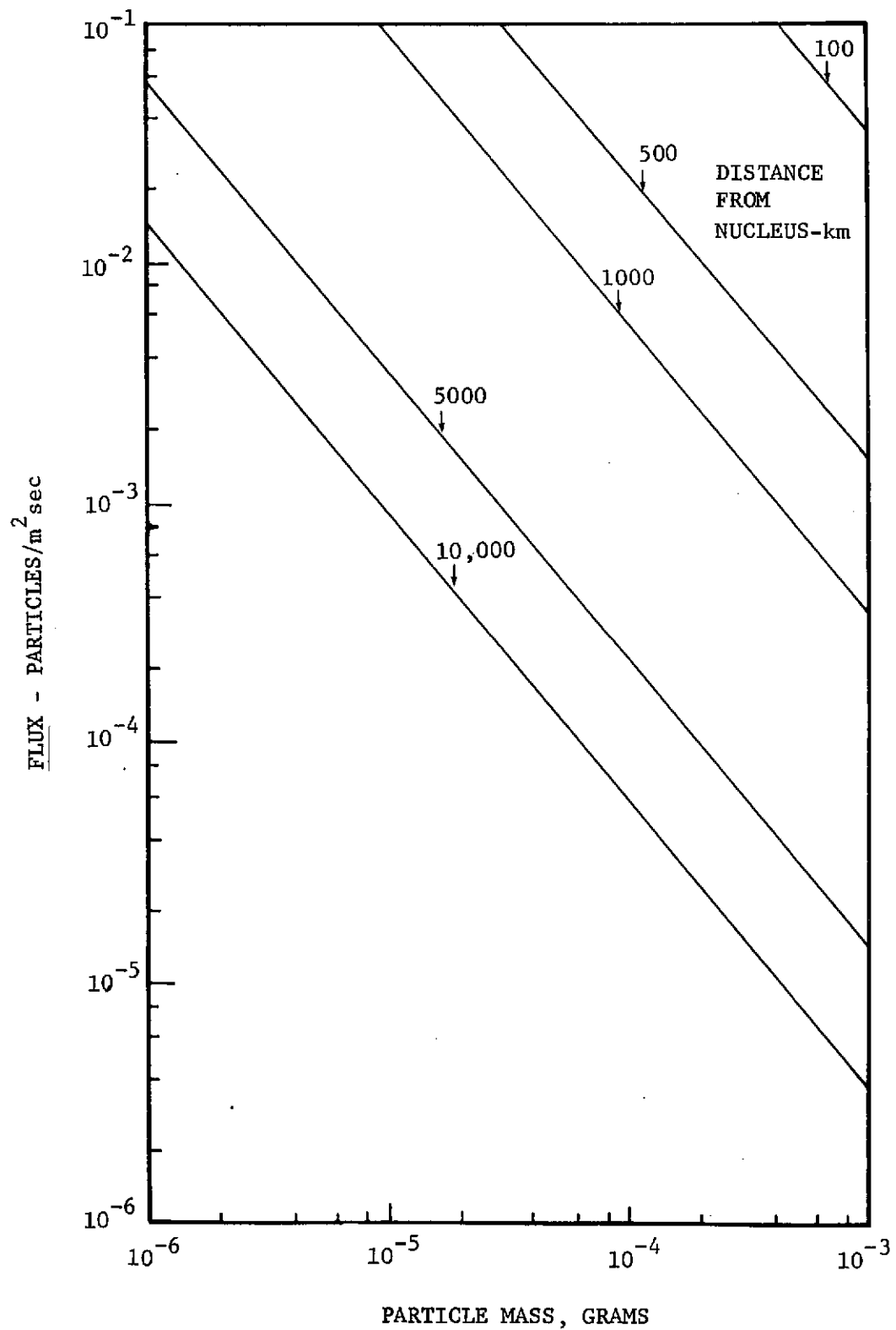


FIGURE B-2 ENCKE PARTICLE FLUX VS DISTANCE FROM NUCLEUS

TABLE B-1 SPACECRAFT AND PROBE SURVIVABILITY
(Particle Emission Rate - 60,000 g/sec; Particle Velocity - 300 m/sec)

	RCA	PROBABILITY OF NO PENETRATIONS* (Vehicle Velocity)	
		18.3 km/sec	26.3 km/sec
SPACECRAFT	10,000	0.9987	0.9968
	5,000	0.9967	0.9920
	1,000	0.9810	0.9548
	500	0.9617	0.9102
PROBE	5,000	0.9997	0.9993
	1,000	0.9982	0.9957
	500	0.9964	0.9914
	100	0.9820	0.9571
	50	0.9642	0.9159
	10	0.8329	0.6436

TABLE B-2 SPACECRAFT AND PROBE SURVIVABILITY
(Particle Emission Rate - 60,000 g/sec; Particle Velocity - 30 m/sec)

	RCA	PROBABILITY OF NO PENETRATIONS* (Vehicle Velocity)	
		18.3 km/sec	26.3 km/sec
SPACECRAFT	10,000	0.9869	0.9686
	5,000	0.9672	0.9229
	1,000	0.8252	0.6294
	500	0.6767	0.3901
PROBE	5,000	0.9969	0.9926
	1,000	0.9825	0.9583
	500	0.9647	0.9170
	100	0.8336	0.6448
	50	0.6945	0.4152
	10	0.1608	0.0122

* One-inch thick polyurethane foam filled honeycomb sandwich material with 18-mil aluminum face sheets.

TABLE B-3 SPACECRAFT AND PROBE SURVIVABILITY

(Particle Emission Rate - 6,000 g/sec; Particle Velocity - 300 m/sec)

	RCA	PROBABILITY OF NO PENETRATIONS* (Vehicle Velocity)	
		<u>18.3 km/sec</u>	<u>26.3 km/sec</u>
SPACECRAFT	10,000	0.9999	0.9997
	5,000	0.9997	0.9992
	1,000	0.9981	0.9954
	500	0.9961	0.9906
PROBE	5,000	0.9999	0.9999
	1,000	0.9998	0.9996
	500	0.9996	0.9991
	100	0.9982	0.9956
	50	0.9963	0.9912
	10	0.9819	0.9569

TABLE B-4 SPACECRAFT AND PROBE SURVIVABILITY

(Particle Emission Rate - 6,000 g/sec; Particle Velocity - 30 m/sec)

	RCA	PROBABILITY OF NO PENETRATIONS* (Vehicle Velocity)	
		<u>18.3 km/sec</u>	<u>26.3 km/sec</u>
SPACECRAFT	10,000	0.9987	0.9969
	5,000	0.9967	0.9920
	1,000	0.9801	0.9548
	500	0.9617	0.9102
PROBE	5,000	0.9997	0.9993
	1,000	0.9982	0.9957
	500	0.9964	0.9914
	100	0.9820	0.9571
	50	0.9642	0.9159
	10	0.8329	0.6436

* One-inch thick polyurethane foam filled honeycomb sandwich material with 18-mil aluminum face sheets.

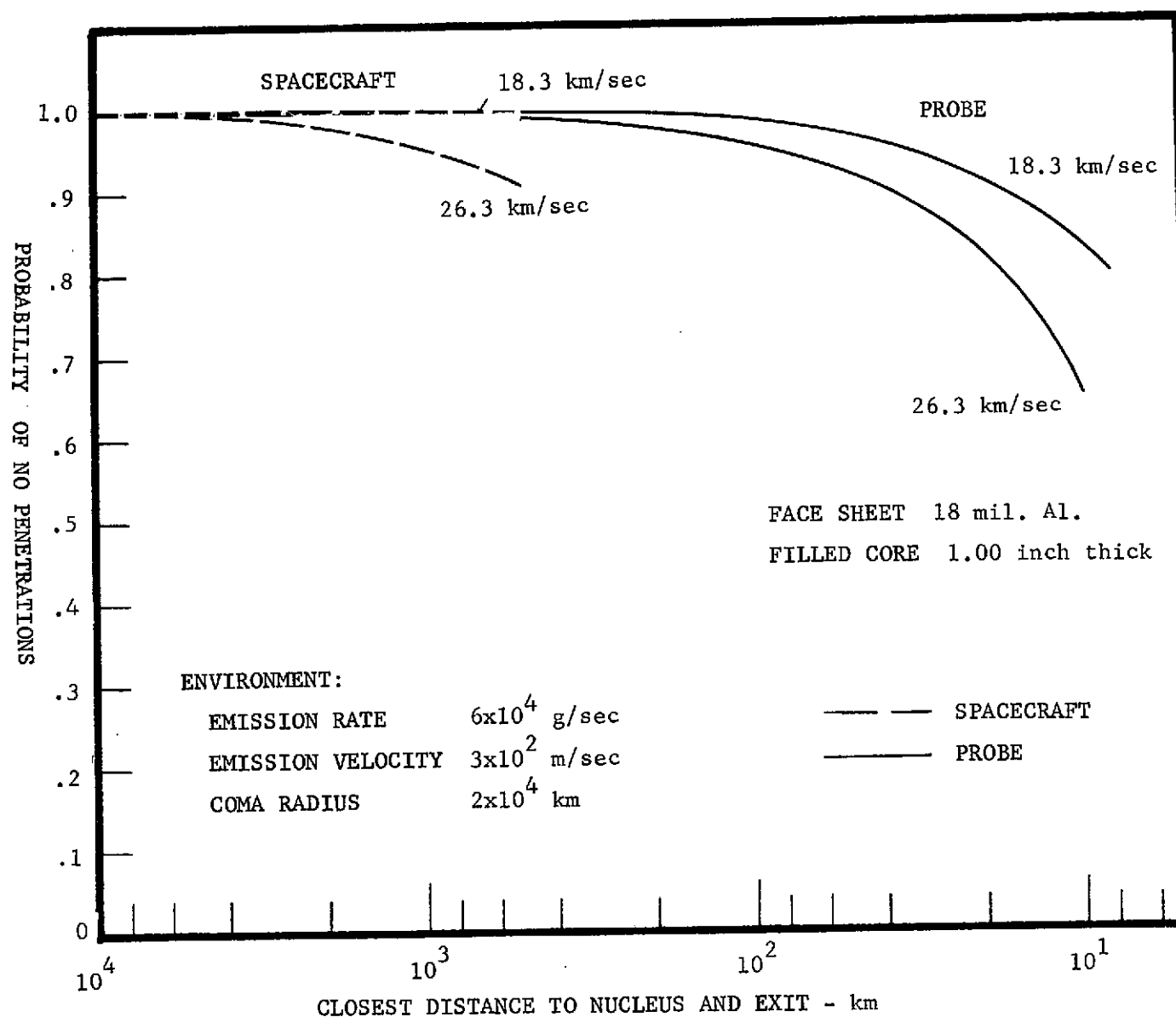


FIGURE B-3 SPACECRAFT AND PROBE SURVIVAL FOR ENCKE ENCOUNTER

Figure B-3 is a plot of Table B-1. The value of 60,000 gm/sec for the rate of particulate-matter emission is considered to be nominal (ref. II-6). A value of 6,000 g/sec (tables B-3 and B-4) is also used in the calculations to allow an order of magnitude uncertainty as a conservative measure. The velocity of particulate material is also shown at two values. The 300-m/sec value is nominal. Terminal gas velocities will reach ~ 1000 m/sec, but, depending upon material mass, drag coefficients, and escape processes, the particulate-matter velocity will be less than the gas velocity. Reference B-4 favors 300 m/sec, and this value has been used. A lower-limit value of 30 m/sec is also included, however.

Table B-1 indicates a probability of no penetration for the spacecraft of 0.9967 at 18.3 km/sec. and 0.9920 at 26.3 km/sec. For the same 60,000 g/sec emission and 300 m/sec velocity, the probe mass probability of no penetrations at 500 km are 0.9964 and 0.9914 at 18.3 km/sec and 26.3 km/sec respectively. Note that the probabilities of no penetrations do start to diverge rapidly (at lower distances) between 18.3 and 26.3 km/sec. (e.g., should the spacecraft transverse the 500 km level from the nucleus, it has only a 0.91 probability at the 26.3 km/sec velocity.). See Figure B-3.

Table B-1, for the probe, shows high survival (high probabilities of no penetration) until very close approaches of 100 to 50 km to the nucleus. Value below these levels are subject to model errors also (see Appendix C.).

Table B-2 indicates the worst combination of larger flux (60,000 g/sec) and slower velocity (30 m/sec). Even then, the 5000 km spacecraft, no penetration probabilities are 0.9672 for the 18.3 km/sec velocity. Comparable probe numbers at 500 km are 0.9647.

Tables B-3 and B-4, for 6,000 g/sec at both 300 and 30 meters sec are more favorable for survival. Numbers of Tables B-1 and B-4 are the same, indicating a trade between emission rate and velocity.

REFERENCES

- B-1 Kessler, D. J., Meteoroid Environment Model - 1970, (Interplanetary and Planetary), NASA SP-8038, Oct. 1970.
- B-2 Frost, V.C., Aerospace Meteoroid Environment and Penetration Criterion, TOR-269 (4650-40)-2, Aerospace Corporation, L.A., Calif., 17 Aug. 1964.
- B-3 Kase, Paul G. "Computerized Design of an Outer Planets Spacecraft Structure to Survive the Meteoroid Environment," Proceedings of AIAA/ASME/SAE, 14th Structures, Structural Dynamics, and Materials Conference, Williamsburg, Va., March 20-23, 1973.
- B-4 Probstein, R. F., "Problems of Hydrodynamics and Continuum Mechanics," Society of Industrial and Applied Mechanics, Phil, Pa., 1968.
- B-5 TRW Systems Group - Study of a Comet Rendezvous Mission, Tech. Report, No. 72-87 , May 1972.

APPENDIX C

APPENDIX C

PROBE COMMUNICATIONS: COMET GAS ENVIRONMENT AND ELECTRON DENSITY STUDY

In order to investigate communications problems that might arise with a probe designed to explore the inner coma of the Comet Encke, the various flow regimes encountered by the probe during its trajectory toward the nucleus must be determined. At sufficiently low ambient densities, gas molecules that collide with the probe surface and are reemitted do not experience subsequent collisions with the freestream particles. This is the free molecule regime. At higher ambient densities, i.e., nearer the comet nucleus, the first collision regime exists where a limited number of gas-phase interactions occur. Shortly after this regime, a cascading effect occurs, gas-phase collisions become dominant, and a shock wave is formed in front of the probe. It is after shock-wave formation, when the ionized processes occur in the shock layer and a plasma layer is formed, that the communications problems appear. This study is intended to establish the distances from the Comet Encke nucleus at which each of the various flow regimes can be expected.

Comet Gas Environment Model

Flow-Field Delineation - The criterion used to define the flow field altitude limits in a rarefied atmosphere is the Knudsen number, K_n , the ratio of a relevant mean free path to a characteristic body dimension. According to Probstein (Ref.C-1) the most realistic mean free path for flow-field delineation is that between particles incident on and those emitted from the probe surface. That is:

$$\lambda_{ei} = \frac{\bar{C}_e}{n_i u_r \pi \sigma^2}$$

with the mean speed \bar{C}_e given by:

$$\bar{C}_e = \left(\frac{8 k T_e}{\pi m_e} \right)^{1/2}$$

and n_i is the number density of incident molecules, u_r the relative velocity

between incident and emitted molecules, $\pi \sigma^2$, the effective mutual molecular cross section, and T_e and m_e the emitted particle temperature and mass respectively.

Taking the characteristic body dimension to be the probe radius R_p , the free molecule regime is defined by Reference C-2 to be that range of parameter values which satisfies.

$$K_n = \frac{\lambda_{ei}}{R_p} \geq 10$$

and the first-collision regime to be that range which satisfies

$$10 > K_n \geq \frac{1}{3}$$

Nominal Model

Basic to establishing the various flow regimes is a definition of the atmosphere, i.e., the number, density and type, n_i , of particles surrounding the comet nucleus. The model chosen for the initial study is basically from Reference C-3, which assumes that the bulk of the gas escaping from the nucleus is H_2O . In the region of interest, i.e., distances from the nucleus on the order of 100-1000 km, the number density distribution of the parent molecules can be represented by:

$$n = \frac{K}{r^2} e^{-r/\tau v} \quad 1/\text{cm}^3$$

where r is the distance from the nucleus, and, for the proposed water vapor model,

$$K = 7.0 \times 10^{12} \text{ km}^2/\text{cm}^3$$

$$\tau v = 3.76 \times 10^4 \text{ km}$$

where v is the gas expansion velocity, and τ is the characteristic time for photodissociation by sunlight. According to Reference C-3, these numbers apply only at a heliocentric distance, R , of 1.0 AU, at which the emission gas temperature is 350°K.

Now, for water vapor

$$m_e = 2.99 \times 10^{-23} \text{ g}$$

$$\sigma = 4.60 \text{ \AA}$$

and, at 1.0 AU,

$$v = 1.11 \text{ km/s}$$

$$\tau = 3.38 \times 10^4 \text{ s}$$

With the probe approaching the nucleus along the sun-comet axis at 24 km/s, then:

$$u_r = U_\infty + v = 25.1 \text{ km/s}, \quad U_\infty = 1.1 \text{ km/s}, \text{ where } U_\infty \text{ is terminal gas velocity.}$$

The energy-accommodation coefficient for particles impacting the probe surface is assumed to be unity, implying that the emitted particles will have the probe surface temperature, which is taken equal to the freestream temperature of 350°K.

Substituting into the appropriate relations yields an equation for the Knudsen number in terms of the distance from the comet nucleus, r :

$$K_n = \frac{\lambda_{ei}}{R_p} = \frac{0.551}{R_p} r^2 e^{-r/3.76 \times 10^4}, \quad R_p \text{ in cm., } r \text{ in km}$$

The exponential term is of the order 1.0 in the region of interest $r \leq 1000 \text{ km}$. Assuming an upper limit on probe radius of 1.0 m there results:

free molecule regime for $r \geq 43 \text{ km}$

first collision regime for $43 > r \geq 7.8 \text{ km}$

Sensitivity Study

The above results are "nominal" regime limits at $R = 1.0 \text{ AU}$ using the comet coma model supplied. An upper limit is established by bounding the various parameters involved. The primary parameters, and the direction in which they

could change in order to cause a decrease in mean free path are:

$$\lambda_{ei} \downarrow \left\{ \begin{array}{l} n_i \uparrow \\ u_r \uparrow \\ T_e \downarrow \end{array} \right.$$

The maximum relative velocity u_r has already been used in the calculation. The emission temperature may be lower than the value assumed of 350°K . A lower limit of 100°K was chosen. The ambient number density is most subject to error. A factor of 10 will be applied to the "nominal" number density variation; this corresponds to the correction of the nucleus vaporization flux which was applied to the basic comet model to account for the fact that Encke is an old comet.

Then:

$$K_n = \frac{0.0294}{R_p} r^2 e^{r/3.76 \times 10^4}$$

so that there exists;

$$\begin{array}{ll} \text{free molecule regime for} & r \geq 184 \text{ km} \\ \text{first collision regime for} & 184 > r \geq 34 \text{ km} \end{array}$$

as upper limits at $R = 1.0$ using the atmosphere provided.

Intercept Distance Adjustments

With the proposed probe intercept expected to occur at about 0.5 AU an estimate of the gas density at this point is required to establish the flow regimes. For $R = 1.0$ and H_2O the parent molecule, the vaporization rate is controlled basically by the solar energy incident on the nucleus. Thus, the vaporization rate shows an inverse square variation with heliocentric distance (ref.C-4). Assuming the gas density to be proportional to this value, a factor of four should be applied to the gas density model at 1.0 AU for considerations at 0.5 AU. In addition, the characteristic time for photodissociation by sunlight varies as R^2 , so that the molecular coma is smaller at 0.5 AU than at 1.0 AU. However, it will still be sufficiently distant so as not to influence

the previous procedure for flow delineation. In this case, and with the parameters other than gas density unaltered, the change from 1.0 AU to 0.5 AU will double the altitude limits established earlier for the free-molecule and first-collision regimes for both the "nominal" and upper bound cases.

Free Electron Distribution Model

Since the closest expected approach to the comet nucleus is ~ 500 km, the probe will probably be in the free-molecule or, at worst, the first-collision regime. In those regimes, a plasma sheath surrounding the probe and containing high concentrations of free electrons is not formed. Thus, the probe passage through the coma should not influence the probe communication, and only resident free electrons need be considered.

In developing the gas density model used as a basis for the flow delineation (ref. C-5) a series of reactions between H_2O and its daughter products were considered. Among these are ionization reactions in which electrons resulted. These considerations indicate, however, that no significant production of free electrons occurs. Thus, it seems that no communication problems should result from the gas composition of the coma.

Refinements to Comet Encke Atmosphere

During the initial flow-delineation effort, a number of assumptions concerning the comet atmosphere were made, e.g. adoption of the Mendis-Holzer-Axford atmosphere (ref. C-5) calculated for $R = 0.8$ (but incorrectly identified in Reference C-3 as occurring at 1.0 AU), and subsequently reducing the density an order of magnitude to account for Encke's age. It now seems that there is sufficient information to construct an atmosphere with less uncertainty and definitely more consistency.

Mendis et al suggest that the H_2O flow velocity determined in their atmospheric calculation is independent of the rate of vaporization, and, thus, their density variation could be rescaled for various production rates. The basic density variation for the parent molecule that satisfactorily fits the numerical results of Mendis et al (ref. C-5) is

$$n = \frac{K}{vr^2} e^{-r/\tau_v} \quad 1/\text{cm}^3$$

The parameter K is dependent on the parent molecule production rate. The value used by Mendis is the result of Delsemme and Swings (C 6). A more recent result by Delsemme and Miller (C 4) will be used in the present estimation. For $R \leq 2.0$, the vaporization rate of H_2O for the steady-state temperature of a rotating cometary nucleus with an albedo of 0.1 can be represented by:

$$Z = n_o v_o = \frac{3.0 \times 10^{17}}{R^2} \quad 1/\text{cm}^2 \text{ s} \quad \text{where} \quad \begin{array}{l} Z \text{ is vaporization rate of } \text{H}_2\text{O} \\ n_o \text{ is number density } 10 \text{ km from the nucleus} \\ v_o \text{ is gas velocity } 10 \text{ km from the nucleus} \end{array}$$

The temperature will be assumed to be constant at a value of 200°K since the Mendis (C-5) velocity distribution is based on this value, and the velocity varies as $v \propto R^{-\frac{1}{2}}$. Then, also from Mendis et al, $v_o = 0.30 \text{ km/s}$, where the subscript o refers to $r_o = 10 \text{ km}$.

The characteristic time for photodissociation, τ , has been estimated earlier for $R = 0.8 \text{ AU}$ as

$$\tau_{0.8} = 3.38 \times 10^4 \text{ s}$$

Then

$$\tau = \tau_{0.8} R^2 = 5.3 \times 10^4 R^2 \text{ s}$$

$$\text{combining the previous results, we have } K = \frac{3 \times 10^{14}}{R^2} \left(\frac{\text{km}}{\text{cm}} \right)^3 \cdot \frac{1}{\text{sec}}$$

$$n = \frac{3.0 \times 10^{14}}{vr^2 R^2} e^{-r/5.3 \times 10^4 v R^2} \quad 1/\text{cm}^3$$

For much of the atmosphere, the H_2O -gas velocity is constant at 1.11 km/s:

$$n = \frac{2.7 \times 10^{14}}{r^2 R^2} e^{-r/5.9 \times 10^4 R^2} \quad 1/\text{cm}^3$$

and the Knudsen number as given by

$$K_n = \frac{2.7 \times 10^{-3}}{R_p} \frac{r^2 R^2}{u_r}$$

r in km
 R in AU
 u_r in km/s
 R_p in m

For flow-field definition, then:

$$r = \frac{1}{R} (3.7 \times 10^2 u_{r p} R K_n)^{1/2} \quad (10^2 \leq r \leq 10^4 R^2 \text{ km})$$

Applying this equation to the flow delineation problem at hand yields:

$$\begin{array}{ll} \text{free-molecule regime} & r \geq 610 \text{ km} \\ \text{first-collision regime} & 610 > r \geq 111 \text{ km} \end{array}$$

at $R = 0.5$.

Figure C-1 shows the derived density variation at 0.5 AU, and figure C-2, taken from Mendis, et al (Ref. C-5), shows the flow velocity at the same location. The previous comments on electron density and communications would still apply, provided communication with probe is not required closer than about 100 km from the nucleus.

REFERENCES

- C-1 Probstein, R. F., "Problems of Hydrodynamics and Continuum Mechanics," Soc. of Industrial and Applied Mechanics. Phil., Pa., 1968.
- C-2 Lefferdo, J. M., Edquist, C. T., and Steel, P.C., "Gas Dynamics Environment of High Altitude Jovian Entry," AIAA Paper No. 72-203, 1972.
- C-3 TRW Systems Group - Study of a Comet Rendezvous Mission, Tech. Report No. 72-87, May 1972.
- C-4 Delsemme, A. H., and Miller, D. C., "Physico-Chemical Phenomena in Comets - III, The Continuum of Comet Burnham (1960 II). " Planet. Space Sci., 19, 1229, 1971.
- C-5 Mendis, D. A., Holzer, T. E., and Axford, W. I., "Neutral Hydrogen in Cometary Comas," Astrophys. and Space Sci., 15, 313, 1972.
- C-6 Delsemme, A. H., and Swings, P., Ann. of Astrophysics, Vol. 15, 1952.
- C-7 Martin Marietta Corp., Jupiter Turbopause Probe Gas Physics Environment and Instrument Response Study, for NASA-Goddard, MCR-71-142, 1971.

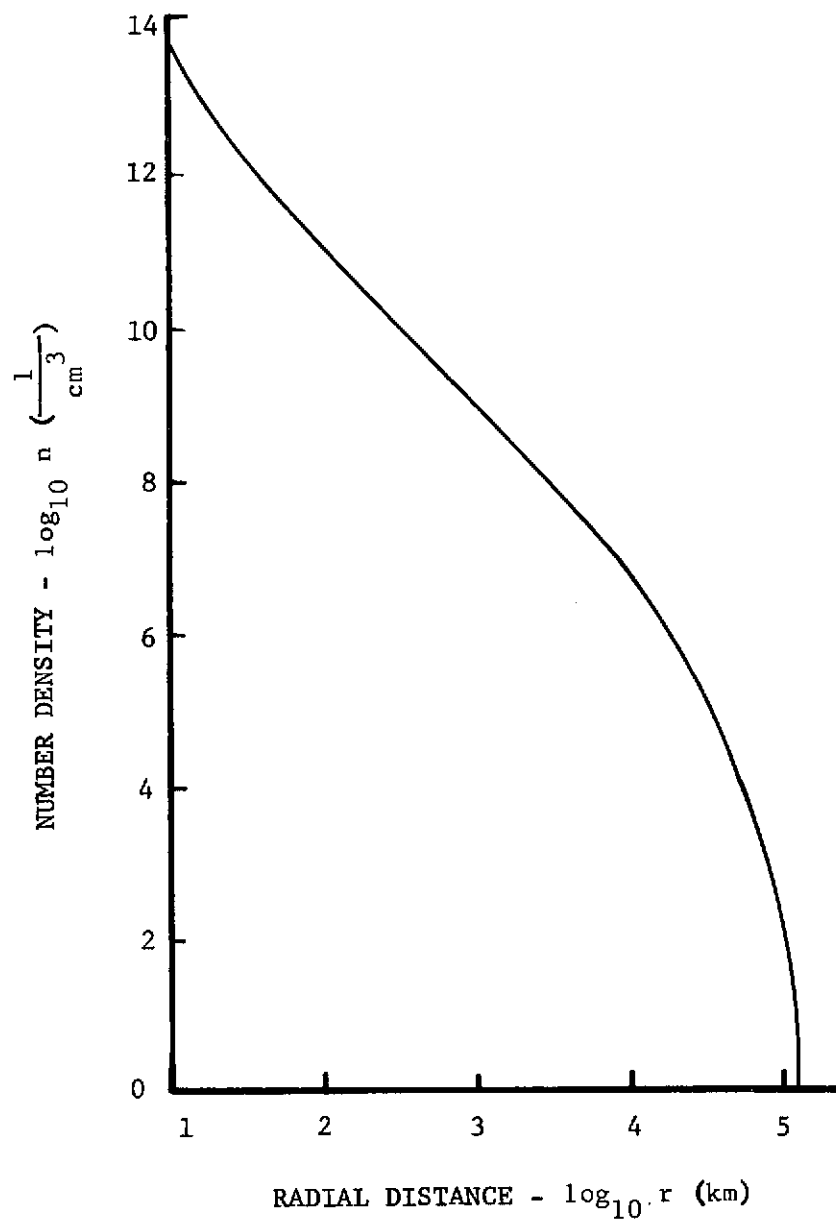


FIGURE C-1 NUMBER DENSITY VS. DISTANCE FROM NUCLEUS AT R = 0.5 AU

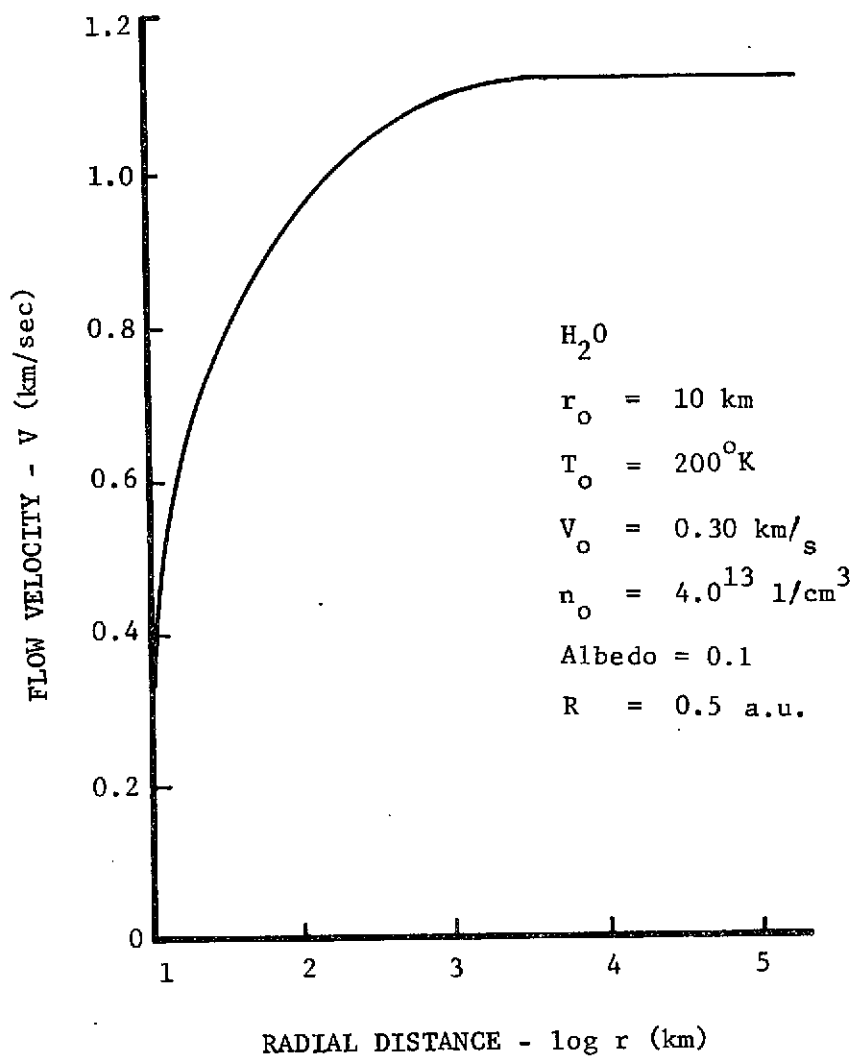


FIGURE C-2 FLOW VELOCITY VS. DISTANCE FROM NUCLEUS, REF. C-5